Enhancing potential field inversion techniques using geological uncertainty: Improving three-dimensional geological models

by
Mark D. Lindsay

School of Geosciences, Monash University
Clayton, Victoria
Australia

and

Géosciences Environnement Toulouse
Université Paul Sabatier (Toulouse III)
Toulouse
France

A thesis submitted for the degree of

Doctor of Philosophy (PhD) - cotutelle

December 2012

Copyright Notices

Notice 1

Notice 2

Abstract

3D modelling aims to solve geological problems, but these are always underdetermined and require prediction to produce geologically reasonable results. There are a series of related issues associated with 3D modelling techniques that require analysis, including geophysical ambiguity, sparse data and the subjective nature of geological interpretation. The combination of these modelling issues results in geological models being subject to uncertainty. In this thesis, we have developed 'stratigraphic variability' to detect and quantify geological uncertainty within 3D models.

Stratigraphic variability determines the likelihood of finding different geological units at any given location within a model. A model suite is produced during uncertainty analysis, which contains a collection of models calculated from a single input data set. The effect of geological uncertainty on 3D model architecture is analysed with a set of 'geodiversity' metrics, a collection of analytical techniques that characterise each model within the model suite geometrically and geophysically. Geometrical metrics include: depth and volume of a geological unit; curvature and surface area of a contact; and geological complexity. Geophysical metrics analyse the observed geophysical response (representing nature), the calculated geophysical response (representing the model) and the residual (the difference between the observed and calculated responses).

Geophysical metrics include: the root-mean-square misfit of the residual; standard deviation of the calculated response; information entropy of the residual; the 2D correlation coefficient of the calculated and observed response and; the Hausdorff distance between the calculated and observed response. Model space is mapped by identifying models that exhibit common and diverse characteristics, with the most diverse models defining the boundaries of model space and most common models defining the centre. The combination of uncertainty detection and model space exploration reveals the range of geological possibility. This thesis demonstrates a set of techniques that better describe the geological problem and provide guidance to geophysical inversion procedures.

We demonstrate stratigraphic variability, geodiversity and inversion techniques on two case studies: the Gippsland Basin, a mature oil and gas prospective region off the coast of southeastern Australia; and the gold prospective Proterozoic Ashanti Greenstone Belt located in southwestern Ghana. Significant results are that: (1) model architecture can vary significantly due to uncertainty; (2) considered addition of data significantly reduces model uncertainty; (3) characterisation of models using geodiversity reveals geologically relevant characteristics of a model; (4) not constructing multiple 3D models from a dataset misrepresents the geological terrane; (5) model uncertainty is complex and affects the architecture of each model differently; (6) geophysical inversion can be assisted using results from both stratigraphic variability and geodiversity and (7) all these techniques can be applied to 3D models that represent different geological terranes.

General Declaration

In accordance with Monash University Doctorate Regulation 17 / Doctor of Philosophy and Research Master's regulations the following declarations are made:

I hereby declare that this thesis contains no material which has been accepted for the award of any other degree or diploma at any university or equivalent institution and that, to the best of my knowledge and belief, this thesis contains no material previously published or written by another person, except where due reference is made in the text of the thesis.

This thesis includes 1 original paper published in a peer reviewed journal and 3 unpublished publications. The core theme of the thesis is using geological uncertainty to improve 3D geological modelling techniques. The ideas, development and writing up of all the papers in the thesis were the principal responsibility of myself, the candidate, working within the School of Geosciences, Monash University, Victoria, Australia under the supervision of Dr. Laurent Ailleres and Géosciences Environnement Toulouse, Université Paul Sabatier (Toulouse III), France under the supervision of Prof. Mark Jessell.

The inclusion of co-authors reflects the fact that the work came from active collaboration between researchers and acknowledges input into team-based research.

In the case of Chapters 1, 2, 3 and 4, my contribution to the work involved the following:

Thesis chapter	Publication title	Publication status	Nature and extent of candidate's contribution
1	Locating and quantifying geological uncertainty in three-dimensional models: Analysis of the Gippsland Basin, southeastern Australia	Published	Preparation of figures and manuscript, 3D model construction, development of technique described within ……90%
2	Geodiversity: Exploration of 3D geological model space	Accepted	Preparation of figures and manuscript, development of technique described within ……90%
3	Investigation of the Ashanti Greenstone Belt with geophysical forward modelling	In preparation	Preparation of figures and manuscript, 3D model construction, development of technique described within ……95%
4	Inversion and geodiversity: Searching model space for the answers	In preparation	Preparation of figures and manuscript, 3D model construction, development of technique described within ……90%

I have (have not (circle that which applies) renumbered sections of submitted or published papers in order to generate a consistent presentation within the thesis.

Signed: [redacted]……

Date:

Acknowledgments

The works presented in this thesis could not have been achieved without the support of many people and organisations. I would like to thank Monash University and the Australian Government for awarding me with an APA scholarship and Université Paul Sabatier (Toulouse III) for welcoming me to their institution.

Firstly, I would like to thank my supervisors Laurent Aillères, Mark Jessell, Pete Betts and Eric de Kemp for their enthusiastic support through every stage of this PhD. While we all never managed to be in the same room at the same time, your willingness to respond to my requests and flights of fancy is greatly appreciated. I hope that we can all share a celebratory drink at some stage in the near future. Special thanks go to Laurent for persisting with organising the cotutelle degree, and Mark and Esther for being so welcoming when my family and I arrived in Toulouse. Thank you also to Stéphane Perrouty for your discussion and amazing ability to cut through French bureaucracy. Thanks also go Florian Wellman, another uncertain geologist, for your enlightening perspectives. Thank you to all the people who have reviewed my papers, abstracts and presentations.

Several organisations and groups have provided much needed support and assistance. Thank you to those who are and were at Intrepid Geophysics; Des FitzGerald, Asbjørn Christensen, Ray Seikel and Stewart Hore for ongoing support with Geomodeller and other topics of interest. Thanks also to Tim Rawling, formerly of GeoScience Victoria, for assistance with the Gippsland Basin model. Thanks to the BGRM and Antonio Guillen and Gabi Corrioux for hosting me in Orléans, providing assistance, and a Christmas party I'll never forget. Thank you to the Society of Economic Geologists Hugo Dummett fund for providing research funds for two years running. Thank you to Monash University, the French Embrassy (Australia) and the Geological Society Australia (Victorian Branch and SGEG) for travel grants. Thank you to the Monash eResearch Centre for the High Performance computing scholarship.

Thank you to those who have shared space with me over the past three years or so. Thank you to Brenton, Maddy, Antoinette, Flic and Steph for being such amazing office-mates and supplying much needed entertainment. Special thanks go to the Monash Structural Geophysics Group – I hope all future meeting are like ours. If not, I'll have to adjust my poor language. Thanks to the postgraduate population at the School of Geosciences, you guys are amazing! To Aude and Jean-Seb in Toulouse, I apologise for my bewildering French but I really appreciate your efforts (in vain) to help me speak the language – merci! Others who made my year in Toulouse truly memorable are Teele, Isabel, Eric, Joaquin, German, Ana, Vasek, Lenka, Luc and Elder.

I would like to gratefully thank my family for supporting me through the entire process. I would like to thank my Mum for inspiration, support and encouragement. I would like to also give my beautiful children a giant kiss for helping me stay focussed and keeping me grounded. Finally, words cannot describe how much the support and love of my wife Amanda meant to me. I could not have done it without you.

Résumé analytique

Executive Summary

Le raisonnement derrière ce projet était de développer des techniques qui pourraient characteriser le niveau de confiance que la communauté géoscientifique a dans les modèles géologiques en trois dimensions (3D). La confiance que l'on a en un modèle est directement liée à la précision du modèle dans la représentation du monde naturel. La précision d'un modèle géologique 3D est vitale pour une évaluation correcte de sites ayant une importance nationale et économique. Les efforts en vue d'obtenir des richesses économiques sous forme de gisements minéraux ou énergétiques (pétrole, gaz, charbon et énergie géothermale), d'atteindre les objectifs de réduction d'émissions de carbone (séquestration du carbone) ou concernant l'élimination des déchets nucléaires peuvent être grandement améliorés par l'utilisation de modèles géologiques 3D précis. Le manque de confiance actuel dans les techniques de construction courantes des modèles géologiques 3D est dû à la nature hautement subjective et interprétative du processus de construction de modèle. Les prédictions basées sur des observations souvent limitées en raison d'un manque d'affleurements ou d'observations faites en trois dimensions des propriétés terrestres ont conduit à des modèles qui représentent le monde naturel de façon erronée. Une technique communément utilisée pour contrebalancer la subjectivité et la dépendance à l'interprétation est de tester les modèles en comparaison avec (et parfois en s'en servant pour les peaufiner) la modélisation gravimétrique et la géophysique magnétique. Le but original de ce projet était d'améliorer les algorithmes courants de façon à (1) mieux combiner les données géologiques et géophysiques et (2) fournir une plateforme plus objective et reproductible sur laquelle construire des modèles géologiques 3D.

Les Directeurs de Thèse pour ce projet étaient Dr. Laurent Ailleres (School of Geosciences, Monash University), Prof. Mark Jessell (Géosciences Environnement Toulouse/ L'Institut de recherche pour le développement), Ass. Prof. Peter Betts (School of Geosciences, Monash University) et Eric De Kemp (Geological Survey Canada, superviseur externe). Des collaborations de recherche étroites ont été établies avec Stéphane Perrouty (GET/IRD), Dr. Des FitzGerald (Intrepid Geophysics) et Dr. Tim Rawling (alors à GeoScience Victoria, maintenant à AGOS, Melbourne University). Une assistance technique et scientifique importante a été procurée par Dr. Antonio Guillen (BRGM, Orléans), Ray Seikel (Intrepid Geophysics) et Dr. Stewart Hore (Intrepid Geophysics).

Deux sites d'études de cas ont été sélectionnés comme exemples de situation en monde réel pour être utilisés dans le cadre de ce projet de recherche. Le Bassin de Gippsland, dans le sud-est de l'état de Victoria, en Australie, est un champ de pétrole et de gaz développé en haute mer. La Ceinture Ashanti Greenstone, dans le sud-ouest du Ghana est un terrane aurifère côtier Paléoprotérozoïque polydéformé situé en Afrique de l'Ouest.

Un partenariat entre le Département des Industries Primaires du gouvernement de l'état de Victoria et GeoScience Victoria (la commission géologique de l'état) a été établi, par lequel les données publiques seraient fournies pour construire un modèle du Bassin de Gippsland. Le Bassin de Gippsland a été choisi en raison de son importance en tant que champ de pétrole et de gaz existant et des plans en vue d'examiner les possibilités de séquestration de carbone dans cette région. L'architecture de bassin est un sujet typique de la plupart des recherches de modélisation géologique 3D et représenterait un exemple nécessaire sur lequel des expériences pourraient être faites.

La Ceinture Ashanti Greenstone a été choisie comme zone d'étude de cas en raison d'une collabo-

ration de recherche existante entre School of Geosciences, Monash University et le LMTG/GET, Université Paul Sabatier (Toulouse III) et IRD. Stéphane Perrouty, doctorant au GET, faisait une étude géologique et géophysique intégrée du sud de la Ceinture Ashanti Greenstone et a produit beaucoup de données qui sont typiquement utilisées dans la construction de modèles 3D. Ce fut une bonne opportunité de produire un modèle 3D pour rehausser l'étude faite par Stéphane et pour fournir une étude de cas géologiquement différente du modèle du Bassin de Gippsland. La modélisation de terranes polydéformés complexes devenant plus importante dans l'exploration des minéraux et il a été jugé nécessaire que les techniques développées au cours de cette étude soient démontrées comme étant efficaces dans ces régions à potentiel minéral.

Les outils et les techniques ont été développés grâce à l'utilisation de logiciels variés sur des plateformes d'ordinateur de bureau et de grille informatique. Geomodeller™ 3D a été utilisé pour construire des modèles 3D afin de faire une modélisation prédictive géophysique 3D. Geomodeller™ 3D est une application de modélisation géologique 3D développée conjointement par Intrepid Geophysics (Brighton, Victoria, Australia) et le BGRM (Orléans, France). La recherche en collaboration avec Intrepid Geophysics a donné accès au logiciel 3D Geomodeller Application Program Interface (API), à partir duquel des techniques primordiales ont été développées. L'automatisation de nombreuses tâches a été facilitée grâce à l'accès à 3D Geomodeller API et a permis plus de développements pour Intrepid Geophysics. Mathworks Matlab® a été utilisé pour développer le code qui a réuni et analyse les résultats générés par 3D Geomodeller. Les processus à utilisation massive de mémoire ont été transférés sur la plateforme informatique Monash Sun Grid où ils demeurent disponibles à l'usage du public.

Chapitre 1 Sommaire

Les modèles géologiques à trois dimensions (3D) sont construits pour représenter de manière fiable une cible géologique donnée. La fiabilité d'un modèle dépend largement des données entrées et est sensible à l'incertitude. Cette étude examine l'incertitude introduite par les données d'orientation géologique en produisant une suite de modèles 3D implicites générés à partir des mesures d'orientation soumises à des simulations d'incertitude. La simulation d'incertitude est un procédé dans lequel les entrées de mesures d'orientation dans le processus de modélisation sont perturbées. La perturbation indépendantes des mesures est accomplie en faisant varier au hasard (simulation Monte-Carlo) les mesures originales de jusqu'à ± cinq degrés. Les mesures d'extension latérale et de pendage pour chaque observation sont toutes deux variées dans les données entrées pendant la simulation d'incertitude.

Le résultat de la simulation d'incertitude est une nouvelle série de mesures à partir de laquelle de nouveaux modèles peuvent être calculés. 100 séries de mesures d'orientation différentes ont été produites dans ce chapitre, mais un nombre infini de mesures peut être produit de cette manière. Le nombre 100 a été choisi car celui-ci produit une quantité suffisamment élevée de données pour produire un échantillonnage adéquat mais est suffisamment bas pour réduire le temps de modélisation et d'analyse des données pour permettre à ce projet d'être accompli dans les délais impartis. De nouveaux modèles ont été calculés une fois que les nouvelles séries de données d'orientation ont été produites. La série de nouveaux modèles en conjonction avec le modèle calculé avec la série de

données originales (le 'modèle initial') a produit la 'série de modèles'. Tous les modèles à l'intérieur de la série de modèles ont été discrétisés en voxets lithologiques et comparés les uns aux autres pour produire une 'grille d'incertitude'.

La méthode de modélisation implicite est présentée en détail dans le Chapitre 1. La méthode implicite est intégrale à cette recherche du fait qu'elle procure à la fois un moyen rapide de calculer les nouveaux modèles et une méthode répétable pour créer des éléments permettant de créer une modèle géologique en trois dimensions. D'autres méthodes de modélisation, telles que la méthode explicite, réclament que l'opérateur numérise manuellement les éléments géologiques et par conséquent implique une interprétation de la part de l'opérateur. La conséquence de l'interprétation est que la même série de données peut produire des solutions différentes selon les décisions prises par l'opérateur durant la modélisation et n'est pas répétable. Les méthodes de modélisation explicites peuvent prendre assez longtemps et la production de modèles multiples (tels que les 100 modèles perturbés produits dans ce chapitre) prendrait bien plus longtemps qu'il n'est possible avec la méthode implicite. Une série de modèles produits par les méthodes explicites contiendrait probablement une grande proportion de préjugés de l'opérateur qui serait difficile à retirer quand les modèles sont comparés l'un à l'autre. 3D Geomodeller utilise la méthode de modélisation implicite 'champ potentiel' et a pu produire automatiquement la série de modèles avec moins de préjugé géologique soit introduit par l'opérateur. La méthode implicite nous a rendus confiants que les différences trouvées entre les modèles étaient celles dues à des mesures d'orientation perturbées et non aux interprétations particulières ou à une opinion personnelle concernant les éléments géologiques. L'incertitude associée aux différentes régions d'un modèle géologique peut être localisée, quantifiée et visualisée par l'analyse de la grille d'incertitude. Cette forme d'analyse de l'incertitude a donné une méthode utile pour évaluer la fiabilité du modèle. Dans le Chapitre 1, la méthode est testée sur un cadre géologique naturel dans le Bassin de Gippsland, dans le sud-est de l'Australie, où des surfaces géologiques modélisées ont été évaluées pour l'incertitude. Le modèle du Bassin de Gippsland a été construit en intégrant les mesures de géologie de champ et l'interprétation géophysique. Les données sur site ont été relevées sous la forme d'observations d'orientation et de cartographie des affleurements à partir du littoral, alors que la plupart du modèle est situé au large, nécessitant une interprétation géophysique basée sur des données aéromagnétiques, gravimétriques et sismiques. Les données de forage n'ont pas été utilisées directement mais ont été intégrées dans l'étude en tant que cartes d'isopaques. Toutes les données utilisées dans cette étude ont été fournies par GeoScience Victoria, cependant une grande partie des données n'était pas en état pour les entrer. La préparation des données a formé un élément significatif de la construction du modèle et est décrite en détail dans le Chapitre 1.

Le concept de variabilité stratigraphique a été introduit et une analyse des données entrées a été faite visuellement. D'autres méthodes de visualisation de l'incertitude offertes par la littérature ont été discutées parallèlement à la méthode choisie dans ce chapitre. La visualisation d'incertitude par la variabilité stratigraphique a été conçue pour communiquer le concept complexe de l'incertitude du modèle 3D aux géoscientifiques d'une manière effective.

Un test a été conduit pour déterminer si l'incertitude du modèle était sensible à une information

additionnelle. Le raisonnement derrière l'accomplissement de ce test était que nous voulions déterminer si de l'information supplémentaire (entrée de données) pouvait réduire l'incertitude, et si c'était le cas, si la grille d'incertitude pouvait être utilisée comme guide pour une future exploration. Le test a été fait en produisant deux séries de modèles, l'une utilisant deux sections sismiques perpendiculaires l'une à l'autre, l'autre utilisant seulement une des sections sismiques. La quantité d'incertitude associée à chaque série de modèles a été calculée comme un volume, similairement aux pratiques d'estimation de ressource. Des seuils d'incertitude haut, moyen et bas ont été établis et les volumes calculés pour la section sismique simple et la série de modèles à deux sections sismiques. L'incertitude globale a été réduite dans la série de modèles à deux sections sismiques à partir de la série de modèles à section simple. Les cartes d'incertitude ont révélé que la plupart de l'incertitude était réduite vers l'emplacement de la section supplémentaire, soutenant ainsi l'efficacité de la détection d'incertitude pour guider la planification.

L'incertitude dans certains sites modèles spécifiques a été identifiée et attribuée aux désaccords possibles entre les données sismiques et isopaches. Des améliorations supplémentaires et des sources de données additionnelles ont été proposées sur la base de cette information. Finalement, une méthode d'introduction de valeurs de variabilité stratigraphique comme contraintes géologiques pour une inversion géophysique a été présentée.

Sommaire du Chapitre 2

Le chapitre 2 commence par examiner la nature interprétative de la compréhension géologique en utilisant le cercle herméneutique. Une compréhension complète de toutes les parties du problème géologique peut seulement être atteinte en comprenant comment elles sont liées au problème dans son ensemble, et la compréhension du problème dans son ensemble ne peut être atteinte que par la compréhension de ses parties. La compréhension qu'un géologue a de ces parties est guidée par son éducation, ses préconceptions et théories qui sont nécessaires pour comprendre les problèmes souvent complexes présentés par une image géophysique ou un affleurement rocheux. Très peu de compréhension géologique peut être obtenue sans interprétation. Toutes les disciplines géologiques demandent une interprétation puisqu'il est nécessaire de faire des reconstructions géodynamiques, construire des modèles de dépôt de minerai ou recréer l'histoire d'une éruption volcanique. Arriver à une réponse interprétative réclame aussi une certaine 'voyance', ou une préconception de la réponse, autrement aucune réponse ne sera jamais obtenue, puisque plusieurs sont souvent possibles. L'équipement géoscientifique (boussole d'orientation, loupe de géologue, spectromètre de masse ICP-MS) a été conçu pour mesurer les phénomènes géologiques considérés comme pertinents aux problèmes géologiques. Les techniques et pratiques d'utilisation de ces équipements ont été formées au cours des années par des praticiens et réclament une interprétation individuelle. La nécessité d'avoir une interprétation veut dire que plus d'une réponse existe pour chaque problème géologique, bien qu'il soit commun de ne jamais en offrir qu'une seule. Notre argument est que les techniques analytiques développées dans cette recherche adressent le problème de la solution unique en offrant une évaluation des possibilités géologiques.

Le chapitre 2 discute des implications de l'incertitude concernant la géométrie des éléments géologiques au sein d'un modèle. Des pratiques de cet ordre vont probablement résulter en un mo-

dèle qui ne représente pas de façon adéquate la géologie ciblée. L'incertitude due à l'intégration et l'interprétation des données a été réexaminée et étendue pour modéliser les explorations spatiales. L'espace modèle a été défini comme une région qui contient toutes les réalisations possibles des possibilités géologiques qui sont offertes par l'ensemble de données plus le modèle qui représente le mieux le monde naturel. Cette incertitude existe à l'intérieur de la série de modèles, la géométrie des éléments géologiques doit aussi être incertaine et varier entre les modèles. Le but du Chapitre 2 était d'identifier quels modèles étaient les 'membres extrêmes' en termes d'attributs géométriques de façon à définir les limites de possibilité géologique.

L'exploration de l'espace modélisé requiert un moyen de comparer et contraster les modèles. Une série de paramètres géométriques ou de 'géodiversité' ont été développés pour mesurer les différents attributs des éléments géologiques dans le Bassin du Gippsland. Comme dans le Chapitre 1, les données entrées ont été soumises à une simulation d'incertitude et une série de modèles a été créée pour former la série de modèles. La série de modèles résultante présente toute une gamme d'architecture géologique qui peut être mesurée en utilisant des paramètres de géodiversité. Diverses relations géométriques (profondeur, volume, surface de contact, courbure et complexité géologique) sont utilisées pour décrire la gamme de possibilités exhibées dans toute la série de modèles. Les modèles de membres extrêmes pour chaque paramètre de géodiversité sont classifiés d'une manière similaire aux descriptions taxonomiques.

Les résultats pour chaque paramètre de géodiversité ont été obtenus en utilisant des scripts écrits en Matlab®. Chaque modèle a été converti en un voxet (une collection de voxels, ou pixels volumétriques) pour permettre le calcul des paramètres. Le paramètre de profondeur détermine l'étendue du moins profond au plus profond pour chaque unité stratigraphique au sein du modèle. Chaque modèle est comparé aux autres pour déterminer le membre extrême le plus profond et le moins profond qui sont représentatifs de chaque lithologie. Le volume est calculé en faisant un compte de voxels de chaque unité stratigraphique à l'intérieur de la série de modèles. Les modèles montrant les volumes les plus grands et les plus petits pour chaque unité stratigraphique sont identifiés comme membres extrêmes représentatifs. La courbure est calculée sur les contacts des unités stratigraphiques. La courbure moyenne détermine la géométrie synforme ou antiforme. La courbure Gaussienne, combinée à la courbure moyenne, détermine si les contacts démontrent une géométrie de dôme/bassin ou de col. Les relations de voisinage à courte distance déterminent combien d'unités stratigraphiques différentes entourent un point d'intérêt donné. Un nombre croissant d'unités stratigraphiques différentes entourant un point donné reflète une plus grande complexité géologique. Finalement, un paramètre qui mesure les relations de contact et la surface associée a été développé. De plus, la gamme de relations de contact dans toute la série de modèles peut être déterminée.

L'analyse des membres extrêmes a fourni des informations utiles pour plus de modélisation d'inversion géophysique. Les volumes peuvent être utilisés pour s'assurer que les unités géologiques n'excèdent pas une taille spécifique et les profondeurs peuvent être utilisées pour s'assurer que les unités géologiques sont limitées dans l'espace. Les mesures de courbure peuvent limiter la quantité de déformation qu'une surface montre au sein du modèle. L'utilisation d'une combinaison de valeurs de voisinage à courte distance et de surfaces de contact peut apporter des contraintes

puissantes aux marges des unités géologiques, assurant ainsi que les relations géologiques et la connectivité sont gardées.

L'analyse des membres extrêmes classe chaque unité stratigraphique de chaque modèle pour chaque paramètre de géodiversité au sein de la série de modèles. Les résultats du Chapitre 2 ont montré qu'aucun modèle n'était présenté systématiquement en tant que membre extrême représentatif. De plus, l'analyse de ces données s'est révélée difficile et la découverte de toutes les tendances conduisant à une identification d'un paramètre influent a été impossible à réaliser avec certitude. Une technique statistique a donc été requise dans l'analyse simultanée de tous les paramètres de géodiversité pour identifier si aucun de ces membres extrêmes n'était différent de manière significative du modèle initial. L'Analyse en Composantes Principales (PCA) a été choisie pour réaliser cette tâche. La PCA est capable de déterminer quels paramètres ont une incidence sur la description de la variabilité entre modèles. Grâce à l'identification des paramètres qui sont les plus influents, les modèles peuvent être comparés quand les résultats de tous les paramètres de géodiversité sont pris en considération. Les modèles géométriquement similaires forment le barycentre du modèle spatial, et les modèles divers (les 'cas isolés') forment les limites.

Des résultats significatifs ont été obtenus. Le volume d'une unité stratigraphique formant le socle s'est révélé comme étant le plus influent dans la production de variabilité géométrique entre les modèles. Intuitivement, le résultat semble logique, puisque tout changement géométrique de cette unité profonde affecterait les unités qui la recouvrent. La définition des limites du modèle a trouvé que le modèle initial n'était pas l'un des modèles les plus courant géométriquement. Le modèle initial s'est trouvé être le onzième plus commun, ce qui veut dire que dix autres modèles contiennent une architecture géologique plus typique. L'implication est que la production d'un modèle unique, comme il serait fait normalement, ignore les dix autres modèles qui pourraient mieux représenter la géologie de la zone étudiée. Il est recommandé que les pratiques qui produisent des réalisations géologiques multiples, telles que celles présentées dans cette recherche, soient adoptées dans la communauté de la modélisation.

Sommaire du Chapitre 3

Le Chapitre 3 étend le concept de géodiversité dans le domaine géophysique. La modélisation géophysique 3D est communément utilisée pour valider les modèles par rapport au monde naturel par l'utilisation de la modélisation prédictive. Il était donc important d'inclure les techniques de modélisation prédictive géophysique 3D dans le groupe de paramètres de géodiversité. La modélisation prédictive 3D compare deux séries de données géophysiques, la réponse observée et la réponse calculée, produisant une valeur inadéquate qui représente le niveau d'accord entre les séries de données. La 'réponse observée' représente le monde naturel et était une série de données de gravité Air Libre obtenues du Bureau Gravimétrique International (BGI). La réponse calculée l'a été à partir du modèle 3D. La combinaison de forme, profondeur et dimension de toutes les unités stratigraphiques et les propriétés pétrophysiques assignées produisent la réponse calculée.

Le Chapitre 3 introduit de nouveau le concept d'incertitude dans la modélisation 3D, en se concentrant cette fois-ci sur la manière dont les décisions sont prises concernant le traitement et le filtrage des données entrées, ce qui peut affecter dramatiquement la réponse calculée d'un modèle 3D.

Malheureusement, ces décisions sont toujours prises sans une connaissance complète du système en cours d'étude. Cela résulte régulièrement, voire toujours, en une représentation déformée des phénomènes naturels par le modèle. Cette représentation déformée des phénomènes naturels peut être attribuée à l'incertitude inhérente au processus de modélisation. L'incertitude est inévitable en modélisation géologique du fait qu'une connaissance complète du système naturel est impossible, bien que nous utilisions de nombreuses techniques pour en réduire la quantité introduite par le traitement, la modélisation prédictive est l'une de ces techniques. Malheureusement, les données géophysiques sont ambiguës et fournissent une solution qui n'est pas unique. Théoriquement, différentes géométries de modèle peuvent produire la même réponse géophysique.

Ce chapitre propose et teste un procédé dans lequel la série de modèles entière à été soumise à une modélisation prédictive géophysique 3D, facilitant ainsi une exploration étendue de l'espace géologique modélisé. Comme dans le chapitre précédent, toutes les mesures de géodiversité ont été combinées dans une analyse multivariée qui a révélé les relations les entre paramètres et défini les limites de possibilité géologique. Le Chapitre 3 examine la Ceinture Ashanti Greenstone, au sud-ouest du Ghana en Afrique de l'Ouest en tant qu'étude de cas pour évaluer l'efficacité de la technique. Des propositions d'étude plus approfondie ont été faites et certains aspects de l'espace modélisé ont été identifiés comme pouvant présenter un intérêt pour l'exploration aurifère.

La Ceinture Ashanti Greenstone est une des ceintures orientées vers le nord-est de roches vertes-granitoïdes à l'intérieur du craton Archéen/Paléoprotérozoïque Leo-Man. Les gisements aurifères allant de vaste à classe mondiale situés dans la Ceinture Ashanti Greenstone sont Obuasi, Tarkwa, Bogoso/Prestia et Damang. Le socle paléoprotérozoïque du sud-ouest du Ghana est formé du Supergroupe Birimien qui est recouvert par le Groupe du Tarkwaien. Deux périodes distinctes d'activité orogénique ont produit les granitoïdes de l'âge éburnéen tonalite-trondhjémite-granodiorite (TTG) avec des granitoïdes granodioritiques, dioritiques et gabbroïques principalement au sud (2180-2150 Ma) et des granitoïdes de l'âge éburnéen (2130-2070 Ma). La minéralisation hydrothermale de l'or a été associée à la Faille d'Ashanti et à d'autres zones de cisaillement majeures. Les gisements d'or alluvial sont associés au contact entre les unités du Birimien et du Tarkwaien.

Des observations sur le terrain préexistantes et des cartes d'affleurement ont été utilisées en combinaison avec les données collectées par Stéphane Perrouty (UPS/IRD) pour générer le modèle initial. Les données de terrain ont inclus des observations structuralles et pétrophysiques de mesures calculées à partir d'échantillons rocheux. L'interprétation géophysique faite par Perrouty était contrainte par l'utilisation de données pétrophysiques, et aidée par les observations sur le terrain. Une couche épaisse latéritique et/ou saprolitique couvre les parties les plus accessibles à l'intérieur de la région, ce qui restreint l'accès à l'affleurement protérozoïque. Par conséquent, une interprétation géophysique de la plupart de la région était nécessaire pour comprendre la géologie entre les zones d'affleurement.

Chaque mesure de réponse géophysique incluse dans la collecte de paramètres de géodiversité a été décrite. Quelques paramètres géophysiques sont des techniques 'couplées', ainsi nommées parce que la comparaison a été faite en paires entre la réponse observée et celle calculée. Les techniques couplées incluent le coefficient de corrélation 2D, la valeur quadratique moyenne (RMS) et la

distance de Hausdorff. Les techniques d'"écart-type' et d'entropie sont typiques des techniques d'analyse d'images non-couplées. La technique d'écart type a été utilisée sur les grilles calculées, la technique de l'entropie a été utilisée sur les grilles résiduelles.

Les résultats obtenus à partir de cette étude montrent que globalement les valeurs déformées RMS sont raisonnablement élevées pour ce type d'étude. Évidemment, on espèrerait des valeurs légèrement plus basses, mais l'amplitude n'est pas assez élevée pour rejeter catégoriquement le modèle géologique. L'analyse des modèles de la valeur quadratique RMS minimum et maximum des membres extrêmes démontre que la plus grande variation d'amplitude déformée se trouve au centre et sur les bords du Bassin du Tarkwaien. Les anomalies de plus grande amplitude semblent concentrées au nord-ouest et au sud-est, mais paraissent élevées dans toutes les grilles résiduelles du modèle. Une raison possible pour cela est que la gravité dans ces zones réponde à des structures plus profondes de l'âge Birimien qui ne sont pas inclues dans le modèle. Le manque de structures modélisées importantes s'est reflété par la suite dans les valeurs déformées relativement élevées. Le résidu observé dans le Tarkwaien n'était pas aussi sévère que ce qui était vu dans les régions nord-ouest et sud-est de la carte, et la géologie modélisée semblait bien correspondre aux données de gravité.

Les paramètres géophysiques ont fourni des méthodes additionnelles de calcul de la déformation entre les grilles calculées et observées. La reconnaissance de tracés de la distance de Hausdorff a offert une technique d'accompagnement utile aux calculs de déformation RMS typiques. La distance de Hausdorff pourrait être une inclusion pour des études futures en raison de sa capacité à détecter les schémas dans les réponses observées qui peuvent exister dans les réponses calculées. L'entropie peut être une technique d'accompagnement utile à associer avec les valeurs RMS. Une RMS basse ne décrit pas toujours la variabilité des valeurs déformées à l'intérieur d'une grille, alors que l'entropie donne une image assez grossière. Une valeur RMS basse rapportée avec une valeur d'entropie élevée représente une image avec une déformation globalement basse mais criblée d'anomalies de grande amplitude. Le choix d'un modèle pour un traitement ultérieur simplement parce qu'il a une RMS basse sans considérer l'entropie correspondante, peut se révéler problématique si des anomalies de grande amplitude sont présentes.

L'Analyse de Composant Principal (PCA) a été faite sur la série de modèles de la ceinture Ashanti Greenstone en utilisant la collecte étendue de paramètres de géodiversité. Deux découvertes principales ont été discutées. La première est que les paramètres de RMS, d'écart type, d'entropie (géophysique) et de complexité (géométrique) contribuent les plus hauts degrés de variabilité géologique de la série de modèles. L'hypothèse originellement déclarée que le volume des formations du socle pourrait expliquer la plupart de la variabilité de la série de modèles s'est révélée fausse. La variabilité en complexité géologique du contact entre les formations du Tarkawaien et du Birimien semble expliquer le mieux la variabilité de la série de modèles, et est aussi étroitement liée à la déformation géophysique. La seconde découverte est que le modèle initial, encore une fois, n'est pas l'exemple le plus commun de possibilité géologique à l'intérieur de la série de modèles. 13 autres modèles sont considérés comme étant plus similaires que le modèle initial. Ceci corrobore des résultats similaires du chapitre précédent qui utilise les paramètres PCA et de géodiversité dans la

série de modèles du Bassin de Gippsland.

La PCA a révélé que la réponse géophysique était associée à un phénomène géométrique. Une future investigation de l'espace modélisé au moyen de l'inversion géophysique peut être simplifiée par l'identification de modèles et d'éléments qui devraient être analysés. Un candidat à l'inversion géométrique a été déterminé comme étant la surface de contact du Tarkwaien/Birimien. Des entrées de modélisation multiples sélectionnées avec la PCA devraient être faites sur le barycentre et les modèles de cas isolés. Le processus d'inversion peut se concentrer sur les éléments de modèle déterminés par la PCA et la géodiversité comme étant importants dans l'obtention d'un modèle qui respecte les données géologiques et géophysiques. Les résultats des Chapitres 2 et 3 soutiennent la conclusion que la production d'un simple résultat dans un exercice de modélisation ignore les autres modèles qui sont probablement plus à même de représenter le monde naturel.

Sommaire du Chapitre 4

Le Chapitre 4 a combiné toutes les techniques décrites dans les Chapitres 1, 2 et 3 pour présenter un plan de travail de modélisation qui a culminé avec l'inversion géophysique. Le but du Chapitre 4 est double : (1) exposer une méthode qui réduise le nombre de décisions subjectives prises lors de la conduite d'une inversion et (2) inclure plus d'informations géologiques dans les procédures d'inversion. Le Chapitre 4 s'est concentré sur la nature subjective de l'inversion. La subjectivité a été identifiée comme existant dans trois domaines : restriction à un modèle d'entrée unique, sélection des paramètres d'inversion et sélection des entrées. Permettre seulement un modèle d'entrée unique restreint l'algorithme d'inversion à une représentation du monde naturel qui contient les connaissances fondamentales, l'expertise et les préjugés inhérents de l'opérateur. De nombreux paramètres d'entrée offerts par les ensembles d'inversion servent à restreindre et enlever les solutions infaisables de la modélisation d'inversion. Les valeurs de paramètres sont conçues pour restreindre les modifications géologiques et géophysiques opérées pendant l'inversion. Les valeurs de paramètres sont souvent considérées comme des substituts pour la confiance que l'opérateur a dans le modèle et tendent à être choisies arbitrairement. Les éléments du modèle qui sont entrés dans l'inversion sont choisis selon leur importance perçue en rapport à l'architecture du monde naturel. Les choix tels que ceux-ci sont typiquement bien considérés, mais sont quand même subjectifs et souvent faits sans effort de production de preuves quantitatives fiables.

Le développement de mesures d'incertitude quantitative et la capacité à catégoriser l'espace modélisé en utilisant la géodiversité aborde la question de la subjectivité de l'inversion. Une étude détaillée de série de modèles de la ceinture Ashanti Greenstone qui a été faite analyse le lien entre l'incertitude, la géodiversité et les résultats de la modélisation de l'inversion géophysique. De hauts niveaux d'incertitude étaient associés aux éléments de modélisation de la Série du Birimien précoce du contact avec la Série du Tarkwaien. Les paramètres de géodiversité soutiennent l'évaluation d'incertitude par la découverte que la signature gravimetrique de chaque modèle correspondait fortement à la variation entre les modèles. L'inversion a été subséquemment conduite sur le socle de la Série du Tarkwaien dans une inversion 'style-socle', où la géométrie et les propriétés rocheuses (par ex. la densité) ont été modifiées itérativement. L'analyse des membres extrêmes et la PCA des paramètres de géodiversité ont guidé le choix des valeurs de paramètre utilisées dans l'inversion,

tout en aidant aussi à l'évaluation des résultats de l'inversion pour une faisabilité géologique. La PCA a défini quels modèles étaient les plus divers et les plus communs. Les trois modèles divers et communs classés le plus haut (six en tout) ont été attribués à la modélisation de l'inversion.
Une corrélation entre les résultats de l'inversion et l'incertitude a été découverte. Il semble que l'algorithme de l'inversion essaie naturellement de modifier les régions du modèle qui sont à la fois géologiquement et géophysiquement ambiguës. De plus, les différences entre les résultats obtenus de chacune des inversions semblent être liés à l'incertitude. Les résultats ont été évalués comme géologiquement faisables, apportant de l'information nouvelle sur la Ceinture Ashanti Greenstone. La procédure décrite au Chapitre 4 a fourni un moyen de réduire certaines des décisions subjectives, inclure plus de données géologiques dans la modélisation de l'inversion et produire des résultats géologiques raisonnables.

Sommaire des publications et congrès

Le Chapitre 1 a été publié dans Tectonophysics.

Lindsay, M. D., Aillères, L., Jessell, M. W., de Kemp, E. A., and Betts, P. G., 2012, Locating and quantifying geological uncertainty in three-dimensional models: Analysis of the Gippsland Basin, southeastern Australia: Tectonophysics, v. 546–547, no. 0, p. 10-27.

Le manuscrit du Chapitre 2 a été soumis à Tectonophysics (19 Juin, 2012) et est actuellement en cours d'évaluation. Le Chapitre 3 sera préparé pour être soumis à Physics of the Earth and Planetary Interiors après que la thèse a été présentée. Le Chapitre 4 sera préparé pour être soumis après que la thèse a été présentée, la décision d'un journal approprié n'a pas encore été prise.

Cinq sommaires détaillés soumis à référence ont été produits à partir de la recherche.

Lindsay, M., Perrouty, S., Jessell, M., Aillères, L., De Kemp, E. and Betts, P.G. (2011) Categorising features of geological terranes with geodiversity metrics: Enhancing exploration of multiple geological models, in Sustaining Our Future: Understanding and Living with Uncertainty, proceedings of MODSIM2011 meeting, Perth, WA, Australia, December 12 – 16, 2011.

Lindsay, M., Ailleres, L., Jessell, M. W., De Kemp, E. A., and Betts, P.G. (2010) Integrating geological uncertainty into combined geological and potential field inversions. In proceedings of GeoMod2010 - University of Lisbon, Lisbon, Portugal, September 27 – 29, 2010.

Ailleres, L., **Lindsay, M.**, Jessell, M., deKemp E., 2010. Can geological uncertainty help reduce potential field ambiguity during inversion modelling? In Young, D., Brown, C., and Seimon, J.(eds) "Geo-computing 2010", Australian Institute of Geoscientists Bulletin, 51, pp. 1-6.

Ailleres, L., **Lindsay, M.**, Jessell, M., deKemp, E., 2010. The role of geological uncertainty in developing combined geological and potential field inversions. ASEG-PESA 21st International Geophysical Conference and Exhibition, Sydney, Aug. 2010. 4p.

Lindsay, M., Aillères, L., Jessell, M. and De Kemp, E. (2009) Improving current potential field inversion techniques: Determining geological uncertainty in implicit modelling applications, in Smart Science for Exploration and Mining: proceedings of the Tenth Biennial Society for Geology Applied to Mineral Deposits Meeting, Townsville, Australia, 17th – 20th August 2009.

Cette recherche a été présentée par l'auteur aux événements suivants :

2009

Dixième Rencontre Biannuelle de Société pour la Géologie Appliquée aux Gisements Minéraux, Townsville, Australie - Poster

Conférence des Universités Victoriennes sur la Science de l'Environnement et de la Terre, Monash University, Melbourne, Australie - Oral

Rencontre des utilisateurs de Geomodeller, Brighton, Australie – Oral

2010

Présentation de Confirmation, Monash University, Melbourne, Australie - Oral

GeoMod2010, Lisbonne, Portugal - Poster

Rencontre Européenne des utilisateurs de Geomodeller, Orléans, France – Oral

Séminaire à l'heure du déjeuner donné à LMTG/GET, Toulouse, France – Oral

2011

Journée des doctorants, GET, Toulouse, France - Oral

Séminaire à l'heure du déjeuner donné à l'École de Géosciences, Monash University, Melbourne, Australie – Oral

Symposium de Mining IQ, Perth, Australie – Oral

Rencontre des utilisateurs de Geomodeller, Brighton, Australie – Oral

ModSim 2011, Perth, Australie – Oral

2012

Rencontre du Groupe de Spécialistes en Tectonique et Géologie Structurelle, Atelier de Modélisation, Monash University, Melbourne, Australie – Oral

Rencontre du Groupe de Spécialistes en Tectonique et Géologie Structurelle, Waratah Bay, Australie – Oral

Congrès Géologique International, Brisbane, Australie - – Oral x2

Introduction

A summary of methods, techniques and issues commonly associated with the construction of three-dimensional geological models

1. Summary

The use of computer-generated three-dimensional (3D) models of geology is an established practice in geosciences, greatly improving our understanding of the geologic mechanisms leading to the formation of sub-surface architecture (Mallet, 1992; Mallet, 2002). There has been slow acceptance of the 3D models by the geoscientific community beyond the hydrocarbon industry (Xue et al., 2004; Kaufmann and Martin, 2008).

3D modelling techniques have been enhanced by improving computing technologies in personal computers, for example, multiple CPUs, large amounts of RAM and powerful 3D graphic cards with multiple GPUs. This has allowed larger datasets to be used and speed of processing increased. A concurrent improvement and availability of specialised software has made 3D modelling more accessible to a wider user base, where GUIs and data interoperability present a user-friendly modelling environment in packages such as Gocad and Geomodeller (Jessell, 2001; Joly et al., 2008; Smirnoff et al., 2008). Complementing these advances are improved geophysical surveying technologies that have led to further enhancement of important information employed in developing 3D geological models (Jessell, 2001; Joly et al., 2008). Overall, it seems that the technologies supplying information to and facilitating the modelling process are continuously improving. Indeed, the information gained from studying these models could benefit many facets of the geoscientific community, from minerals exploration (Fullagar et al., 2004; Strykowski et al., 2005; Murphy et al., 2006; Rawling et al., 2006; Feltrin et al., 2009) to environmental applications (Marinoni, 2003; Wycisk, 2009). So why are there only a small number of practitioners outside of the hydrocarbon industry? Clearly, there must be outstanding concerns regarding the usability and usefulness of 3D models from the majority of geoscientists.

In general, 3D models are built using a combination of traditional geological data, such as geological maps, drill-core logs, cross-section interpretations and geophysical information, such as gravity and magnetic data (Martelet et al., 2004). Geological maps provide information on how geological structures observed at the surface may extend to within the subsurface. Deciding what geometry these structures exhibit is augmented and constrained by both drill-core logs

and cross-section interpretations. All mapping techniques that provide data to the modelling process are open to interpretation and often require it (Frodeman, 1995). 3D geological model building techniques rely on subjective interpretations and predictions based on limited observations of the Earth's properties. All 3D models contain a degree of uncertainty. The source of uncertainty in geological modelling can be grouped into three categories (Cox Jr, 1982; Mann, 1993; Davis, 2002; Bond et al., 2010; Wellmann et al., 2010).

Type 1 uncertainty relates to data imprecision, error and bias. Field measurements taken by different geologists can vary, not due to a lack of skill or training, but simply because some of these observations can be quite difficult to identify and measure (Thore et al., 2002; Jones et al., 2004; Gallerini and De Donatis, 2009). Type 1 uncertainty also encompasses data sub-sampling. An abundance of data collected from a small area, such as a mine, is usually required to be sub-sampled and reduced to representative points for input into a modelling package (Putz et al., 2006). This is typical when regional scale model is being built from data collected at the local scale. Type 2 uncertainty relates to predictability and intrinsic randomness. A lack of outcrop, inconsistent or sparse measurement of rock properties and a lack of 3D information (such as how far particular rocks may extend at depth) require interpolation to represent an entire geological structure (Aitken and Betts, 2008; Maxelon et al., 2009; Zanchi et al., 2009). Type 3 uncertainty relates to a lack of knowledge. A model may not contain structures that do exist in the natural world, such as lithologies, folds, faults or shear zones that may significantly affect model topology.

The combination of these effects can create model uncertainty and possibly result in spurious model geometry and discrete regions where geological architecture is not well understood. Removing uncertainty from 3D models would be the ultimate aim, but this could only be achieved by employing the unrealistic proposition of physically observing the entire target region. A more realistic option would be to mitigate the effects of uncertainty by developing a measure of influence. Uncertainty will always be present due to the nature of 3D modelling and the problem of sparse measurements, so quantitative determination of uncertainty can assist the generation and application of 3D models. The benefits of determining uncertainty in this manner are twofold: (1) regions displaying high levels of uncertainty can be delineated and used to guide where further geological data collection and interpretive work should be conducted and (2) uncertainty values can be used as a gauge when assessing models to guide operator confidence.

The potential for 3D models to benefit geosciences is high, but the process of model-building is complex. Therefore, a detailed examination of the critical aspects of the 3D model building process is provided. The various data types used to create and correct 3D models are examined, followed by a discussion of the software packages and styles of modelling that allow the operator to integrate and process input data, including the geophysical inversion process. Finally, characteristics of the modelling process are reviewed to describe methods that have been developed to determine, mitigate or exploit uncertainty.

2. Data types

There are challenges inherent to any geological study. Collected data is multi-variate and is often under-sampled to adequately represent the possible variables (Davis, 2002). Developing an understanding of the possible complex geometrical structures that can be interpreted from geology can be difficult. This is compounded when geological observations leading to the development of architectural interpretations are sparse. Interpolating what structures may exist between geological observation points is significantly assisted when used in conjunction with geophysical datasets, but major assumptions and considerations need to be made before this can be achieved. Studies by de Kemp (2000), Fullagar et al. (2004), Joly et al. (2007; 2008), Frank et al. (2007), Aitken et al. (2008), Calcagno et al. (2008), Guillen et al. (2008) and Maxelon et al. (2009) exemplify this by attempting to explain previously poorly-understood 3D geological problems using computational analytical techniques. The focus and scale of these studies varies considerably, from reconstructing a deformation history (Aitken and Betts, 2008; Maxelon et al., 2009) to developing an understanding of the relationship of a shear zone to magmatic events and intrusive geometries (Joly et al., 2007; Joly et al., 2008) or better defining the depth of an Pb/Zn ore-body at the mine scale (Fullagar et al., 2004). By no means do these studies define the extent geomodelling can be applied, but all display a common reliance on particular geological and geophysical data types from which models are generated. This section introduces the different types of data used in geomodelling, their strengths and weaknesses and how they are employed in constructing 3D models and interpretations.

2.1 Geological Data

Geological data provides the foundation for any study that aims to develop a 3D understanding of sub-surface architecture. Drill-core and field measurements are advantageous as the observations can directly augment the conceptual 3D model within the geologist's mind and be added to a structural map without requiring computer processing, as is the case with geophysical measurements.

Geological data often provides the only basis from which a 3D geological model can be made, especially in cases where geophysical data lacks appropriate controls (for example, petrophysical constraints or high quality data collection and processing) (Maxelon et al., 2009). Some contributions geological data makes toward the 3D model entails identifying structural constraints (such as kinematic and geometric indicators), identifying stratigraphy and outcropping lithological boundaries, and the composition of different lithologies gathered from petrology. 3D models can be constructed without the use of potential field geophysical data. Examples of these types of studies include de Kemp (2000), Dumont et al (2008) and Zanchi et al. (2009). These studies do not rely on geophysics to constrain or complement the geological data, either as the geophysical data may not be available or of sufficient quality (de Kemp, 2000) or the suite of available geophysical measurements are thought to be unreliable (Maxelon et al., 2009).

The French (Dumont et al., 2008) and Italian Alps (Zanchi et al., 2009) provide excellent study areas to produce 3D models as relatively abundant outcrop allows a rare view to large areas of geological outcrop. The Dauphiné zone in the Western French Alps hosts spectacular poly-deformed outcrop in the hanging-wall of the La Garde thrust in addition to extensive historical structural data supplied by many previous studies (Dumont et al., 2008). The same can be said for the Zanchi et al. (2009) study where outcrop allows the direct observation of the structures being modelled. The most pressing concern seems to be management of the abundant data available to the authors and integrating it into the model, a theme which is either discussed in or the focus of other recent papers (Putz et al., 2006; Joly et al., 2008; Gallerini and De Donatis, 2009; Howard et al., 2009; Maxelon et al., 2009).

The perceived positive properties of geological data can lead to potential issues. Models that have been constructed using the benefit of geological data to constrain geophysical inter-

pretation can be assumed to be more robust than those that have relied purely on information derived from potential field data (Schmidt and McDougall, 1977; Martelet et al., 2004; Aitken et al., 2008; Stewart and Betts, 2010). Geological measurements constrain geophysical interpretation by reducing the number of possible solutions offered by the ambiguous geophysical data. Unfortunately, the 3D modeller often does not collect all the geological or geophysical data, nor is able to perform extensive quality assurance unless supplied with the data. Howard et al. (2009) suggests an organisational framework based on work done by the British Geological Survey to address these deficiencies. Historical data will often still lacks measures of confidence or quality even if these changes were adopted by multiple organisations, so the 3D modeller is left assuming (and hoping) that input data is high quality.

Another source of ambiguity contained within geological data is the geologist's interpretation of the terrane. The stratigraphic, fault-fault, faults-folds and faults-stratigraphy relationships determined by the geologist fundamentally control the resulting 3D model topology. Measurements taken from a particular stratigraphic unit are assigned to a conceptual container that has relationships (such as relative age and deformation history) with other geological units. Structures inferred or measured within this unit are also subjected to the relationships interpreted by the geologist. All efforts are made to ensure that interpretations are scientifically valid, but new information can come to hand that produces a different viewpoint. Tectonic evolutions of an area are constantly being revised or changed, and there are usually at least two different geological interpretations for the area (for example, the differing evolutionary views of Broken Hill as a nappe fold sequence (Marjoribanks et al., 1980) or a fold and thrust belt (White et al., 1995). Geological data therefore relies heavily on the interpretive skills of the geologist and also subject to ambiguity (Frodeman, 1995).

It is clear that ambiguity inherent in geological data is difficult to account for, especially when only sparse data is available. For this reason, the assumption that geological data is a more reliable source of information than geophysical information is flawed. These aspects should be considered when assessing a 3D model for further use practical applications such as geophysical inversions, engineering surveys or exploration programs.

2.2 Geophysical Data

Not all study areas are blessed with the same quality and quantity of outcrop as the French and Italian Alps. In covered terranes, such as those typical to Australia, outcrop is often very difficult to find or too weathered to take appropriate structural measurements. Many studies that attempt to resolve sub-surface architecture in covered terranes (Betts et al., 2003; McLean and Betts, 2003; Strykowski et al., 2005; Rawling et al., 2006; Aitken and Betts, 2008; Aitken et al., 2008; Edmiston et al., 2008; Williams et al., 2009) have required the use of geophysics to provide much of the data from which geological interpretations can be made. Scattered or sparse field observations can be incorporated into larger-scale interpretive exercises when correlated with geophysical data, providing a powerful platform from which regional geological studies can be conducted (Gunn et al., 1997; Betts et al., 2007).

There are several geophysical techniques that can be employed to develop 3D models. Seismic reflection datasets are used to provide cross-section views of the study area, developing a relationship between different structures and stratigraphic layers (Strykowski et al., 2005; Susini and De Donatis, 2009). Electrical methods, such as induced polarisation (IP) and DC resistivity are effective at detecting geological boundaries, such as faults and lithological contacts, and are used extensively in minerals exploration (Oldenburg et al., 1997; Meju, 2002; Wijns and Kowalczyk, 2007). A common practice is the use of gravity or magnetics in 'basement' terranes (Jessell, 2001), often in combination, to identify geological structures. An increase in the amount of high-resolution data from both gravity and magnetic surveys has promoted their use in many research studies in addition to powerful image processing techniques that can emphasise different petrophysical properties. By producing a variety of maps using these image processing techniques, diverse observations can be made to aid interpretation (Figure 1) (Morozov et al. (2009), Luyendyk (1997); Milligan & Gunn (1997) and Aitken et al. (2008) and references therein).

2.2.1 Gravity and magnetic surveys

Gravity datasets exploit the density contrast between different lithologies to aid geophysical interpretation. The gravity survey technique measures the spatial variation of gravitational acceleration over a discrete point on the Earth's surface, inferring density contrasts of the

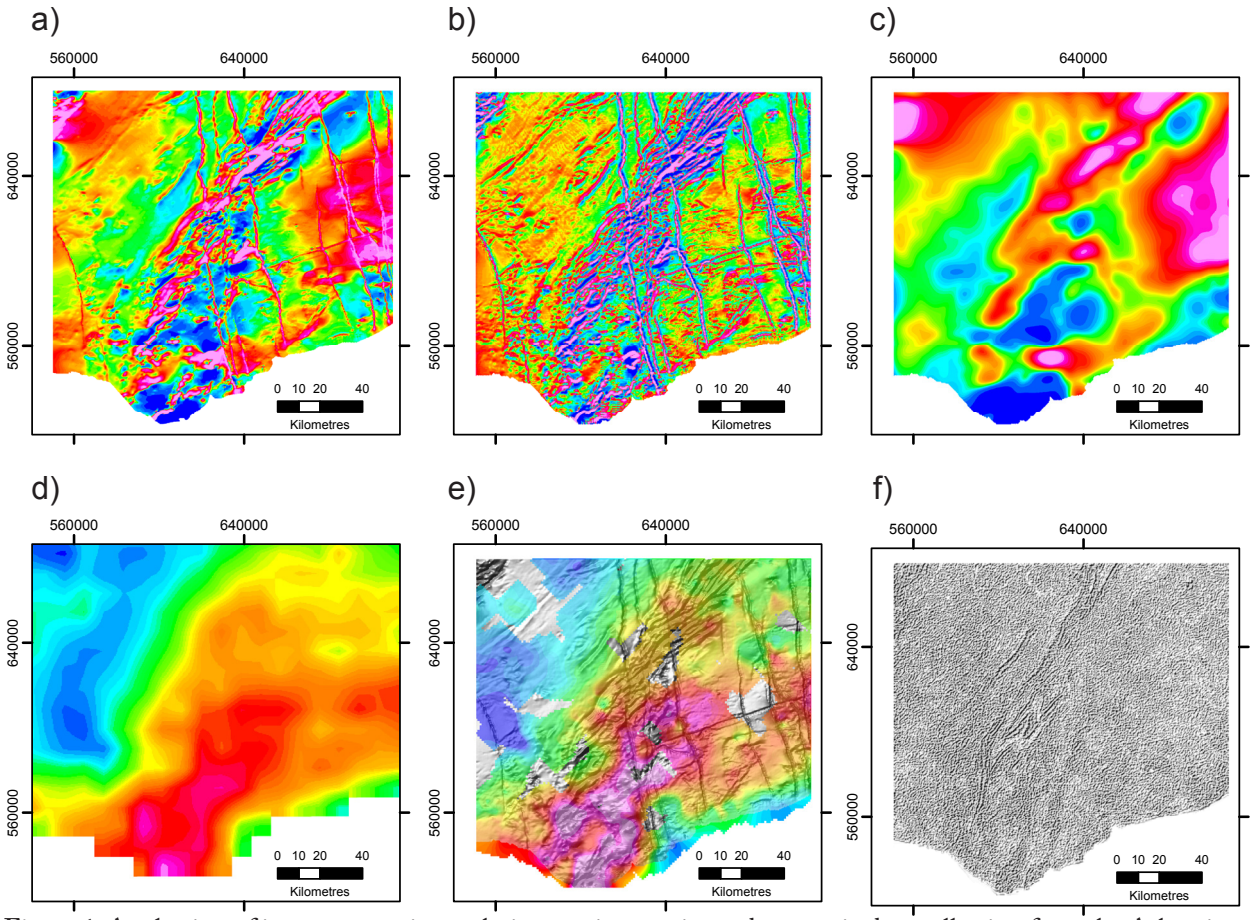

Figure 1. A selection of image processing techniques using gravity and magnetic data collection from the Ashanti Greenstone Belt, southwestern Ghana, western Africa. (a) Reduced-to-the-Pole (RTP) aeromagnetic image showing a high frequency region through the centre of the image and high magnitude linear anomalies signifying dykes; (b) aeromagnetic image in the first vertical derivative (1VD) accentuating a high-frequency magnetic anomalies; (c) RTP image reduced to the pole and upward continued to four kilometres, highlighting magnetic anomalies in the east, north and northwest. Note the signature of the dykes has been subdued; (d) Pseudocolour regional gravity Bouguer colour image showing a large trough in the centre and southwest of the image; (e) combination image of 1VD aeromagnetic (greyscale) sun-shaded from the southeast and pseudocolour Bouguer gravity image showing the correlation of a textured magnetic signature with a higher magnitude gravity response; (f) aeromagnetic greyscale image with an auto gain control filter enhancing more subtle trends and continuity of the response. Note folds shown in the centre and to the north of the image.

lithologies under that point, which can then be used determine and constrain the spatial distribution of petrophysical properties (Jessell, 2001; Kearey et al., 2002). In comparison, magnetic surveys detect variation in the Earth's magnetic field. Broadly speaking, rocks composed of a relatively high amount of magnetic minerals (for example magnetite, maghaematite and pyrrhotite) (Clark, 1983; Telford et al., 1990; Airo, 2002) will produce a higher response than rock composed of low amounts of magnetic minerals. The spatial distribution of high and low magnetic response can reveal information about the composition of the rocks over which the survey was conducted. It is important to note that while magnetic surveys tend to be a higher resolution (i.e. the survey line spacing is smaller) than gravity, not all rocks contain magnetic minerals, while all rocks possess a density. Therefore, where a magnetic survey may not reveal a change in lithology if all rocks

possess the same magnetic mineral content (possibly due to hydrothermal alternation or high-grade metamorphic events) it is possible that a gravity survey may reveal them.

2.2.2 Geophysical ambiguity

Geophysical interpretation can be a beneficial tool for many geological studies. Some may not have been possible without the information geophysical surveys provide (see McLean & Betts (2003), Aitken & Betts (2008), Williams et al. (2009), Metelka et al. (2011) and Perrouty et al. (2012). It is therefore critical to acknowledge the inherent ambiguity when interpreting geophysical datasets. The number of possible outcomes that can fit the observed response may render interpretations meaningless unless certain petrophysical constraints are applied (Nettleton, 1942; Fullagar et al., 2004). It stands to reason that geological constraints should be included in 3D modelling exercises to mitigate the effects of geophysical ambiguity (Jessell, 2001). Common practice is to take appropriate petrophysical samples relevant to the potential field under study; magnetic susceptibility for magnetic surveys and density measurements for gravity (see Talbot et al. (2000; 2004), Wu et al. (2005), Guillen et al. (2008), Williams et al. (2009), Metelka et al. (2011) and Perrouty et al. (2012) for examples). When applied appropriately, a particular geophysical response can often be correlated to different lithologies within a study area (Grant, 1985; Betts et al., 2007). Consequently, identification of geological structures such as folds and faults can be interpreted with more certainty, leading to more scientifically robust conclusions.

3. Geomodelling techniques

Maxelon et al. (2009) distinguish two geomodelling techniques used to model complex geological architecture: explicit and implicit. Both styles of geomodelling are performed using different methods of defining modelled objects that depends on the software package, but both utilise the kriging data interpolation technique (and its derivations) to 'join-the-dots' and add information where data points do not exist.

3.1. Data interpolation and kriging

Much of the data used in geomodelling exhibits characteristics of regionalised variables; they are spatially correlated over short distances, but at larger distances may be statistically independent. Semivariogram and covariogram functions can describe the degree of spatial continuity of this input data and, using kriging techniques, estimation of value at unsampled locations can be made (Chilès and Delfiner, 1999). While kriging is classified as a linear regression technique, it differs from traditional linear regression by not assuming that random sampling has taken place, nor that the variates are independent (Davis, 2002). Kriging accommodates the assumption that measurements are dependent on geological processes that have operated within the area, and should be reflected in the spatial variation of measurement values. Semivariogram analysis of the data is performed prior to kriging to identify spatial trends within the data (Figure 2). The 'range' of the semivariogram is the distance at which measurements become uncorrelated and the 'sill' is the limit of correlation. Anisotropy within the data can be determined where the range of semivariograms is dependent on direction (Chiles and Delfiner, 1996). The 'nugget' determines

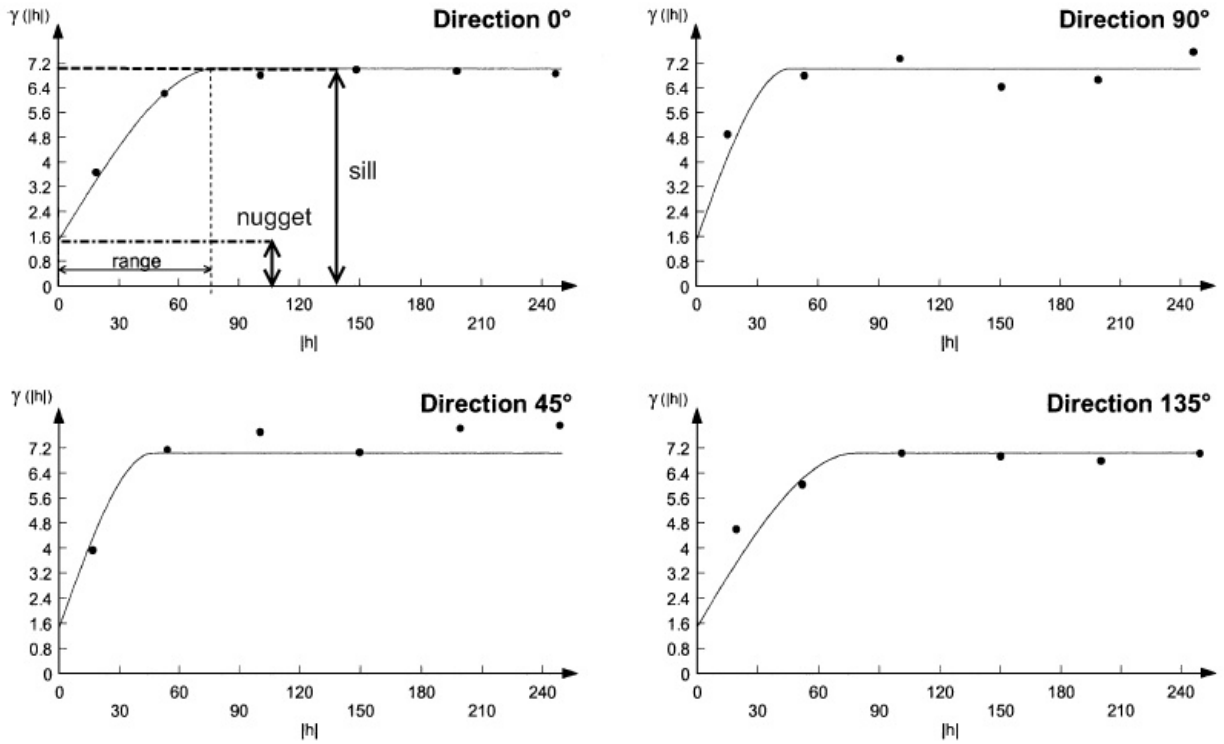

Figure 2. Semivariograms displaying anisotropies in data variance. By using the same dataset and observing the change in semivariogram range with direction, a trend can observed along the 135° axis where the range is largest. Distance from the point under study is shown on the x-axis, variance of data is shown on the y-axis. Adapted from Marinoni (2000, 2003).

the amount of error associated with the sampled data and the confidence with which it can be observed. The next step toward obtaining kriged data is to define a search ellipse that outlines an estimation grid over the region of interest (Chiles and Delfiner, 1996). While kriging is used extensively in geological studies, its basic form does not allow for modelling more than one variable or if there is covariance observed between variables (Chilès and Delfiner, 1999; Davis, 2002). Geophysical data can provide an example.

Magnetic geophysical surveys record the spatial variation in magnetic susceptibility based on the content of magnetic minerals within the rock, such as magnetite, maghaematite and pyrrhotite (Clark, 1983; Telford et al., 1990; Airo, 2002). In a general sense, increasing abundance of these minerals would indicate an associated increase in magnetic signature, a relationship that could be effectively modelled using kriging with two variables with that exhibit a clearly defined covariance.

The reality is different however, as each of these minerals have different ranges of magnetic susceptibility and corresponding influence on the magnetic signature (Telford et al. (1990) provide a more detailed examination of this topic). Other geological factors can affect this relationship, such as fluid flow, metamorphic activity and weathering that make the relationship even less clear as each can increase or decrease magnetite content and subsequently affect the measured magnetic susceptibility (Betts et al., 2003). Another geostatisical method, cokriging, addresses this issue by accommodating the analysis of multiple regionalised variables that have been sampled at the same locations (Chilès and Delfiner, 1999; Davis 2002). The kriging covariance of multiple variables is complemented with spatial cross-covariances between each of the variables and can provide information on the importance of particular dataset relationships while identifying further possible correlations between variables (Goovaerts, 1998). Cokriging facilitates a better understanding of data distribution and correlation and allows us to produce models that accommodate variable relationships between datasets and model elements.

3.2. Explicit modelling

Explicit modelling defines each object within the model as a mesh or data structure. A surface that defines the extent of the object, either as two-dimensional grids, parametric or

triangulated surfaces is created using points entered by the operator (Figure 3). A diverse range of methods are available to create these surfaces, including Bezier surface interpolation (de Kemp, 1999), splines, geostatistical kriging variants (Chiles and Delfiner, 1999) and discrete smooth interpolation (DSI) (Mallet, 1992).

It is important to note that DSI allows a variety of constraints to be incorporated into model calculations that involve single objects or a number of geometrically or topologically related objects (Mallet, 1992; Mallet, 2002). The benefit of explicit modelling comes from the ability to manually manipulate these surfaces, though accommodating large amounts of orientation data can be restrictive, especially if not located on modelled surfaces. Unrelated orientation data may need to be filtered, pre-processed or manipulated manually which is a labour-intensive activity that can make any model updates (i.e. addition of drill-core logs or field measurements) time-consuming (Jessell, 2001). Various tools and methods have been proposed to mitigate the data management drawbacks and sometimes excessive data entry requirements of explicit modelling, (de Kemp, 1999; de Kemp, 2000; Kaufmann and Martin, 2009; Zanchi et al., 2009) including a 'support vector machine' which attempts to automate the 3D model generation process (Smirnoff et al., 2008). Two examples of explicit modelling software packages are Gocad™ (http://www.pdgm.com/gocad-base-module/) and SURPAC.

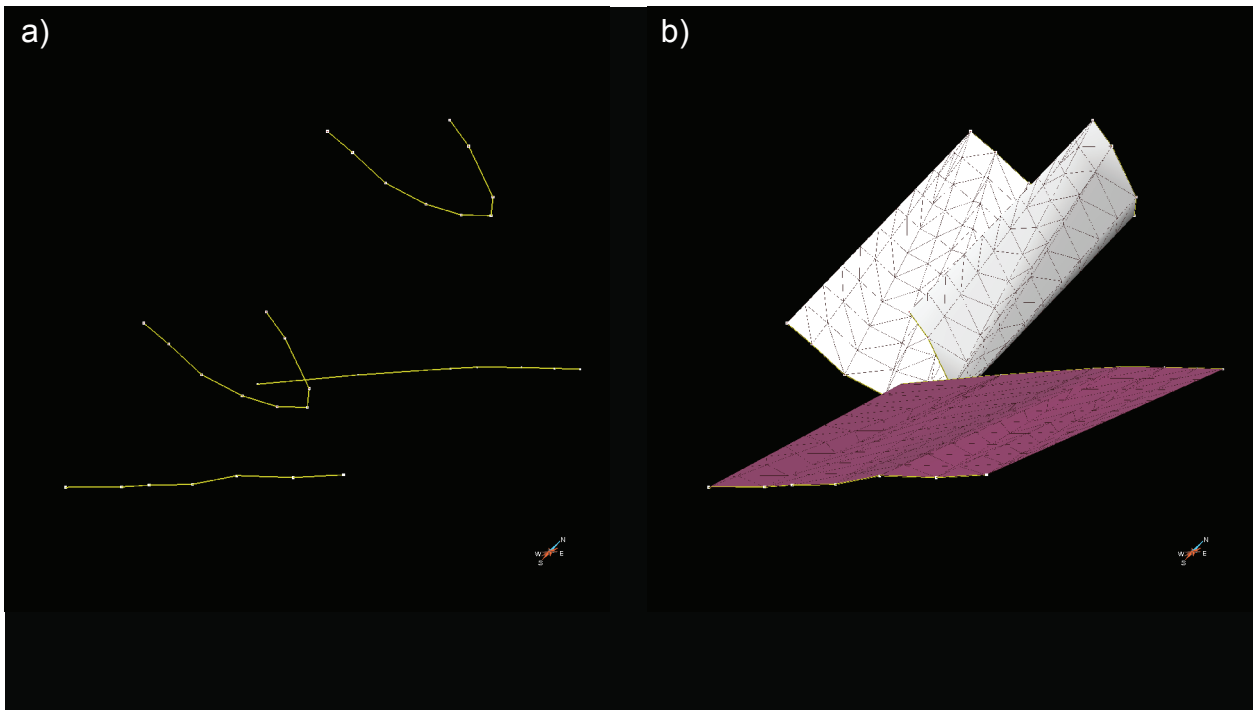

Figure 3. Example of creating a geological surface in an explicit modelling environment. GoCAD is used for this example. a) Two pairs of curves have been digitised from a set of nodes (points) and linked with a polyline. b) Surfaces are created by linking each curve pair. Further operations, such discrete smooth interpolation (DSI) (Mallet, 1992), can be used to smooth these objects.

3.3. Implicit modelling

Maxelon et al. (2009) states that in contrast to explicit modelling, implicit modelling uses iso-surfaces of one or several scalar fields in 3D space to generate geological interfaces. Geological orientation data is represented by vectors (for example, dip angle, dip or younging direction) defining the gradients of the scalar field and geometry of the iso-surface. Stratigraphic contacts, and other geological features such as fault locations, are located via iso-values within the model. The scalar field is calculated by interpolation between data points generating iso-surfaces (Figure 4). Other geologically conformable surfaces can be modelled based on data associated with different interfaces (Lajaunie et al., 1997), a particularly useful capability if data is sparse or biased to one geological formation or structure. Implicit modelling allows updates to be easily integrated into existing models if new data becomes available.

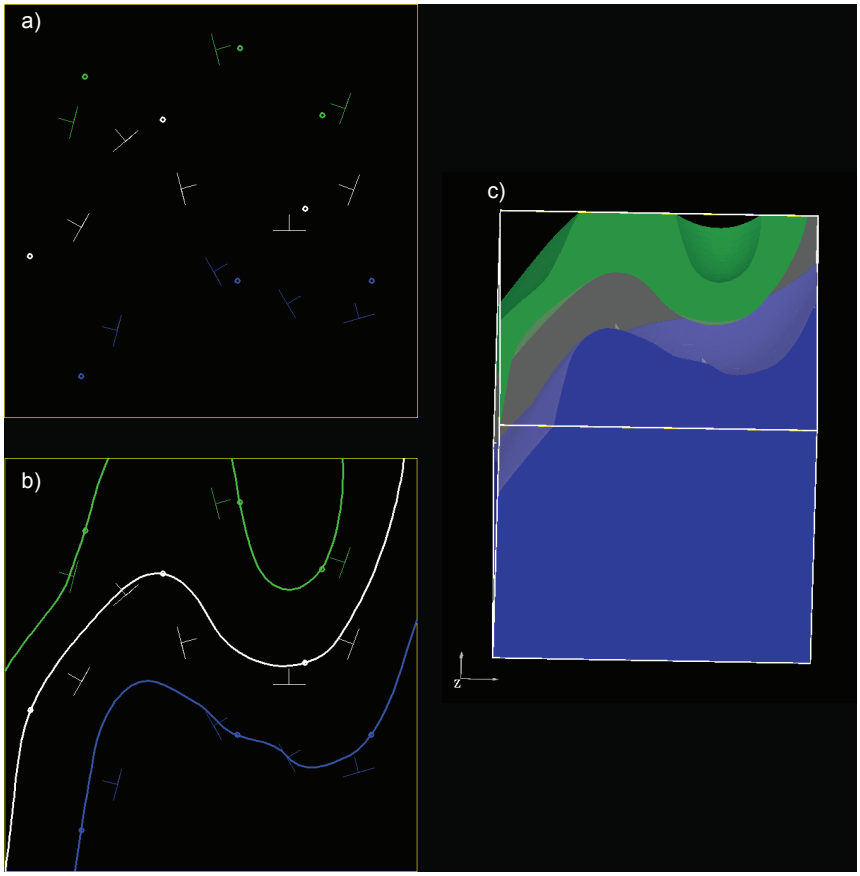

Figure 4. Example of creating a geological surface in an implicit modelling environment. 3D Geomodeller is used in this example. a) Digitised geological map of three formations in blue, white and green. Outcrop points are depicted as circles, dip and strike are depicted by the standard convention. b) Interpolated geological map determined by the potential field method. The solid lines represent contacts between the three formations. Note how both contact and orientation (strike and dip) points are honoured to produce an antiform-synform pair. c) 3D representation of the input data looking down-dip.

Implicit modelling does not always produce surfaces with desired geometries. If information contained within the data points does not allow geological geometries that are known or suspected, the operator is required to adjust the point attributes to 'force' the surface into the desired shape. Adjusting the variogram to impose particular geometries on surfaces can also be employed, though this will affect all surfaces associated with the data. This is a major consideration and source of subjectivity that should be acknowledged when constructing 3D models with the implicit technique. Examples of implicit modelling software are 3D GeoModeller™ (www.geomodeller.com) (Figure 5), Gocad SKUA® (http://www.pdgm.com/products/skua.aspx), and the Gocad 'Geochron' technique, which uses the age of geological horizons to generate scalar field gradients (Caumon et al., 2012; Frank et al., 2007; Moyen, 2005; Royer et al., 2006).

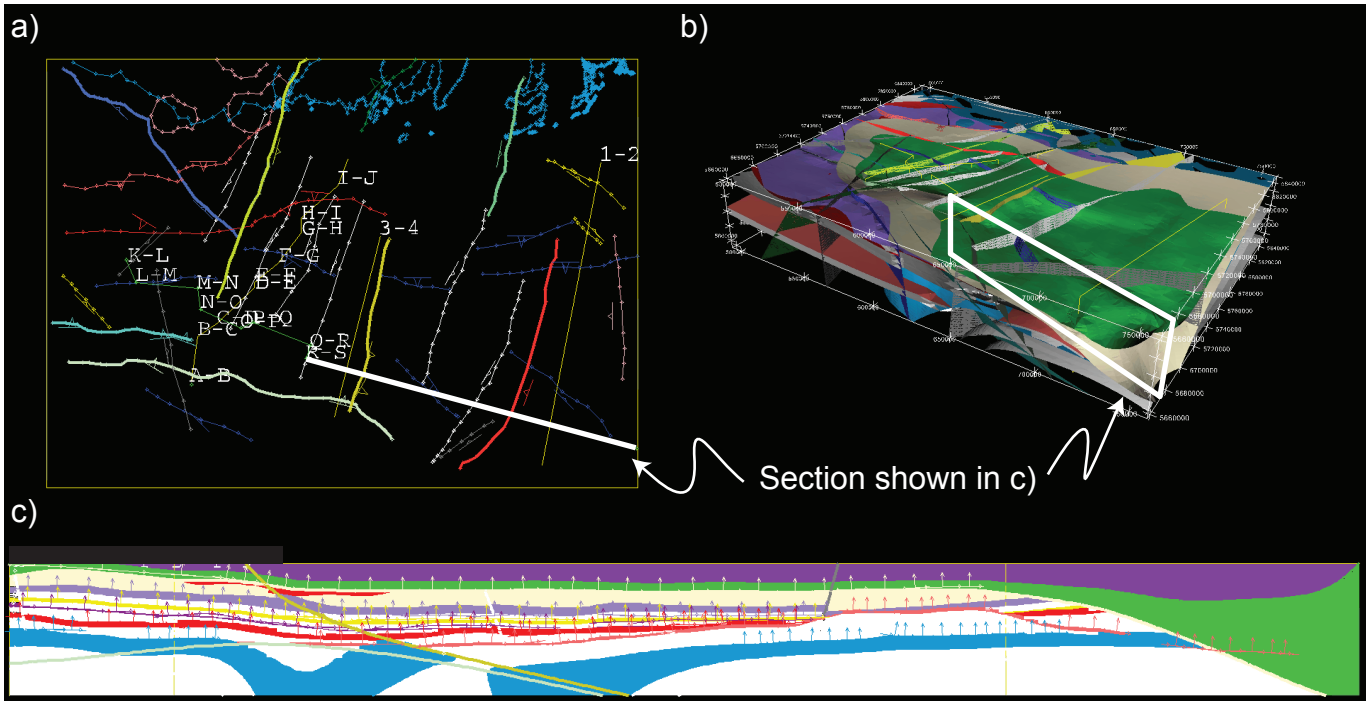

Figure 5. 3D geological model of the Gippsland Basin, southeastern Victoria, produced with an implicit modelling software package, 3D GeoModeller: (a) structural data colour-coded according to formation and fault; (b) 3D model view looking from the southeast; (c) E-W cross-section and interpolated geology.

4. Geophysical inversions

Geophysical inversions are powerful modelling techniques that exploit the spatial data coverage offered by geophysical surveys to generate an assessment of 3D geological models. In very broad terms, an inversion is a process where an algorithm determines the best fit between a measured geophysical dataset and the calculated model (Tarantola, 1984; Oldenburg et al. 1997;

Sambridge, 1999; Boschetti and Moresi, 2001; Fullagar et al., 2008; Guillen et al., 2008; Aitken et al., 2012) and allow the 3D modeller to test model veracity with respect to the measured geophysical signature. The geometry or properties of surfaces in any particular model are modified by the inversion process to better match the geophysical signature. The results can show either geometric or petrophysical differences between the modelled surfaces and those represented by geophysical data (or the 'residual'). The residual can be used as form of sensitivity analysis to find the measure of fit or correlative overlap between the geological and geophysical data. This process does have bias toward geophysical integrity as it relies on geophysical data to correct model properties or geometry. This has implications for geological integrity (Fullagar et al., 2000) as to how inherent ambiguities in geophysical interpretations allow many inverse solutions result from one set of observations.

4.1. Definitions and jargon-busting

It is necessary to describe and define the many technical terms that are used in much of the literature before going into detail about the inversion process. These definitions are provided by Tarantola (2005) unless cited otherwise.

A little background to inverse theory will assist understanding the geophysical inversion process. If a theory describing aspects of a physical system is known, then predictions about measurements from that system can be made. Two types of problems are presented when making such predictions: the forward and inverse problem. The forward problem consists of predicting measurements given a set of parameters and involves a unique solution (assuming all parameters are known), whereas the inverse problem uses the results of observations to infer the parameters of the system presenting multiple solutions. A diversion from the forward problem definition can be seen regarding geophysical forward modelling. This process requires the operator to interactively construct a geological cross-section by assigning appropriate petrophysical values to lithologies and then tailoring their geometry to both represent feasible geology and an observed potential field (Figure 6). In this situation a number of geological solutions may accurately represent the observed response, and can be compounded further when magnetics and gravity are combined in the one forward model. While the potential for multiple solutions contradicts

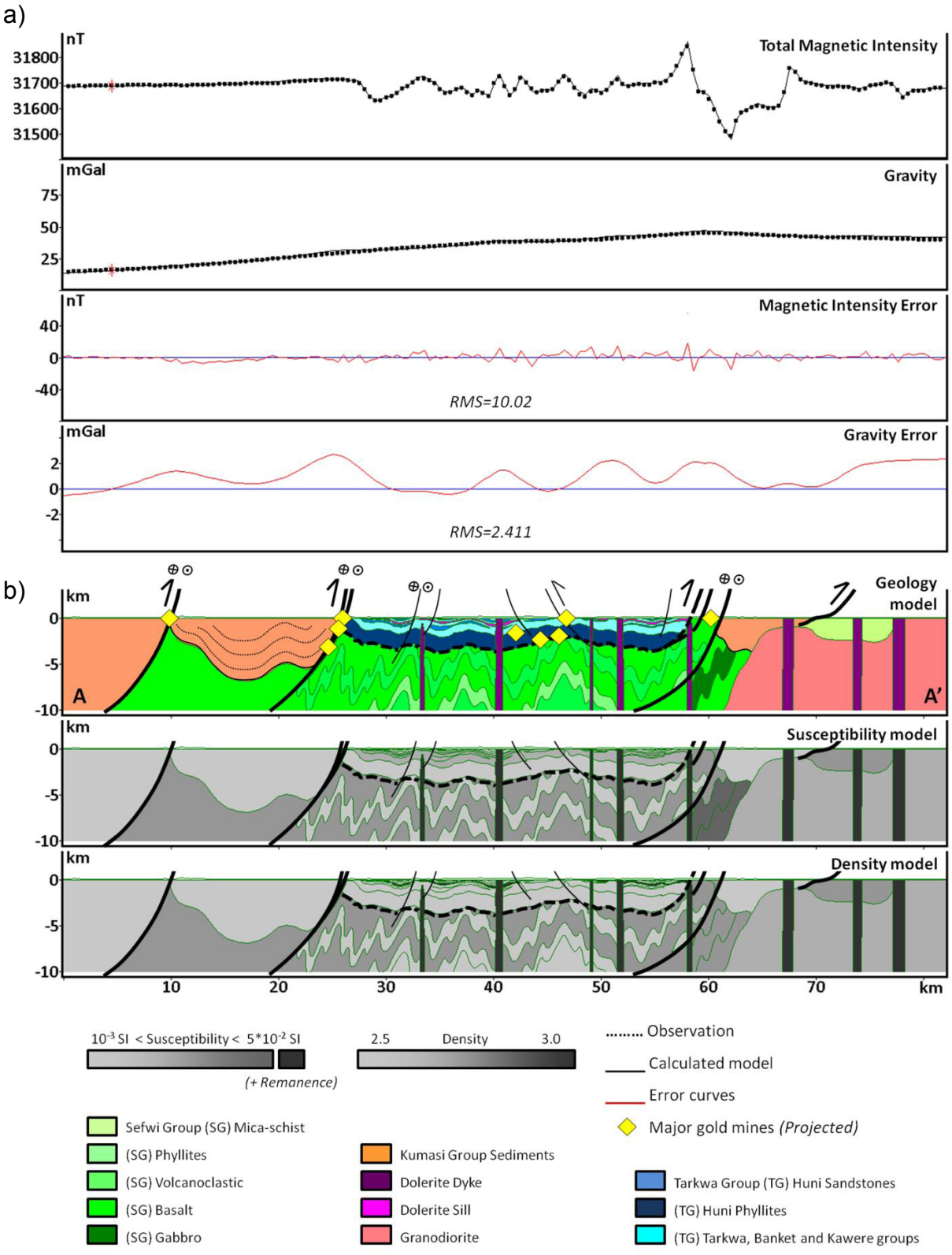

Figure 6. Example of a forward model showing geology resolved to (a) magnetic and gravity signatures. b) Corresponding lithologies are represented by different colours. The susceptility and density models are shown to display the relative contribution of each structure to the potential field. After Perrouty et al. (2012).

the definition of a forward problem, the reason why more than one solution may be found is that not all parameters are known. We never know the exact geological architecture or spatial distribution of petrophysical measurements. As exact geological architecture is never known, predictions about the location of modelled geological features must be performed a priori to provide a starting point. The 'known' parameters, of which the a priori model is a member, are not so much known as predicted. A priori models, being predictions, can be changed to improve misfit when required. If this occurs, the challenge becomes an inverse problem, where multiple parameters are unknown.

When dealing with geological inverse problems, an initial model is used as a starting point to which the inversion process is applied. This geological model is usually constructed in an implicit or explicit geomodelling package. Geological attributes represented by the a priori model is then measured against a set of observable parameters and results are used to guide modification of the a priori model. More simply put, the a priori model represents what is currently understood whereas the inverted model is created once new data has been integrated. The inversion process relies on three abstract concepts: (1) the physical system, (2) the model space, and (3) the model. The physical system describes (i) the physical parameters, (ii) physical laws that enable forward problems to be solved for the system under study and (iii) how results observed from observable parameters can be used to infer the values of model parameters (i.e. the inverse problem). Examples of physical systems are stars for an astrophysicist or a mineral system for an economic geologist. The model space is a representation of possible models with a given set of parameters. Any point within model space represents the entire range of models that can be calculated within the physical system using a particular set of defined parameters. The point may represent only one model for a completely physically constrained deterministic example, but multiple models for examples where the parameters are either incomplete or unknown, or for stochastic examples. Parameters are the physical quantities that characterise the system and define the boundaries of the model space. Using the mineral system example, the defined parameters may be hydrothermal fluid flux, a set of fault structures and knowledge of the lithology. Therefore, potential models may only be those that can be formed within the predetermined fluid flux range, on fault surfaces and within the specified lithology. Other possible parameters could be the size of the mineral system, the commodity or commodities being targeted and their depth. While the consequences of not

defining the model space appropriately may result in the number of possible models to be quite large and possibly unmanageable, this may be desirable. By allowing as many models as possible the likelihood of producing the closest representation of real geology increases, though the likelihood of finding said representation decreases.

'Optimising' or 'optimisation of the data' describes the process of producing an optimal, or single 'best' model from a set of inversions based on minimising the misfit between the measured and modelled data (Jessell, 2001; Fullagar et al., 2004; Tarantola, 2006; Guillen et al., 2008). It is the responsibility of the geologist to assess then accept or reject the model based on geological accuracy or feasibility when adopting an optimising approach to inversions. Optimisation is a more traditional approach to running and producing inversion models. In contrast is the falsification approach suggested by Mosegaard and Tarantola (1995) and Tarantola (2006), whereby observations enable the operator to reject possible or impossible solutions, rather than seeking the best available. The argument for this approach is based on the scientific principle that observations cannot be used to produce models, only to falsify them (Popper, 1983). According to Tarantola (2006), there is a natural human instinct to observe a result from the inversion process with less scepticism over time, so much so that uncertainty inherent in the model (either as a function of geophysical ambiguity or variation in geological measurements) is ignored or never considered. Models with a high level of uncertainty may be viewed with the same confidence as those with little, contributing to poor decision making.

Another key term that requires examination is 'discretisation'; a process whereby a continous model is represented as a set of discontinuous, finite objects such as 3D volumetric pixels, or 'voxels', collectively known as 'voxets'. Discretisation is necessary as voxets provide better numerical resolution for partial differential equation calculations employed by modelling applications (Guillen et al., 2008; McLean et al., 2008; Williams et al., 2009). A voxel contains location information (x,y,z or u,v,w format) and the relevant physical attributes, such as magnetic susceptibility, density or lithology. While it is easier for the inversion process to use voxels rather than vectors and surfaces, detail can be lost in the process of discretisation. Geology is very rarely exhibited by a perfect cube (at least at the regional scale), therefore one must acknowledge that data fidelity has been compromised to enhance the modelling process.

4.2. Geophysical inversion methods

The aim of geophysical inversion is to validate geological models from geophysical data by automatically solving the forward problem multiple times. The iterative approach adopted by the inversion process is necessary due to the many possible results that can be correctly represented by potential field observations. An objective function is chosen to assist in decreasing the number of possible outcomes that adequately fit the data. The type of objection function is decided prior to modelling and takes into consideration the geological complexity and nature of geophysical information input into modelling (Oldenburg et al., 1997). Some inversion schemes use Monte Carlo sampling techniques to obtain an adequate and manageable sample of the millions of possible inversion results (Guillen et al., 2008). Inversion is then performed on a discretised version of the input geological model and then modified to reduce the misfit detected against the geophysical signature. Statistical techniques are used to decide which inverted model is selected as the most appropriate (Fullagar et al., 2008; Guillen et al., 2008; Fullagar, 2009).

4.3 Conducting an inversion

VPmg (Vertical Prism magnetics gravity) is an inversion package that can work alongside Gocad. Fullagar et al. (2008) describes two general types of inversion method: property and geometry. The property inversion has two variants: homogenous and heterogenous. The homogenous property inversion assumes that each discrete geological body has the same geophysical properties value throughout. A homogenous property inversion allows the process to adjust rock properties (either susceptibility or density measurements) without changing the geometry of the input model, while allowing the operator to assess and adjust the contact locations in the resulting model to reduce the misfit. The heterogeneous property inversion allows discrete geological bodies to be divided into parts, enabling the petrophysical properties within the discrete body to vary (McLean et al., 2008; Aitken, 2010). Heterogeneity is introduced to simulate the high degree of petrophysical variation displayed within some (if not all) lithologies in order to obtain smaller misfit and residual values. The heterogeneous property inversion can be particularly helpful to reconcile magnetic remanence, an effect that can cause many issues in the inversion process

by introducing magnetic susceptibility values orders of magnitude higher than those commonly seen (Reid et al., 1990; Muxworthy and McClelland, 2000). Finally, the property inversion can be configured to change values in pre-determined geologic domains by removal of other rock types from the calculations. This allows further refined inversions to be conducted that either accelerates the process, performs sensitivity analysis in 'what-if?' scenarios or forces the process to ignore areas that are considered to be close to reality due to direct observation information(drill logs, field mapping).

A geometric inversion does not modify rock properties, but adjusts geological surfaces in the z-direction to achieve a better misfit. Subsequently, geometric inversion necessitates that petrophysical properties are extensively measured and integrated into the inversion process. Input of inadequately sampled or non-representative petrophysical values are likely to result in spurious and unfeasible geometries (Fullagar et al., 2008). Similar to fixing petrophysical properties in property-style inversion, surfaces can be fixed in a geometrical inversion. Geological surfaces can be 'fixed' by constraints dervied from data obtained from drill logs or field observations. Fixing surfaces can be achieved by adding 'pierce points' to surfaces that correspond to known geological contacts or structures.

Guillen et al. (2008) describe a different process, dubbed a 'total litho-inversion', used in conjunction with 3D GeoModeller. This inversion utilises Bayesian probability functions to quantify the spatial distribution of rock properties and lithologies within a given model (Lane and Guillen, 2005). The flaws of optimisation stated by Tarantola (2006) are addressed by using varied geometries to test a range of possible models, though these are still highly dependent on the geometry of the a priori model. A probability distribution over model space is produced to guide deduction of the final model. The benefit of generating a probability distribution is that Monte Carlo sampling of solutions can be applied using the Metropolis algorithm (Mosegaard and Tarantola, 1995; Bosch et al., 2001). This method is broadly described as a process that allows the exploration and analysis of multiple model possibilities resulting from complex a priori information and ambiguous geophysical input data (Mosegaard and Tarantola, 1995; Tarantola, 2005). The inversion process for both 3D GeoModeller and VPmg share a somewhat similar workflow, but fundamental differences are seen. A comprehensive outline for 3D GeoModeller is described in Guillen et al. (2008) and workflows for VPmg are described in Fullagar et al. (2000; 2004;

2008), McLean et al. (2008) and Williams et al. (2009).

Williams (2006) outlines the University of British Columbia – Geophysical Inversion Facility (UBC-GIF) software which uses a model objective function to derive a geological model from the observed potential field response (Li and Oldenburg, 1996, 1998; Oldenburg et al., 1997). UBC-GIF inversion attempts to find a physical property model that (1) requires the smallest amount of modification as possible from the a priori model ('smallness') and (2) contains as few high magnitude residual effects as possible ('smoothness'). A number of parameters and constraints are available to the operator to customise the inversion: including noise (a reflection of noise in the observed potential field data); weighting the solution toward smallness or smoothness; upper and lower property bounds for the observed field and; providing geological constraints in the form of inferred or known geological interfaces and/or volumes. The consequence of this level of inversion customisation is that the operator can impart control over the solution and assign parameters appropriate to the types of input data and the problem. However, it may not be possible to accurately assign the correct parameters without making generalised assumptions about the data, which could be miscalculated and have negative effects on the quality of the result (Williams, 2006). Williams (2006) also suggests that unless there is a robust and detailed 3D model available as an input, a 'zero reference model' should be used , in other words, an a priori model that contains no geological constraints. Given that most geological models are underdetermined, a zero reference model would therefore have to used in most cases, aside from some rare mine-scale detailed models are available. This form of geologically unconstrained inversion greatly increases the number of possible solutions, and reduces the likelihood of finding a geologically feasible result.

A significant drawback for geophysical inversion concerns that a priori sampling and the inversion process may exclude models that better resemble reality. The methods described above only offer a provision for one input model. This issue stems from the problems of sparse data sampling that endemic to the geosciences (Frodeman, 1995; Groshong, 2006). The data input into the inversion process may be comprehensive, but due to the necessity of interpretation the geological system will never be entirely described. Therefore the processes of sampling undertaken in the generation of the a priori 3D model and subsequent inversion processes cannot optimise the data with complete certainty. It is possible the resulting model adequately represents

reality for the purposes of the study if the operator is prudent in the process of data collection, interpretation, modelling and inversion is conducted properly. This requires the operator to exercise prudent judgement on the data, method and results to ensure that the process is not compromised by overly relying on geomodelling and inversion algorithms to provide the answer. The inversion process can offer overconfidence by producing readouts like misfits and residuals that may reduce required scepticism when analysing the results. In other words, geophysical inversions should not be treated like a 'black box' , where data is collected, entered and presented without healthy scepticism and objectivity.

4.4 Assumptions and issues

The aim of solving the inverse problem is to determine the parameters that explain data distribution. It is also necessary to make assumptions so a workable method can be used to obtain a solution (Jessell, 2001; Guillen et al., 2008). Certain assumptions made during inversion modelling cannot be avoided. The quality of input may be unquantified and assuming data is adequate may produce results fundamentally removed from a useful outcome (Boschetti and Moresi, 2001; Jessell, 2001). While it seems clear that geoscientists should be aware of all assumptions inherent to the inversion process, especially those that cannot be removed from the method or software package, it is not always the case. This attitude is partially related to Tarantola's (2006) assertion that human nature tends to lead people to ignore the possible uncertainty or error in a model resulting from a geophysical inversion (or any complex data modelling process). Consequently, there is potential for assumptions to be ignored, forgotten or simply not considered when observing a model, potentially resulting in flawed interpretations or accepting inversion results when they should be rejected. In order to aid the acknowledgment of these issues, common assumptions made during the inversion process are listed here to promote necessary caution during the pre- and post-processing stages.

4.4.1. A mean value is assumed for petrophysical properties outside the bounding box in 3D space.

A discrete volume has to be defined by bounding coordinates when an inversion is performed to limit the volume of data being calculated. Inversions require the volume outside

the bounding box to be assigned a petrophysical value appropriate to the field being calculated to provide some continuity in geophysical response at the margins. These values are often given a mean value, such as 2.67 g/cm^3 (the average density of the crust) for gravity inversions. The issue is that far-field geophysical anomalies outside the bounding box can affect the fields observed within, and will not be accounted for if a mean density value is assigned to the outside volume. For example, if a large gravity-high existed outside of the bounding box it would have an effect on the gravity field within. If the inversion was set to assume a mean density value outside the bounding box and the gravity anomaly was not acknowledged, inconsistent results would occur.

4.4.2. Homogenous petrophysical properties adequately represent discrete lithological units

Mean petrophysical values are assigned to lithological units when a homogenous property inversion is employed, often determined from forward modelling (Williams et al., 2009). This is very unlikely in reality, as these measurements often vary significantly spatially, especially in deformed, metamorphosed or altered terranes. The heterogenous property inversion has been developed to accommodate this, but still requires each lithological unit to be discretised and all other lithologies removed from calculations. Therefore each lithological unit is considered independently of each other, in contrast to various geological processes that may have affected one, some or all units concurrently.

Heterogenous properties inversions also rely on sampling to accurately represent petrophysical heterogeneities throughout the rock unit. Sampling error can therefore affect the inversion modelling process by not representing the actual petrophysical heterogeneity within the rock unit.

4.4.3. Discretised models accurately represent geology.

Discretisation requires the operator to determine a resolution based on voxel size for the volume to be inverted (Oldenburg et al., 1997; McLean et al., 2008; Prutkin and Casten, 2009; Williams et al., 2009) (Figure 7). The choice of voxel size needs to balance a desire for high model detail with a corresponding increase in computational demand. The scale of project, size of target or speed at which the model is calculated often determines the resolution. Computation requires discretisation for the process to be completed, but the resulting cubes (voxels) may not

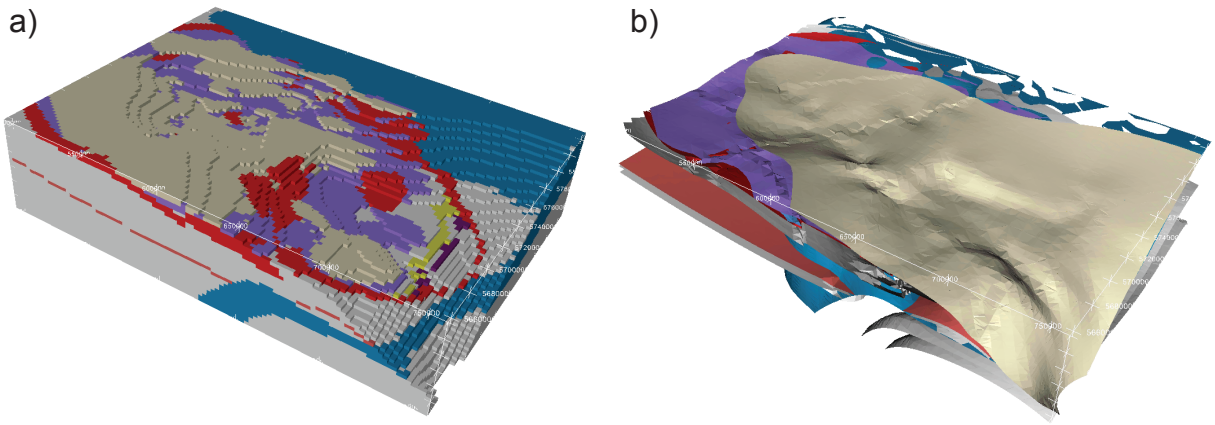

Figure 7. A discretised 3D model of the Gippsland Basin, southeastern Australia (viewed from the southeast). (a) shows a discretised version of (b). Note how geological contact surfaces in (b) are converted to cubic voxels in (a). All faults and some surfaces in (b) have been removed to aid visualisation of the underlying surfaces.

represent reality well. If the resolution is too low, small geological structures or lenses of lithology that may important to understanding the geological problem (such as magnetically remanent dykes) may have not have been modelled or included in calculations, resulting in flawed interpretation and results.

4.4.4. Single model input

In most studies there are often two or more versions of tectonic evolution. Take, for example, the two prevailing Broken Hill models of Marjoribanks et al. (1980) (nappe fold sequence) and White et al. (1995) (fold and thrust belt). Both offer a robust hypothesis describing the complex geological evolution of Broken Hill area. Currently there is no method by which these models can be quantitatively compared in terms of geological feasibility, even if an a priori model based on each was created. The problem is that current inversion processes do not allow topological changes to occur during modelling (Guillen et al., 2008), however solutions have been proposed (Cherpeau et al., 2012). This can be overcome by producing a priori models that represent the different, currently accepted topological models that describe the study area, but does not completely address the practicality of the issue. Different topological relationships are complex and are subsequently time-consuming to understand and integrate into an a priori model, forcing the operator to choose one topology over the others. Consequently inversion results are biased towards the chosen topology.

Multiple model versions are possible when different interpretations are taken into ac-

count. Geophysical and geological interpretations can differ, from deciding on the geometry of a fault or basin, to what lithology a particular stratigraphic unit should be. Differences such as these can produce varied models built using the same topology.

Significant issues requiring detailed discussion are: (1) that VPmg and 3D Geomodeller geophysical inversions only utilise geophysical methods to calculate the likelihood of the model; (2) that model uncertainty is not quantified and (3) multiple models are not compared or assessed during the inversion.

5. Uncertainty

The everyday use of the word uncertainty relates to doubt regarding a particular observation or concept. Further, statisticians use uncertainty to describe how predicted or observed data may vary with respect to the 'true' value, a concept which strongly relates to the 3D modelling processes. Uncertainty is inherent in any modelling solution, as it is in all knowledge held regarding the real world (Tarantola, 2005). In many cases uncertainty is negligible, but when assumptions, such as those listed in Section 4.4., are made when performing inversions, the number of sources and magnitude of uncertainty can be high. Quantifying the uncertainty associated with a 3D geological model prior to or after inversion would be a useful measure to assess the effectiveness the 3D modelling workflow. Understanding how uncertainty affects the model during inversion can aid in understanding the study area. It has been suggested by Mosegaard & Tarantola (1995) that inversion could be iteratively performed until uncertainty approaches zero, though this approach toward optimisation is discouraged as presenting a single solution can result in a mistaken belief that the model is 'truth', rather than a representation of nature provided by the data (see Tarantola (2006) and Section 4.1). Quantifying uncertainty is also important when assessing ore resources, planning exploration programs, identifying permissive locations for geothermal energy or geosequestration reservoirs. It contributes to better decision making by supplying more useful information to the user and increases the confidence with which one can view and apply interpretations made from a model that is essentially an estimation (Chilès et al., 2004).

5.1. Sources of uncertainty

Aside from geophysical ambiguity (Section 2.2.2), many and varied sources of uncertainty have been identified in oil and gas exploration (Thore et al., 2002; O'Dell and Lamers, 2005), geotechnical surveys (Marinoni, 2003; Samadi et al., 2009) minerals exploration (Shcheglov, 1991; Chilès et al., 2004), geological mapping (Jones et al., 2004) and geophysical surveys (Bowden, 2007). The breadth of interest alone suggests that quantifying this variable is considered an important exercise, but also infers that many sources can influence it. O'Dell & Lamers (2005) state that uncertainty involved in assessing oil reservoirs for resource extraction is linked with knowledge of reservoir architecture and compartmentalization, location of faults and fractures and other structural considerations. They also add that factors, such as compositional grading, may be more influential in resource-assessment decisions if associated uncertainty was calculated adequately. Thore et al. (2002) go further to discuss not only structural and mechanical considerations, but the uncertainty involved in processing geophysical data and the inherently subjective practice of geophysical interpretation.

Marinoni (2003) discusses how sources of 'algorithmic' uncertainty associated with data interpolation can be linked with the 'smoothing' of interfaces observed in kriging. Smoothing describes how variability in a model is reduced below that which may be observed in reality. Reducing variability may seem to be a desirable outcome, but detail is lost when too much variability is removed. The Marinoni (2003) study found that a lack of detail can present problems for using the model for prediction.

Jones (2004) and Bowden (2007) discuss a particularly interesting notion that uncertainty associated with the final product of a study, either a 2D geological map, 3D model (Jones et al., 2004) or geophysical survey (Bowden, 2007), can be attributed to human behaviour. Bowden (2007) cites a lack of specialised knowledge in field operatives as a chief source of error in the reporting of radiometric ground surveys and their lack of knowledge unnecessarily introduces uncertainty to the results. Jones et al. (2004) attributes much uncertainty from the interdependence of data, information and knowledge and the prevailing scientific paradigm of inductive reasoning. Central to these themes are three types of knowledge that can be associated with varying degrees of uncertainty (Table 1). 'Explicit' knowledge is that which can be easily

Table 1. Summary of knowledge accessibility. Adapted from Jones et al. (2004).

Knowledge Type	Example	Geological Example
Explicit	Journal articles	Detailed outcrop map
	Lecture material	Geophysical line data
	Textbook content	
Implicit	Working hypotheses	Field observations within a notebook
	Undocumented road directions	Unpublished observations leading to accepted geological theory
Tacit	Riding a bicycle	Geophysical interpretation
	Walking	Recognition of structures in heavily altered or deformed terranes
	Speaking a language	Transformation of structural data into 3D interpretation

communicated, expressed and understood by others. 'Implicit' knowledge is that which is not yet in a format as easily expressed but can be when queried and discussed(Frodeman, 1995). 'Tacit' knowledge (Polanyi, 1962) is that which exists within ones intellect, but may not be easily accessible by others as the owner may not be able to express it appropriately or they are not aware they possess it. Tacit knowledge can be equated to instinct, intuition and 'gut-feeling' and forms the basis for many cornerstone geological activities, including 3D modelling and both geological and geophysical interpretation .

5.2. Determining and utilising uncertainty

All sources of uncertainty can adversely affect the practical application of 3D models. Too much uncertainty within a model can result in model predictions being entirely random, rendering the model and predictions useless. It is therefore crucial that the level of uncertainty can be quantified, either to be used as a threshold further processing (such as inversions) can operate within, or as a value presented with a model informing the observer the magnitude of associated uncertainty. An example of quantifying uncertainty can be seen in the Marinoni (2003) study where the presence or absence of clays and silt exhibits a binary response. This was achieved by a process called 'indicator kriging' (Journel, 1983) which allows the operator to assign a

probability of encountering the clay and silt layer at each data point (in this case, boreholes). The operator is then able to visualise the kriged results and assess which probability model best represents reality.

There are two issues with this method: (1) the use of probability thresholds between more than two variables (for example, if there were three different lithologies rather than two - which is often the case) has a significant computational cost; (2) the assessment of the kriged model outcome is an interpretive exercise and represents the use of tacit knowledge. While the uncertainty associated with data interpolation and kriging is mitigated using the indicator kriging approach, uncertainty is re-introduced in a form much harder to quantify and account for as it is based on the geological expertise of the operator.

Uncertainty associated with human behaviour and interpretation is not easily measured as these activities tend to be qualitative assessments (Jones et al., 2004). To account for this fuzzy logic has been proposed as a means to assign confidence values to observations made by a geologist and introduce a quantitative means to which overall uncertainty can be determined (Bonham-Carter, 1994; Kasabov, 1996). Fuzzy logic requires tacit knowledge to be expressed as explicit knowledge (Brown et al., 2000) by requiring the geologist to first consider the observation or interpretation and then represent confidence by giving it a value between 0 and 1 . This practice is still subjective, not to mention time-consuming when using traditional mapping methods (map board and notebook) and rarely performed (Jones et al., 2004).

Another form of uncertainty found in geomodelling is the algorithmic uncertainty associated with interpolation of geological interfaces (Lajaunie et al., 1997). This method (discussed in Section 3.3.) interpolates surfaces using a 'dual' form of cokriging, attempting to find the most likely location for a geological interface in model space between known data points. This suggests that information contained within the model space between known data points is not precisely defined and therefore contains a certain amount of uncertainty. The magnitude of uncertainty within model space increases correspondingly with the distance from observation points (Figure 8).

Determining the magnitude of algorithmic uncertainty is unfortunately not straightforward. Chilès et al. (2004) suggest a geostatistical method to determine levels of uncertainty associated with data interpolation for potential field-style geomodelling in 3D GeoModeller. The

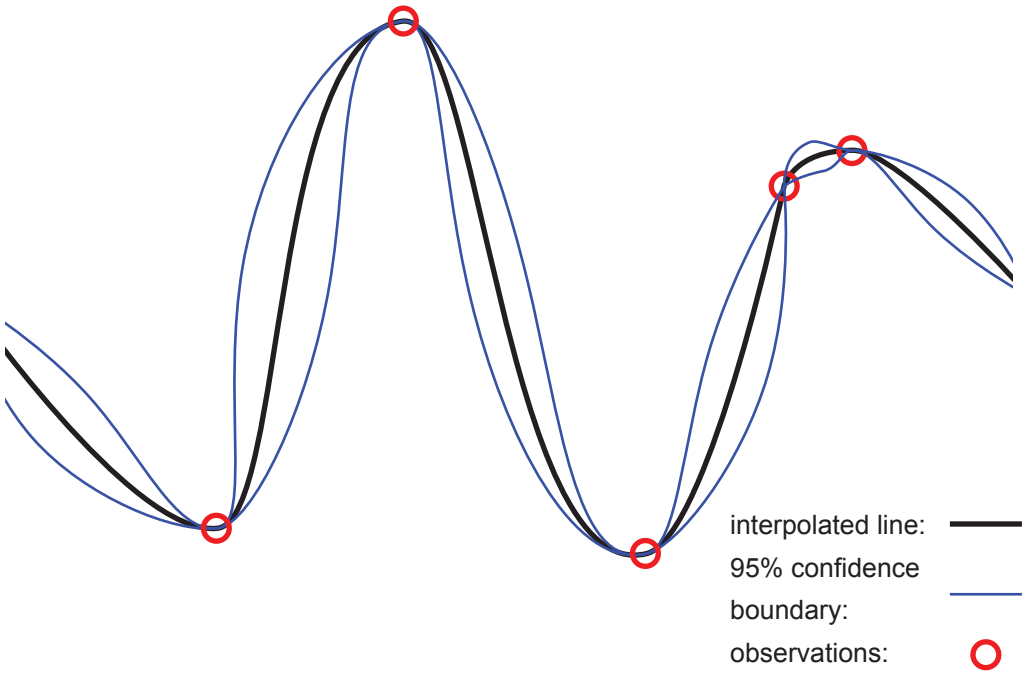

Figure 8. An interpolated surface (red) using 1D observations. The blue boundaries represent the area that the interpolated line could be placed within 95% certainty. Note how the distance from the interpolated line to the 95% certainty boundary increases with distance from each observation. Also note that the distance from the interpolated line to the 95% confidence boundary depends on the variogram model.

potential fields, or iso-surfaces, are determined by a dual form of cokriging, requiring the operator to input the covariance model and estimation variance (Section 3.1). The dual form of cokriging performed in 3D GeoModeller has two advantages: (1) that computing time is reduced as the cokriging system is solved and (2) visualisation is more easily achieved if executed with a marching cube algorithm (where nodes of the grid are predicted and intermediate points between are estimated to complete the iso-surface). One of the limitations of this approach is that the covariance model chosen by the operator may not be appropriate. The advantage of a numerical assignment of these variables is that a quantitative assessment of their respective contribution to the interpolation process can be made and reproduced by others in conjunction with model appraisal (Tangestani and Moore, 2001, 2003). Unfortunately, the choice of each value is made using tacit knowledge and is subjective and can become an almost arbitrary process, adding further uncertainty to the process.

A significant disadvantage using dual cokriging for interpolation is interpolation error and uncertainty cannot be determined, but a different approach can be taken to counteract this. Chilès et al. (2004) suggest that by using a standard cokriging system the covariance standard deviation can be calculated and algorithmic uncertainty can be inferred. This is performed by

using the covariance fitted from the data to ascertain a reasonable cokriging standard deviation. Subsequently, the likelihood that an interface passes through a particular point can be determined by combining the covariance of the potential field and the cokriging standard deviation. The cumulative likelihood of a set of interfaces passing through associated points then allows the probability of an area hosting an interface to be expressed in terms of standard deviations (S(x)). An example is shown in Chilès et al. (2004) that an area defined by a likelihood of S(x) <2 includes about 95% (i.e. two standard deviations from the mean) of the modelled interface (Figure 9), or the modelled interface has an uncertainty value of about five percent.

A major assumption in this approach is that the covariance of the potential field exhibits a Gaussian probability curve. Chilès et al. (2004) find this a reasonable assumption when applied

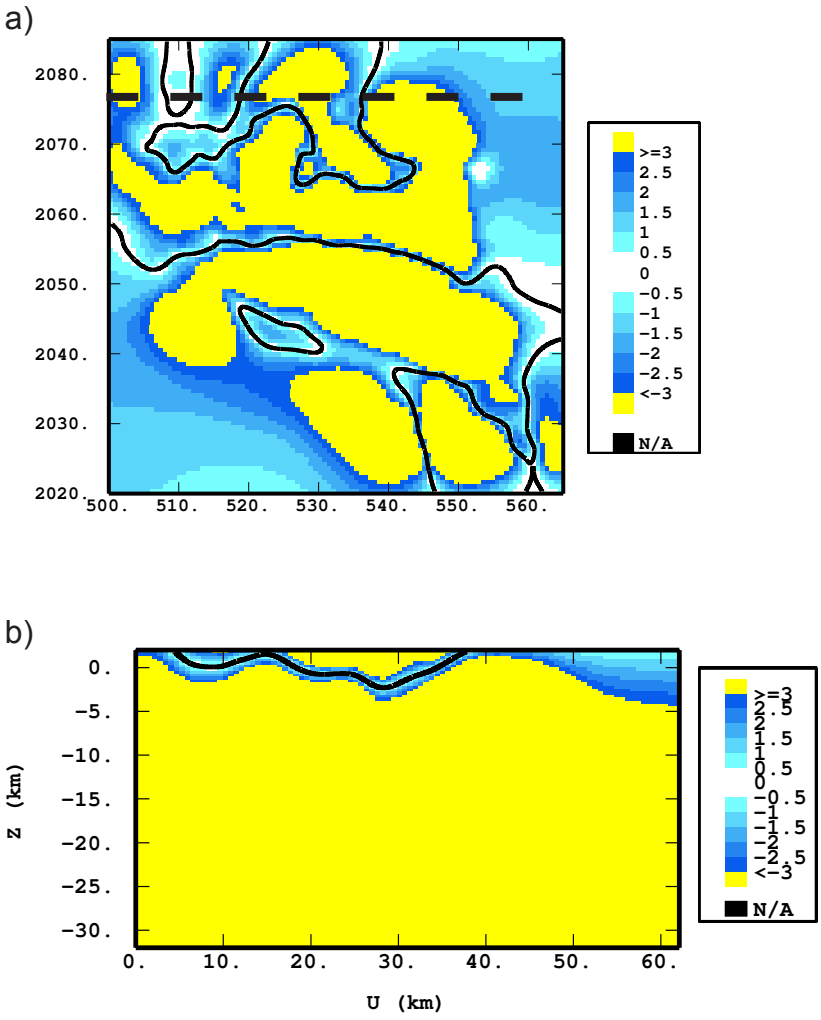

Figure 9. Depiction of uncertainty of the top layer of a gneiss unit, Limousin (Massif Central, France). (a) Plan view of modelled geology within 65 kilometre x 65 kilometre zone and 500 metres of elevation. (b) East – west cross-section located by the dashed line in (a) of 62 kilometre length and 34 kilometre depth. S(x) is represented by the colour scale at right of (a) and (b), the cokriged potential field interface is represented by the solid black line. Note that the 'true' interface is most likely to be found in the white and pale blue areas (between S(x) 0 and ± 0.5) which corresponds to about 95% of the modelled interface location. Adapted from Aug (2004) and Chilès et al. (2004).

to less complex geological problems. Unfortunately, this assumption is not always safe to make, especially in older, non-basin terrains, where many geological processes have been active over a long period of time. These relatively complex geological terranes rarely exhibit geological attributes (example, grain size, sorting, mineral composition) according to probabilities of a Gaussian curve, which are subsequently not adequately reflected in a computed potential field.

It is evident that while a quantitative measure of uncertainty is desirable, it is difficult to calculate accurately. It also appears that there is no single solution; different problems (geological, geotechnical or geophysical) require different approaches. Moreover the challenge of quantifying the human experience and understanding by assessing tacit knowledge first suggested by Polanyi (1962) is a task that still inspires intensive research in varied disciplines (see Cooley (2007), Rix & Liévre (2008), Braude (2009) and Ray (2009) for examples). Adequately accommodating potential for variability and error in interpretive exercises is clearly an immense task.

3D modelling is an accepted and important discipline in the geosciences as an effective method to visualise, analyse and represent geology. The aim of most geoscientific disciplines is to develop a model that explains measurements or observations and facilitates predictions. 3D models themselves are an integrated representation of various geoscientific disciplines. The applications of 3D models have been discussed, such as applications to ore deposit targeting, large-scale plate reconstructions, resource evaluation and mine engineering. The combination of structural geology and geophysical interpretation improves the quality of information used to build 3D models.

The 3D modelling discipline is also dynamic. Explicit and implicit modelling packages and inversion procedures discussed in this review are constantly being updated and improved to aid and increase the operator's geological understanding of the target area. Moreover, the digital nature of these modelling techniques allows cross-compatibility between applications, so that surfaces or volumes developed in one package can be exported for use in another. The development of new interpretation techniques also provides impetus for improvement with many of the cited authors having successfully used 3D modelling techniques to solve complex geological problems by improving on existing methods. The result is that 3D modelling is now a requirement for many enterprises within research, government and organisations.

It is clear that much has been achieved in the field of 3D modelling, but issues still

remain that require consideration. Perhaps two of the most significant issues facing 3D modellers are the heavy reliance on geophysical data and determination of geological uncertainty. Underestimating or not acknowledging uncertainty contained within the a priori geological model can have compounding effects on the results of geophysical inversion. Further, different sources of uncertainty need to be determined whether they are from algorithms or measurement and observation.

6. Thesis aim and structure

The aims of this thesis are: (1) to locate, quantify and visualise model uncertainty; (2) determine the effect of model uncertainty on model elements; (3) perform an exploration of model space and; (4) demonstrate a modelling workflow incorporating existing techniques developed from this project. Three 3D models were created and used for testing and analysis during this research. The first is a synthetic model that was used for proof-of-concept and features in Chapter One. The second is a 3D model of the Gippland Basin, southeastern Australia (Lindsay et al. (2012) and features in Chapters One and Two. The Gippland Basin model was built using public data and with significant assistance from the Department of Primary Industries, Victorian State Government. The third model is of the Ashanti Greenstone Belt, southwestern Ghana, west Africa (Perrouty, 2012) and features in Chapters Three and Four. The Ashanti Greenstone Belt model was built in collaboration with Stéphane Perrouty of Géoscience Environnment Toulouse, Université Paul Sabatier (Toulouse III).

This thesis is separated into four chapters. Chapter One introduces the problem of uncertainty in the geosciences. The geology of the Gippsland Basin, southeastern Victoria, Australia, is reviewed and the methods used to build an initial representative 3D model are described. Uncertainty simulation is described. The term 'model suite' is introduced and described as collection of models produced by subjecting the initial model to uncertainty simulation. The concept of stratigraphic variance is presented as means to measure, locate and visualise model uncertainty. Sensitivity analysis is performed and determines that model uncertainty can be reduced through judicious addition of data.

Chapter Two introduces the concept of 'geodiversity' and model space exploration. Geo-

diversity describes a collection of methods that characterise differences in architecture between models. The concept was developed as the presence of uncertainty within a model suggests that model elements must display different geometries from one model realisation to another. Geodiversity metrics were developed to categorise the geometrical aspects of different model elements. Quantification of geometry allows comparison with other models to determine the location and magnitude of differences. Metrics include depth of unit, volume, contact surface area, curvature and geological complexity. End-member models are identified from each metric providing a limited view of which models exhibit diverse (or common) architecture. Principal component analysis (PCA) is employed to simultaneously analyse all metrics and models to determine the configuration of model space. PCA also identifies any metrics that are associated with uncertainty. The Gippsland Basin model is used as a case study in Chapter 2. Most workflows produce a single geological realisation. PCA and geodiversity analysis produces evidence against model optimisation practices as the initial model is found to not be the most likely geological representation of the input data.

Chapter 3 expands on techniques described in Chapter 2 by including geophysical analysis into the geodiversity suite of metrics. Geophysical analysis is a key stage in regional-scale 3D modelling and the inclusion of some form of geophysical categorisation was necessary. Geophysical metrics include residual RMS, Hausdorff distance (Huttenlocher et al., 1993), standard deviation, entropy and 2D correlation. All geometrical and geophysical geodiversity metrics are used to analyse the Ashanti Greenstone Belt, southwestern Ghana, west Africa. Results from this chapter demonstrate that there is covariance between the geological complexity of the base of the Tarkwaian and the geophysical response. Geophysical analysis shows that Birimian-age features need to be better modelled to better represent the geophysical response. Arguments against only producing a single model are reinforced by PCA as the initial model is again found to not be the most common.

Chapter 4 demonstrates all the techniques developed through this research in an integrated study of the Ashanti Greenstone Belt. The aim was to conduct inversion with less subjective decisions while producing a geologically reasonable model. Birimian-age geological structures are included in the model according to recommendations made in Chapter 3. Uncertainty of the model suite is determined and analysed. Geodiversity techniques are employed and end-

member and principal component analysis results presented. Inversion modelling is performed on diverse and common representatives of model space, identified using geodiversity PCA. Inversion parameters are chosen according to results from uncertainty, end-member and principal component analysis. Inversion results are collated and found to display correlation to model uncertainty. Inversion modelling produces a realistic geological model that is validated by geophysical data. The workflow presented in Chapter 4 demostrates that inversion modelling can be conducted with less subjectivity and more geological input than current inversion workflows to produce a geologically reasonable model.

Chapter 1 amendments

Amendments to Chapter 1 are listed here due to this chapter being previously published in Tectonophysics.

Page 40, paragraph 3: add "developing" and read "The difference between a single realisation, or 'best' model approach and developing multiple realisations from input data…"

Page 41, paragraph 2: delete "assist or retard", add "are pivotal" and read "Determining which data points are pivotal to the calculation…"

Page 44 paragraph 5: add "or geometry" and read "preconceived model topology or geometry…"

Page 52 paragraph 2: delete "an optimal" and replace with "the most likely".

Page 67 paragraph 1: add space between "depth" and "conversion"

1

Locating and quantifying geological uncertainty in three-dimensional models: Analysis of the Gippsland Basin, southeastern Australia

Mark D. Lindsay [a,b], Laurent Ailleres [a], Mark W. Jessell [b,c], Eric A. de Kemp [d], Peter Betts [a]

[a] School of Geosciences, Monash University, PO Box 28E, Victoria, 3800, Australia
[b] Université de Toulouse, UPS, (OMP), GET, 14 Av. Edouard Belin, F-31400, Toulouse, France
[c] IRD, GET, F-31400, Toulouse, France
[d] Geological Survey of Canada, 236-315 Booth St. Ottawa, Ontario, Canada K1A 0E9

Tectonophysics, 546-547 (2012) 10 - 27; doi:10.1016/j.tecto.2012.04.007

Abstract

Geological three-dimensional (3D) models are constructed to reliably represent a given geological target. The reliability of a model is heavily dependent on the input data and is sensitive to uncertainty. This study examines the uncertainty introduced by geological orientation data by producing a suite of implicit 3d models generated from orientation measurements subjected to uncertainty simulations. The resulting uncertainty associated with different regions of the geological model can be located, quantified and visualised, providing a useful method to assess model reliability. The method is tested on a natural geological setting in the Gippsland Basin, southeastern Australia, where modelled geological surfaces are assessed for uncertainty. The concept of stratigraphic variability is introduced and analysis of the input data is performed using two uncertainty visualisation methods. Uncertainty visualisation through stratigraphic variability is designed to convey the complex concept of 3D model uncertainty to the geoscientist in an effective manner. Uncertainty analysis determined that additional seismic information provides an effective means of con- straining modelled geology and reducing uncertainty in regions proximal to the seismic sections. Improve- ments to the reliability of high uncertainty regions achieved using information gathered from uncertainty visualisations are quantified in a comparative case study. Uncertainty in specific model locations is identified and attributed to possible disagreements between seismic and isopach data. Further improvements to and additional sources of data for the model are proposed based on this information. Finally, a method of introducing stratigraphic variability values as geological constraints for geophysical inversion is presented.

Keywords: Stratigraphic variability, Gippsland Basin, Implicit 3D modelling, Uncertainty grids, Model suite exploration, Structural geology

1. Introduction

The quality of three-dimensional (3D) representations of geology is measured by their ability to reliably reproduce the geometry and distribution of essential elements of a geological target. To do this a reliable 3D model needs to reconcile all available geological and geophysical data from a study area (Guillen et al., 2008; Jessell, 2001). Further it is fundamental that the model is able to simultaneously represent geology at the surface (where structural field observations may be more abundant) and at depth (where observations are inevitably less abundant). The quality of input data used to construct geological models, such as bedding, structural fabric orientations or lithological contact information, is intrinsically linked to the quality of the final product. Uncertainties contained within the input data for 3D model architecture can potentially reproduce unreliable geology. The aim of this is paper is to communicate a new method that as- sesses, locates and visualises the effects of data uncertainty.

Previous studies into the effects of data uncertainty involve methods that assess variability introduced by human or machine during data collection, processing (including data reduction during pro- ject upscaling) and interpretation (Bond et al., 2010; Bowden, 2007; Jones et al., 2004; Thore et al., 2002). The solution is often an attempt to reduce the effects of data uncertainty before its integration into the model. In contrast, the method described here follows recent contributions by Caumon et al. (2007), Jessell et al. (2010), Viard et al. (2010) and Wellmann et al. (2010) that assess the final 3D model for geological uncertainty. It is assumed that the input data contains uncertainty and this method does not attempt the difficult task of removing it prior to input. Instead the method provides an assessment of uncertainty after data input and includes a suite of possible 3D models that can be evaluated simultaneously.

The difference between a single realisation, or 'best' model approach and multiple realisations from input data is highlighted by Bond et al. (2010) as the difference between inexperienced and experienced geoscientists. A group of geoscientists of varying experience was asked to interpret a synthetic seismic section. The results of their efforts were assessed, including success in picking seismic horizons correctly, the content and quantity of discussion between candidates and the type

and quality of annotations added to interpretations. While better results from the more 'successful' candidates could be attributed to their experience in the geoscience field, it was also their experience that led them to acknowledge that finding the 'right answer' with the available information was unlikely. In fact, the assumption amongst the more successful subjects was the interpretation was likely to be incorrect, but with the available data it was the best that could be obtained. The low likelihood of finding the correct answer, or model, from sparse datasets is therefore not a revolutionary concept, rather is it a common assumption within the geosciences. Interestingly, and contrary to this understanding, input data is commonly used to create one optimised or 'best' model by modellers. This study argues that no 'best' model exists and that all members of the model suite are geologically possible. The key is to find the regions of difference between the models.

An interesting direction for this research is to measure data density effects on the model quality (e.g. Putz et al., 2006). Determining which data points assist or retard the calculation of reliable model structures can streamline data input. Further, this type of information can identify which points provide useful geometrical or geological constraints and can help delineate essential data input on this basis. While these effects could be studied using the technique present in this paper, downsampling data points would introduce additional experimental effects that are difficult to characterise within the scope of this introductory study. This research direction is a deserving subject for a separate paper, and is therefore not presented here.

The first section of this paper examines particular aspects of input data sensitivity, identified by Jessell et al. (2010), and uses techniques described in their contribution. It also examines the nature of geological input data and how it is used in 3D modelling applications by describing a method that visualises the location and magnitude of geological uncertainty through a 'geological perturbation' technique. Examples of this technique are provided with both simple and complex geological settings. Simple, synthetic models provide clear examples of how this technique can visualise geological uncertainty in 3D.

The second part of this paper examines a case study from the Gippsland Basin, southeastern Australia to display how this technique can be applied to a natural geological setting. The Gippsland Basin is an offshore geological environment displaying relatively complex geological fold and fault relationships within a mature oil and gas field environment. An assessment of un-

certainty is conducted on the Gippsland Basin model, and suggestions are made and carried out to improve model reliability. Analysis into the effects of additional input data is provided, as well as an explanation of how the technique can provide important information to guide field studies and aid the discovery of key localities. Lastly, a use for the data generated by the technique in geophysical inversion is proposed.

2. Geological uncertainty

The process of creating a 3D model begins with the collection of relevant data that will support the creation of a digital representation of geology. The types of data required are varied and the relative importance of each depends on scale (from mine scales to crustal scales), application and target. In practice, however, 3D model construction often suffers from a lack of geological information, independent of scale, due to sparse outcrop limiting field observations and inadequate borehole or geophysical data. This often means that all available data is utilised, regardless of original purpose, application or collection scale (Kaufmann and Martin, 2008; Royse, 2010). Interpretation of geology from geophysics may need to be performed prior to input into a 3D modelling package to better understand regions lacking geological observations, (e.g. Aitken and Betts, 2009). Determining whether the same lithological contact is continuous under cover or determining the morphology of a structure (Figure 1a) is a decision made using geological expertise and is often aided with the use of geophysical interpretation (Betts et al., 2003; Gunn et al.,1997; Joly et al., 2007).

Forward modelling of geophysical data is often part of 3D model construction workflows, aiding the constraint of geological surfaces in cross-section (Jessell, 2001). The price of using geophysical data to aid geological interpretation in the process of creating a 3D model is the introduction of a possible additional source of uncertainty. Geophysical data ambiguity is not a new issue and has been well covered since Nettleton (1942) began critically assessing the interpretations of his contemporaries. It was recognised in his and further studies that a number of possible outcomes could fit a particular geophysical data set and render any interpretation meaningless without the proper geological controls (Clark, 1983, 1997; Gunn, 1997). Endeavours to remove geophysical ambiguity from geophysical interpretation is a critical component of any related study and is usual-

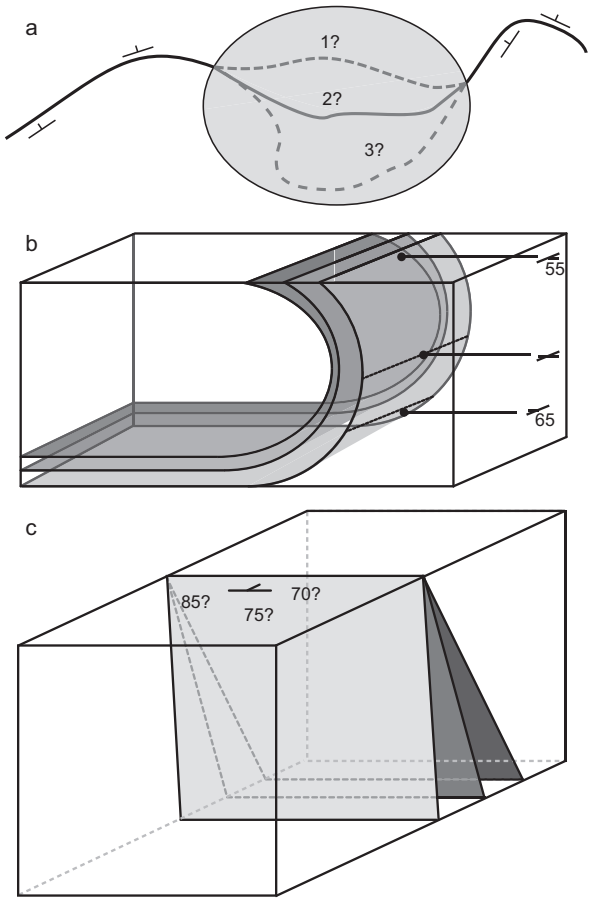

Figure 1. (a) Most geological mapping requires a degree of interpolation. In this example three possible options (though many more exist) are presented to the geologist, but only one will be recorded. This decision is made by the geologist, often with the benefit of prior knowledge and experience of the terrane. Unfortunately, the other possibilities are lost to others viewing the map, which may more accurately resemble the true geology.(b) Some geological measurements do not completely represent the observed surface. In this example of a recumbent fold limb, a dip measurement of 55˚ at the surface is reasonable, but fails to convey that the bedding dip angle changes to sub-vertical if taken at the first dashed line(fold axis) and eventually reverses with depth (second dashed line). This situation is also prevalent in poly-deformed terranes.(c) Weathered terranes often require an estimated measurement of a geological surface. When an estimated measurement is entered into a 3D model the resulting geometry can have compounding effects on the model, especially at depth. The location of a geological surface can vary considerably at depth even with a small measurement error at the surface.

ly performed, often with much effort, by collecting petrophysical data appropriate to the geophysical potential field being utilised (e.g. Joly et al., 2008; Nabighian et al., 2005; Williams et al., 2009).

Inherent uncertainty is not only confined to geophysical data. Uncertainty also needs to be considered when using geological data. Measurements taken when field mapping and drill-core logging are typically 3D observations recorded in a 2D (bedding contacts, fault plane, fold hinge or foliations) or 1D context (lineation or fold plunge). The uncertainty of these measurements and their interpretation can generally be associated with any of the following considerations (Jessell et al., 2010; Jones et al., 2004; Thore et al., 2002; Torvela and Bond, 2010; Wellmann et al., 2010):

• Does the observation represent the geological surface or vector at depth? It is possible

that the angle or strike/plunge of a structure varies from the surface measurement to that at depth (Figure 1b). Additionally, 3D models are often constructed at the regional scale using data collected in detailed field mapping. This requires the downsampling of data to a few 'representative' points that may fail to adequately represent the geological element.

• What impact does scale have on the modelled structures? Downsampling of data also has implications related to model scale. Orientation measurements used in the calculation of the implicit potential field and subsequent modelled geology may have been obtained from local geological structures, such as parasitic folds or fault splays. Uncertainty can be introduced if the local structure cannot be adequately resolved in detail when the model is calculated with regional scale parameters. The inverse is also true, where regional scale data (such as seismic or gravity) is used to generate small-scale structures.

• Are bedding contacts easily discernible? Determining the orientation of bedding planes requires a degree of estimation for both strike and dip if bedding contacts are not clear. For example some geological terranes are weathered to such a degree that confidence in the measurement is low. Any error in estimating the dip of these contacts can have problematic effects, as different orientations have increasing ranges of geometrical possibilities with increasing depth (Figure 1c).

• Do existing theoretical models affect input data? Current understanding and hypotheses concerning a particular geological terrane can oversimplify geological reality. Interpretations may underestimate the complexity of the geology. The resulting model may misrepresent the geology, resulting in an unreliable product. Again, the inverse is also true, where over-interpretation may result in a model that is too complex.

Field data may also be vulnerable to error if the modelling is not being performed by the field geologist. Critical knowledge of the terrane and knowledge of the reliability of measurements may be lost. Processes have been developed to reduce this effect by introducing workflows that encourage the field geologist to record levels of confidence in measurements (Jones et al., 2004). Normally, implicit knowledge of the terrane remains difficult to transfer to others as it is tacit knowledge (Jones et al., 2004; Polanyi, 1962). This includes knowledge of the interpretive and mapping skills of the geologist and a priori information that is taken into the field. Measurements may be taken with a particular preconceived model topology in mind resulting in biased observations being recorded.

3. Implicit 3D geological modelling

A requirement of the technique described here is to use an implicit 3D modelling application. The advantage of implicit modelling over other techniques (such as explicit techniques) is the speed at which models can be re-calculated with additional data to produce repeatable and objective results. Explicit modelling techniques require the operator to manually add vertices to construct geological structures. Some automated processes, such as Discrete Smooth Interpolation (DSI) (Mallet, 1992), are available to assist in creating geologically reasonable structures, but essentially the explicit methods require significant operator input to produce a feasible model. Consequently, a significant amount of time is required to produce each model and the results are not repeatable. Explicit techniques are not appropriate in terms of time and repeatability as many models are being produced from a single data set in this study. In contrast, implicit modelling features are beneficial to the method, allowing automated model calculation, rapid model realisation and repeatable results. An implicit geological modelling application, 3D Geomodeller (www.geomodeller.com), was chosen as the modelling and simulation platform for this study.

3D Geomodeller utilises the 'implicit potential field' method to construct geological interfaces as implicit surfaces (Lajaunie et al., 1997). In this context, 'potential field' describes a scalar function from which geology is generated. The objective is to model geological interfaces based on three principles: (i) geological interfaces define the contact between geological formations; (ii) structural field data orientations (i.e. strike and dip) sampled within geological formations are used to model the interfaces separating formations and (iii) all modelled interfaces are part of an infinite set of surfaces that are aligned with the orientation of the implicit potential field (Calcagno et al., 2008) (Figure 2a–c).

Certain requirements are needed for this form of modelling to take place. A stratigraphic column must be specified and formations within the column must have at least one location data point and one orientation data point before they can be calculated. Geology is calculated from the implicit potential field that is a scalar function $T(p)$ of any point $p = (x, y, z)$ within 3D space where T can represent a relevant geological process that can be assigned a numerical value (i.e. time of

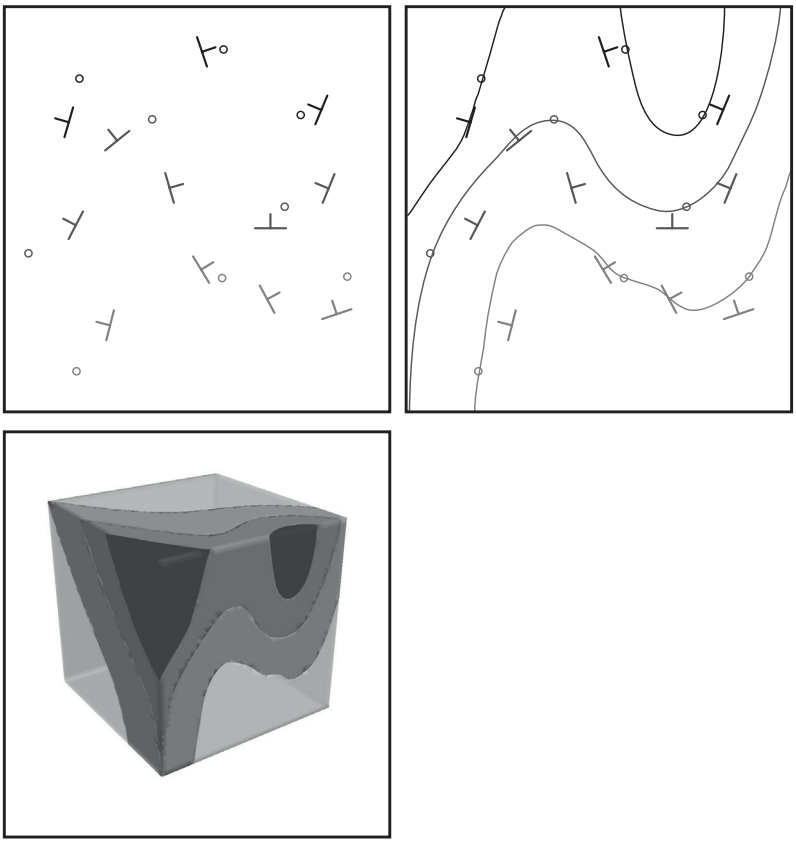

Figure 2. Example of creating a geological surface in an implicit modelling environment. 3D Geomodeller is used in this example. (a) Digitised geological map of three formations in black, dark grey and light grey. Outcrop points are depicted as circles, dip and strike are depicted with the standard convention. (b) Interpolated geological map determined by the potential field method. The solid lines represent contacts between the three formations. Note how both contact and orientation (strike and dip) points are honoured to produce an antiform–synform pair. (c) 3D representation of the input data.

deposition or geological age). The implicit potential field is an isosurface of the scalar field, and a geological contact can be considered to be where reference isovalues change from one lithology to another. The implicit potential field is interpolated from cokriging of the geological contact (contact location) and orientation (contact geometry) data and allows the determination of geological interfaces that honour the input data (Lajaunie et al., 1997).

The stratigraphic column defines the geological units being modelled, which can then be sorted into geological 'series' to represent a group of geological formations (Figure 3a). Each series has an implicit potential field calculated separately to the others. The interaction each series and implicit potential field has with other series and implicit potential fields is defined by its chronological position and behaviour exhibited with respect to older formations. Behaviour is set as either an 'erode' relationship, where older units are cross-cut or truncated, or 'onlap' where a series is allowed to be present if space permits without modification of the underlying older series (Calcagno et al., 2008). Each geological unit has a numerical attribute, that allows identification of the strati-

graphic unit (Figure 3a) at a given X, Y, Z co-ordinate. Faults are interpolated in a similar manner to lithologies. Fault-specific orientation data defines the fault dip and fault trace data points define fault location. The age of a fault is defined in two ways: (i) by interactions between faults and geological units (Figure 3b) and (ii) faults and other faults (Figure 3c). A fault may only affect some units in the stratigraphic column and can also terminate on another fault.

Model topology is defined by assigning both chronological and relationship parameters between geological units and faults in the model. The chosen topology is probably only one of multiple possible versions that exist for the terrane under study, so the choice of relationships becomes a subjective decision made by the geologist. Unfortunately, multiple topologies cannot be explored simultaneously at this stage, but by changing these relationships manually and re-calculating the model, different topologies can be realised to test various scientific hypotheses for geological feasibility.

a

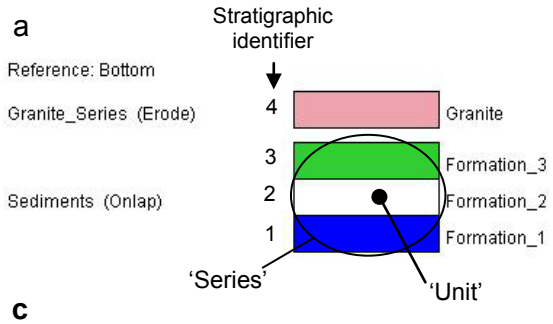

b

	Fault 1	Fault 2	Fault 3
Granite		✓	
Sediments	✓	✓	✓

c

Stops on	Fault 1	Fault 2	Fault 3
Fault 1		✓	
Fault 2			
Fault 3	✓	✓	

Figure 3. Example of possible relationships between different geological elements. (a) Stratigraphy showing three conformable ('onlap') sedimentary units in one series that are cross-cut ('erode') by a younger granite unit. Note how the numerical attribute is assigned in ascending geochronological order. (b) Fault–stratigraphy relationship matrix defining which series are faulted by which fault. This matrix shows that Fault 2 must be a late fault as it affects all series defined in the pile (and therefore younger the Faults 1 and 3 which only affect the older 'Sediments' series). Faults 1 and 3 must be older than the granite, but younger than the sediments. (c) Fault–fault relationship matrix defining how faults 'stop on' or are cross-cut by other faults. This matrix only describes geometrical relationships between faults and not necessarily their relative ages.

4. Method

Rather than attempt to remove uncertainty from the input data, this paper assumes that the input data contains uncertainty and attempts to simulate its effects through 'geological perturbation'. Perturbing a set of structural field measurements allows different model possibilities to be generated and assessed. This 'geological perturbation' method attempts to simulate uncertainty by randomly adjusting observed strike and dip measurements within a range of 10° to produce a suite of 'what-if?' scenarios. This process is analogous to an 'en-masse' field mapping survey by a large number of geologists. The maps produced by the end of the survey all tend to look similar, but differ slightly in various ways due to geological uncertainty. In addition, the geologists may have focussed on some areas more than others or taken measurements from different fabrics at the same outcrop. The benefit is that collectively these maps may produce interpretations that change our geological understanding of the study area.

4.1. Calculating, quantifying and visualising model uncertainty

By adjusting strike and dip values of the input orientation data we can reveal the location and magnitude of uncertainty contained within the model. We define uncertain regions as those where the location, morphology or orientation of geological structures are different between models. Geological structures that can vary include fault surfaces, folds or lithological contacts in terms of their geometry, orientation, scale, shape and position. It is considered that an increase in uncertainty is inversely proportional to the reliability of the model, so it is critical to understand where these regions are. Uncertainty information can be used to aid subsequent data collection activities to further constrain the model and increase reliability.

The visualisation and processing of uncertainty data is achieved by calculating a 3D uncertainty grid: a record of stratigraphic units found at discrete locations within each model, calculated from perturbed measurements. Locations within each model are described within the grid by an X, Y and Z reference. Once processing has been performed, a function describing stratigraphic variability is used as a proxy for uncertainty during visualisation and is assigned to the appropriate location.

4.2. Procedure

Four steps are required to produce, process and visualise an uncertainty grid.

A. Construction of 3D model

The process begins with the construction of a reference model, normally the final product in most workflows. All available and relevant data should be used to produce this model. Critical to this technique is that strike and dip orientation data is used as: (i) they are required by the implicit potential field technique and (ii) they are the components that are perturbed to allow varied models to be calculated.

B. Variation of geological orientation data

The model is perturbed by varying the input orientation data strike and dip measurements (related to foliations and faults) by ± 5° from original reference model measurements. Five degrees was chosen as a reasonable amount of variation that may be observed between measurements taken by different geologists, especially in weathered, covered or highly-deformed terranes where the relationship between larger and smaller scale structures is not clear. A stereoplot comparison of synthetic and varied measurements is shown in Figure 4. Any number of perturbations can be calculated and is restricted only by the power and storage space of the computing platform. In this study, each model suite contains 100 perturbed models and the reference model (101 models in total).

C. Calculation of model suite and model interrogation

Each perturbed model is re-interpolated using the implicit potential field method to accommodate the new, varied orientation input data (Figure 5). Next, each model is interrogated to collect stratigraphic data at specified *X, Y* and *Z* axis intervals. The interrogation process is performed within a given set of parameters along each axis (in UTM projection metre units): an initial co-ordinate (*X*, *Y*, *Z*); a final co-ordinate (*X'*, *Y'*, *Z'*) and a sampling frequency (X_n, Y_n and Z_n). The sample interval along each axis can then be determined and the cell size of the uncertainty cube can be defined (X_s, Y_s, Z_s) (1). If required, volume and area of a particular formation or uncertainty region within the model can be determined, within the constraints of the cell size.

$$[X_s\ Y_s\ Z_s] = \frac{([X'\ Y'\ Z'] - [X\ Y\ Z])}{[X_n\ Y_n\ Z_n]} \quad (1)$$

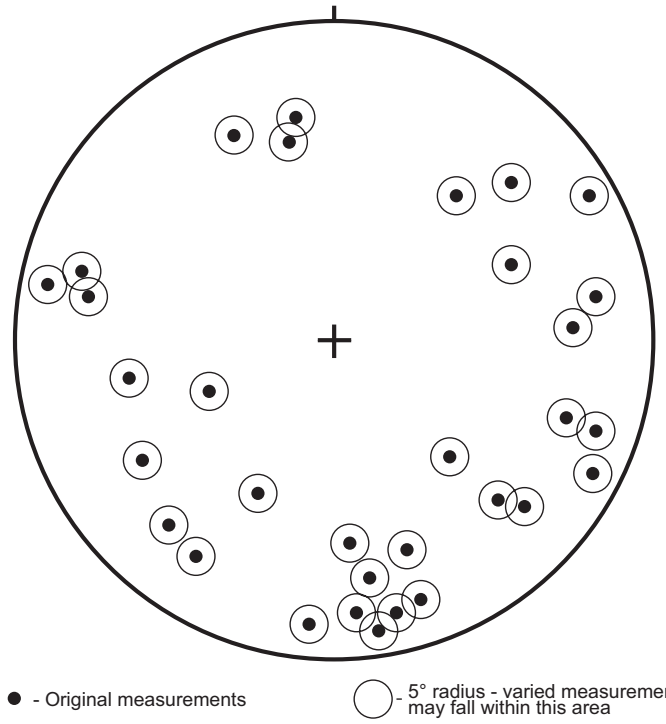

Figure 4. Stereonet plot comparison of original, or initial, measurements and a five degree zone of possibility circling each original measurement. The zone indicates where varied measurements may be plotted after being subjected to uncertainty simulation.

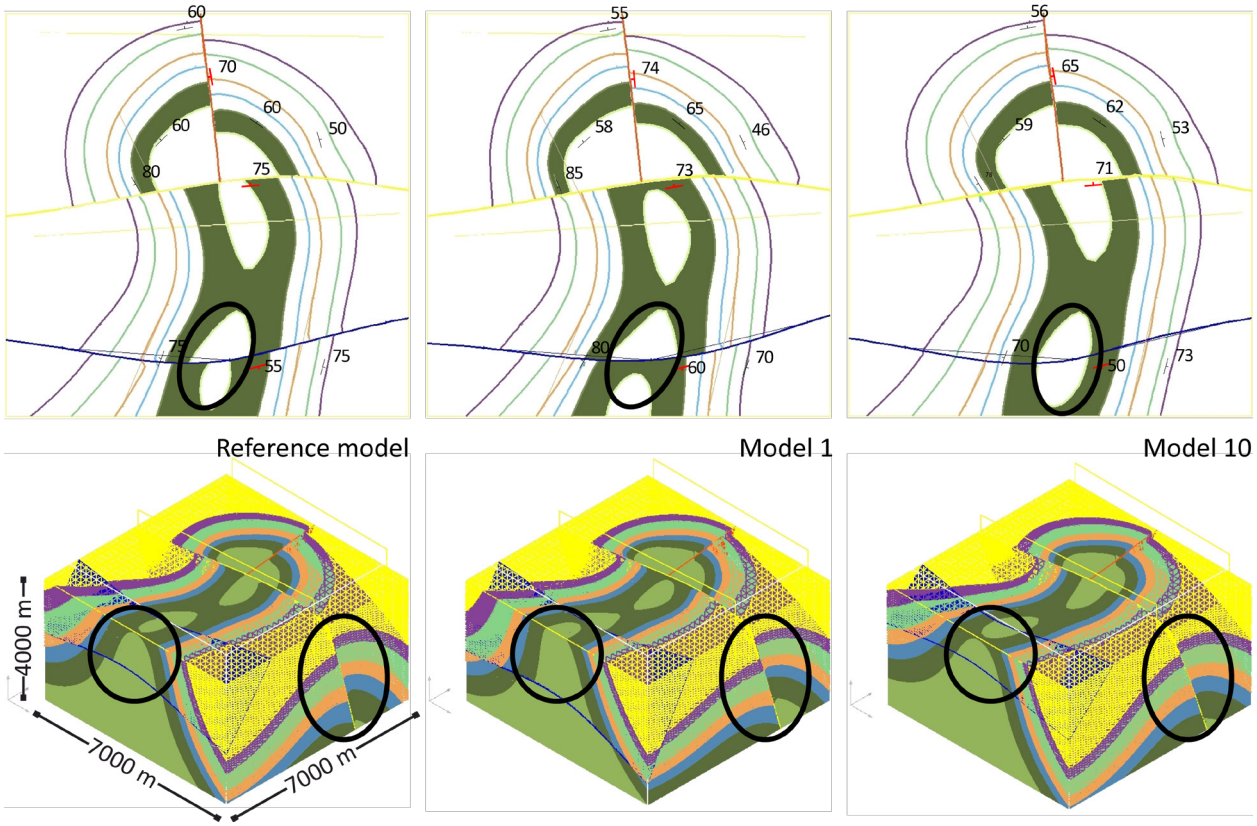

Figure 5. Three synthetic models constructed from a perturbed data set. The 'Reference model' contains the original strike and dip observations. The top row of images shows a surface map view of the geology interpolated by a potential field method (Section 3 and Fig. 2a–c). The bottom row of images shows an oblique view of the corresponding 3D block models. The black circles show regions of noteworthy difference between each model on both map and block diagram views. The most important differences are associated with faulting structures.

The process is able to determine a stratigraphic unit within the model at each sample location (Figure 6). The detected stratigraphic unit is returned as a simple integer, the value of which represents its relative location within the stratigraphic column (the 'stratigraphic identifier' or stratigraphic ID — see Figure 3a). A value of "1" represents the 'basement' or base formation, with values increasing with each successive overlying formation. The next model is interpolated and the interrogation process is repeated using the same sampling parameters with the results concatenated to the uncertainty grid. The process is repeated for the remaining model perturbations. The result is a grid of stratigraphic units describing a sample of each individual model (Table 1).

D. Quantification of uncertainty cube using stratigraphic variability. Visualisation of model uncertainty is now possible by importing the uncertainty grid into a 3D visualisation package. This technique uses Gocad® for this purpose. Locations that show different possible stratigraphic units can be identified by making manual comparisons between each model perturbation, but doing so in this qualitative manner is time-consuming and difficult. A quantitative approach is more time effective, easier and offers more information about the magnitude and variability of uncertainty. The concept of stratigraphic variability has been developed to meet this requirement. Stratigraphic variability is intended to serve a dual purpose by describing model uncertainty spatially and useful for further analysis by providing a value that is statistically valid.

In a simple sedimentary sequence the stratigraphic unit identifiers could be considered ordinal data, with each number representing the relative position of each stratigraphic unit. Ordi-

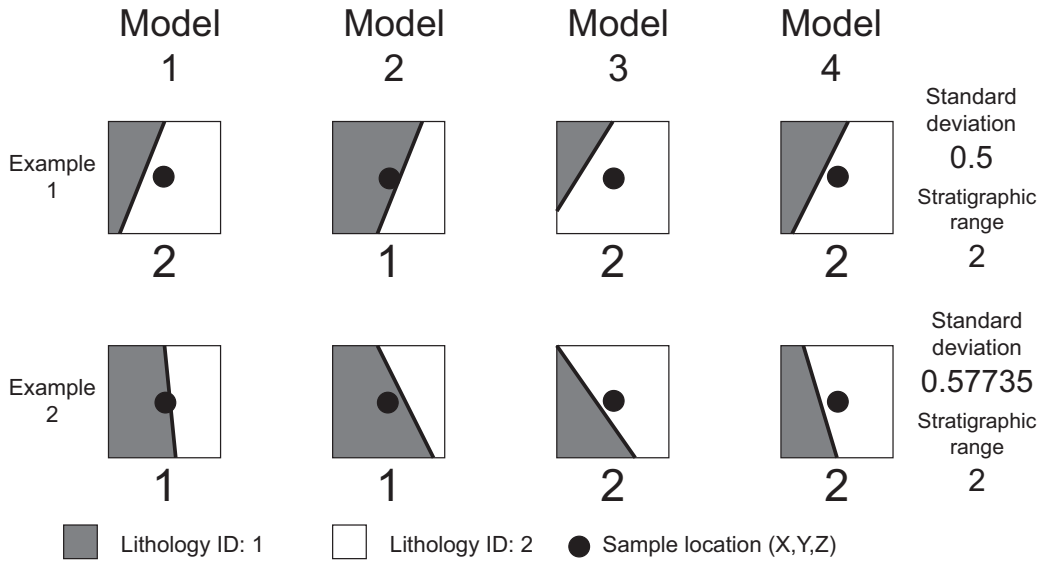

Figure 6. Example of model uncertainty. Here a standard deviation is used as a relative measure of variability and stratigraphic range (L) refers to number of possible stratigraphic units detected by this technique at this location.

Table 1. Sample of the uncertainty grid. Coordinates of the sample location are given on the left-hand side, the results are given on the right-hand side of the table. In the model columns, 'Ref' refers to the reference model and '1,2,3,4…' etc. refer to successive model perturbations.

Coordinates			Model										
X	*Y*	*Z*	Ref	1	2	3	4	5	6	7	8	...	*n*
492630	5731250	-3000	8	8	8	7	8	8	8	8	8	···	8
492630	5731250	-3500	7	7	7	7	7	7	7	7	7	···	7
492630	5731250	-4000	7	7	7	7	7	7	3	7	7	···	7
492630	5731250	-4500	3	3	3	3	3	3	3	3	3	···	3
492630	5731250	-5000	3	3	3	3	3	3	3	3	3	···	3
492630	5731250	-5500	6	3	3	6	3	3	6	3	3	···	3
492630	5731250	-6000	5	5	5	5	3	5	5	5	3	···	5
492630	5731250	-6500	5	5	5	5	3	5	5	5	3	···	5
492630	5731250	-7000	4	4	4	4	4	4	4	4	3	···	4

nal data requires that the number set is ranked, or ordered, so that appropriate statistical treatment can be applied. The presence of igneous units, such as a granitoid, complicates this definition. The depth location of younger granitoids within an older sedimentary sequence can violate the definition of ordinal data where the granitoid cross-cuts or intrudes older units. In other words, the units are not ranked from oldest (basement) to youngest (cover) everywhere in the model if units are intruded or cross-cut by younger granitoids at depth, and therefore can no longer be treated as ordinal data. The number sequence is no longer ordered if based on stratigraphy and the assigned geological evolution of the model. The technique treats the sampled data in this technique as categorical to avoid using inappropriate statistical measures.

Each number represents a description of an individual stratigraphic unit, and not a relative position, so categorical values can only be treated in a limited number of ways as compared to continuous or ratio data types (Agresti, 2007; Davis, 2002). Data descriptors such as mean and standard deviation, while yielding results, are meaningless when generated from categorical data and are only useful when indicating relative magnitudes of uncertainty. However, the mode of the generated data does produce values that adequately describe both an optimal model and proportions representing variation.

Stratigraphic variability is composed of two separate values (2). The first represents the number of possible stratigraphic units (L) that exist at a given point. Only the stratigraphic units that exist at that point (i.e. the unique values) are counted. For example, if stratigraphic units '1', '2', '4' and '7' were sampled from a location then L has a value of 4.

$$L = |S|$$
$$S = \{I_1, I_2, ...I_n\} \quad (2)$$

where I is a unique number within set S. S is a set of integers representing all possible stratigraphic units, at a given point, within the nth model of the model suite.

The number of stratigraphic possibilities by itself does not completely describe uncertainty data as it does not accommodate the frequency of variation possible at each location. The second part of stratigraphic variability determines the degree of frequency, P. P is calculated by determining the proportion of models that do not equal the mode stratigraphic unit, at a particular location, across the model suite (3).

$$P = \frac{|X \neq Mode(S)|}{|M|} \quad (3)$$

where X is a model location with an associated stratigraphic unit and M is the model suite. The 'mode stratigraphic unit' is the most common stratigraphic unit across the model suite for a particular X, Y, Z-defined location. For example, if at location X: 590,000, Y: 610,000 and Z: - 4500 the distribution of detected stratigraphic units across 100 models was Unit 1: 5, Unit 2: 55, Unit 3: 23 and Unit 4: 17, the stratigraphic mode unit would be 'Unit 2' (55 occurrences). The mode stratigraphic unit is not the stratigraphic unit that is detected from the initial model.

For example, suppose the mode stratigraphic unit for a given location in the model suite is '4'. A P value of 0.07 would indicate that 93% of the models in the model suite also exhibit the same stratigraphic unit ('4') and 7% differ from '4' at that location. This method uses a percentage differing from the mode for two reasons: (i) this information describes the frequency of variability between models and (ii) it also provides a value that increases with variability, creating a difference between locations where L is equal, but the stratigraphic variability differs. Figure 7 shows a sample from an uncertainty cube generated from Gippsland Basin data demonstrating why both L

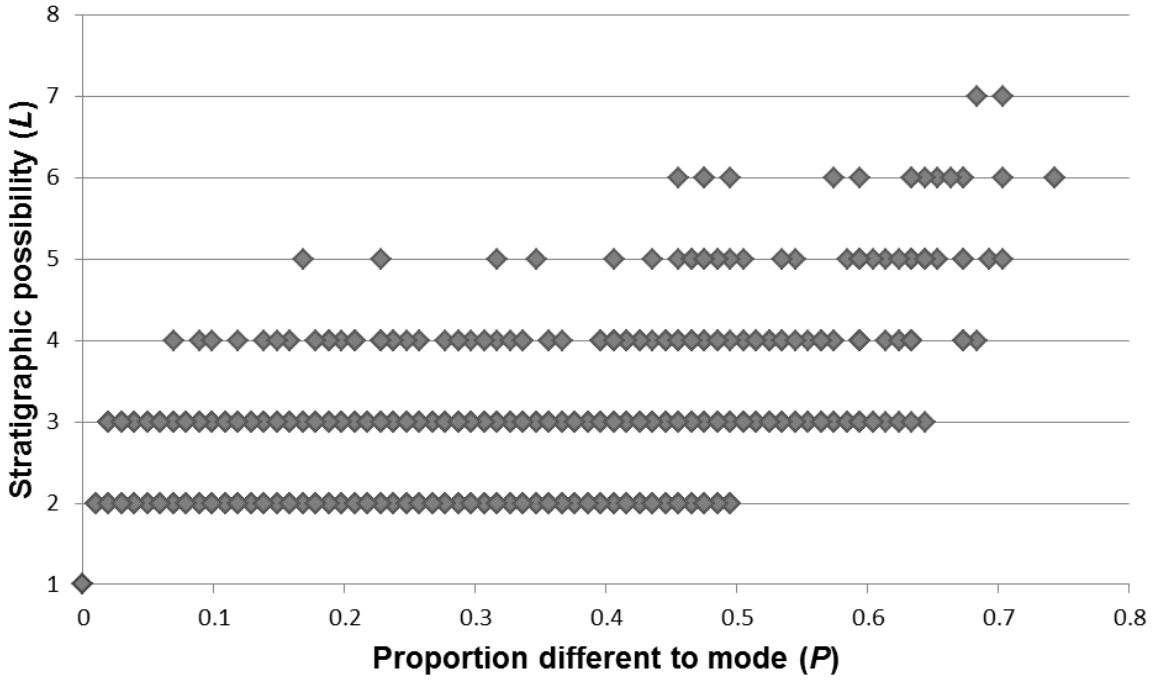

Figure 7. Plot of *P* versus *L* values, sampled from 15,890 Gippsland Basin data locations. A positive trend is observed, but no correlation (R^2 = 0.082). It is clear that both stratigraphic possibility and mode proportion need to be included for the property to be useful as they represent different aspects of uncertainty. For example, an *L* value of '*4*' yields *P* values between 0.170 and 0.683. Both locations show 4 stratigraphic possibilities and but differ greatly in the amount of variability. Note that the point at (0,1) represents all locations displaying no uncertainty (no difference to the mode and only one stratigraphic possibility).

and *P* values are required. It shows that *L* and *P* values, for a given location, display a loose trend of increasing proportions different to the mode with increasing stratigraphic possibility. There is a degree of variability present, especially for lower magnitudes of stratigraphic possibility. Therefore the property needs to accommodate the amount of lithological variation observed across the model suite for a given location to adequately describe the associated uncertainty. As *L* represents the number of possible stratigraphic units detected at a given location across the model suite, the number of stratigraphic units defined in the stratigraphic pile should also be considered. For example, *L* = 4 indicates relatively less uncertainty in a stratigraphic pile of 20 units than a pile with five units. *L* can be normalised by the total number of stratigraphic units defined in the pile for the purposes of comparing model suites based on different stratigraphic piles. The pre-normalised value is kept intact for this study to retain the explicit description of stratigraphic possibilities.

Uncertainty can be described in better detail if both *L* and *P* values are used. For example, values *L* = 3 and *P* = 0.14 describe a location within the model suite where three different stratigraphic units have been detected and 86% of the models displayed the same stratigraphic unit as model suite mode for that location. These values indicate a moderate level of uncertainty in this

location as there are three stratigraphic possibilities, but most of the values represent the mode. In contrast, L = 6 and P = 0.37 indicate a relatively high level of uncertainty, as there are six possible stratigraphic units and only 63% of models display the model suite mode value for that location. The benefit of using both values allows us to delineate regions with a particular L value according to P, revealing more detail about the spatial characteristics of model uncertainty. Using L and P values separately or in combination aids visualisation and model queries. Thresholds can be using either L or P values assigned to colour maps or used in voxet generation to better describe model uncertainty to the operator.

5. Methods of visualisation

Visualisation of stratigraphic variability as a proxy for uncertainty reveals important aspects of the 3D model and input data. Uncertain regions can be easily located and identification of particular uncertain geological components of the model can be performed. A coincident representation of uncertainty has been chosen, where both modelled geology and associated uncertainty are displayed simultaneously (MacEachren et al., 1998). Different aspects of uncertainty can be revealed using either point data or voxet volumes. Voxets are a set of regularly-spaced voxels (or volume elements) that present data as volumes, rather than as polygons. Wellmann and Regenauer-Lieb (2011) use a similar voxet-based method where information entropy values are assigned to individual voxels. The information entropy property displays the amount of information that is missing from each location, restricting the full prediction of the system.

Magnitude of uncertainty is useful to identify particular uncertain components of the model. In Figure 8a–c we have assigned a blue-white-green-yellow-red colour map to stratigraphic variability values. Low uncertainty is associated with the blue points and high uncertainty with the red points. The location and magnitude of model uncertainty quickly become evident. Points displaying no uncertainty have been made transparent to aid visualisation. High uncertainty is associated with the fault intersections of the northern east–west thrust fault and the north–south thrust fault. L values of five and six have been calculated in this region, particularly at depth. These regions represent the highest geological variability across this model suite. This can be explained by the combined effects of three attributes, fault displacement, fault orientation constraints and bed-

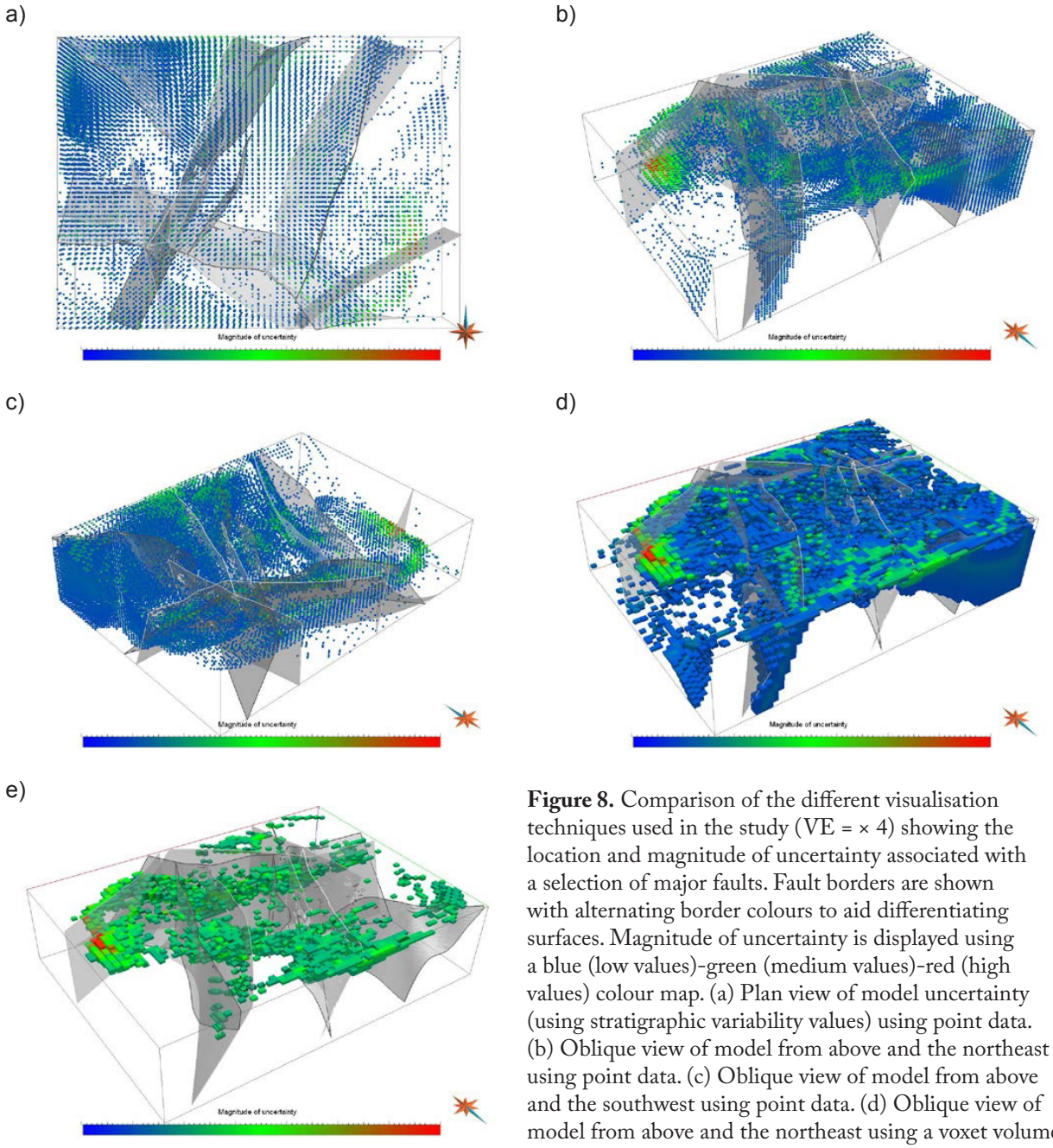

Figure 8. Comparison of the different visualisation techniques used in the study (VE = × 4) showing the location and magnitude of uncertainty associated with a selection of major faults. Fault borders are shown with alternating border colours to aid differentiating surfaces. Magnitude of uncertainty is displayed using a blue (low values)-green (medium values)-red (high values) colour map. (a) Plan view of model uncertainty (using stratigraphic variability values) using point data. (b) Oblique view of model from above and the northeast using point data. (c) Oblique view of model from above and the southwest using point data. (d) Oblique view of model from above and the northeast using a voxet volume to show stratigraphic variability values, excluding the first 25 percentiles. (e) Oblique view of model from above and the northeast all cells with an *L* value = 2.

ding orientation constraints. Variation in stratigraphic displacement across the fault plane allows more lithological variation as the fault plane orientation changes between models. Each modelled fault is described by one fault orientation measurement. No other measurements assist constraint of the fault surfaces, so when the fault orientation measurements are varied, the fault plane orientation varies freely. Bedding orientation measurements also affect the geometry of bedding surface intersection with the fault surface. Each lithology is defined by limited orientation measurements, therefore a high degree of orientation variation is allowed. The combined effects of sparse data, as-

sociated with fault and bedding orientation parameters, have produced a region of high uncertainty.

Uncertainty volumes can be calculated to describe the model, a procedure similar to resource volume calculations (Figure 8d–e) (see Singer and Menzie, 2010). Volume calculations can help identify areas of high uncertainty similar to the point data technique described above, but are also useful to compare different sets of input data according to uncertainty volume. One application of this technique is to measure how model uncertainty changes with additional orientation measurements.

6. Uncertainty in the Gippsland Basin

The Gippsland Basin in southeastern Australia has been used as a case study to demonstrate the utility of determining, quantifying and assessing 3D model uncertainty. During construction of this model (Figure 9a–b) it was found that additional information was needed to reduce uncertainty located in certain regions. Two model suites are presented, Case Study A and Case Study B. Both model suites were constructed using information provided by Geoscience Victoria (Department of Primary Industries) and Geoscience Australia. Case Study A was constructed using all information and only the interpreted seismic sections K–S taken from the interpretation of Moore and Wong (2002). Case Study B uses the same input data, but includes all available seismic section information from the Moore and Wong (2002) study (seismic sections K–S and A–J). The results show how additional information can reduce uncertainty and serves to improve model reliability.

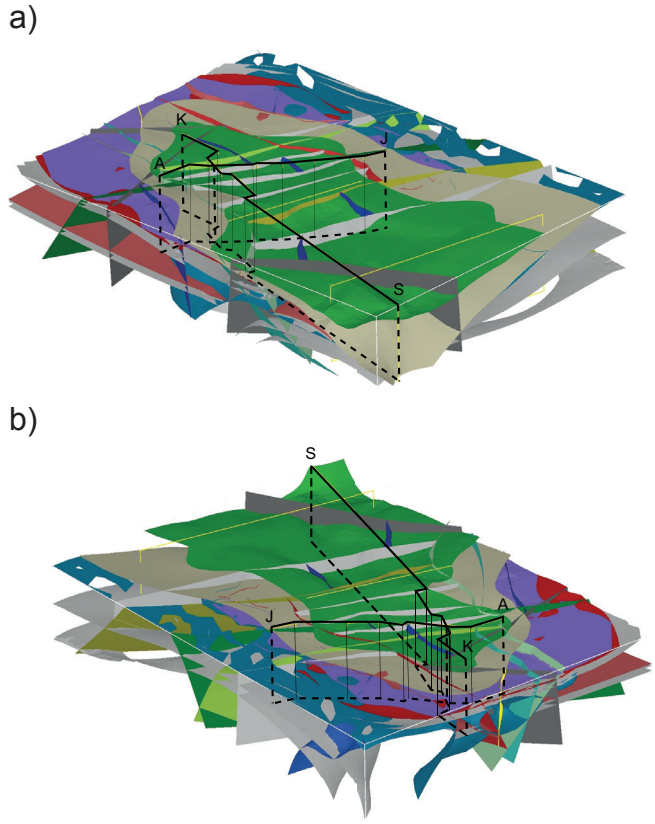

Figure 9. 3D block diagram of the Gippsland Basin, viewed from the southeast (a) and northwest (b). These images show surfaces rather than volumes so aspects of the model architecture can be more easily viewed. Locations of seismic sections A–J and K–S used in model construction are shown.

The models created in the A and B case studies are a simplification of what could be modelled and only major stratigraphic units and faults have been included. We suggest that presenting low fidelity models provides a more effective method in which to display our technique. The geology is therefore described in terms of what has been input into the model, and does not include every possible unit observed in the Gippsland Basin region. The input stratigraphic unit descriptions, relationships and adaption for model input are shown in Figure 10. The fault networks have been defined according to fault relationships described in the following section.

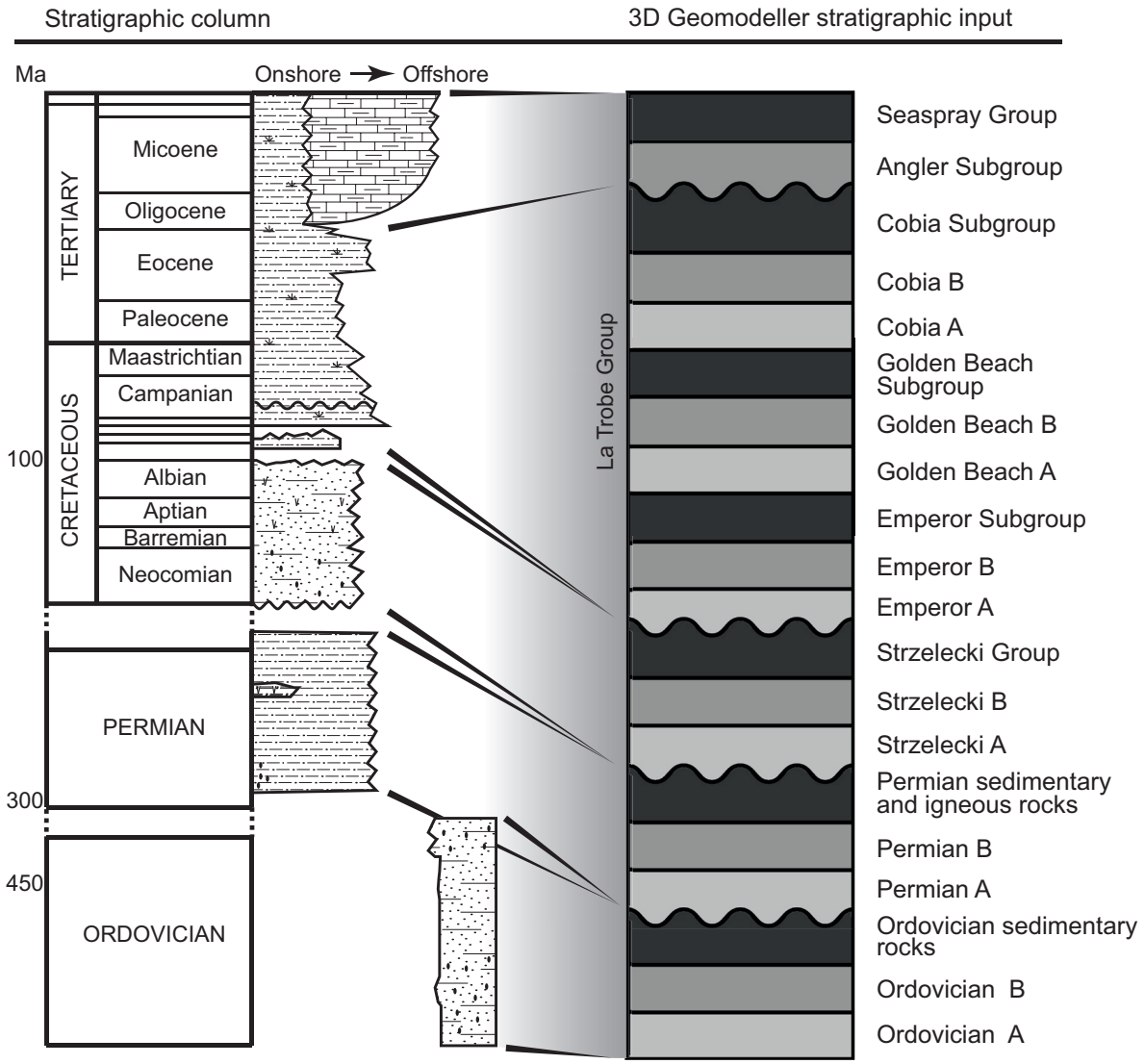

Figure 10. Gippsland Basin stratigraphic column (adapted from Moore and Wong (2002)) correlated to 3D Geomodeller stratigraphic input. Units with the suffix 'A' and 'B' have been added to increase stratigraphic resolution (Section 6.2.1).

6.1. Background geology

The Mesozoic to Cenozoic Gippsland Basin is a mature oil and gas field located in south-eastern Australia that hosts brown coal deposits and is prospective for CO2 sequestration (Cook, 2006; Rahmanian et al., 1990). The basin extends from an onshore setting around Western Port Bay offshore into Bass Strait and includes the Melbourne, Bass, Tabberabbera, Kuark and Mallacoota Zones of the Palaeozoic Lachlan Fold Belt (LFB) (Willman et al., 2002). The 80 km by 400 km depocentre trends asymmetrically east–southeast and is underlain by Palaeozoic basement (Moore and Wong, 2002; Rahmanian et al., 1990).

The basement unit for these models is labelled as Ordovician sediments, a collection of various units forming the same basement in the seismic interpretation of Moore and Wong (2002). Overlying the basement unit is the Permian sediments and igneous unit series, a representation of various Permian and Jurassic sedimentary and igneous units (Schmidt and McDougall, 1977).

Sedimentation during the Cretaceous resulted two in distinct units, the volcaniclastic Strzelecki Group, generally regarded as economic basement (Haq et al., 1987), and the lacustrine and marginalmarine quartose-derived Latrobe Group (Moore and Wong, 2002; Veevers, 1986; Veevers et al., 1991). The Latrobe Group is the primary target for oil and gas (Rahmanian et al., 1990) and comprises the Em-peror, Golden Beach and Cobia Subgroups (Bernecker and Partridge, 2001; Moore and Wong, 2002). The Emperor Subgroup lacustrine sediment deposition was primarily controlled by early rift-related north–east trending faults over the northern and central parts of the basin (Bernecker et al., 2001; Smith et al., 2000). The western edge of the Cobia Subgroup is considered to be bounded by the Wron Wron Fault System (Moore and Wong, 2002). The Seaspray Group and the Angler Subgroup resulted from further thermal subsidence and marine transgression during the Oligocene (Holdgate et al., 2002; Mitchell et al., 2007). The Angler subgroup forms the base of the Seaspray Group and is characterised by calcareous mudstones and marls (Gallagher et al., 2001).

Moore and Wong (2002) describe the complex fault interactions in the Gippsland Basin as sets of older, straighter basement faults with similar orientations displaced by younger faults with varied orientations. The relationship between basement and younger faults is attributed to a

competency contrast between the more rigid basement and softer overlying basin sediments. Two regions of young faults can be observed. The north and west fault sets typically trend northeast–southwest and exhibit steeper dip angles and may have been active as late as the Late Oligocene to Early Miocene. The western faults trend east to west and show possible Quaternary reactivation (Gray and Foster, 1998).

6.2. Input data

The input data used to construct the Gippsland Basin models were taken from the sources listed in Table 2 and shown in Figure 11. Seismic data was acquired through a combination of Geoscience Australia and company surveys, including those from Esso, Petrofina and Shell. The average internal velocities used to processing the data were: sea water (1480 ms^{-1}); Seaspray Group (2800 ms^{-1}), Latrobe Group (3400 ms^{-1}), Golden Beach/Emperor/Cobia Subgroups (3900 ms^{-1}) and Strzelecki Group (3900 ms^{-1}). A combination of well ties (listed above each well location in Figure 12) and breaks in seismic property was used to identify seismic reflectors. The seismic interpretations shown in Figure 12 were digitised from Moore and Wong (2002). Sections A–J were not included in Case Study A, but were included in Case Study B in the attempt to improve model reliability after uncertainty assessment was performed. Geophysical potential field interpretation was performed to identify faults. Both gravity and magnetic data sets were used in combination to identify steep gradients in the geophysical response (Figure 13). Steep geophysical gradients suggest a rapid change in geophysical character perpendicular to the gradient direction and can infer the presence of a geological interface (Clark, 1997; Grant, 1985). Isopach and bathymetry data was used to create datasets of 3D interface points to aid the interpolation of the top of the Seaspray, Latrobe and Strzelecki groups and the Ordovician sedimentary successions (Figure 11). Isopach data was supplied by Geoscience Victoria. A large proportion of input geological orientation data was interpreted from both geophysical potential field interpretation and seismic section. Mapped onshore outcrop information was used in input data; offshore geology was more difficult to constrain and required the use of isopach and bathymetry data combined with seismic interpretation.

6.2.1. Improving the detection of model uncertainty

There are circumstances where uncertain fault surfaces (i.e. poorly constrained fault sur-

Table 2. Input data, purpose and sources.

Data	Purpose	Source
Geophysics – Aeromagnetics and gravity	Geological interpretation of faults	Geoscience Australia
Geophysics – 2D seismic	Geological interpretation of faults and stratigraphy	Geoscience Victoria – Department of Primary Industries
Isopach maps	Constraints for stratigraphic horizons	Geoscience Victoria – Department of Primary Industries
Bathmetry observations	Constraints for stratigraphic horizons	Geoscience Australia
Geological maps	Constraints for onshore outcrop geology Stratigraphic column	Geoscience Victoria – Department of Primary Industries
Stratigraphy	Development of stratigraphic pile	Literature (see references listed in section 5.1

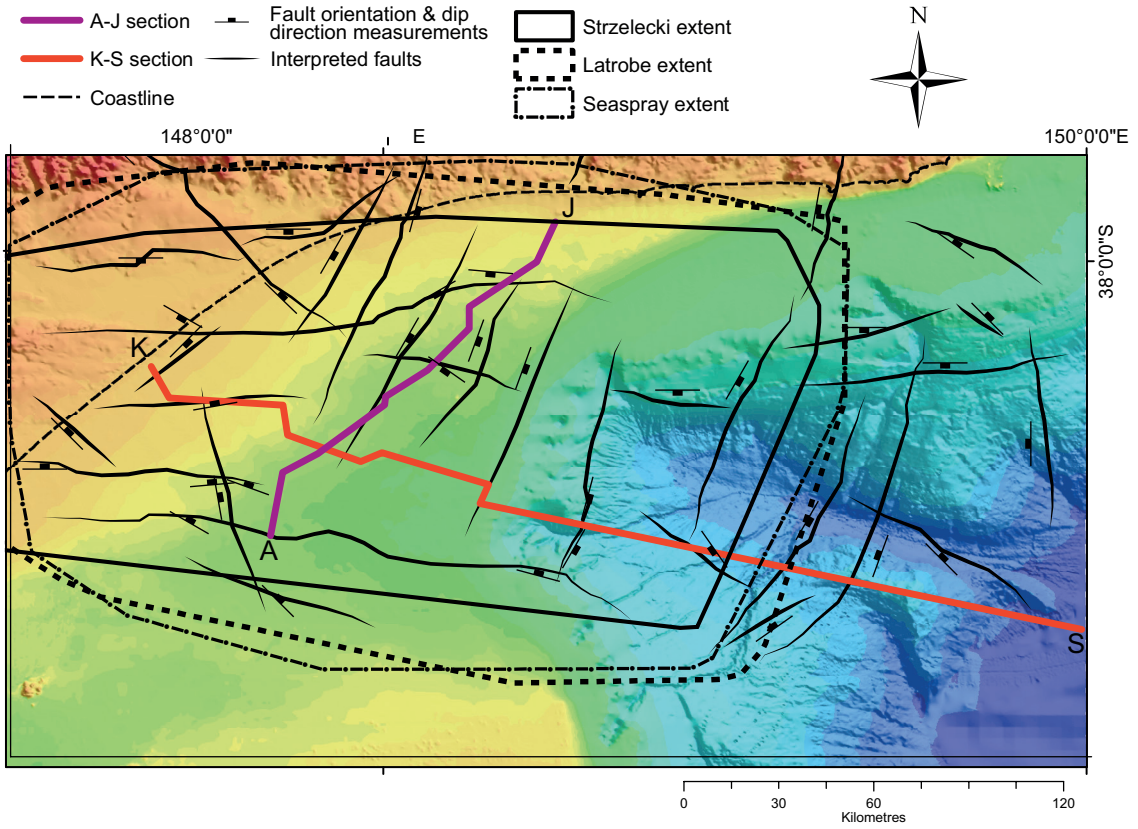

Figures 11. Location and distribution of input data. Fault and dips interpreted from potential field data (Figure 13) are overlain on gridded bathymetry data. The extents of isopach information, depicting the tops of three major stratigraphic formations are outlined. Location of seismic sections A–J and K–S are shown blue and red respectively.

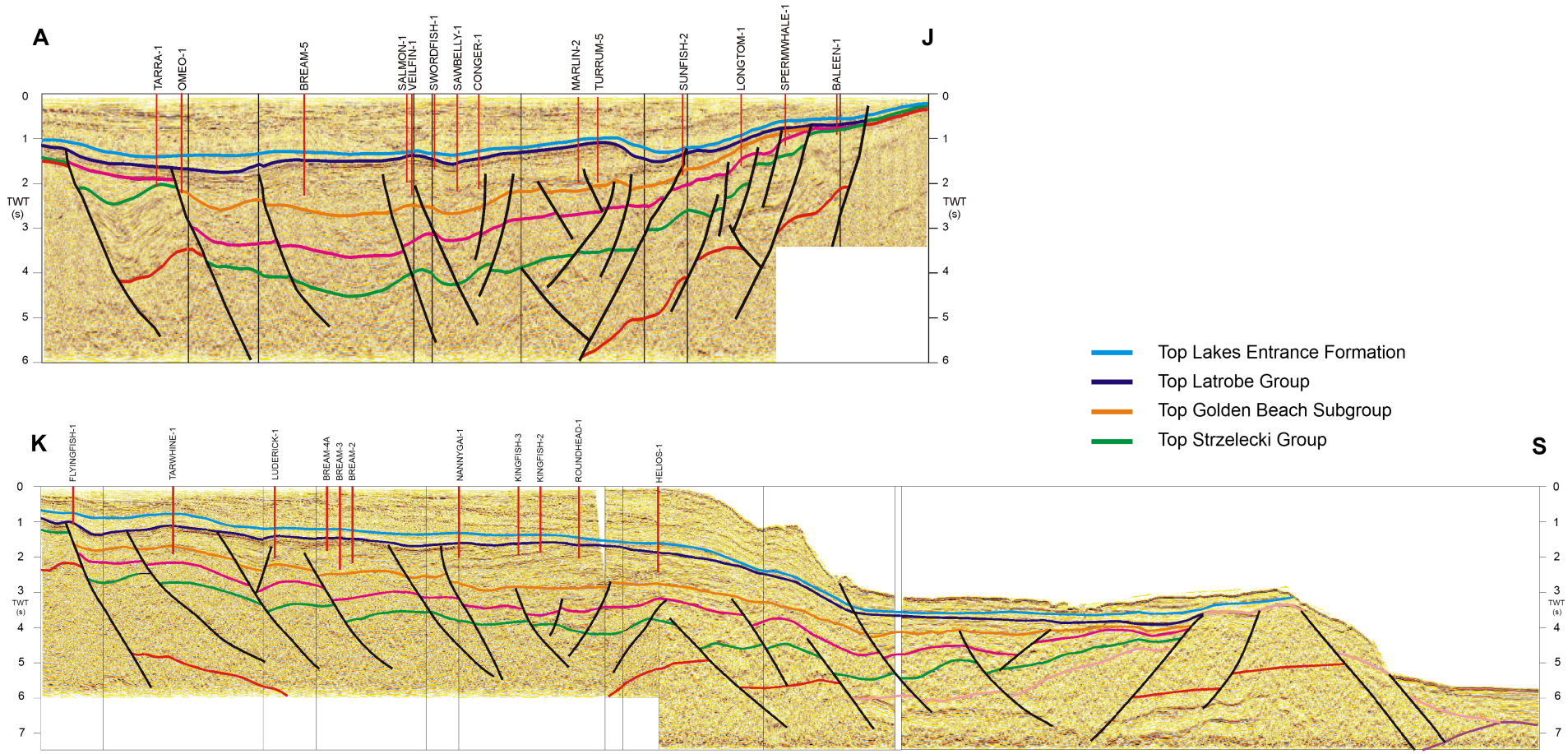

Figure 12. Interpreted seismic sections A-J (top) and K-S (bottom) used as input data for the Gippsland Basin case study. Interpretation was performed by the Department of Natural Resources and Environment. Adapted from Moore and Wong (2002).

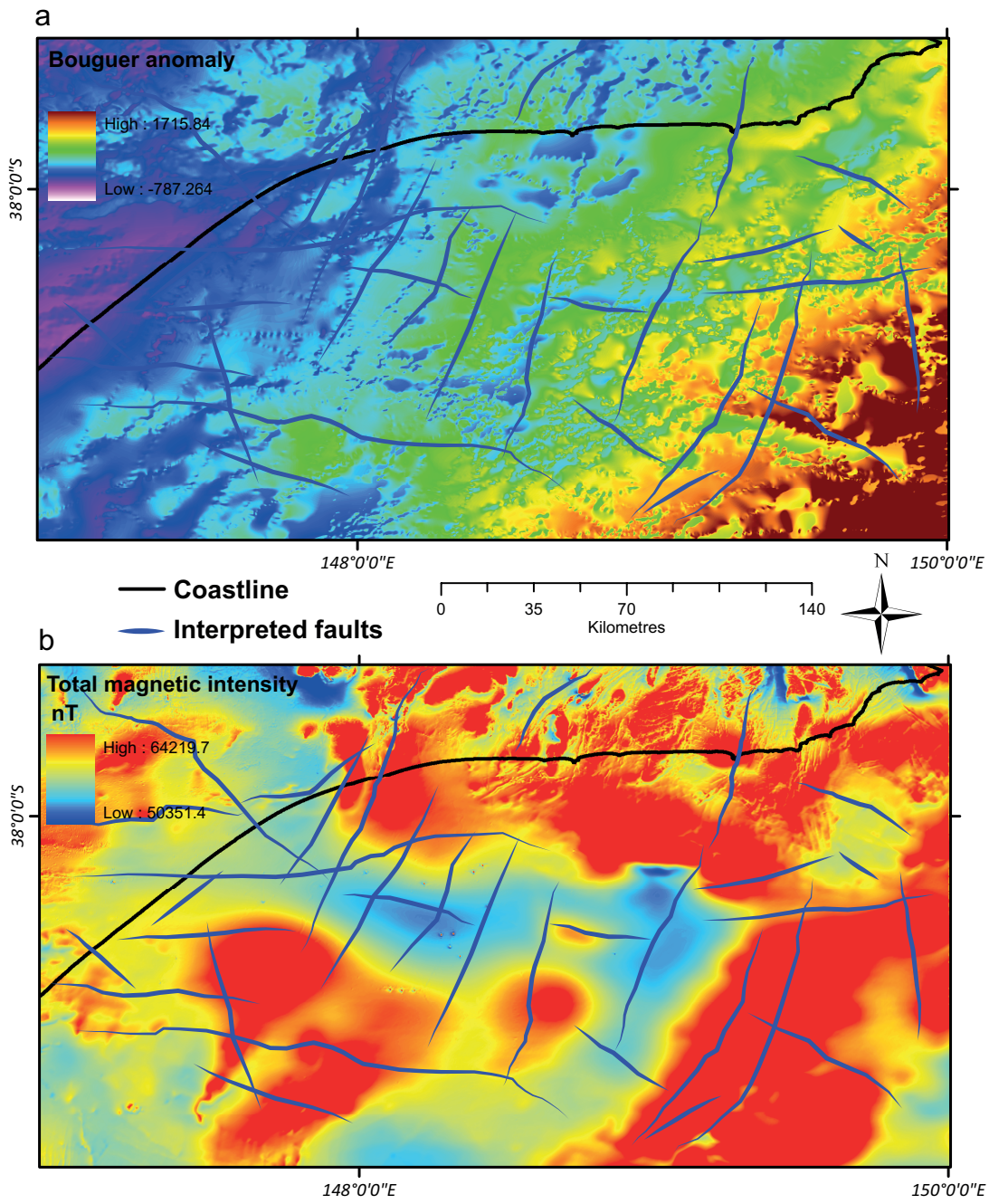

Figure 13. Interpreted geophysical potential field datasets used as input for the Gippsland Basin case study. (a) Bouguer gravity anomaly shown with a southeast directed 'hillshade' effect for enhancement. (b) Total magnetic intensity anomaly shown with no 'hillshade' effect.

face orientations that change due to input data perturbations) are not completely detected. Non-detection occurs if the displacement of the fault is not greater than the thickness of the stratigraphic unit due to the same stratigraphic unit being detected on both the hangingwall and footwall of the fault (Figure 14). In the example shown in Figure 14a, the blue unit was assigned a value of one and the white a value of two. The orientation of the fault surfaces does differ from model to model within the model suite, but only a portion of the surface is detected by the technique (Figure 14b). Different fault locations will not be detected if the stratigraphic unit each side of the fault

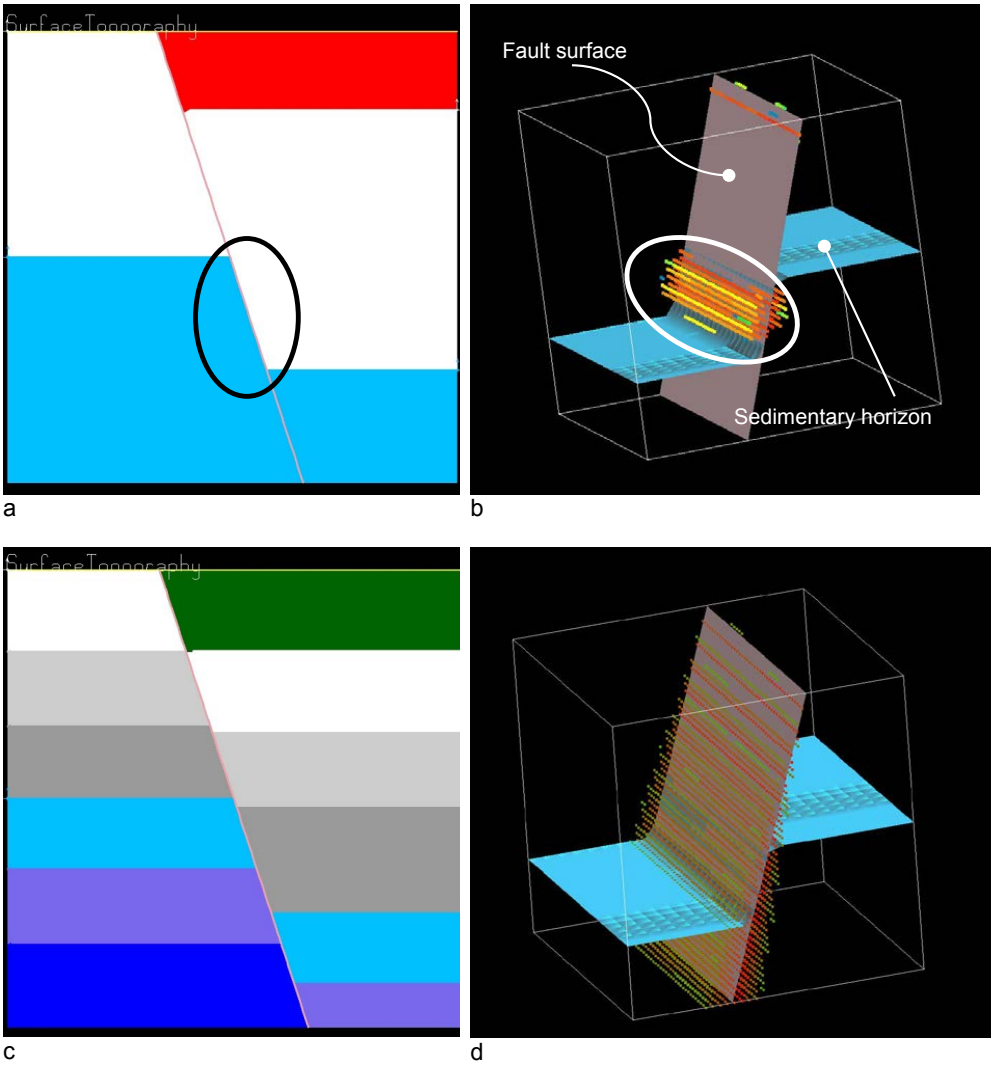

Figure 14. When fault displacement is less than stratigraphic thickness fault surfaces may not be completely detected. This example shows a modelled normal fault represented in section view (left) and in 3D on the right. Note that only where the blue and white units (circled — left) are adjacent is there the possibility of uncertainty (shown with point data) being detected (circled — right). With the addition of virtual formations (c) the uncertainty along the entire fault surface can be resolved (d).

are the same as only differences in the values assigned to stratigraphic units are detected with this technique. Additional virtual stratigraphic units were added to mitigate these effects (Figure 14c). Each of these additional virtual units was included in the appropriate 'series', so were included in the implicit potential field calculations of the originating formation. The 3D spatial properties of the virtual units were not treated any differently than the originating unit and were calculated from the same input data.

The practice of adding virtual units increases the 'stratigraphic resolution' of the model, enabling entire uncertain faulting surfaces to be detected when smaller displacements are observed (Figure 14d). Stratigraphic resolution has been increased in the Gippsland Basin model as some

sedimentary layers are thick and fault displacements may not be large enough to avoid the situation described above. Each series has two additional layers added for this purpose, except the top series 'Seaspray_Group', as the thickness of this group is not large enough to warrant additional formations.

6.3. Uncertainty assessment in the Gippsland Basin

Poorly constrained regions and structures in the Gippsland Basin model can be located using methods of uncertainty visualisation. Particular areas of increased uncertainty identified in Figure 15, highlighted in red on the plan maps, are located in the north (1), northwest (2) and southern parts (3) of the model. Areas (1), (2) and (3) are all associated with faults and the effect of faulting on the cross-cut strata. These faults are not well constrained by orientation measurements as they are based on (i) one orientation measurement, (ii) the relationship they have with other faults (i.e. whether they cross-cut or are cross-cut by other faults) and (iii) whether they are defined in the seismic cross-sections K–S. The elongate region of uncertainty running with an east–west axis, just south of the seismic section (region '3') is not defined in the section itself, so does not benefit from any cross-section constraints. The result is that the geology is allowed to vary to a larger degree, displaying higher associated uncertainty values than geology that is represented in the cross-sections.

There are also lack of orientation measurements constraining stratal geometry and distribution in regions of high uncertainty. Onshore observations that we could confidently relate to offshore components are rare and generally relate to formations older than the model basement. In addition, the combined isopach and bathymetry data inputs are largely clustered in the centre and eastern areas of the model, leaving the west relatively unconstrained (Figure 11). Strata in the uncertain areas rely heavily on the seismic section K–S due to the absence of other data. The over-reliance on section K–S to constrain geological surfaces due to sparse data can also been seen in the northern part of the map where high uncertainty values are observed. Region 2 displays levels of uncertainty due to both high degrees of faulting and the lack of seismic data that could add geometrical constraints to these at depth.

An area of high uncertainty located on the 4000 m depth plan section view of Case Study

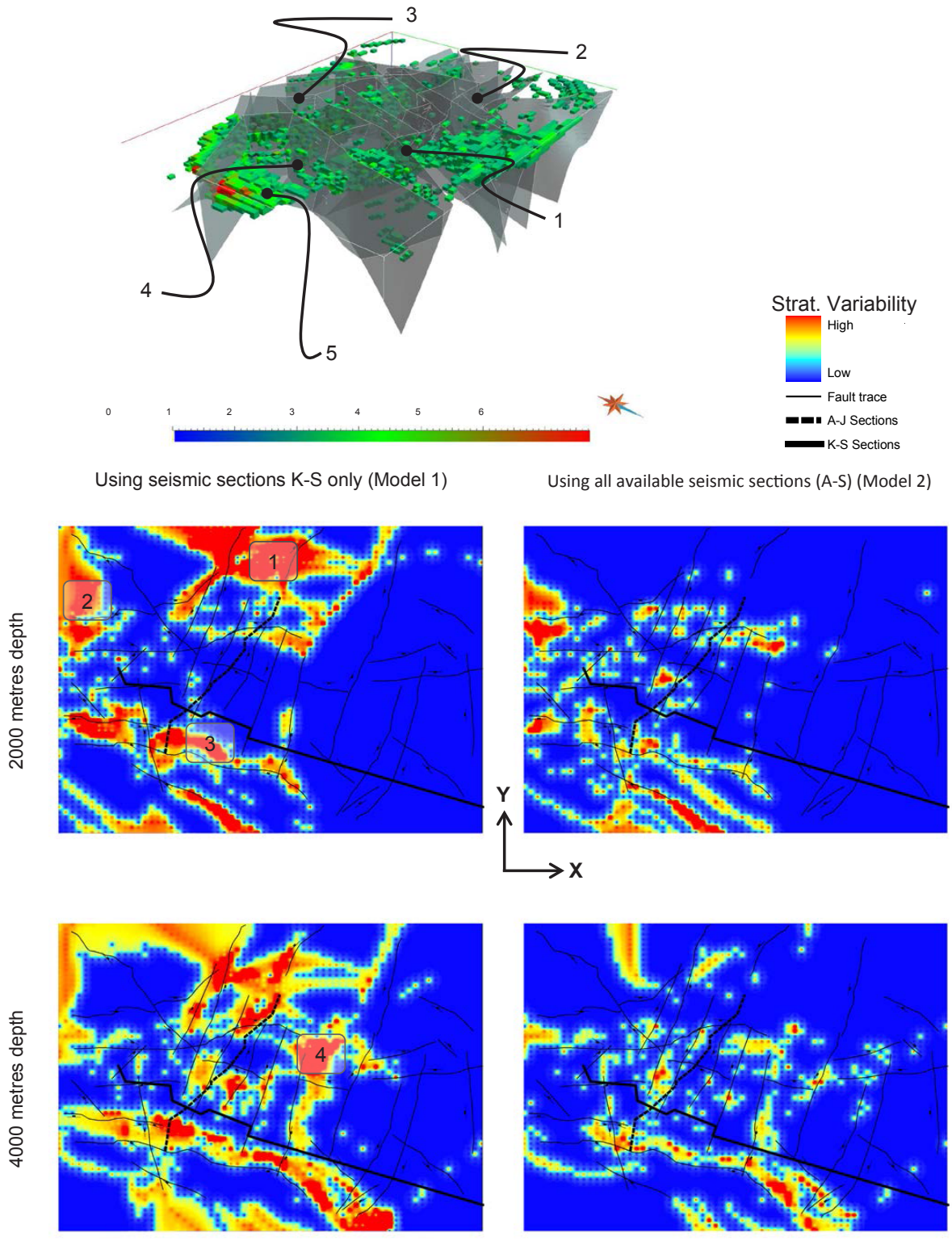

Figure 15. Comparison of stratigraphic variability observed at 2000 m and 4000 m depth. All maps are in plan view. Note areas of high stratigraphic variability (uncertainty) located to the north, northwest and southwest of Case Study A. Labelled regions are correspondingly labelled in the 3D view of uncertainty (voxet model, L = 2, grey surfaces are faults). Significant improvements to uncertainty values have been made in these areas with the addition seismic section information in Case Study B. Another interesting feature is the association of uncertainty with the faults and in some cases the dip of the fault can be determined by the uncertainty gradient. For example, the east–west fault in the south of the map shows a northerly dip, which is confirmed by associated strike and dip orientations.

A (region '4') is due to the intersection of a number of faults and structural complexity resulting from the interaction of strata and the Central Deep. Picking tops from the seismic data of the Strzelecki, Emperor and Golden Beach subgroups in this region was considered 'arbitrary' by Moore and Wong (2002). Estimates of the tops were made based on an interpretation that the Emperor Subgroup thickens to the north and the Strzelecki and Golden Beach Subgroups thicken to the south. It seems that the seismic horizon interpretations do not necessarily correlate to the isopach data. This has resulted in modelled surfaces that vary considerably across the model suite as the implicit potential field method attempts to reconcile the seismic and isopach data. Added complications may have arisen from depth conversion of two-way-time (TWT) data. Errors in depth-converting TWT data are likely to affect the entirety of this model as it is notoriously difficult to perform without incorporating some error (Cameron, 2007; Suzuki et al., 2008). Time–depth curves of wells were used by Moore and Wong (2002) to determine a seismic velocity model to calculate depth values. Five average internal velocities were used to represent entire density variation of the Gippsland Basin. Local rock density heterogeneity will not be accommodated if bulk density values are assumed. Subsequently some regions of the study area will be mis-represented where local density variations differ from the global averages determined in the velocity model. The result is that horizons interpreted in regions of anomalously high or low density values (with respect to the global average) will not be correctly located spatially. It is most likely that the source of disagreement between data types is caused by a combination of interpretive and data-conversion difficulties.

None of these issues were entirely unexpected in the construction of this model. It was expected that some disagreement between model realisations would be present, given the data types and relative geological complexity. What is important is that the degree and location of disagreement can be shown by detecting the uncertainty in the model. It was subsequently decided that an additional seismic section should be added in an attempt to better constrain the regions of high uncertainty.

6.4. The benefit of additional information

Seismic sections A–J from the Moore and Wong (2002) study were added to the model,

an incarnation named Case Study B. Sections A–J start in the southwestern quadrant of the model and extend northeast, intersecting sections K–S just west of the model centre, stopping in the northern centre (Figure 11). The results in removing uncertainty can be seen qualitatively in the Case Study B maps (Figure 15). Uncertainty in the northern region of interest (1) has been significantly reduced in Case Study B and areas (2) and (4) have also been reduced, but to a lesser extent. Region (3) still displays a high degree of uncertainty, though it has been reduced below that displayed in Case Study A.

Change in uncertainty is quantified by calculating the difference in volume for different L values (L = 2, 4 and 6) (Figure 16). The differences between these values in Case Study A and Case Study B are also shown. The differences equate to a percentage decrease of 64.5 (L = 2), 53.7 (L = 4) and 87.5 (L = 6), showing that adding seismic sections A–J to the model improved the potential for geology to be more reliably modelled.

6.5. Discrete regions of uncertainty

Overall improvements to model uncertainty were addressed by adding additional information to the model. There remain regions of high uncertainty within the model (Figure 15, re-

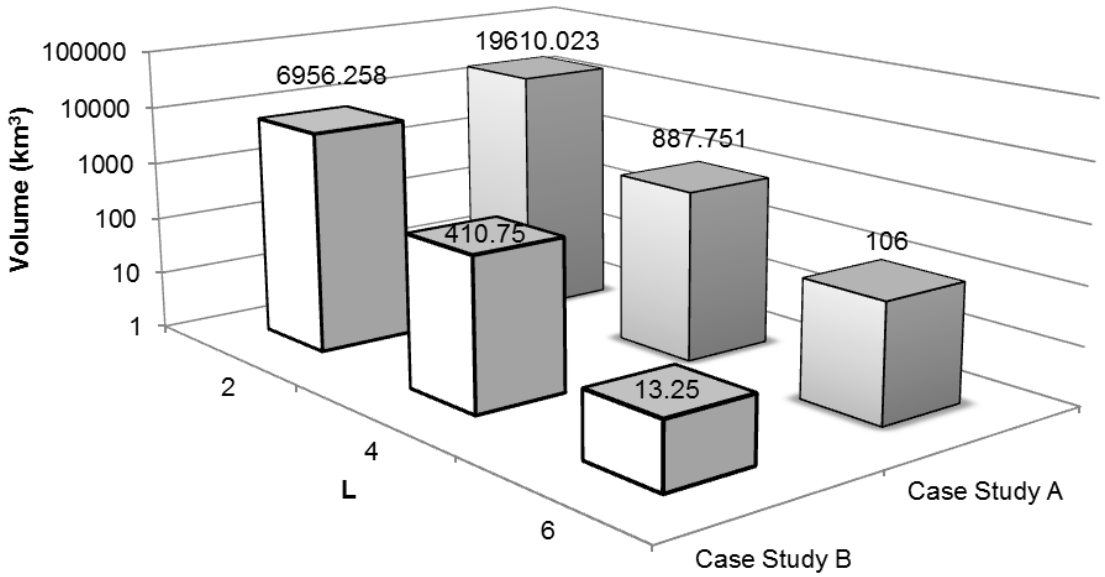

Figure 16. Change in uncertainty due to additional data. Volumes of stratigraphic possibilities (L) have been separated into three thresholds representing low (L = 2), medium (L = 4) and high (L = 6) levels of uncertainty. Levels of uncertainty contained within model Case Study A to Case Study B are plotted against a logarithmic volume scale (km^3). Reductions in uncertainty seen between Case Study A and Case Study B are due to the addition of seismic section information.

gion '5') in the Central Deep. One explanation is that there is no isopach information to aid strata geometry. Most of the information in this region is defined by the seismic section R–S and fault interpretations made from geophysical potential field data or seismic interpretation. This is compounded by difficulties in seismic interpretation of formation tops in the Gippsland Deep (Moore and Wong, 2002). It is clear that there are issues when attempting to correlate faults interpreted by geophysical potential fields to those interpreted from seismic data. Uncertain regions are generated by using ambiguous input data during model construction. This is true for geophysical data, in terms of non-unique solutions for geophysical potential field interpretation and the aforementioned issues relating to seismic data interpretation and integration into a 3D model. While it is tempting to avoid using geophysical data to prevent the possibility of making ambiguous observations, is it not feasible. Problems of sparse data require the use of geophysics in regional scales studies, such as that undertaken by Moore and Wong (2002). The key is locating, mitigating and understanding the nature of model uncertainty.

7. Discussion

The method presented here has shown it is possible to locate and calculate the magnitude of uncertainty within a 3D model of real geology. The method has allowed assessment of the Gippsland Basin model for inherent uncertainties and has aided the identification of data sources that may disagree. It appears that constraining the geology in central parts and an eastern region of the basin is particularly problematic due to heavy reliance on difficult to interpret seismic information. Additional information can provide geological constraints that reduce uncertainty, as has been shown. Consideration must be made that new information may also introduce additional uncertainty. The disagreement between the isopach-derived and interpreted seismic data, an occurrence not uncommon in basin studies (Suzuki et al., 2008), highlights how different data types do not necessarily reduce uncertainty by constraining each other, but create a situation where uncertainty is increased. Therefore it is likely the degree of geological complexity in the northwestern, central and eastern regions of the model is higher than that which can be interpolated using the current data inputs.

Stratigraphic variability values provide the operator with an intuitive method with which to understand two fundamental, but separate, components of model uncertainty: stratigraphic possibility (*L*) and stratigraphic variability frequency (*P*). These concepts are simple, easy to calculate and meaningful to the non-expert. Both the normalised stratigraphic possibility and variability values are model independent and do not require redefining for different geological settings. Both values are calculated from statistical methods, so are therefore repeatable and objective. This method also generates a variety of model perturbations in the process of determining uncertainty that can be assessed individually to provide an expanded view of what may be possible geologically.

It is important that the information generated by this technique is presented with an appropriate visualisation tool to adequately communicate the complexities of model uncertainty to the operator (Gershon, 1998; Thomson et al., 2005). Other effective methods of uncertainty visualisation exist (MacEachren et al., 1998; Viard et al., 2010; Wellmann and Regenauer-Lieb, 2011; Zuk and Carpendale, 2006) and have been considered for the purposes of this technique. The 'heat-map' colour scheme has been chosen because it is intuitive for most geoscientists and allows an appropriate amount of colour variation to effectively show the attributed quantities. The magnitude of uncertainty is directly related to colour and variations in data are clear to the operator. Regions of uncertainty are then identified using a combination of point data and stratigraphic variability values assigned to a colour map. Thresholds can be applied to the colour map to delineate high or low ranges of uncertainty. The features of stratigraphic variability allow the spatial variation of uncertainty and associated geological elements to be easily identified.

Another means to visualise model uncertainty is provided by assigning stratigraphic variability values to voxets. The use of voxets also allows the calculation of uncertainty volumes, in contrast Wellmann et al. (2010) who focus on visualising uncertainty with surfaces. Knowledge of uncertainty volumes provides a particularly useful comparative measure for assessing uncertainty between different model versions or quantifying the effect of additional data sets on model iterations. Importantly for this study, uncertainty volumes provide a descriptive quantity that can be used for reporting purposes when reviewing a model for reliably representing a geological target.

A different method to quantify uncertainty has been suggested by Jessell et al. (2010) that employs a distance penalty function applied to the model suite where stratigraphic observations are compared against predictions. The closest modelled location(s) sharing the same properties as

an observation point are determined and Euclidean distance is calculated. The results provide a distance misfit error that describes the geological variability of a model suite within a local area. The benefit to using this method is that stratigraphic units can be reclassified into ordinal data and subdomains of related geological units can be defined. The results can then be subjected to a wider range of statistical treatments. Additional measures derived from different statistics would be advantageous to detecting and quantifying uncertainty. A drawback to using distance misfit error is that only uncertainty contained within a local area is measured, whereas the stratigraphic variability describes uncertainty at a discrete location. In addition, adjusting the method for this technique to a local area distance calculation presents a challenge in how to define an 'observed' location or the reference model itself. This paper defines the 'reference model' as that which is produced using unperturbed orientation measurements. This definition of a reference model is not an unbiased estimate, as it depends on the internal parameterisation of the implicit scheme applied. Another definition for a reference model could be the 'mode model', as it represents the most common stratigraphic units for every given point across the model suite. The mode model incorporates all the perturbed orientation datasets, not just a single orientation dataset, and accommodates more geological possibility. The mode model is derived statistically from a voxet and does not necessarily retain any geological connectivity or feasibility. A solution to this problem is to find a model in the model suite that corresponds exactly to the mode model, which, if it exists, could be legitimately classified as the reference model.

Multiple realisations of a single geological concept are being analysed in this study. Multiple realisations of multiple geological concepts can be analysed if topological relationships are varied in combination with orientation observations. The implicit method requires topological input in the form of a stratigraphic column (with appropriate 'onlap' or 'erode' relationships between units), a defined fault network and fault–stratigraphy relationships. If any topological relationships are perturbed, fundamental changes to the model will occur and produce far greater variability in the model suite than if, as in this study, only the input orientation observations are perturbed. There is good reason to perform topological perturbation. Most geological terranes have multiple tectonic evolution hypotheses and could be comparatively tested using topological perturbation. Appropriate analysis of these results would require the process to reject models on the basis of geological impossibility, a concept that is open to vigorous debate. The boundaries of model space

are greatly expanded by allowing topological perturbation and more degrees of freedom, requiring increased model suite members and subsequently requiring faster model calculation and sampling. These are minor challenges to resolve when considering the benefits. Geological possibility, and therefore uncertainty, is not being fully explored if different model topologies are not included in analysis.

The production of a model suite and uncertainty analysis has an additional educational application. Generating multiple models can aid management decisions and educate non-geoscientists. The degree of variation observed between models due to small perturbations of the input data highlight the problems of sparse data inherent in geosciences. These concepts are often not well acknowledged outside of scientific disciplines like geosciences and astronomy. One of the conclusions from the Bond et al. (2010) study was that to better prepare geoscience students for professional life, discouragement of striving to find the 'best' answer and accepting multiple answers needs to be effectively communicated. This conclusion can also be applied to management personnel that have not been trained within the geosciences. Acknowledgement that a single 'correct' answer is not necessarily available can be aided by this technique by visualising the degree of uncertainty within a particular model.

7.1. Improving understanding of model uncertainty

Improvements can be made to better assess uncertainty contained within 3D models. There are possible augmentations to this technique that may offer more information to the operator.

a) Higher resolution sampling. Model sampling parameters used in this study can be improved in two ways. A vertical bias exists as the sampling interval on the Z axis is 500 m, whereas on the X and Y axes it is 4140.625 m and 3200 m respectively. It would be preferable to have all axes equal to ensure no directional bias exists and to have smaller intervals to ensure that the geometry of inherent uncertainty can be more accurately defined. The restriction in this case was due to hardware requirements. The assessment was conducted on a personal laptop (250GB HDD) and smaller sampling is restricted heavily by hard disk space. It would be preferable for future studies to be conducted on high-capacity

computing platforms to address this.

b) Use of continuous variables. The stratigraphic identifier used in this study to describe the stratigraphic unit at a given point returns a categorical variable. As such, there are limited statistical treatments that are available for analysis. One solution would be to identify both the type of stratigraphy (currently done) and the implicit potential field value the model is interpolated with. The implicit potential field value is a continuous variable and would give a value revealing where sample location is in the stratigraphic unit and proximity to other geological interfaces (contacts, faults). This information would very useful in terms of developing better techniques to analyse, visualise and use uncertainty data to improve model reliability. It would also remove the need to add additional formations to increase stratigraphic resolution.

c) Calculation of stratigraphic distance. Accommodating uncertainty between both stratigraphy and lithology can be achieved with the use of a weighting schema and additional information from the 3D Geomodeller implicit potential field. Currently no consideration of geochronology and unconformable relationships is made when calculating uncertainty. Locations which display lithological variability within the same stratigraphic group, such as variation between the Angler Subgroup and the Seaspray Group (both part of the Seaspray Series) (Figure 10) could have a lesser weighting than variability between the Angler Subgroup (Seaspray Group Series) and the Cobia Subgroup (Latrobe Group Series). This difference in weighting can be justified as an erosional unconformity that separates the Angler and Cobia units, whereas the Angler and Seaspray units are generally considered to be conformable. Knowledge of the implicit potential field value and gradient would be beneficial to accurately calculate stratigraphic distance. The implicit potential field value would allow calculation of Euclidian distance in three dimensions, as the position within stratigraphy would be known. The implicit potential field gradient value would assist in describing the direction of stratigraphic anisotropy within the geological layer and from this the orientation of the stratigraphic distance vector could be found.

7.2. Geological constraints for geophysical inversion

Calculating stratigraphic variability produces information that could potentially provide geological constraints for geophysical inversion. Current inversion techniques provide geological constraints in the form of petrophysical rock property distributions (Guillen et al., 2008; Jessell et al., 2010; Li and Oldenburg, 1998), 'pierce points' assigned to stratigraphic horizons in drill-holes (Fullagar et al., 2000) or weightings applied to entire surfaces (Fullagar et al., 2008) that restrict movement during geometrical inversion. However, existing techniques do not integrate all available geological data into the process, such as orientation measurements, and therefore cannot be expected to honour all data inputs. The information provided by this technique could offer a method to constrain the geophysical inversion process. Both L and P values, together representing stratigraphic variability, could provide an adjustment threshold for cells during inversion. If the possible cell solutions are limited to what is defined by their associated L and P values, then the final inverted model will more likely to represent a realistic geological situation as it honours all the data.

For example, if $L = 3$ and $P = 0.23$ for a cell at X, Y, Z, then the inversion process would be limited to varying the cell to the three possible stratigraphic units identified by this technique. The 0.23 P value, indicating what frequency the stratigraphic unit differs from the mode, can be used as a weighting coefficient representing the likelihood of this cell being changed during inversion. A consideration in using stratigraphic variability as a constraint to geophysical inversion is that the process may fail and render no result, which is potentially more useful than if the process completes successfully. A failed inversion executed with these geological constraints as input would suggest that the geological reference model, input data and the geophysical data used in the inversion may differ to a degree beyond what geologically feasible.

8. Conclusion

Uncertainty in 3D geological models can be located, visualised and quantified in the pursuit of building a reliable 3D geological model. Uncertainty can be used to identify potentially unreliable regions in 3D models, requiring additional data constraints. Reduction of uncertainty

is also measurable, and can be used to explore whether adding more data is beneficial. A principal assumption in this study is that the input data, potentially of high quality, is not without error. Attempts to correct the data and remove error are not performed. Instead this study offers a process where a suite of geological possibilities can be generated from a single input data set through perturbations of the data. Significant reductions of model uncertainty can be achieved by using appropriate data in key locations within the 3D model. The location and magnitude of uncertainty also reveal regions that bear further geological or geophysical analysis. Uncertain regions can be treated by adding more data, or may guide future surveys and studies if data is unavailable. Producing an uncertainty grid and stratigraphic variability values is a step towards the goal of a geophysically and geologically constrained inversion process that produces models that honour both geophysical and geological data.

Acknowledgements

We gratefully acknowledge the assistance of the team at Intrepid Geophysics, Melbourne, Australia, who supplied the 3D Geomodeller API and provided technical support. This study would not have been possible without financial support and datasets supplied by Tim Rawling and Geoscience Victoria, Department of Primary Industries, Melbourne, Australia. We would also like to thank the Society of Economic Geologists and the Hugo Dummett Memorial Fund for awarding funding in support of this study. Finally, we acknowledge the thorough and constructive feedback provided by two anonymous reviewers and Alan Gibbs of Midland Valley.

1a

Chapter 1 presents a method that locates and quantifies the magnitude of uncertainty with 3D geological models. The stratigraphic variability technique provides a step towards understanding how perturbations in orientation input data can produce substantially different model architecture. Adding information to a model to regions of high uncertainty is demonstrated to have a measureable effect on reducing model uncertainty. However, stratigraphic variability does not provide an understanding of how geometries of geological bodies, faults and stratigraphic contacts are affected by model uncertainty. Chapter 2 demonstrates a series of measures that characterise model architecture geometrically in order to record differences between models. There are multiple ways model elements can vary from model to model, so a variety of techniques were developed to detect variability within a model suite resulting from uncertainty simulation. Each technique was developed to be geologically relevant, independent of other measures or sources of information.

Conceptual development of geodiversity metrics was straightforward, whereas implementation of these methods required significant testing and quality assurance. Implementation proved challenging as automated processing was a key requirement. Matlab© was chosen as the platform to automate categorisation tasks as it allows a large variety operations to be 'looped', or repeated, using different inputs.

Looping allows multiple models and multiple model elements to be analysed without the need for manual analysis. Manual analysis always presents problems where human error (i.e. input error or unintended differences between input parameters) produces non-representative results. Manual analysis is also slow and labour-intensive, restricting the efficiency of the procedure and desirability to the wider scientific community. It is hard to promote a technique requiring operations to be manually executed on each model element in each model, potentially involving thousands of user-initiated operations.

Another challenge to the success of the method was choosing an appropriate means to report results. The importance of being able to easily identify anomalous results was highlighted in Chapter 1, and will influence the uptake of these techniques by the geoscientific community. Although many of the issues faced in the transition from determining model uncertainty to understanding geodiversity were more technical then geological, they were nonetheless important as geological understanding would have suffered had they not been resolved. Chapter 2 has been submitted for review to the journal Tectonophysics.

2

Geodiversity: Exploration of 3D geological model space

Mark D. Lindsay [a,b], Mark W. Jessell [b,c], Laurent Ailleres [a], Stephane Perrouty [b,c] , Eric A. de Kemp [d], Peter Betts [a]

[a] School of Geosciences, Monash University, PO Box 28E, Victoria, 3800, Australia
[b] Université de Toulouse, UPS, (OMP), GET, 14 Av. Edouard Belin, F-31400, Toulouse, France
[c] IRD, GET, F-31400, Toulouse, France
[d] Geological Survey of Canada, 236-315 Booth St. Ottawa, Ontario, Canada K1A 0E9

Submitted to **Tectonophysics** on 19 June, 2012, manuscript number TECTO8400.

Accepted.

Abstract

The process of building a 3D model necessitates the geoscientist to reconcile field observations, geophysical interpretation, geological data uncertainty and the prevailing tectonic evolution hypotheses and interpretations. Uncertainty is compounded when clustered data points collected at local scales are statistically upscaled to one or two points for use in regional models. Interpretation is required to interpolate between sparse field data points using ambiguous geophysical data to support field data in covered terranes. It becomes clear that multiple interpretations are possible during model construction, but typically only a single interpretation is permitted. Uncertainties are introduced into the 3D model during construction from a variety of sources and through data set optimisation that only produce a single model. Practices such as these are likely to result in a model that does not adequately represent the target geology.

A set of geometrical or 'geodiversity' metrics are used to analyse the Gippsland Basin, southeastern Australia is analysed using by subjecting input data to uncertainty simulation prior to model input. The resulting sets of perturbed geological observations are used to calculate multiple geological 3D models that display a range of geological architecture. Biodiversity measures degrees of variation within different organisms, ecosystems or the entire Earth. This concept has been adapted for the geosciences to quantify geometric variability, or 'geodiversity', between models. Various geometrical relationships (depth, volume, contact surface area, curvature and geological complexity) are used to describe the range of possibilities exhibited throughout the model suite. End-member models for each geodiversity metric are classified in a similar manner to taxonomic descriptions. Further analysis of the model suite is performed using principal component analysis (PCA) to determine important features and geometrical characteristics. The outliers of the model suite are identified and model space boundaries and composition determined that potentially identify undiscovered model 'species'.

Keywords: Uncertainty, 3D modelling, Model space, Principal component analysis, Gippsland Basin

1. Introduction

In much the same way the diversity of animal species at a particular location can be described using biodiversity metrics (Simpson, 1949; Miller and Foote, 1996; Roy and Foote, 1997), multiple geological models within a model suite can be described using a set of geological diversity, or 'geodiversity', metrics. Many biodiversity metrics now exist to assess species diversity, providing insights into subtle relationships and interactions recorded in the data (Magurran, 2004). The translation of diversity metrics into the geosceiences is performed to address the repercussions of geology being a fundamentally interpretive science (Frodeman, 1995).

Frodeman (1995) applies the hermeneutic (interpretive) circle of Heidegger (Heidegger, 1962, 1963) to the progress of geological understanding. The hermeneutic circle states that central to comprehending parts of a geological problem is understanding their relationship to the whole, and comprehension of the whole geological problem is only achieved from an understanding of its parts. The geologist's interpretations of the whole and parts are guided by preconceptions and theories that are relied upon to make sense of a rock outcrop or geophysical image. These preconceptions and theories are necessary when performing geological or geophysical interpretation and are assimilated into the geologist's skillset through training and experience. Very little knowledge about any geological terrane can be obtained without interpretation. Geodynamic reconstructions, ore deposit models and volcanic eruption histories would not exist without the ability of the geologist to take geological evidence and forensically reconstruct processes that cannot be directly observed.

Frodeman (1995) acknowledges that some sense of the answer, or 'foresight', is required to collate the abundance of data and interpretations into a feasible concept. Without foresight, the answer may not be recognised. The scope of what may be considered a possible answer is predefined by the scientific principles and goals of the geologist than those acquired through the scientific activity itself.

The equipment employed by the geologist (field compass, hand lens, petrology microscope, ICP-MS machine), their operation and associated data processing technique also prede-

termine the answer by shaping the types of information collected and subsequent interpretations. Geological interpretations are not static and continue to evolve over time as more knowledge is gained through the emergence of new techniques, equipment and natural and numerical analogues. The comparison of different editions of the same geological mapsheets provide an example of the evolution of geological understanding. Some deeper geological features in early editions may be subdivided in later editions as subsurface imaging techniques are used. Faults and folds may appear in later editions due to additional field work being undertaken. The stratigraphic column may change if the tectonic evolution of the region is revised. The desire to constantly seek more information to better understand the scientific problem is the fate of the interpretive science. Unfortunately only one answer is usually provided, where many others may exist. Geodiversity metrics offer an approach that allow the parts of a geological problem to be communicated relative to the whole of geological possibility.

The detection and visualisation of uncertainty within 3D geological models has been highlighted as an important issue (Jones et al., 2004; Bond et al., 2007; Caumon et al., 2009; Bond et al., 2012) and is the focus of recent contributions (Cherpeau et al., 2010; Jessell et al., 2010; Wellmann et al., 2010; Wellmann and Regenauer-Lieb, 2011; Lindsay et al., 2012). 3D geological modelling relies on input data to determine the correct spatial relationships between various geological elements (Jessell et al., 2010). The model relies completely on the capability of input data to provide sufficient information to locate and describe these geological elements. Unfortunately, input data is subjected to varying degrees of error and uncertainty in collection and processing, adversely affecting the accuracy of the model, predominantly due to sampling and upscaling procedures involved in data collection through to model construction (Thore et al., 2002). Geophysical data supplies an infinite number of mathematically feasible solutions (Nettleton, 1942) without appropriate use of petrophysical constraints or a priori geological knowledge (Gunn, 1997; Saltus and Blakely, 2011). Petrophysical constraints contain their own uncertainty, due to a few measurements being extrapolated using mathematical functions employed to simulate natural property heterogeneity throughout a rock body with varying, and potentially unknown, degrees of success (Jessell, 2001). This contribution follows advances made by Jessell et al. (2010), Lindsay et al. (2012), Wellmann et al. (2010) and Wellmann and Regenauer-Lieb (2011) describing uncertainty detection techniques. These studies have shown that multiple models displaying overall similar, but possibly

significant differences in geological architecture can be created from the same data set. Model differences are now being detected and quantified as model uncertainty. Concepts facilitating uncertainty detection are expanded here in a geometrical exploration of model space. The necessity for model space exploration is exemplified by variability in geological architecture between models. This contribution aims to describe geological variability and how geological elements may change between models using a selection of geometrical measures. A fundamental difference between this and previous studies is that global variations i.e. the geological unit/formation as a whole entity is analysed, rather than at discontinuous local (point) locations.

A key aspect of this and the Jessell et al. (2010), Wellman et al. (2010), Wellman and Regenauer-Lieb (2011) and Lindsay et al. (2012) studies is that removal of error or uncertainty from data prior to input is not performed. Instead, multiple models are calculated from perturbed input data in an attempt to understand the range of geological possibilities that exist when data uncertainty has been taken into consideration. A 'model suite' is generated, containing a cluster of models displaying similar geological geometries at the 'barycentre', or geometrically divergent models displaying extreme geometries that define a boundary of geological possibilities that can be generated from the input data set.

The use of the term geodiversity in the modelling context of this study should not be confused with its use in conservation that, while related, describes the diversity of processes, morphology and mineralogy of the earth. Fundamental aspects that are addressed to describe model suite geodiversity are: (1) identifying if the models display differences; (2) how these models are different and (3) what modelling implications can be drawn from the information that geodiversity metrics provide. A description of how a model suite is generated is provided, followed by the method by which geodiversity metrics are calculated. The geodiversity metrics are then applied to a case study located in the Gippsland Basin, southeastern Australia. Principal component analysis (PCA) of geodiversity metric results are presented and allow definition of model space composition boundaries, together with identification of metrics that contribute most to model space definitions.

2. Model suite generation

A model suite is created by calculating many models from a single input data set. Generating a model suite is a realistic admission that full knowledge of modelled system is unattainable, which is true for most, if not all, geological modelling scenarios. Creating multiple models from variations of the same input data allows different geological architecture to be generated, explored and compared. Uncertainty simulation is used to produce the model suite (Lindsay et al., 2012). A single model is first created from the input data, typically including field measurements, interpretation of potential field geophysics (including seismic, gravity and magnetic datasets) and drill hole data using 3D Geomodeller, an implicit geological modelling application. 3D Geomodeller uses the scalar potential field method to rapidly calculate geological interfaces as implicit surfaces (Lajaunie et al., 1997). Geological interfaces represent surfaces where the potential for one unit exceeds that of another iso-potential, forming the contact between different geological units (see Calcagno et al. 2008 for additional information). The implicit modelling method requires that three different sources of geological information are specified before model calculation can take place:

a) A stratigraphic column. This describes the temporal relationships between the geological units being modelled

b) The location of geological contacts for each stratigraphic group must be known at some locations.

c) Orientation data in the form of strike and dip measurements describing the orientation of geological interfaces.

The uncertainty simulation used in this contribution varies the orientation measurements from the data set ± five degrees. Five degrees has been chosen to represent the amount of variation observed when taking field measurements, interpreting interface orientations from geophysics or performing data upscaling. The principle behind ± five degrees of variation is that it can often be difficult to determine whether the measurement adequately represents the geological structure after upscaling (Figure 1a) or at the different scales (Figure 1b). Each data set perturbation is then

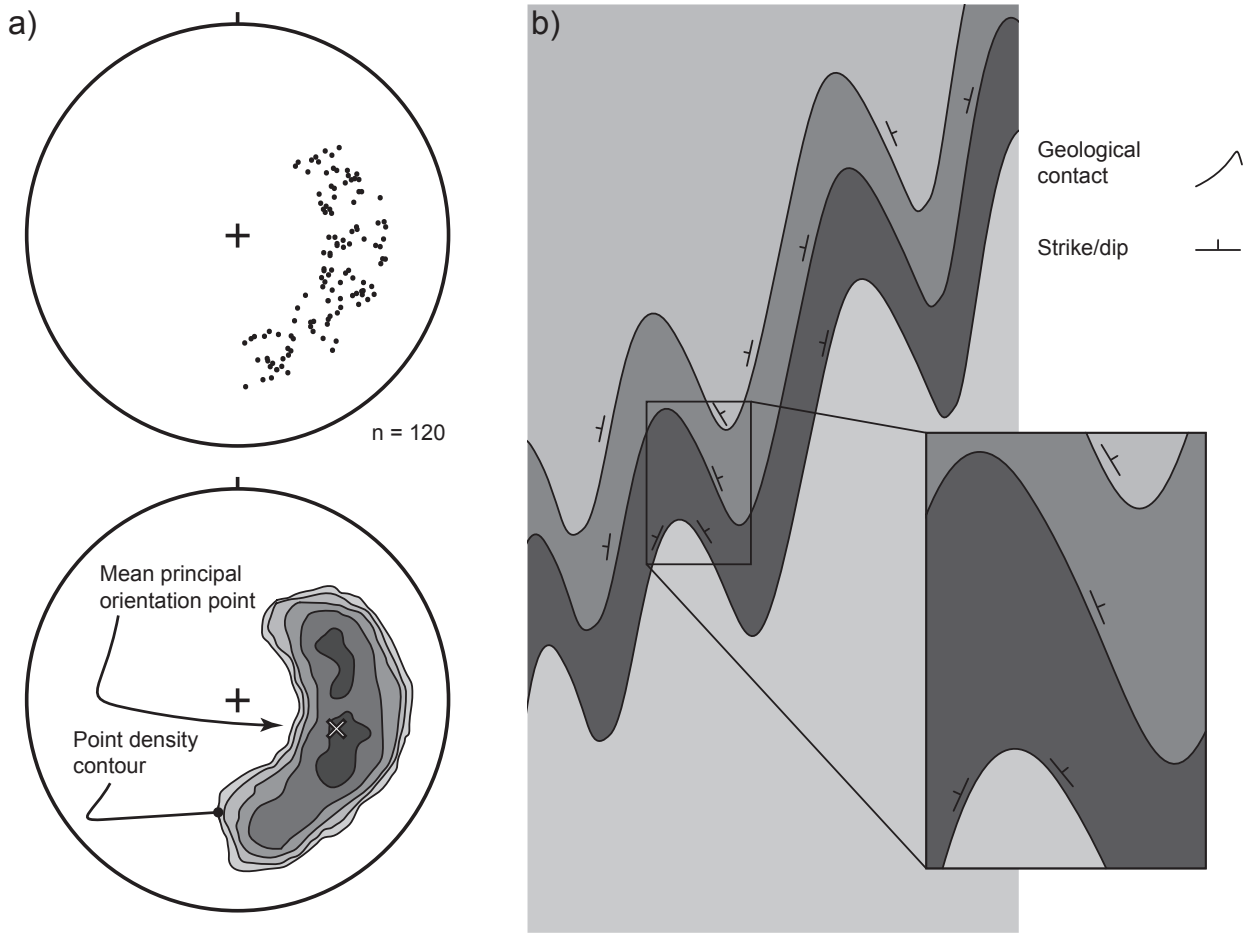

Figure 1. a) Upscaling field data for input into a 3D geological model. 120 field measurements taken at the local scale (top) are reduced to a single 'representative' point (bottom – 'mean principal orientation point') using point density statistics. This is a valid statistical technique, but may not best represent the measured natural geology. b) Typical scale and issue encountered in a mapping exercise. The inset box shows a structural trend along a nor-northwest – east-southeast axis, also consistent with the strike/dip measurements that have been recorded. At the regional scale, and with additional measurements, the trend is nor-northeast and west-southwest.

used to recalculate the model potential field to accommodate the new, varied input data. The results of uncertainty simulation can be seen in the synthetic model suite sample shown in Figure 2. There is potential to generate millions of models in this manner, but for the purposes of this study we have generated 100 new models, all based on perturbed input data, for a total of 101 (including the original model based on unpeturbed data). A sample of this size allows a reasonable comparison of the geometrical possibilities within the model suite.

3. Geodiversity metrics

Geodiversity metric calculation is performed using MATLAB® scripts. Calculation is performed by first converting each model into a 'voxet', a set of volumetric pixels (voxels) that

represent the model as a grid in 3D located space. The voxet parameters are stored in Universal Transverse Mercator (UTM) co-ordinates so that distances (including depth) and location, can be measured in metres and related back to the real-world area of interest. The property of each cell is the 'stratigraphic ID', an integer that represents the relative position of a geological formation within the stratigraphic column. A stratigraphic ID value of '1' represents the basement unit of the model, whereas a stratigraphic ID value of '2' represents the unit overlying the basement and so on (see example in Figure 8).

The geodiversity seen within the model suite is clear when comparing the models seen in Figure 2. The different degrees of displacement along faults in the 3D block models diagrams and the geometry of rock outcrop can easily be identified. The differences are often more subtle than can be seen when using purely visual comparative techniques in more complex natural models, such as when studying the difference in curvature of a geological contact or volume and depth for

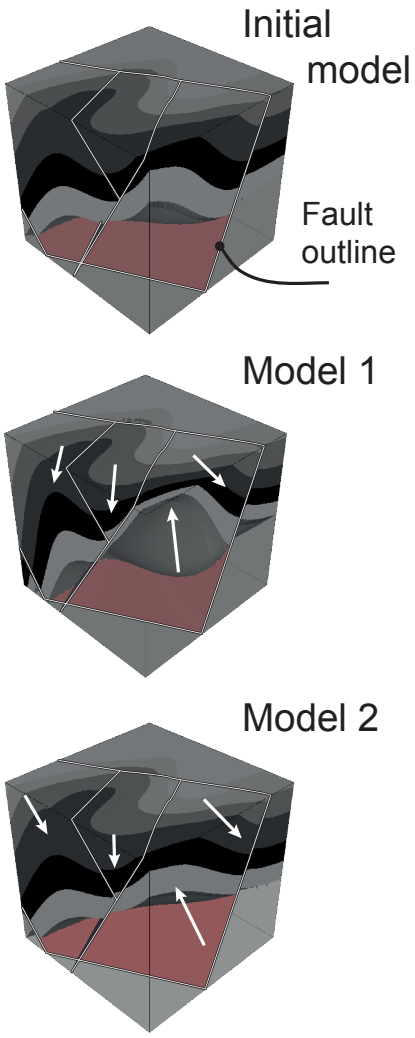

Figure 2. A comparison of an initial synthetic model with perturbed models 1 and 2. The main regions of variability are highlighted with arrows. Fault surfaces are bordered in black and white.

an entire formation. Some model properties, such as the volume or depth ranges of a particular geological unit of interest, require quantitative analytical methods to provide useful information to the operator.

Manually inspecting each model within a suite with many members for differences and variability is too time consuming to be practical in most cases. A set of analytical techniques have been developed to automatically assess model suite geodiversity, avoiding the need for manual model inspection. Geometrical characterization of model suite geology can be performed to allow relevant comparisons to be made and important information to be extracted.

3.1. Formation depth and volume

The shallowest and deepest extents of each stratigraphic unit can be determined from each model. This type of information can be of interest to both traditional geoscientific industries, such as oil, gas and minerals exploration (depth of reservoir or deposit) and groundwater and environmental management (depth of aquifer), but also to emerging energy industries such as geothermal and coalbed methane exploration. Shallowest extent of a formation is calculated by determining the depth of the shallowest voxel in the formation under study and vice versa for the deepest extent (Figure 3). It is also possible to calculate the volume of each stratigraphic unit within each model of the suite. Particular units can be delineated and examined for economic or scientific research interest to answer questions regarding geological possibilities. Volumes are determined by multiplying the count of formation voxels with the voxel volume (Figure 3).

3.2. Average mean curvature

Calculating the average mean curvature of a geological contact provides information describing geological interface deformation. Curvature is determined by rotating a section plane around the surface normal ($\vec{N}$) at *P*, a point on a folded surface (Figure 4a). The section plane running through the folded surface that shows the maximum magnitude of curvature is principal curvature k_1. Principal curvature k_2, is a plane perpendicular to k_1 , so that $k_1 > k_2$ (Lisle and Robinson, 1995; Lisle and Toimil, 2007). The sign of principal curvature values indicates sense of curvature:

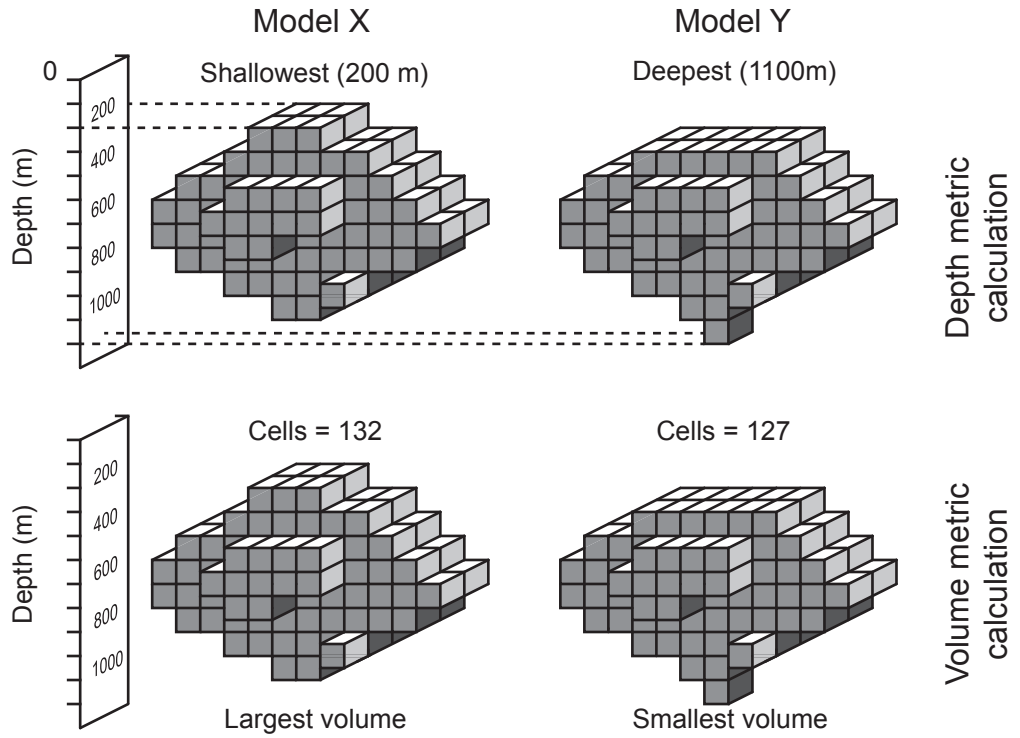

Figure 3. Formation depth and volume calculations. The geological bodies are shown as a set of voxels rather than surfaces, according to the method of analysis. Formation depth analysis detects the location of the deepest or shallowest voxel attributed to a particular geological unit. Volume analysis is performed with a voxel count of the geological unit.

positive indicates convex-upward and negative indicates concave-upward. Mean curvature (M) is the arithmetic average of k_1 and k_2,

$$M = \frac{k_1 + k_2}{2} \quad , \tag{1}$$

and represents an antiformal (convex) surface when $M > 0$ or a synformal (concave) surface when $M < 0$. If $M = 0$ it indicates the surface is a flat plane (neither concave or convex) or a surface where $k_1 = -k_2$, what Lisle and Toimil (2007) refer to as 'perfect saddle'. Interference patterns can be identified by calculating Gaussian curvature (G), which is the product of k_1 and k_2

$$G = k_1 . k_2 \, . \tag{2}$$

A positive G value indicates that both principal curvatures have the same sign (the surface resembles a dome, or if inverted, a basin) and a negative value indicates the principal curvatures have different signs (the surface resembles an antiformal or synformal saddle) (Mynatt et al., 2007). Curvature calculations can locate and determine the magnitude of curvature (or folding) observed within a contact. Figure 4b shows how further analysis of mean and Gaussian curvature in combination can reveal folding directions along two perpendicular axes, allowing the identification of fold geometry (i.e. antiformal synforms or synformal antiforms) (Lisle and Toimil, 2007).

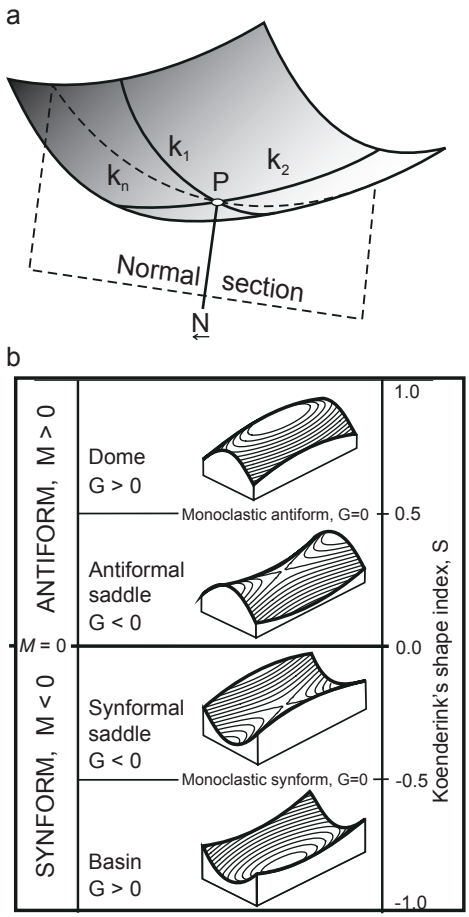

Figure 4. a) Principal curvatures k_1 and k_2 at point '*P*' on a folded surface with normal curvature k_n. $\vec{N}$ is the surface normal at point *P*. b) Fold classification scheme based on mean curvature (*M*) and Gaussian curvature (*G*) values. After Lisle and Tiomil (2007) and Mynatt et al. (2007).

The following describes the procedure used to calculate curvature for surfaces within a model. Locations are determined from the centroid of each voxel.

1. Two geological units are chosen, designated U_1 and U_2 for the purposes of this description. The curvature of the contact between U_1 and U_2 is being calculated.

2. Filter voxels where the lithology property does not equal U_1 or U_2.

3. Find locations where U_1 and U_2 are adjacent and filter the remaining voxels.

4. The contact between U_1 and U_2 may not be continuous throughout the model. The surface can be crosscut by unconformities, igneous intrusions or faulting structures. Misleading results will be obtained when non-adjacent points are triangulated as this creates a surface where one does not exist. Points adjacent in 3D are labelled as a distinct region using a 26-connected neighbourhood test (Figure 5a).

5. Delaunay triangulation is performed separately on each region to create the mesh from which curvature calculations are performed. Regions with four or less points are

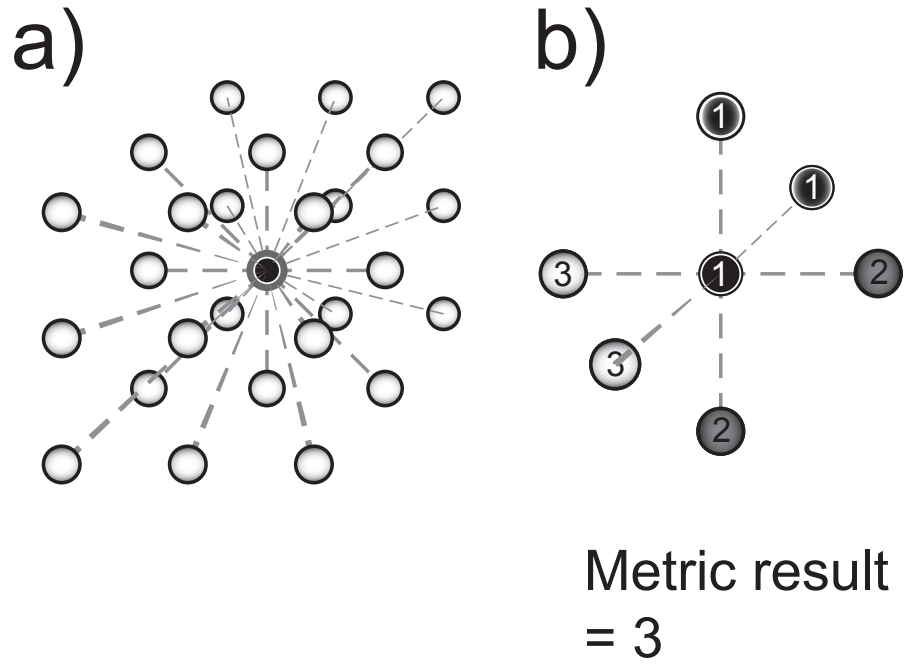

Figure 5. a) 26-Connected neighbourhood used in the k-nearest neighbour algorithm for region connectivity. The sample location is highlighted in black, representing the centroid location of the sample voxel. Points in white represent the surrounding voxel centroid locations. If any of these white points are the same stratigraphic unit as the sample they are considered to be connected, or adjacent, to the sample and will be included in the same region for curvature calculation. b) Short distance '6 neighbour calculation' showing the sample location assigned with a stratigraphic ID of '1'. The metric result equals three because the sample location is surrounded by three stratigraphic units.

filtered from the voxet to conform with concept known as the 'Delaunay condition' (Lee and Schachter, 1980; Sloan, 1993). The Delaunay condition ensures that no overlap occurs during triangulation.

6. Curvature calculations are performed using the method of Ole Kaven (2009) which is based on the work of Chen and Schmitt (1992) and Dong and Wang (2005). The measures for k_1, k_2, M and G are recorded for each point in the region.

7. The sum of curvature measures for each voxel within each region is determined for the surface under study. The arithmetic mean for each of the curvature measures are calculated for all voxels making the surface (including the distinct regions). The result is a value that represents overall curvature for the surface.

3.3. Neighbourhood relationships

Neighbour relationships can describe the manner in which different stratigraphic units

are juxtaposed. We employ short-distance metrics, which are those that only examine voxels directly adjacent to the sample voxel. This contribution evaluates the union (or contact) between two units and the geological complexity of a location. Neighbourhood relationships are calculated with a *k*-nearest neighbour algorithm (*k*-NN). This method classifies objects based on training areas within the model and finds the closest points in terms of Euclidean distance (Friedman et al., 1977; Bremner et al., 2005). The distances determined by this technique are used to constrain which voxels are counted as neighbours. Only the shortest distances measured along eastings, northings and depth axes (a six neighbour relationship - Figure 5b) are included when determining short distance geological relationships.

The surface area of the contact between stratigraphic units is identified together with the proportion of overall contacts within the 3D volume. This information can be beneficial to mineral exploration studies, where the contact between particular units can lead to the identification of a potential mineral resource. For example, an explorer may be interested in what conditions and which model within the model suite displays the largest surface-area between modelled psammitic and psammopelitic units being used to target a Broken Hill-type deposit.

A measure representing geological complexity has also been developed using short-distance neighbour relationships. The number of different adjacent stratigraphic units directly adjacent to the sample voxel can be identified (Figure 5b). For example, if a sample voxel had one type of stratigraphic unit adjacent, then the voxel is surrounded by the same stratigraphic unit. This would indicate that the cell is located away from the extremities, in an area of low geological complexity. Complexity increases as the number of differing adjacent stratigraphic units increases. A value of 'two' indicates that the cell is on a geological contact between two different units. A value of 'three' indicates that the cell on a triple-junction between units. Individual voxels can give information about the complexity of a given point, but a mean value for an entire formation can represent the geological complexity for the whole formation. Geological complexity information can be used to determine which stratigraphic units or structures within the model may be more difficult to target in drilling programs.

4. Principal component analysis (PCA)

Simultaneous analysis of variability within geodiversity metrics can describe the geometrical variation between models within the model suite. The measured attributes of analysed metrics can be used to identify which models are 'outliers' and display a large difference from the more common and similar examples within a model suite. Model similarity defines a 'barycentre' of the model suite in geometrical terms depending on the metrics under examination. Further, and perhaps more interestingly, the models that display a large degree of difference from the barycentre can identify model suite 'end-members', either for individual or all metrics. Knowledge of end-members helps to define the limits of geological possibility, given the input dataset, method of model calculation and geodiversity metrics employed.

This contribution employs multiple geodiversity metrics. While expert opinion may hypothesise that co-variance exists between each geodiversity metric, it is required that rigorous analysis be performed to confirm this hypothesis. For example, the differences seen between models in terms of formation volume and formation depth, are likely to be unrelated. The problem has become multidimensional, and multivariate analysis must be used to adequately analyse the complexities of the model suite. PCA has been chosen to perform this task. Jolliffe (2002) describes PCA as an exploratory data technique that allows complex data interactions to be displayed by orthogonal transformation of the data and re-organisation in terms of relevance to the attribute being analysed . The original, potentially correlated variables (in this case the geodiversity metrics) are converted into uncorrelated variables or principal components. The conversion of data is performed so that the first principal component displays the greatest variance, with each component thereafter displaying progressively lower degrees of variance. This means that each component contains a combination of variability across all the metrics, rather than measuring the variability of just one. The combined effect on variability of all the metrics can be measured, and also allows metrics using different units of measurement to be included. Each further component contains the next highest degree of remaining variance, so long as it is uncorrelated to preceding components (Jolliffe, 2002). A common cause (or causes) behind the influence a metric has over model variability can be identified combining metric variability into principal components.

Principal components are calculated in the following manner:

1. Statistics (mean, subtract deviations from mean, calculation of the covariance matrix)
2. Sort eigenvectors and eigenvalues of the covariance matrix in descending order
3. Determine contributions of eigenvectors to eigenvalues
4. Determination of basis vectors
5. Projection of the z-score-converted original dataset onto basis vectors.

PCA has been chosen instead of other multivariate techniques such as Factor Analysis and Nonnegative Matrix Factorization due the larger range of visualisation methods available. PCA was performed in MATLAB, primarily with the 'princomp' function (http://www.mathworks.com.au/help/toolbox/stats/princomp.html). The coefficients, or 'loadings', of the linear combinations of the metrics that were used to calculate the principal component data are obtained from this function (Jolliffe, 2002). Plotting loadings as vectors can show the contribution in variability a particular metric has toward the principal components (see Figure 6). Hotelling's T^2 statistic is also calculated with the MATLAB 'princomp' function, allowing models to be ranked according to their multivariate distance from the centre of the dataset and aiding identification of model suite outliers and barycentre examples (Hotelling, 1931; Krzanowski, 1995).

A two-stage PCA method is employed. The first stage determines which individual stratigraphic units best describe variability within each metric. Each stratigraphic unit is analysed using depth, volume and short-distance neighbourhood relationship metrics. The stratigraphic unit from each metric that best describes variability within the model suite is identified from loading vectors. The metrics contributing most variability to the first two principal components are retained and collated into a combined matrix with other geodiversity metrics representatives. The combined matrix is then assessed using PCA in stage two. Figure 6 shows a workflow for this process using four example stratigraphic units *W*, *X*, *Y* and *Z*. Units *X* and *Y* are seen to contribute most to the first principal component and second component variability respectively, for the volume metric. Units *W* and *Z* contribute most variability to the depth geodiversity metric. The volume measures for units *X* and *Y* and depths for *W* and *Z* are collated into a single matrix with the measures from other metric representatives. It is now possible to determine (1) which metric best describes model suite variability overall and (2) which models represent the outliers and barycentre of the model

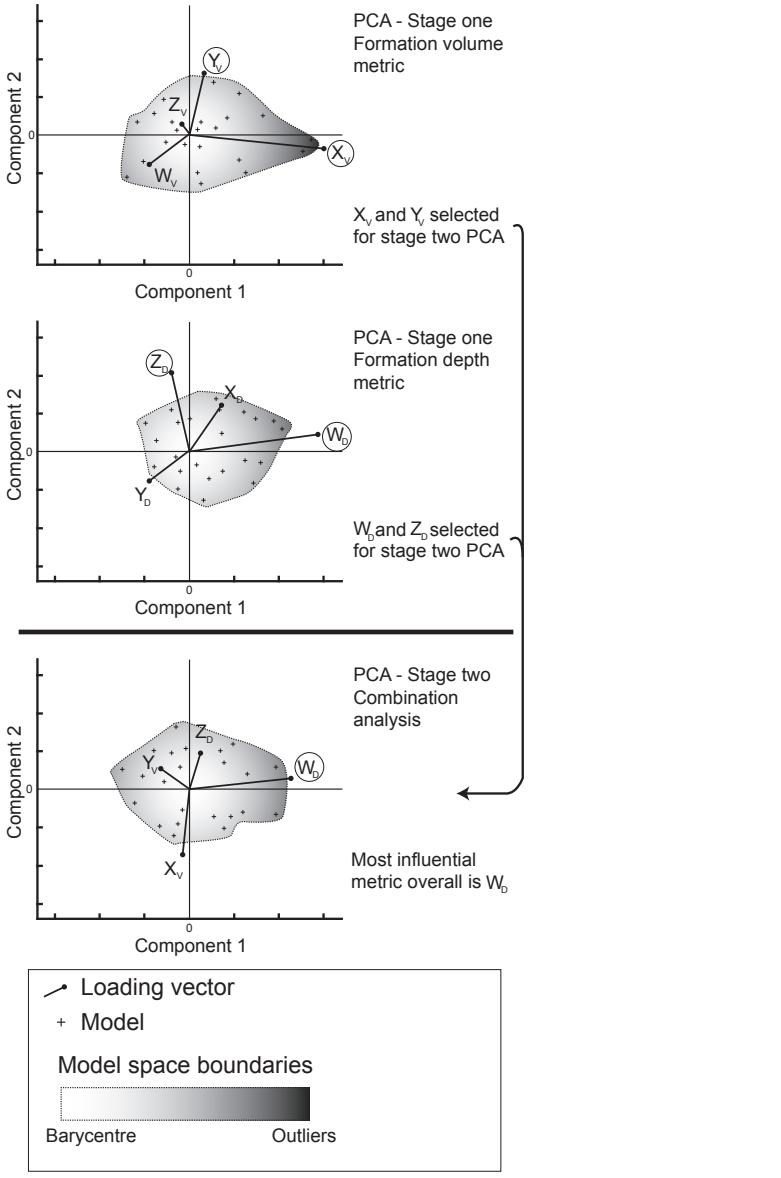

Figure 6. Flowchart displaying the two-stage PCA method used in this contribution. A model suite containing 20 models is used in this example. Above the solid black line are the first stage analyses of formation volume and formation depth geodiversity metrics. The combination analysis is shown below the black line. Loading vectors that plot close to the component axes represent the association of variability for that component and the length of the vector indicates the magnitude of variability represented. The model space boundaries are shown with a dashed line and shading indicates regions of barycentre or outlier model space.

suite. In the Figure 6 example, the depth of unit *W* has been determined to be the most influential in terms of geological variability between models.

5. Gippsland Basin, southeastern Australia

A geological data set representing the Gippsland Basin, southeastern Australia (Figure 7a) has been used to build a 3D model case study (Figure 7b) to discover what type of information can be obtained from geodiversity metrics and PCA in a natural setting. A variety of data types

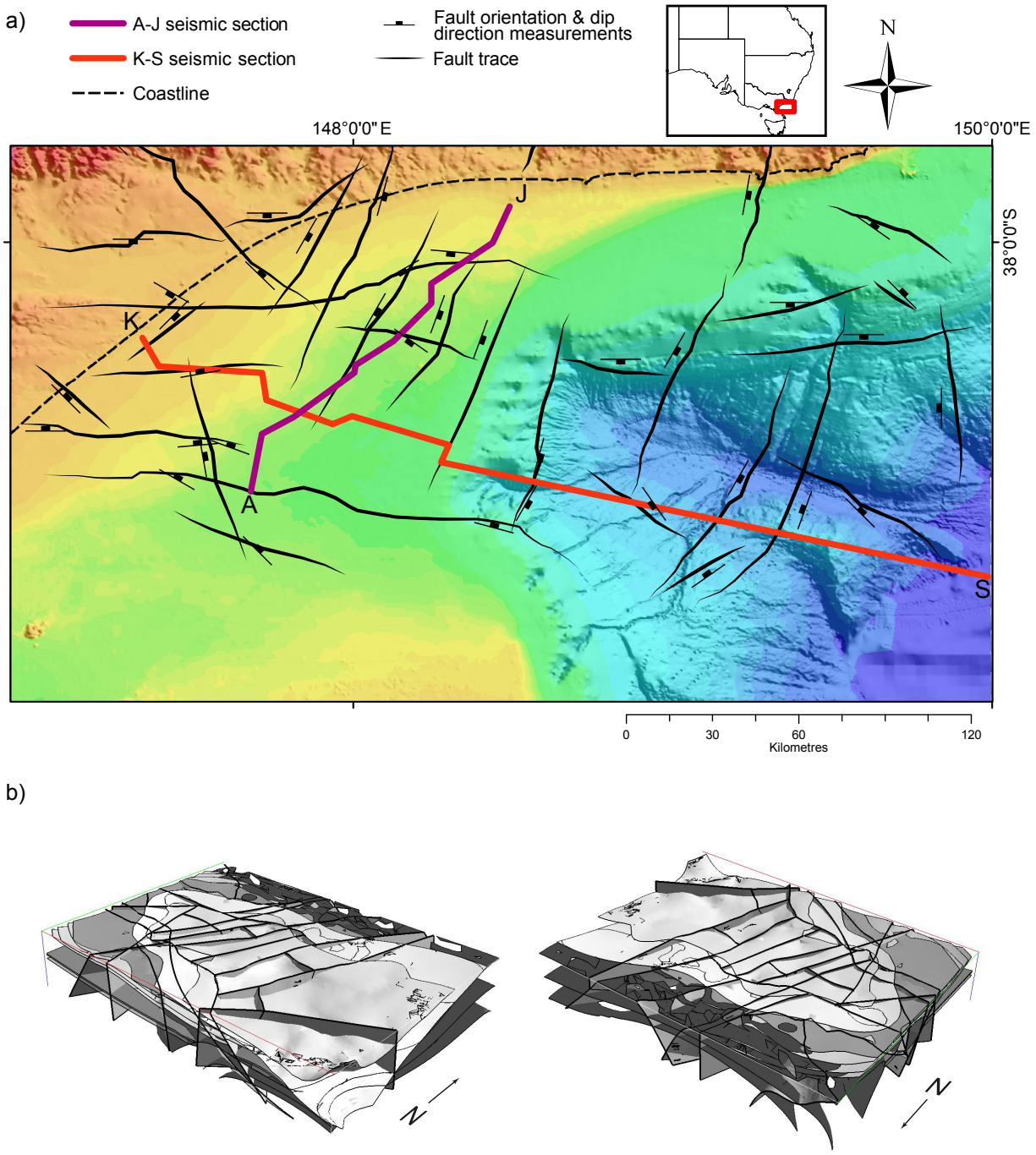

Figure 7. a) Location and fault map of Gippsland Basin, southeastern Australia. Shaded background represents bathymetry. Modified after Lindsay et al. (2012). b) 3D model of the Gippsland Basin shown from the southeast (left) and northwest (right). Fault surfaces are highlighted with thicker borders.

have been used when building this model, including hard rock observations, geophysical interpretation (2D seismic, aeromagnetic and gravity data), bathymetry information and well logs (Lindsay et al., 2012). Each geological formation within the model has been assigned a stratigraphic ID based on position within the stratigraphic column (Figure 8). Geological relationships shown in the stratigraphic column have been taken from the literature (Rahmanian et al., 1990; Willman et al., 2002). The Mesozoic to Cenozoic Gippsland Basin is a mature oil and gas field located in

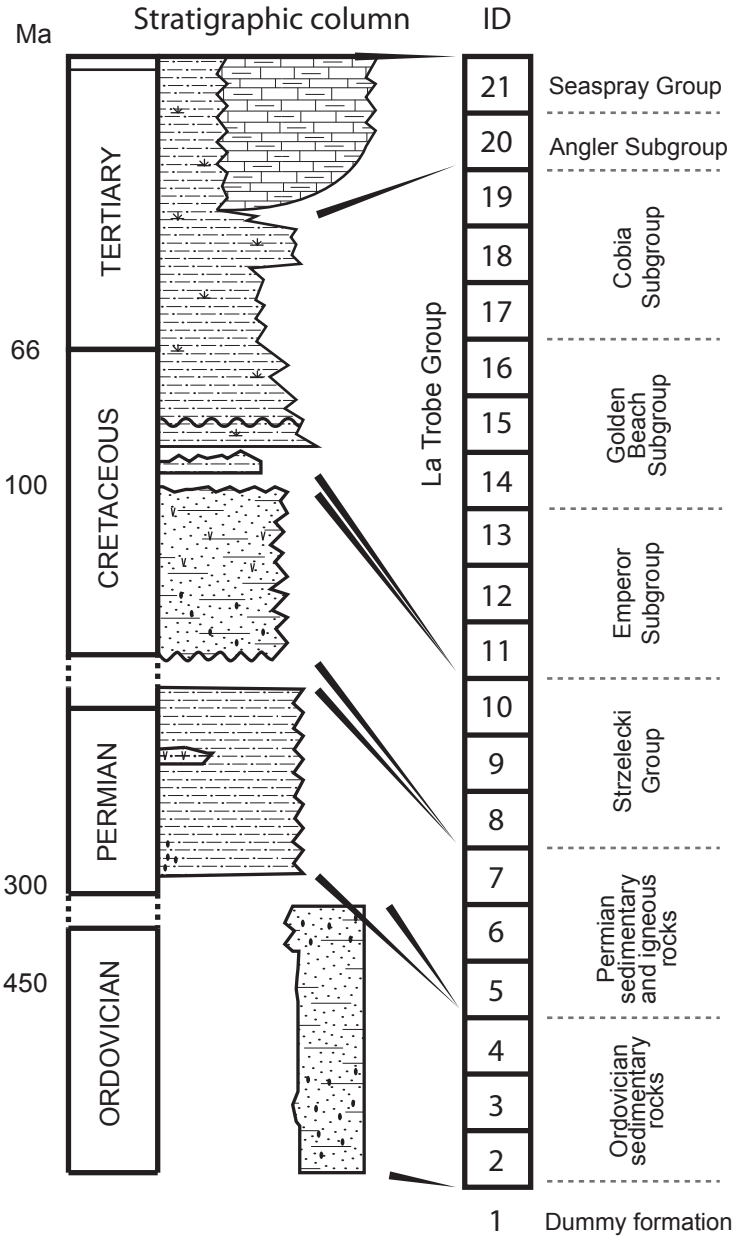

Figure 8. Stratigraphic column used to generate the Gippsland Basin model and the associated stratigraphic IDs for each unit. The 'Dummy formation' (ID: 1) is used by 3D Geomodeller to fill space at the base of the model. After Lindsay et al. (2012).

southeastern Australia that also hosts brown coal deposits and is prospective for CO2 sequestration (Rahmanian et al., 1990; Cook, 2006). Ordovician formations comprise the basement of the model and the Oligocene to Pliocene Seaspray and Angler comprise the cover sequences. The Paleocene to Late Miocene Latrobe Group is primary target for oil and gas and includes the Cobia, Golden Beach and Emperor Subgroups (Bernecker et al., 2001). The basin is cross-cut by a number of transfer and normal faults, with the model fault-bounded to the west, north and south. The initial assumption was made that either the volume or depth of formation metrics would have the greatest influence on model suite variability as the model has layer-cake stratigraphy typical of a basin.

6. Modelling results and discussion

6.1. Geodiversity end-members

Simple ranking of geodiversity metrics selected as the best representatives of model variability reveals the range of geological and geometrical possibilities available in the model suite (Table 1). The selection process of representative stratigraphic units is explained more fully in Section 6.2. The degree of variability that can be observed within a model suite for a given metric is shown by maximum, minimum and range values. These simple statistics quantify geometries that can be used in subsequent modelling or analysis. Viewing the spread of values in Table 1 and comparison with the initial model (i.e. the model generated from an unperturbed dataset) emphasises the high degree of uncertainty that can exist within a model suite. The last row in Table 1 shows the initial model distance from the studentized mean using standard deviation as measurement units. The results show that the initial model varies from the model suite mean, especially for km (1.43) and depth (1.11) metrics, highlighting that the initial model is unlikely to be the best, or at least most common, representative of the dataset.

Table 1. PCA-selected geodiversity metrics and associated end-member model representatives. The model representing the model suite end-member for each metric is bracketed. A comparison with the initial model created from unperturbed data is shown on the last two rows. Distance the initial model is from the geodiversity metric model suite average is shown using the number of standard deviations away from the sample mean. The magnitude of some distance values (bold) emphasises how the initial model is not necessarily the best representative of model suite possibilities.

	SDN – Strat ID 14	Contact surface area 3 & 4 (km^2)	k_m	k_g	Depth of Strat ID 16 (m)	Volume of Strat ID 3 (km^3)
Max	4.14 (15)	1840 (97)	$5.02x10^{-5}$ (38)	~ 0 (81)	-5500 (100)	3910 (30)
Min	3.56 (80)	1754 (56)	$-5.95x10^{-6}$ (65)	$-5.02x10^{19}$ (40)	-3500 (2)	3681 (16)
Range	0.59	86	$5.61x10^{-5}$	$5.02x10^{19}$	2000	229
Initial model	3.89	1781	2.82E-05	-9.7E+18	-5500	38185
S away from the model suite mean	0.025	**0.53**	**1.43**	**0.78**	**1.11**	0.15

The data in Table 1 provides some useful constraints that define geometrical end-members within a model suite. This information only describes part of problem, as all elements of the model are defined by a combination of these metrics. Comparing each metric with respect to its end-members or the entire ranked list of models will reveal little as no single model appears more than once as an end-member representative, nor does there appear to be any obvious relationships between the ranked lists. Finding a boundary for least likely models, nor which models are the most likely, cannot be found using direct comparative methods alone. A multivariate statistical technique, such as PCA, is therefore employed to combine these metrics to i) find the model suite barycentre and boundary and ii) find the geodiversity metric that best describes model variability.

6.2. Model suite analysis

Figure 9a shows loading and score plots for short-distance neighbourhood relationships taken from stage one PCA conducted on the Gippsland Basin model suite. Each vector represents a stratigraphic unit. The direction and length of the vector indicates how each stratigraphic unit contributes to the two principal components in the plot. Figure 9a shows that stratigraphic units

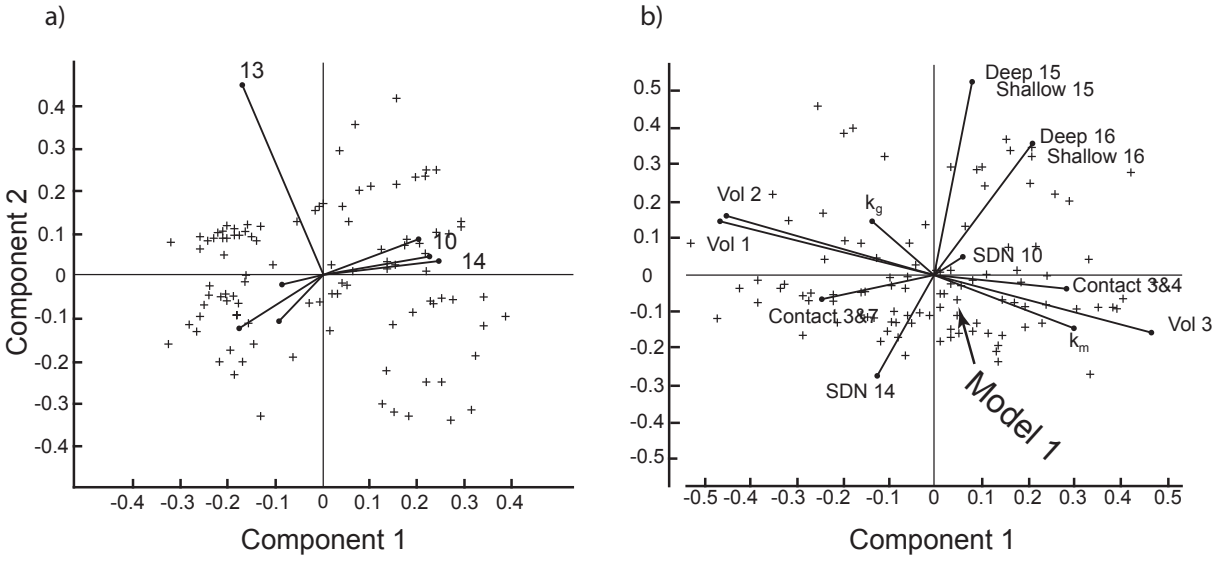

Figure 9. a) Stage one PCA plot of short distance neighbour relationships (Section 3.3). Only significant loading vectors have been plotted. The loading vector associated with lithology 14 (bottom of the Golden Beach Subgroup – Figure 8) shows the greatest influence on model variability due to the proximity to the component one (x-) axis. Lithology 14 is retained to form the combined matrix used in stage two PCA. b) Stage two combined PCA plot. Each loading vector is labelled according to the metric used and the stratigraphic ID selected from stage one: Deep = deepest unit; Shallow = shallowest unit; SDN = Short distance neighbour; Contact = contact surface area (contact units are both listed), Vol = volume; k_m = mean curvature, k_g = Gaussian curvature. The location of Model 1, the initial model is indicated with an arrow. Note that Model 1 is not the closest model to the model space barycentre.

fourteen (bottom of the Golden Beach Subgroup – see Figure 8), ten (top the Strzelecki Group) and fifteen (middle of the Golden Beach Subgroup) contribute the most to the first principal component (x axis), whereas thirteen (top of the Emperor Subgroup) contributes the most toward the second principal component (y axis). Units fourteen and ten (top of the Strzelecki Group) are selected as representatives of short distance neighbour variability on the basis of loading vector plots. The same selection process is performed on the other geodiversity metrics described in Section 3. A combined matrix of representative metrics is formed and subjected to PCA. From stage two PCA it can be determined which models represent the barycentre of the model suite and models that represent the outliers. Figure 9b shows the results from the combined geodiversity metric PCA from the Gippsland Basin. All geodiversity metrics defined in Section 3 have been input to determine which models are classed as outlier representations of the model suite, and those that represent the barycentre when all metrics are taken into consideration. Hotelling's T^2 scores for each model are sorted to identify the rank for each of the model suite members. Models 40, 30 and 38 define the most diverse, or outlier model. The most common, or barycentre are found to be models 95, 61 and 20. A significant result is that initial model (Model '1') does not appear in top-three barycentre models. The initial model is ranked 11th, meaning that there are 10 other models considered more representative of the model suite. This finding has negative implications for modelling workflows that consider only one realisation of input data necessary. One 3D realisation of a data set severely limits the study to a narrow view of geological possibility and likely misrepresents both the data set and the geological terrane under study.

Figure 9b shows the most influential metric of model suite variability for the Gippsland Basin is a member of the Ordovician basement (volume of stratigraphic unit three, see Figure 8). As this basement unit underlies most of the stratigraphy in a basin environment, any geometrical perturbations of this unit will have subsequent effect on the volume of the formation, which in turn affects the spatial location of all overlying units, including the oil and gas prospective Latrobe Group units. Further revisions of the model can be aided by these results. Measurements, observations and data types that are effective at constraining the volume of Gippsland Basin stratigraphic unit three can be pursued. If these aspects of the model can be better constrained, the possibility of high variability between models may decrease, which subsequently reduces overall model uncertainty. The variety of geodiversity end-member models identified within the Gippsland Basin

model suite also suggests that using a number of metrics is appropriate to encompass the variety of model geometries presented when a data set has been subjected to uncertainty simulation.

End-member information shown in Table 1 also provides useful information. A range of feasible values describing 3D model geometries can be obtained through geodiversity metrics to provide constraints for inversion processes. Volumes can be used to ensure geological units do not exceed a specific size and depths can be useful to ensure that geological units are spatially constrained. Curvature measures can constrain the amount of deformation a surface exhibits within the model. Using a combination of short-distance neighbourhood values and contact surface areas can provide powerful constraints at the boundaries of geological units, ensuring geological relationships and connectivity are retained.

7. Conclusions

The geodiversity metrics used in this study can be useful to various geoscientific studies. The metrics describe the type and quantity of geometrical variability that may be encountered when generating a 3D model from a single geological input data. Difficult to obtain geometrical information can be obtained from the model suite and allow comparison with other model suites. The Gippsland Basin model suite has been analysed to determine end-member models for particular metrics, providing constraints for inversion processes. PCA has been used to define the model space boundaries and the outlier and barycentre models for both individual geodiversity metrics and combined metrics. The outlier models may become new 'species' of model that require further investigation. The presence of these new 'species' may drive additional research directions and aid selection of exploration techniques and targeting locations. The relative contribution of different stratigraphic units within individual metrics has been assessed to find their contribution to model suite variability, answering questions relating to the specific aims of a geoscientific study and improvements in the case study model. Areas of interest can be easily located using these metrics, as the data is georeferenced within the voxet. Different metrics can also be identified as contributing more or less to model suite variability. Additional metrics can be easily incorporated into future end-member and principal component analyses as they are developed, increasing the potential for extracting additional geometrical and model suite information. The geodiversity metrics shown

here are certainly not exhaustive, and more can be developed and incorporated into the process.

The information produced from end-member and PCA analysis of geodiversity metrics allows the geoscientists to identify which metrics more effectively inspect, quantify and represent the breadth of geological possibility. Some of the issues concerning the interpretive nature of geology can be addressed by assuming that uncertainty is inherent within input data and producing a model suite. Biodiversity measures the diversity of species to explain complex relationships and function within an ecosystem. The parts of a 3D geological model are examined in relation to the whole of the model, and model 'species' are considered in relation to the entire model suite. Producing a single 3D geological model from a data set has been shown to misrepresent what is geologically possible. PCA of geodiversity metric results taken from the Gippsland Basin model suite reveals that the initial model produced using the input data is not the most representative, and there are 10 other models that are more representative of the data. With this knowledge one is lead to consider which diverse model geometries define boundaries of model space. The geological possibilities that may have been filtered by preconceptions, foresight and equipment biases can now be revealed by multivariate analysis of geological possibility.

Acknowledgements

Thanks go to Geoscience Victoria, Department of Primary Industries, Victoria, Australia; the Society of Economic Geologists Hugo Dummett Memorial Fund and Intrepid Geophysics for technical assistance and access to the 3D Geomodeller API (Application Programming Interface).

2a

The combination of geodiversity and principal component analysis provide a powerful means by which to examine model suite uncertainty. The geodiversity concept also initiates a model space search for geological possibility. The discovery in Chapter 2 that the initial model did not display the most common model geometries has provided evidence in support of workflows that produce multiple models. The geodiversity metrics employed in Chapter 2 describe important geometrical aspects of model elements in the Gippsland Basin model suite. What is missing is a set of metrics that describe geophysical aspects of a model.

Geophysical techniques are very common and useful in 3D geological modelling. Geophysical interpretation of potential field data is commonly used to aid geological interpolation between outcrops, especially in regions of sparse data. It was decided that some manner of geophysical measure was necessary to include into the stable of geodiversity metrics. A typical stage in any modelling workflow is to determine the 3D forward geophysical response of a model for comparison against the observed response obtained through geophysical surveying. The hypothesis is that as geophysical data usually provides the greatest coverage over a region of interest, the observed geophysical response will provide the most complete representation of the natural system. The root-mean-square (RMS) of the misfit between the calculated and the observed responses typically represents the overall distance between the 3D model and the natural world. Additional geophysical metrics that measure different aspects of the calculated and observed geophysical response were included into the geodiversity stable in an attempt to account for geophysical ambiguity.

The 3D Geomodeller™ modelling application is used to generate the forward response of each 3D model. An application program interface (API) is provided with the modelling application that allowed access to a range of functions from within the software making task automation possible. In Chapter 3, forward modelling is automatically performed for the entire model suite and produced calculated response grids are model and corresponding RMS misfit values. The calculated response grids are imported into Matlab©. A range of image processing functions and script looping allow all geophysical metrics to be tested and incorporated into the modelling workflow. The aim of geophysically characterising a model suite is to move the workflow closer to a geophysical inversion procedure that acknowledges multiple geological and geophysical possibilities.

A new model suite is analysed in Chapter 3. The Ashanti Greenstone Belt, southwestern Ghana, west Africa is modelled in collaboration between Monash University and Université Paul

Sabatier (Toulouse III) (Perrouty et al., 2012). The Ashanti Greenstone Belt is a palaeoproterozoic metamorphic terrane, geologically different to the Gippsland Basin model analysed in Chapters 1 and 2. Analysis of the Ashanti Greenstone Belt model is performed to determine if the techniques developed in Chapters 1 and 2 are transferrable to a model in a different geological terrane. Performing the techniques on the Ashanti Greenstone Belt model suite also reveals whether these techniques are just as effective in mineral prospective terranes as in oil and gas prospective terranes. Chapter 3 is currently in preparation for submission to the Geophysical Journal International.

3

Investigation of the Ashanti Greenstone Belt with geophysical forward modelling

Mark D. Lindsay [a,b], Stephane Perrouty [b,c], Mark W. Jessell [b,c], Laurent Ailleres [a]

[a] School of Geosciences, Monash University, PO Box 28E, Victoria, 3800, Australia
[b] Université de Toulouse, UPS, (OMP), GET, 14 Av. Edouard Belin, F-31400, Toulouse, France
[c] IRD, GET, F-31400, Toulouse, France

In preparation for submission to **Geophysical Journal International**.

Abstract

The process of three-dimensional (3D) modelling forces the operator to consider data collection and processing error while making assumptions about geology, requiring interpretation to arrive at the most likely or logical geological scenario. These kinds of ambiguities lead to a situations where multiple model realisations can be produced from a single input data set. Typically decisions are made during the modelling process with the aim of reducing the number of possible models, preferably to produce a single geological realisation. These types of decisions involve how input data is processed and what data is included, and are always made without complete knowledge of the system under study. This regularly, if not always, results in natural geometries being misrepresented by the model, which can be attributed to uncertainty inherent in the modelling process. Uncertainty is unavoidable in geological modelling as complete knowledge of the natural system is impossible, though we use many techniques to reduce the amount introduced through the process. A common technique used to reduce uncertainty is geophysical forward modelling, and the misfit between the calculated and observed response provides a means to gauge whether changes in model architecture improve or degrade the quality of the model. Unfortunately, geophysical data is in itself ambiguous and provides a non-unique solution, and different model geometries can produce the same geophysical response.

We propose a process whereby multiple models, collectively known as the 'model suite', are produced from a single data set that allows an exploration of geological model space. Various 'geodiversity' metrics have been developed to characterise geometrical and geophysical aspects of each model. Geodiversity measurements are combined into multivariate analysis that reveals relationships between metrics and defines the boundaries of the possible geological models. A previous study using geodiversity metrics on the Gippsland Basin is extended here by including geophysical metrics. We use the Ashanti Greenstone Belt, southwestern Ghana in West Africa as a case study to assess the usefulness of the technique. A critical assessment of the 3D model is performed and aspects of the model space are identified that could be interest to gold explorers.

Keywords: Geophysical forward modelling, 3D modelling, Principal component analysis, Ashanti Greenstone Belt, Geodiversity

1. Introduction

Two-dimensional (2D) and three-dimensional (3D) geophysical forward modelling is a useful tool commonly used in geoscientific studies to validate or falsify geological models against the observed geophysical data. Both variations compare an 'observed' geophysical response against a 'calculated' response. The calculated response signal is measured from a representation of geology contained within a 2 or 3D model. The shape, depth and size of a stratigraphic unit in combination with the contrast of assigned petrophysical properties produce a signal. Other elements in the model, such as faults or dykes, are also taken into consideration. The combinations of signals from the modelled geological units and structures are calculated and are convolved to produce the calculated field, for examples Betts et al. (2003), Joly et al. (2008), Williams et al. (2009) and Perrouty et al. (2012).

Together with petrophysical information, the geometry of the geological model plays a key role in the process of geophysical modelling. The aim of this study is to discover whether relationships exist between particular geometrical parameters exhibited in a 3D model and the geophysical response. For example, the geophysical response may be heavily influenced by the volume or geological complexity of a particular geological formation within a model. Discovering a relationship of this nature will enable model refinements to be guided toward finding a model that honours both geological and geophysical data. However, determining a relationship is difficult as the interaction between model geometries, petrophysical properties and geophysical response is complicated. A model space exploration is a useful means by which to achieve this goal.

We produce a number of 3D geological models based on the same input data set to produce a model suite, a collection of models that exhibit similar, but not identical, model architecture. Each one of these models is considered geologically feasible and may a priori provide the best realisation of the natural world possible, given the input data. The model suite can be analysed in its entirety to determine uncertainty, the range of geometrical possibility and geophysical misfit. We perform an exploration of geological and geophysical model space using the Ashanti Greenstone Belt, southwestern Ghana as a case study. A set of 'geodiversity metrics', quantifying both geo-

metrical and geophysical aspects of the 3D model (Jessell et al., 2010; Lindsay et al., 2012b), are used to determine geological end-members existing within the model space. A geodiveristy metric is a measure, such as volume, surface area or geophysical misfit, that characterises an aspect of a model and allows comparison against other models within the model suite. A multi-variate statistical technique is employed to simultaneously compare all the metrics and determine their effect on the model suite. Analysis of the results is performed using Principal Component Analysis (PCA) which allows: (1) determination of the model space boundaries, a theoretical limit to geological possibility defined by models exhibiting the most unusual architecture; (2) identification of uncommon and common models in terms of both geometry and geophysics and (3) an understanding of which metrics can contribute most to uncertainty in modelling.

1.1. Geodiversity principles and the link to model uncertainty

Uncertainty is inherent in any modelling process and is particularly evident in 3D geological modelling (Cherpeau et al., 2010; Chugunov et al., 2008; Gershon, 1998; Jessell et al., 2010; Thore et al., 2002). 3D modelling suffers from a lack of geological information as there is never complete coverage of data that describes the entire system. Outcrop is usually limited, restricting field observations, and can be under-sampled when available. Geophysical data may not supply complete coverage nor be available at the required resolution for detailed interpretation. Uncertainty caused by data sparseness is exacerbated by input data errors, caused during collection, processing or preparation for input to the geological model (Bond et al., 2010; Yeten et al., 2004). Issues such as upscaling data (where clustered data points are subsampled to a representative point prior to input) are well-known but typically tolerated. The effects of upscaling, sampling and data error and resulting uncertainty have been examined by Putz et al. (2006). They found that their model remained reasonably robust until 50 percent of input data had been subsampled prior to model generation. After the 50 percent threshold, the model progressively degrades with increasing degrees of downsampling until observed geology is barely recognisable. 50 percent is not a threshold that applies to all models. The level at which models degrade beyond being recognisable depends on the redundancy between data and the interpolation algorithm, which also relates to model complexity.

Recent studies have shown how uncertainty can be located, quantified and possibly reduced using different methods (Jessell et al., 2010; Lindsay et al., 2012a; Thomson et al., 2005; Viard et al., 2010; Wellmann and Regenauer-Lieb, 2011). Geodiversity metrics were developed as a means of measuring uncertainty, as the presence of uncertainty implies that model geometry must be variable (Figure 1). Varied geometry then suggests that the various elements of each model, be they the volume of a granitoid or surface area of a contact will vary as well. Geodiversity metrics are a method to analyse geometrical variations of model elements and determine the upper and lower bounds for each metric in order to establish model suite end-members. The volume of a modelled granitoid can serves as an example. The model with the smallest volume of granitoid can be identified, and the model with the largest volume of the same granitoid can also be identified. Therefore the model that contains the granitoid with the smallest volume becomes the minimum end-member representative for the volume of the granitoid, and the model exhibiting the largest volume for the granitoid becomes the corresponding maximum end-member representative.

Geometrical aspects of a 3D model are not the only metrics of interest to geoscientists. Geophysics is an integral component of many modern geological studies, and is used heavily in the 3D modelling process. Geophysical metrics can be included in the suite of geodiversity metrics in order to quantify the capacity of the model suite to match the observed geophysical field. End-members for different geophysical metrics can be identified just like their geometrical counterparts, and used to aid further modelling efforts. Finding whether any geometrical metrics can be

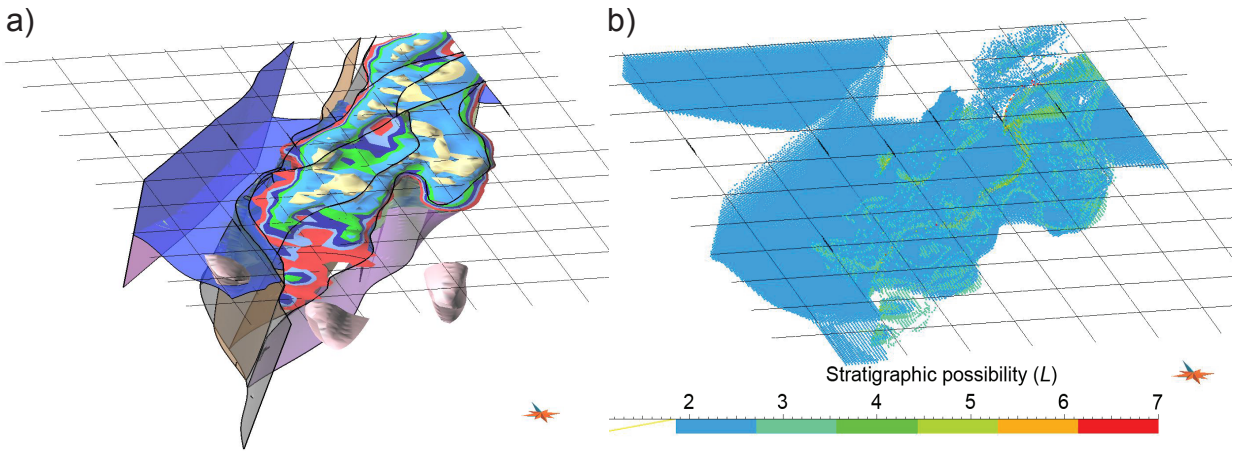

Figure 1. Visualisation of uncertainty in the Ashanti Greenstone Belt model. Note that grid lines have 10km spacing. Geological contacts (colours correspond to the stratigraphic column in Figure 2) and faults (thick black borders) from the initial model are shown in a). Uncertainty within the model is shown in b), with the degree of uncertainty (stratigraphic possibility) shown using a colour code (blue is lowest uncertainty, red is highest). The stratigraphic possibility (L) is the number of possible stratigraphic units that can be found at a given point for all the models in the model suite (Lindsay et al. 2012).

linked with geophysical metrics is of particular interest, providing a guide to which geometrical aspect of the model should be examined to most efficiently decrease geophysical misfit and lead to a model that honours both geophysical and geological data.

2. Method

2.1. Geophysical forward modelling

The geophysical forward modelling method used in this contribution discretises the 3D geological model into a 3D grid, or 'voxet'. Each cell, or 'voxel', is assigned a stratigraphic unit identifier based on the geological model. Next, each voxel is assigned a petrophysical value representative of the assigned stratigraphic identifier and appropriate to the geophysical response required. In this paper, the gravitational response is being modelled, so density is the assigned petrophysical property. The sum of the contribution of each voxel to the field is calculated using an analytical expression (Holstein, 2003; Holstein et al., 1999; Okabe, 1979; Plouff, 1976). The heterogeneity of petrophysical properties predicted to occur within a stratigraphic unit can be simulated by the definition of probability distribution functions (Figure 2). A 3D model of the southern Ashanti Greenstone Belt and corresponding calculated gravitational response is shown in Figure 3.

2.2. Comparison of geophysical images.

A residual grid is created by subtracting the calculated response grid from the observed response grid. The measure of geophysical misfit is often expressed as a root-mean-squared value, or 'RMS',

$$x_{rms} = \sqrt{\frac{1}{n}\left({x_1}^2 + {x_2}^2 + \ldots + {x_n}^2\right)}, \tag{1}$$

calculated from the residual grid that is the difference between the observed and calculated signals. Figure 4 shows the observed, calculated and residual grids for the initial model, i.e. the model that was calculated using an unperturbed data set.

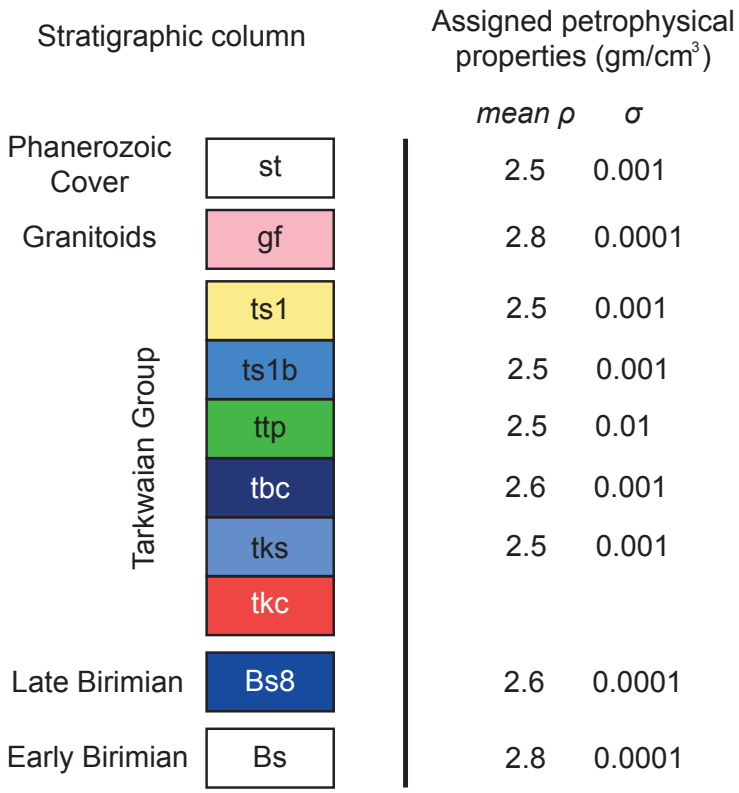

Figure 2. Input parameters used in construction and geophysical modelling of the Ashanti Greenstone Belt model. a) Stratigraphic column based on recently revised tectonic evolution (Perrouty et al. 2012). b) Petrophysical properties and distribution statistics assigned to each formation (Metelka et al. 2011; Perrouty et al. 2012).

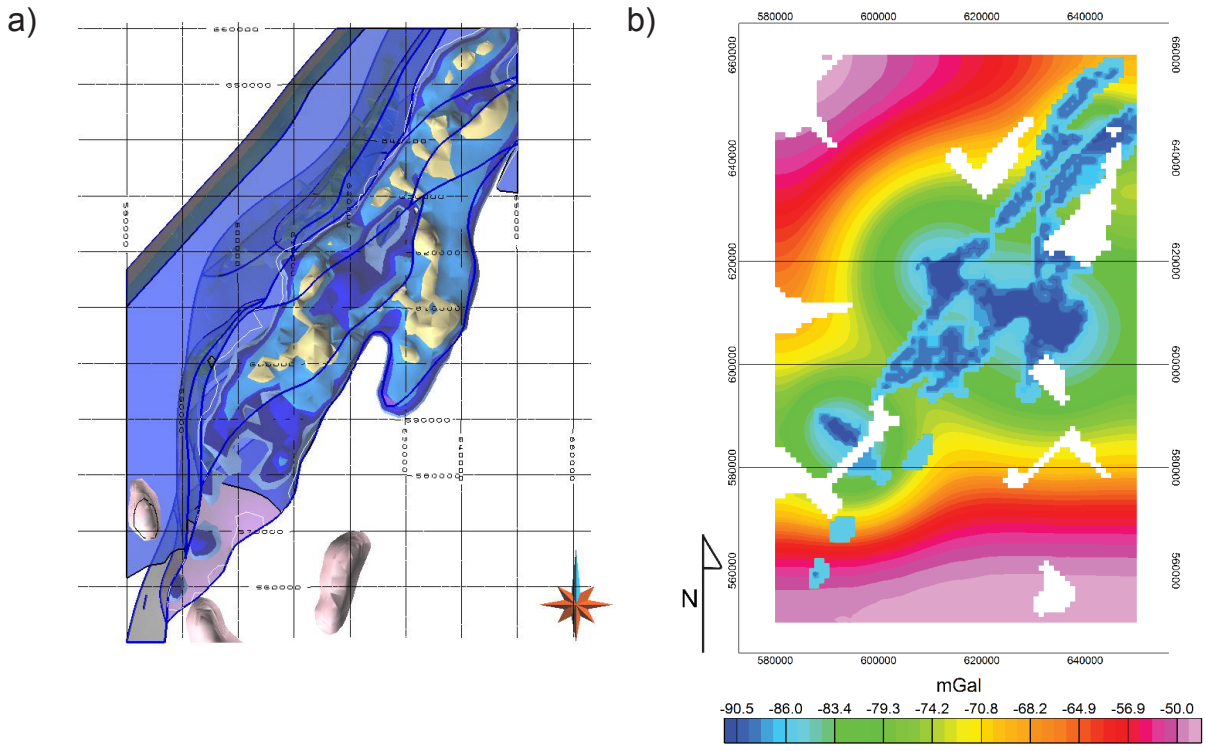

Figure 3. Calculating the geophysical response from a 3D model. a) shows a view of the Ashanti Greenstone Belt 3D model from above. Faults have been shown with blue border and stratigraphy is shown with opaque surfaces. b) shows the calculated geophysical gravity response of a). Note the 'white spaces' in b) indicating no interpolated gravity response. This 'white space' is particular to the 3D geophysical forward modelling procedure and associated parameters.

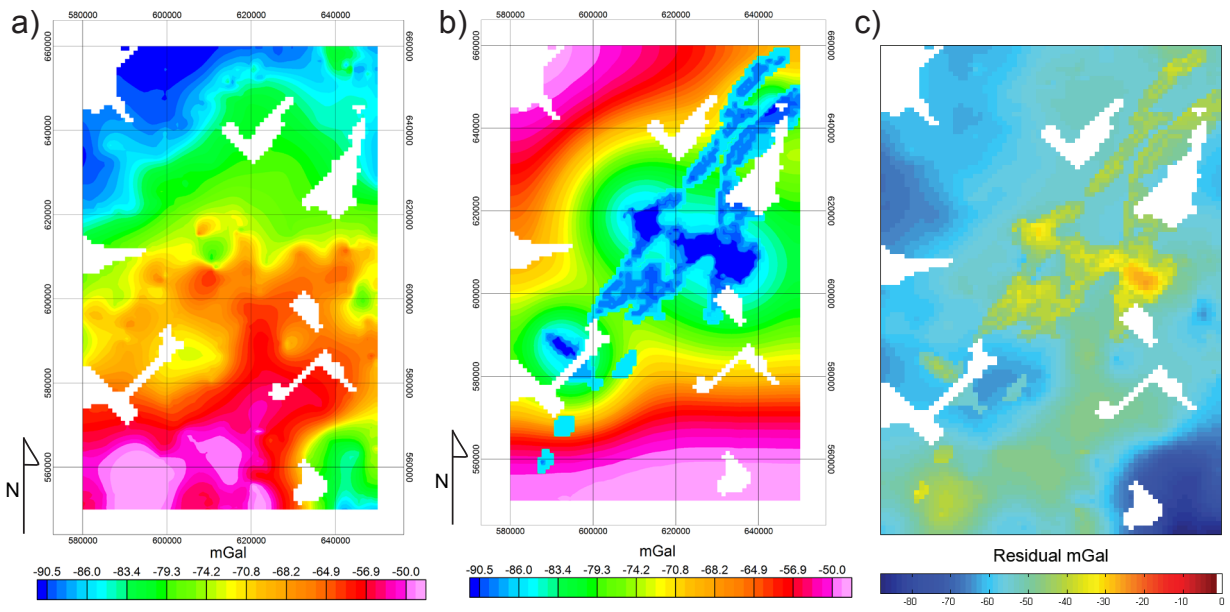

Figure 4. Example of 3D geophysical forward modelling from the initial Ashanti Greenstone Belt model. a) shows the observed gravity grid, which is based on survey data, b) is the calculated response of the initial model and c) is the residual, calculated from the difference between a) and b). 20 kilometre grid line spacing for a) and b).

2.3. Statistical analysis – global

The following techniques have been included in this study to obtain a scalar value for each calculated geophysical response. Some of these values are obtained by calculating the residual between the observed and calculated response. and include the 2D correlation coefficient, root-mean-squared (RMS) and the Hausdorff distance. The standard deviation and entropy techniques are typical image analysis techniques. The standard deviation technique was performed on the calculated grids, the entropy technique was performed on the residual grids. The scalar value obtained through these techniques is global, in other words, a value that represents the entire grid, not local regions within the grid. The global approach was implemented to adhere to the requirements of PCA. A requirement for performing PCA is that a single value represents each geodiversity metric (geometrical and geophysical) for each model in the model suite. While useful, non-global, or local image analysis of each of the geophysical grids would produce multiple values for each metric. All values obtained for one model would need to be reduced to single value for use in PCA, making a local analysis averaged.

2.3.1. Standard deviation

The standard deviation of an image is a common technique in image analysis as it represents the underlying intensity probability distribution, and it can be used to measure the degree to which potential field grid values vary across the entire image. Using standard deviation of the calculated response as a geodiversity metric allows the variability of each grid to be compared.

$$s = \left(\frac{1}{n-1} \sum_{i=1}^{n} (x_i - \bar{x})^2 \right)^{\frac{1}{2}} . \quad (2)$$

We can ask ourselves why would one model have a higher standard deviation than another? Can this be resolved due to a particular geometrical feature of the model? For example a granitoid with a high petrophysical contrast to the country rock that is larger in a model than others, may result in a relatively high standard deviation for the calculated response and assist examination of input petrophysical constraints.

2.3.2. Entropy

Entropy (*E)* is used to measure the average bits per pixel over an entire image, representing its global information content (O'Gorman et al., 2008). The type of entropy used here is 'Information Entropy' which is derived from the Shannon Entropy model (Shannon, 1948; Wellmann and Regenauer-Lieb, 2011):

$$E = -\sum_{i}^{N} p_i \; log \; p_i \quad , \quad (3)$$

where *E i*s the sum of all products of p (probability), of each possible outcome (i) out of N total possible outcomes. Where $E = 0$ it indicated that the image is dominated by large regions of the same value (Figure 5a). In a system of two integer values 0 and 1 (1-bit system) the $E_{max} = 1$ (Figure 5b). The image is made of equal proportions of possible values in this case, therefore $E = 1$ reflects that at any point it is equally likely to find a '0' or a '1'. Figure 5c is still a 1-bit system (values 0 or 1), but two out of three lines along the Y-axis are '1'. The proportions are no longer equal as it is 66.66% likely to find '1' and 33.33% likely to detect '0' at any given point and $E = 0.9135$. E_{max} will increase with the range of values within the data set under study. This is shown in Figure 5d where a range of five integers (one through five) are found in the randomly generated image.

Information entropy is a useful tool in exploring model space uncertainties. Wellmann et al. (2010) have used Information Entropy as a visualisation technique to communicate where

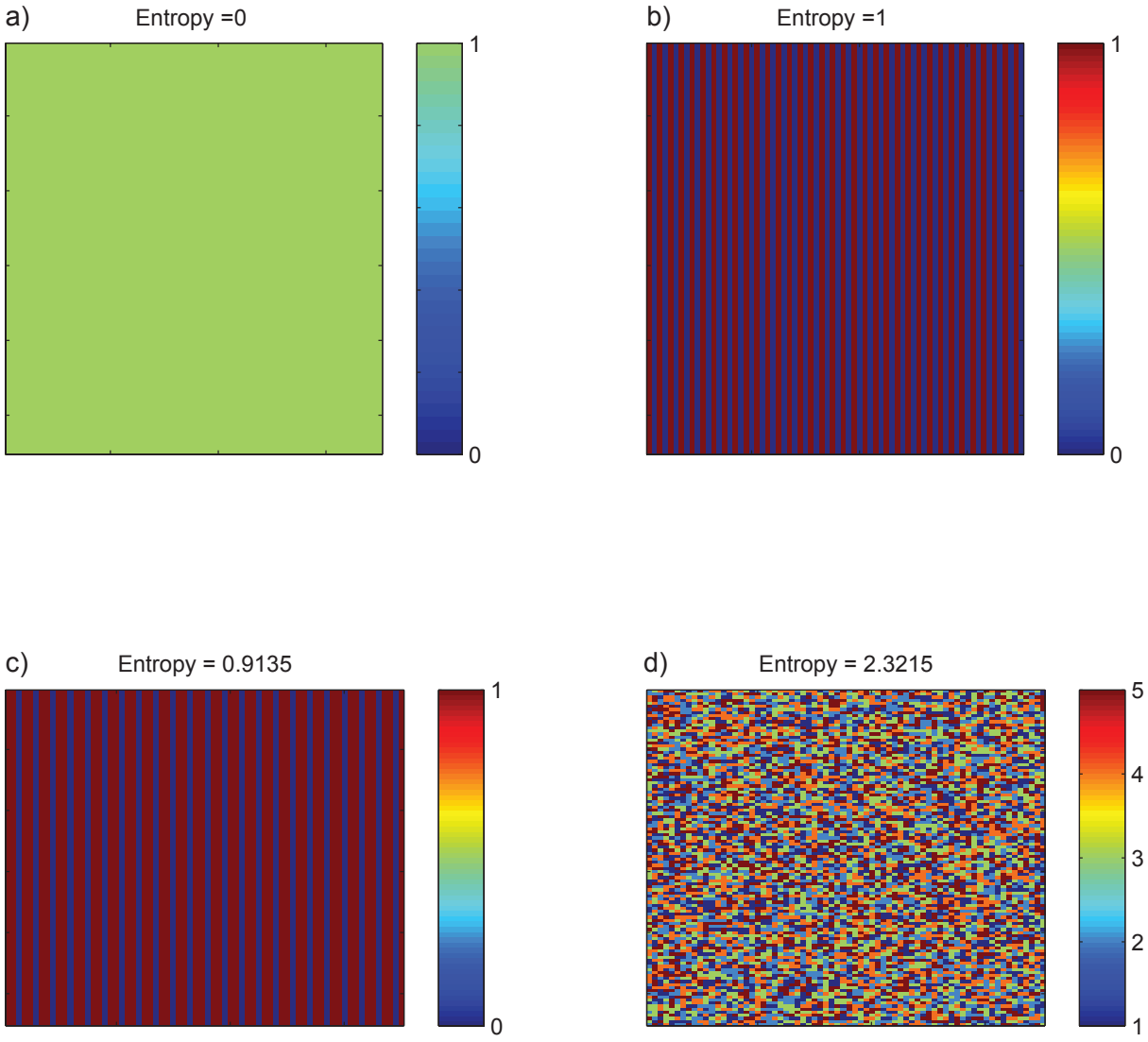

Figure 5. A set of four images showing how information entropy (E) can identify information content in an image. a) shows E = 0, meaning that entire image contains the same value and all pixels in the images can be predicted to 100% accuracy based on the value of one pixel. b) an image with two integer possibilities (0 or 1), alternating bands across the image will result in the highest amount of E for a binary system. While instinctively one would assume that the regular bands are easy to predict, in fact as there are equal proportions of 0's and 1's throughout the image, the possibility of picking a 0 or 1 at any given point is equally likely (50% for each value). There is no single value that is more likely to be found, so E =1, the highest value for a binary image. c) a binary image with a 66% chance to find '1' and 33% chance for '0', E is slightly lower, reflecting less randomness in the image. d) shows an image generated using a random function of integers 1 through 5. E is relatively high as the number of possibilities has increased, and the relative proportions of each integer are similar.

uncertainties within 3D models exist. We use the concept to analyse the residual grids produced by the automatic forward modelling technique to find grids that are smoother and contain less variability in values.

2.3.3. 2D correlation co-efficient

2D correlation co-efficients are typically calculated in geophysical and engineering applications to track changes in 2 and 3D objects. The subject of 2D correlations are often images as the algorithm is able to measure how closely an image of an object subjected to deformation resembles

the original state over a time period. The correlation is '2D' as it is performed between matrices, rather than between two vectors (Figure 6). The 2D correlation *r* is calculated using

$$r = \frac{\sum_m \sum_n \left(A_{mn} - \bar{A}\right)\left(B_{mn} - \bar{B}\right)}{\sqrt{\left(\sum_m \sum_n \left(A_{mn} - \bar{A}\right)^2\right)\left(\sum_m \sum_n \left(B_{mn} - \bar{B}\right)^2\right)}}, \quad (4)$$

where $\bar{A}$ is the global mean of image one (observed geophysical response) and $\bar{B}$ is the global mean of image two (the calculated geophysical response). The correlation between the images is not a subtractive comparison, such as performed in the RMS method, rather it measures whether patterns in the image resemble each other. The purpose of using this technique to compare observed and calculated responses is that if the correlation coefficient is high, the spatial variation of values in both the calculated and observed responses is similar.

2.3.4. Hausdorff distance

The Hausdorff distance measures how far points in two different subsets are from each

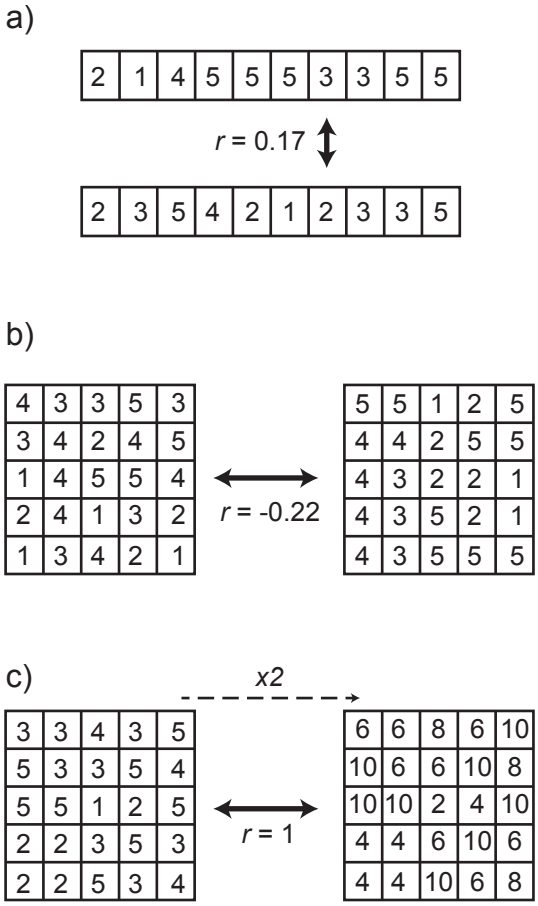

Figure 6. Features of 1 and 2D correlation functions. a) Correlation between two sets of vector data showing little to no linear dependence. b) 2D correlation between two matrices showing little linear dependence. c) The correlation function recognises that the second matrix has been created simply by multiplying the first matrix by two, returning a score indicating complete linear dependence.

other. The distance can then be used to understand the level of resemblance two superimposed objects have to each other. The Hausdorff distance has been typically used in machine vision (Rucklidge, 1997; Wang and Suter, 2007) and pattern recognition applications (Gao and Leung, 2002; Olson and Huttenlocher, 1997; Sim et al., 1999) to compare and find patterns in one image that may be present in another (Huttenlocher et al., 1993). Geophysical grids can be compared using the Hausdorff distance. If we assume that the geophysical forward response of a given 3D model is a subset of the model space, then the observed response of the potential field is also a subset of the same model space, but represents an as yet undiscovered 3D model (Foudil-Bey, 2012).

The Hausdorff distance (d_H)can account for dilation and limited degrees of rotation and translation of one image with respect to the other (Figure 7). Geometrical differences between model suite members will be reflected in their respective calculated geophysical responses. The recognition of similar patterns is not performed via standard geophysical misfit algorithms, so it is interesting to determine whether using the Hausdorff distance as a metric for model comparison can be more effective.

The Hausdorff distance is calculated using the following equation. *X* and *Y* are two non-empty subsets of a metric space (*M, d*). The Hausdorff distance between these two sets $d_H(X,Y)$ is

$$d_H(X,Y) = max\left\{ \sup_{x \in X} \inf_{y \in Y} d(x,y), \sup_{y \in Y} \inf_{x \in X} d(x,y) \right\}, \quad (5)$$

where *sup* is the supremum, *inf* is the infimum and *x* and *y* are points within sets *X* and *Y* respectively. In the application of the Hausdorff distance used here, *X* is a grid of the observed response, *Y* is a calculated forward response grid of some model and *x* and *y* are values of a given cell within the grid. The supremum is defined as the least element of subset *Y* of set *X* that is greater than or equal to all elements of *Y*. The infimum is defined as the greatest element of subset *Y* of set *X* that is less than or equal to all elements of *Y* (Figure 8). In other words, the infimum defines the lower bounds of subset *Y* within set *X*, whereas the supremum defines the upper bounds of subset *Y* within set *X*. Therefore the Hausdorff distance finds point *x* from set *X* that is farthest from any point in *Y* and measures the distance from *x* to the nearest neighbour in *Y*.

2.4. Geometrical geodiversity metrics

Seven geodiversity metrics have been employed to categorise the Ashanti Greenstone

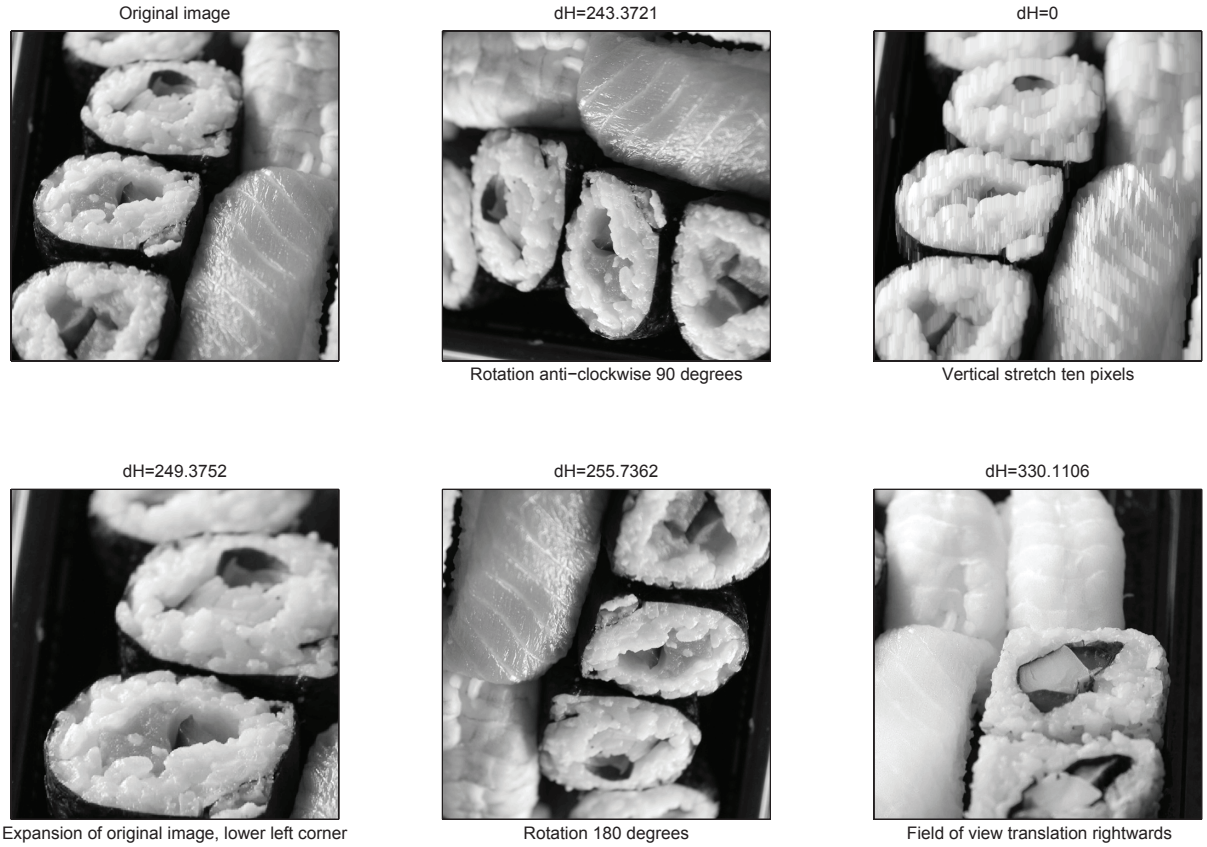

Figure 7. Hausdorff distances (dH) calculated between an original image (top-left) and images subjected to different morphological operations. Note that the stretch example produces zero Hausdorff distance.

Belt model (Table 1). A short review of the geometrical metric method (volume, depth, surface area, curvature and complexity) is provided in this section, though additional details can be found in Lindsay et al (2012b). Being able to quantify a particular aspect of a model allows comparison with other models in the model suite. Comparison then allows identification of end-member representatives for each metric. Quantification also allows each metric to be compared against one another to determine whether there are metrics that can best explain uncertainty contained within the model suite. All the geophysical metrics are used to provide a global measure of the calculated geophysical response or misfit with an objective representation of nature in the observed response. The geophysical metrics have been included in the geodiversity collection to discover if the geophysical response can be associated with any of the geometric geodiversity metrics according to the stated hypothesis.

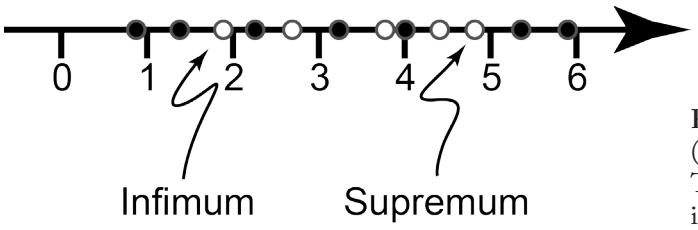

Figure 8. A number line shows a set of numbers (white and black balls) and a subset (white balls). The infimum and supremum of the subset are indicated.

Table 1. Summary of geodiversity metrics and their function. Detailed descriptions of the geometrical metrics and their function can be found in Lindsay et al (2012b).

Name	Subject	Measurement	Output
Geometrical geodiversity metrics			
Volume	Voxet	Metres^3	Volume for each formation
Depth	Voxet	Metres	Shallowest and deepest occurrence of each formation
Curvature	Surface	k_m: Mean curvature k_g: Gaussian curvature	Average k_m and k_g values for each formation
Contact relationships	Surface	Area (metres^2)	Contact surface area and contact relationships
Geological complexity	Voxet	Number of different lithologies around point-of-interest	Scalar value representing geological complexity
Geophysical geodiversity metrics			
Root mean square (RMS)	Residual grid	Global measure of geophysical misfit	Scalar value
Standard deviation	Calculated grid	Global measure of geophysical variability	Scalar value
Entropy	Residual grid	Global measure of geophysical variability	Scalar value
2D correlation coefficient	Comparison between observed and calculated grids	Global measure of geophysical covariance – recognises similar patterns	Scalar value
Hausdorff distance	Distance between observed and calculated grids	Global measure of geophysical misfit – accounts for pattern translation, rotation and dilation	Scalar value

The following geometrical geodiversity metrics were developed to analyse the geometry of 3D geological model elements. Note that this list of metrics is not exhaustive. Many other metrics may exist that are also effective at measuring the effects of uncertainty on model geometry.

2.4.1. Formation depth and volume

The deepest and shallowest extents of each stratigraphic unit are determined using this metric. Each model in the suite can be analysed to find if any model shows that a stratigraphic unit is significantly deeper or shallower than it is in others. Information like this can be useful to assist

in identifying under what conditions a stratigraphic unit may be shallower. Most units in a model that displays either flat-lying geology, low uncertainty or both will share the same deepest and shallowest extents with other models within the model suite which makes identification of end-members difficult. Therefore, the unit that has the most volume at the depth extent under study is considered the end-member. For example, the deepest extent of 'Unit A' is found to be 8500 metres and was found in models 3, 6 and 70. In Model 3, Unit A has 3000 m3 at 8500 m depth, Model 6 has 4000 m3 and Model 70 has 3500m3 at 8500 m depth. Model 6 is determined to be the end-member for the deepest extent of Unit A, as it has the most volume at 8500 m depth. Volume of each unit is calculated by counting the voxels assigned to that unit and multiplying by the voxel volume.

2.4.2. Average mean curvature

Most surfaces within a 3D geological model are curved as they attempt to represent the natural world. Defining the curvature of a surface can be useful, especially if curvature is conducive to producing an economically viable target. Antiformal traps are highly sought after in oil, gas and minerals exploration and determining where they exist can aid exploration activities. Curvature may also influence the geophysical response of a model. Potential links between a particular style or degree of curvature and high or low geophysical misfit can aid model refinement and improve the modelling workflows.

We use a technique described by Lisle and Robinson (1995) and Lisle and Toimil (2007) that rotates a surface around its normal until the maximum curvature ('k_1') is found. The surface that is perpendicular to k_1, 'k_2' is also recorded. k_1 and k_2 are known as the principal curvatures. The sign of principal curvatures indicates their polarity, negative indicates concave-upward, positive indicates convex-upward. Mean curvature (M) is calculated from the arithmetic mean of k_1 and k_2:

$$M = \frac{k_1 + k_2}{2}. \quad (6)$$

$M < 0$ represents a concave (synformal) surface, $M > 0$ represents a convex (antiformal) surface and $M = 0$ either represents a flat plane or a 'perfect saddle' (Lisle and Toimil, 2007). The product of k_1 and k_2 is the Gaussian curvature:

$$G = k_1.k_2, \quad (7)$$

which can be used to identify specific folding interference patterns. Positive G values show that both principal curvatures k_1 and k_2 have the same sign, and represent a dome or basin.

Negative *G* values indicate that principal curvatures have different signs, and represent antiformal or synformal saddles (Gray et al., 2006; Mallet, 2002; Mynatt et al., 2007). Use of curvature calculations as a geodiversity metric allows comparison of specific geological interfaces with a model and model suite using quantitative methods.

2.4.3. Contact relationships

A contact relationship metric has been developed to quantify the surface area of modelled stratigraphic units, and to identify which units are in contact with other units within the model. Contact relationships are recorded by determining which stratigraphic units are adjacent to each other and surface area is calculated from a voxel count of the regions where that adjacency exists. Table 2 shows an example of the relationships between stratigraphic units found in the initial model of the Ashanti model suite. This matrix provides a useful guide to geological relationships that exist in the model that may not be immediately evident without thorough visual investigation. Information of this kind can provide a useful means to cross-validate the resulting model with the contact relationships that are described by the input geological data.

2.5. Using 3D geophysical forward modelling in combination with geodiversity

The geophysical response of a model will always rely on the 3D geological architecture it represents. Integration of geophysical misfit and geodiversity metrics allows data exploration to identify which, if any, geodiversity metrics may influence geophysical misfit. Finding a single

Table 2. Voxel count and contact relationships between stratigraphic units generated in the initial model of the Ashanti model suite. Stratigraphic units are labelled in the column and row headings. A voxel count of '0' indicates these units are not in contact within this model volume.

	'Bs'	**'bs8'**	**'tkc'**	**'tks'**	**'tbc'**	**'ttp'**	**'ts1b'**	**'ts1'**	**'gf'**
'Bs'	0								
'bs8'	23885	0							
'tkc'	1708	5910	0						
'tks'	123	2127	2418	0					
'tbc'	11	880	2220	2083	0				
'ttp'	1	99	2194	1249	1667	0			
'ts1b'	1	59	870	1289	1922	1095	0		
'ts1'	0	12	27	19	32	32	668	0	
'gf'	1025	134	0	0	0	0	0	0	0

metric, or combination of metrics, that influence geophysical misfit can help modellers refine their models to reduce geophysical misfit between the observed response and the calculated response.

Caution must be taken with this research direction. It is not intended that any relationship discovered between a geodiversity metric and geophysical response be exploited to manipulate the misfit into a more 'agreeable' result. We emphasise the importance of geological feasibility with respect to the geophysical misfit. For example, if a covariant relationship between the volume of a particular unit and geophysical misfit is found, the volume should not be adjusted in isolation simply to decrease the misfit. Changes to the volume of that unit should be considered with respect to geology, so that unrealistic realisations of the geology are avoided. The intent is to guide the modeller toward finding alternative data sources that better resolve the geometry of the geological formation through additional data (Lindsay et al., 2012). Adding data is not necessarily going to improve the geophysical misfit, especially if the data is inappropriate to improve the realisation of the anomalous modelled geology. For example, if volume was found to be linked to geophysical misfit of the model suite, adding 3D seismic interpretation to the input data set may improve the misfit of the model suite and provide a more accurate and reasonable geological realisation.

2.6. Data Analysis using Principal Component Analysis (PCA)

Each model can be analysed and then ranked using geodiversity metric results. The models exhibiting the greatest and smallest (i.e. the end-member representatives) volume of a particular geological unit are easily identified, as are the volume ranks of all other models. This information can be very useful, especially for further processing and modelling such as geophysical inversion. But potentially more interesting is discovering where a particular model sits in an overall ranking scheme that incorporates all geodiversity metrics. This type of analysis defines where a model resides in relation to other models within model space. For example, finding whether the initial model (the model calculated from non-perturbed data) exhibits typical characteristics is important. The initial model is normally the only model considered in current modelling workflows. If this model does not exhibit typical characteristics, the practice of producing one single model should be seriously questioned.

Simultaneous analysis of results from techniques that measure both geometrical and geo-

physical phenomena require a specialised set of tools. Typical methods measuring correlation, such as Spearman's Rank or Pearson's *r*, operate pairwise and only two variables are measured simultaneously. To adequately understand the relationship between different geodiversity metrics, we require a method that can compare different observations, sometimes with different scales of measurement. Further, we want to be able to reduce the number of geodiversity metrics to a select few that best represent the degree of variability observed through the model suite. PCA falls within the 'feature transformation' group of methods that fit these requirements, while also providing visualisation techniques that assist in understanding the interaction between variables and model space definition. Formally, PCA is an exploratory data technique that analyses the interaction between geodiversity metrics through orthogonal data transformation, where data is then re-organised in terms of relevance to model suite variability (Jolliffe, 2002). PCA identifies which geodiversity metric contributes the most toward model suite variability and defines the model space. 'Outlier' models form the boundary of model space. Outlier models are those models that exhibit geometrical and geophysical characteristics that show the biggest combined difference when compared to other models. 'Barycentre' models form the centre of model space and display characteristics that are similar when considered in combination. Defining the model space is an important exercise as it characterises what is possible geologically given the modelling method, geodiversity metrics and input data set. Knowledge of the model space parameters assists definition of geological possibility, given the input dataset, method of model calculation and geodiversity metrics employed. We performed the PCA in Matlab with the 'princomp' function (http://www.mathworks.com.au/help/toolbox/stats/princomp.html). The multivariate distance of the model from the centre of the dataset (i.e. the model's rank within model space) is determined using Hotelling's T^2 statistic, also obtained from the 'princomp' function (Hotelling, 1931; Krzanowski, 1995).

A detailed account of the PCA procedure is described in Lindsay et al (2012b). The PCA is carried out in two stages. The first stage involves analysing the contact relationship, volume, depth and complexity metrics individually. Each metric measures the corresponding observations for each stratigraphic unit within the model suite. PCA is performed on the stratigraphic units to find which units contribute the most to model variability for that metric. For example, if the hypothetical units *XYX* and *ABA* were found to contribute the most to model suite variability, *XYX* and *ABA* are then representatives of the volume metric. They would then be used with other representa-

tive units in the second stage 'combined' PCA.

The remaining metrics, including all the geophysical varieties, do not require filtering in a first-stage PCA procedure as a single value representing the entire model (e.g. the RMS or Hausdorff distance) is produced. The curvature metric was not subjected to PCA as curvature was not calculated for every stratigraphic unit through the model suite. The computation time required for the curvature procedure is high, so target geological contacts were chosen manually. The decision for which contact should be analysed for curvature was based on which exhibited the highest surface area, and therefore was most likely to vary and have a resulting effect on model geometry. This decision was made possible due to information provided by the contact relationship metric (e.g. Table 2).

3. Geological review – Ashanti Greenstone Belt, southwestern Ghana

The Leo-Man craton forms the southern Archaean / Palaeoproterozoic section of the West African Craton. In the south of the craton in southwestern Ghana, four Palaeoproterozoic greenstone-granitoid belts can be found (from east to west); the Kibi-Winneba, the Ashanti, the Sefwi and the Bui. Each belt is separated by a sedimentary basin (from east to west); the Akyem (or Cape Coast Basin), Kumasi and Sunyani Basins. The Ashanti Greenstone Belt has economic significance as it hosts a number of large and world-class gold deposits, including Obuasi, Tarkwa, Bogoso/Prestia and Damang (Allibone et al., 2002; Feybesse et al., 2006; Pigios et al., 2003; Tunks et al., 2004).

3.1. Mineralisation and gold prospectivity

Gold mineralisation can be identified in two ways (Perrouty et al., 2012): spatially associated with the Ashanti Fault and other major shear zones or along the contact between the Tarkwaian and Birimian units. Tarkwaian-hosted deposits display two styles of mineralisation. The first is observed only in quartz lithic conglomerates within the Banket Formation (eg. Tarkwa Mine). Economically viable deposits are constrained to a few horizons locally named 'Banket Reefs'

(Blenkinsop et al., 1994) and is thought to be of palaeoplacer origin (Hirdes and Nunoo, 1994; Sestini, 1973). A second mineralisation style, observed within Tarkwaian units, are the hydrothermal deposits that occur along the Birimian / Tarkwaian contact (eg. Damang Mine). A contrasting mesothermal mineralisation style is associated with the Birimian Supergroup and is associated within quartz ± carbonate veins within graphitic-mylonitic shear zones. World-class gold mines such as the Ashanti deposit are hosted within the Obuasi/Main Reef fissure (Allibone et al., 2002; Tunks et al., 2004).

3.2. Modelling the Ashanti Greenstone Belt

The purpose of building the Ashanti Greenstone Belt model was to determine the geometry of the Tarkwaian Basin (Figure 9). The depth and morphology of the basin base is of particular economic interest as it plays host to existing and potential placer gold deposits. Existing understanding of Tarkwaian Basin depth is controversial. Hastings (1982) and Barritt and Kuma (1998) predict the basin is between 1500 and 2500 metres, but these estimates assume an older version of stratigraphy that has low density Birimian metasediments underlying the higher density Birmian metavolcanics. Depth estimates based on gravity inversion and interpretation may therefore underestimate basin depth and granitoid geometry (Perrouty, S. – unpublished thesis chapter). Current stratigraphic relationships developed through updated information (Adadey et al., 2009) has encouraged construction of this model. The new map proposed by Perrouty et al (2012), structural measurements, stratigraphy (Figure 2a) and geophysical interpretation have been input to create the 3D model of the Ashanti Greenstone Belt, southwestern Ghana.

3.3. Datasets obtained from fieldwork

Pre-existing field observations and outcrop maps from Loh et al. (1999), BHP Billiton and Golden Star are used in combination with data collected by Perrouty et al (2012). This field data includes structural observations and petrophysical measurements calculated from rock samples. Geophysical interpretation was constrained using petrophysical data, and field observations aided geophysical interpretation. A thick lateritic and/or saprolitic layer covers most accessible areas

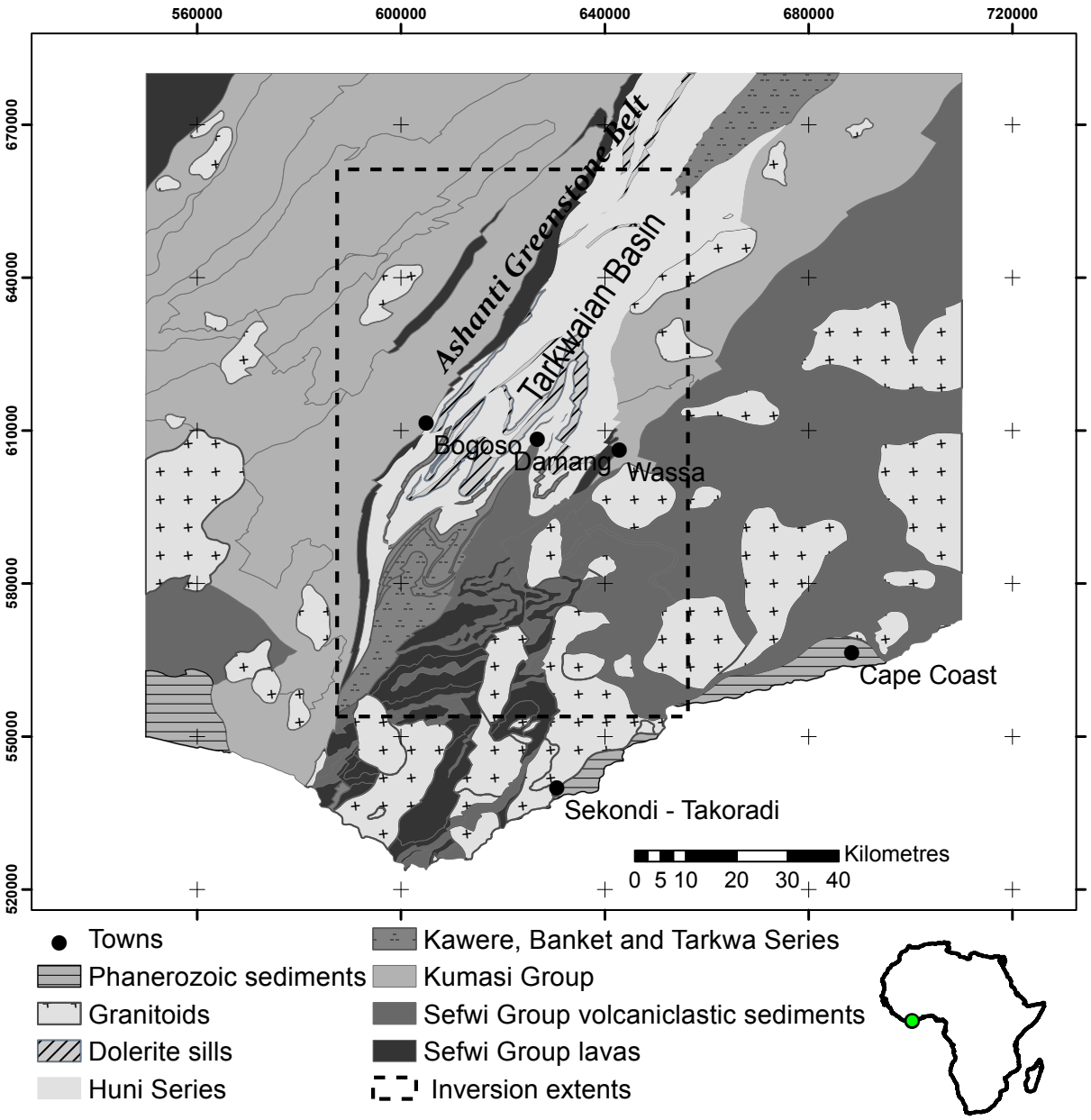

Figure 9. Geological map of Ashanti Greenstone Belt, southwestern Ghana. Note the location of the modelled region over the Ashanti Greenstone Belt and the Tarkwaian Basin.

within the region that restricts the occurrence of Proterozoic outcrop. Geophysical interpretation was therefore necessary to gain geological understanding between outcrop areas, resulting in much of the region requiring interpretation.

3.4.1. Gravity data

Gravity data has been used to provide a potential field data set to cross-validate magnetic interpretation and better image deeper structures in the region. A number of datasets have been compiled to create the gravity data used in the validation of this model. A pre-processed Free Air anomaly grid dataset was obtained through the International Gravimetric Bureau (BGI, http://bgi.omp.obs-mip.fr/) and contains a combination of BGI on- and off-shore data, satellite data and

Getech ground data (African Gravity Project 1986-1988, http://www.getech.com/history.htm). Spatial resolution is 2.5 arc-minutes, or close to 4.6 kilometres per pixel.

Figure 10 shows a steep gravity gradient to the west of the Tarkwaian Basin that marks the location of the Ashanti Fault. Other less dramatic anomalies represent Eburnean granites and Eoburnean granitoids.

3.4. 3D modelling and model suite creation

3D Geomodeller (http://www.geomodeller.com/geo/index.php) is used to integrate field, geophysical and satellite data into a coherent and geologically feasible model. 3D Geomodeller uses an implicit method to integrate all input data to create scalar potential field of conformable lithological formations (Lajaunie et al., 1997). Note that the 'scalar potential field' is different to the geophysical potential field that is used to generate some of the input for the model. Geological

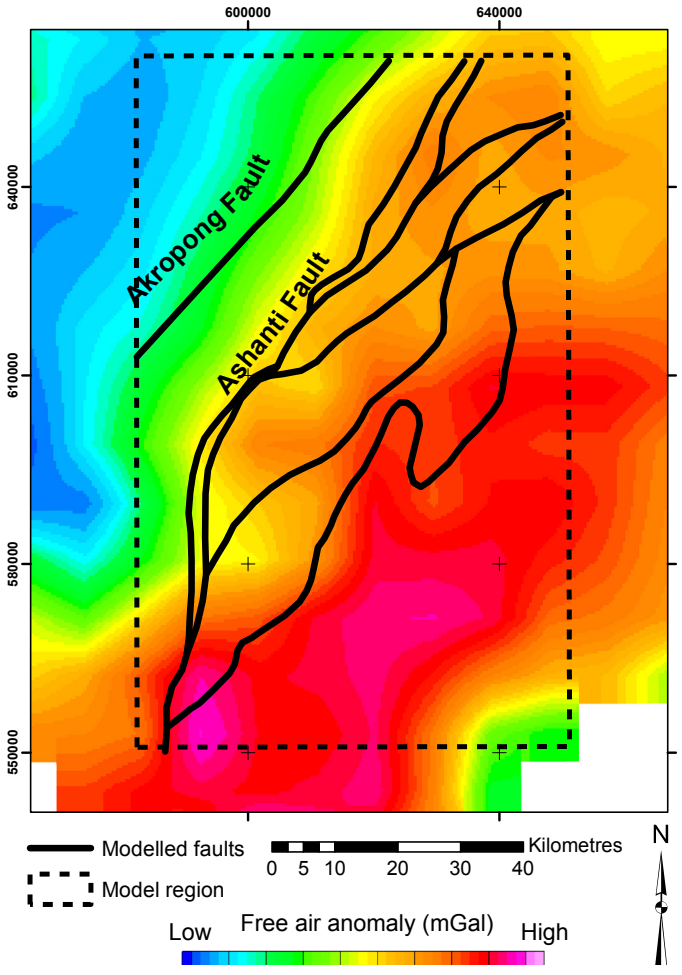

Figure 10. Gravity response of the Ashtanti Greenstone Belt with an overlay showing the location of modelled faults.

interfaces are identified from the scalar field through a process of cokriging all scalar fields and a 3D model is constructed. Three types of input data are required for the 3D Geomodeller implicit method to function: (1) geological contact locations; (2) geological orientation measurements and (3) a stratigraphic column with defined geological relationships. The contact locations define where interfaces exist within the model, the orientation measurements give the interfaces their geometry and the stratigraphic column defines adjacent geological relationships. Fault relationships can also be defined allowing complex fault networks and timing relationships between fault and geological units to be defined. A complete description of the 3D Geomodeller method and associated techniques is described by Calcagno et al. (2008).

We consider the first model that was created to be the 'initial model'. The initial model is the model that is created in a normal 3D geological modelling workflow. It represents the best-efforts of the modelling team to produce a consistent model that attempts to honour all the input data. Lindsay et al. (2012a) describes how the initial model is subjected to uncertainty simulation to create the model suite and is then included in the model suite as a member that is no more or less likely to exist in nature than the other perturbed models. Uncertainty simulation consists of taking the orientation measurements (including those assigned to faults) from the input dataset and reassigning their values to within ±5 degrees (both strike and dip) of the original measurement. The reassignment is performed as a Monte Carlo simulation to avoid bias. For example, a measurement of 325/40E could be perturbed so that measurement within model '1' of the model suite would be reassigned 323/35E, model '2' reassigned 320/42E and so on. Each model is then recalculated using the new measurements and with other perturbed models create the model suite: a set of geometrically similar, but diverse examples of geological possibility. Voxets are generated from each of the members of the model suite and are used for geodiversity analysis.

3.5. Predicting the resulting geophysical response from varied geometries

It was initially thought that the volume of a unit would be closely related to the overall geophysical misfit calculated during forward modelling. Given that one particular unit may take up a high proportion of the model volume, it would be reasonable to expect that the unit would

correspondingly have influence over the overall geophysical response. This relationship is not without some considerations. The petrophysical properties assigned to the high-volume unit must have some contrast to the surrounding unit otherwise it would be geophysically indistinguishable from other geological units. Further, if the high-volume unit is flat-lying, especially if it exists only at depth, then it will also be difficult to distinguish from other units. The flat-lying unit will simply add its response to the units that overly it, so it needs to outcrop, or at least have experienced some deformational process to fold or tilt beds so that the top surface is irregular in some manner.

4. Results and discussion

The results are presented in two parts: (1) as a pure end-member analysis, where end-members for each representative metric (determined in the first-stage PCA where necessary) are presented with the corresponding measurement and (2) the results of the combined PCA, where the combined analysis of geodiversity metrics is presented with a depiction of model space.

4.1. End-member analysis

Results from geodiversity analysis are shown in Table 3. It becomes evident that knowledge of these end-members and their corresponding measurement reveals several interesting aspects of the model suite. Firstly, the geometrical metrics display considerable variation in the range between end-member values. The range of possible volumes for the Late Birimian formation ('***Bs8***') is 1553.1 km^3, whereas the depth metrics only show a range of 200 metres between end-member representatives. Considering that the smallest interval between the measured depth of a given formation is 200 metres (voxel size is 200 metres on the Z axis), the results are essentially binary in that the stratigraphic unit is either one of two depths (1400 or 1200 metres for ***Bs8*** and 400 or 200 metres for the base of the Tarkwaian Series '***tks'***). The depth for the shallowest extent for Bs8 does allow for three possibilities (1000, 1200 and 1400 metres), but none of these results allow for much fidelity in terms of detecting different depths. In contrast, the volume is calculated by counting the voxels within a formation, and the range between the smallest and largest volume allows a far greater spectrum of results (between 321915 to 352977 voxels, a range of 31062 vox-

Table 3. End-member representatives for each geodiversity metric and the corresponding observation. Note how each end-member is represented by a single scalar value. This is a requirement for input into PCA, but also allows commonality constraint values to be determined.

Metric	Measures	Minimum End-member	Maximum End-member
Geometric geodiversity end-members			
Volume	Volume of Bs8	Model 37: 16095.75 km3	Model 21: 17648.85 km3
Volume	Volume of tks	Model 78: 197.95 km3	Model 21: 229.7 km3
Complexity	Complexity of tkc	Model 70: 3.1141	Model 26: 3.3186
Complexity	Complexity of Bs	Model 61: 1.3825	Model 1: 1.9825
Depth - deepest	Deepest occurrence of Bs8	Model 11: 1400 m	Model 100: 1200 m
Depth - deepest	Deepest occurrence of tks	Model 31: 400 m	Model 12: 200 m
Depth - shallowest	Shallowest occurrence of Bs	Model 101: 1400 m	Model 32: 1200 m
Depth - shallowest	Shallowest occurrence of Bs8	Model 92: 1400 m	Model 61: 1000 m
Contact relationship	Contact between Bs and Bs8	Model 32: 21348 voxels	Model 72: 26464 voxels
Contact relationship	Contact between Bs and tkc	Model 90: 1106 voxels	Model 32: 2975 voxels
Curvature	km of contact between Bs8 and tks	Model 57: 2.9995e-05	Model 28: 1.8792e-05
Curvature	km of contact between Bs and Bs8	Model 54: -4.6455e-05	Model 84: 7.4882e-04
Curvature	kg of contact between Bs and Bs8	Model 89: -1.0559e+21	Model 31: -1.4424e-08
Curvature	kg of contact between Bs8 and tks	Model 8: -4.1816e+14	Model 12: -6.5508e-08
Geophysical geodiversity end-members			
RMS	RMS misfit between observed and calculated response	Model 37 - 8.2963	Model 26 - 8.4930
Standard deviation	Global measure of geophysical variability within the calculated response grid	Model 70 - 17.4038	Model 39 - 17.5306
Entropy	Global measure of geophysical randomness within the residual grid	Model 70 - 4.9151	Model 39 - 4.9509
2D correlation coef.	Comparison between observed and calculated grids – accounts for similar patterns	Model 32 - 0.9465	Model 37 - 0.9503
Hausdorff distance	Global measure of geophysical misfit – accounts for pattern translation, rotation and dilation	Model 26 - 482.8557	Model 76 - 487.8138

els) than the depth metric. Much smaller variation in geometry can be detected in the volume of a formation throughout the model suite, suggesting that the volume metric will be more useful as a variable in PCA. Decreasing the voxel Z-axis interval may improve the effectiveness of the depth metric, but the impact on computing requirements (both storage and computation) would need to be considered. Decreasing the Z-axis interval will dramatically increase the number of voxels in the voxet and the trade-off between improvements in variability detection for the depth and other metrics would have to be assessed. Despite depth metrics being less useful for detecting model suite variability, they would nonetheless provide useful information to explorers using the model for prospectivity analysis. Access to the possible depths of a prospective geological unit can make decisions about targeting easier. The economic viability of a prospect can hinge on predicted ore depth, so depth end-member knowledge allows a quick assessment of this variable.

The complexity metric shows that the ***tkc s***tratigraphic unit has an average of between 3.1141 and 3.3186 different lithologies at any given point. This result is high in comparison to the 1.3825 to 1.9825 calculated for the Early Birimian ('***Bs***'). A relatively high degree of complexity that also describes model suite geometrical variability (determined during first stage of PCA) suggests that tkc is an important unit within the model suite. The location of ***tkc*** in the stratigraphy makes the complexity result even more interesting as tkc forms the base to the Tarkwaian basin and is gold prospective. Intuitively, the average of over three different units at any given point seems high and indicates that this unit may define the geometry of units overlying it. It may also be that the geological complexity of tkc is associated with gold prospectivity.

The relatively large range of values seen within the contact relationship metrics ***Bs*** and ***Bs8*** (5116 voxels) and between ***Bs*** and ***tkc*** (1869 voxels) reveal how geometrically variable the model suite is. The large range indicates that the surface area between these contacts can be easily influenced by model uncertainty. The ***Bs***/***Bs8*** contact variability shows that the contact between the Early and Late Birimian units is inadequately constrained. This is confirmed as only a single orientation point defines the orientation of this contact. The ***Bs8***/***tkc*** contact is gold prospective, so a large range of values may suggest that this model suite may not offer enough certainty for use with further prospectivity modelling. These results do not necessarily mean that the model suite cannot be used, but that the variability of this geometrical aspect of the model suite should be kept in mind in future applications.

The curvature results reveal some aspects of the ***Bs***/***Bs8*** and ***Bs8***/***tkc*** contacts that are difficult (if not impossible) to determine from visual analysis of the surfaces. The average mean curvature (k_m) of the gold prospective ***Bs8***/***tks*** contact shows that all the surfaces throughout the model suite display an overall antiformal curvature. This result seems to be counter-intuitive to geological reason. The ***Bs8***/***tkc*** contact forms the basement to the Tarkwaian Basin which one would expect to be synformal, even with the four deformation events that have shaped it to the present day geometry. Visual inspection also suggests the same conclusion (Figure 11). The reason for this seemingly anomalous result is the fact the curvature is calculated between adjacent voxels. Overall curvature appears to be synformal, influenced heavily by curvature at the edges of the basin. However, throughout the centre of the basin the curvature exhibits more antiformal geometry, more than the synformal, resulting in the average mean curvature detected by the geodiversity metrics.

An interesting result from the Gaussian curvature (k_g) metric is that all the results return a negative number. This results from both principal curvatures (k_1 and k_2) having opposite signs, meaning that the surfaces all exhibit a saddle or inverted saddle geometry (Lisle and Toimil, 2007). The magnitude of k_g values range from close to zero (model 31, ***Bs***/***Bs8*** - model 12, ***Bs8***/***tks***) to extreme (model 89, ***Bs***/***Bs8*** and model 8, ***Bs8***/***tks***), meaning that models 31 and 12 exhibit almost cylindrical fold geometry, whereas models 89 and 8 would exhibit distinctive saddle geometries. The saddle geometries are intuitively expected given the polyphase deformation history of the

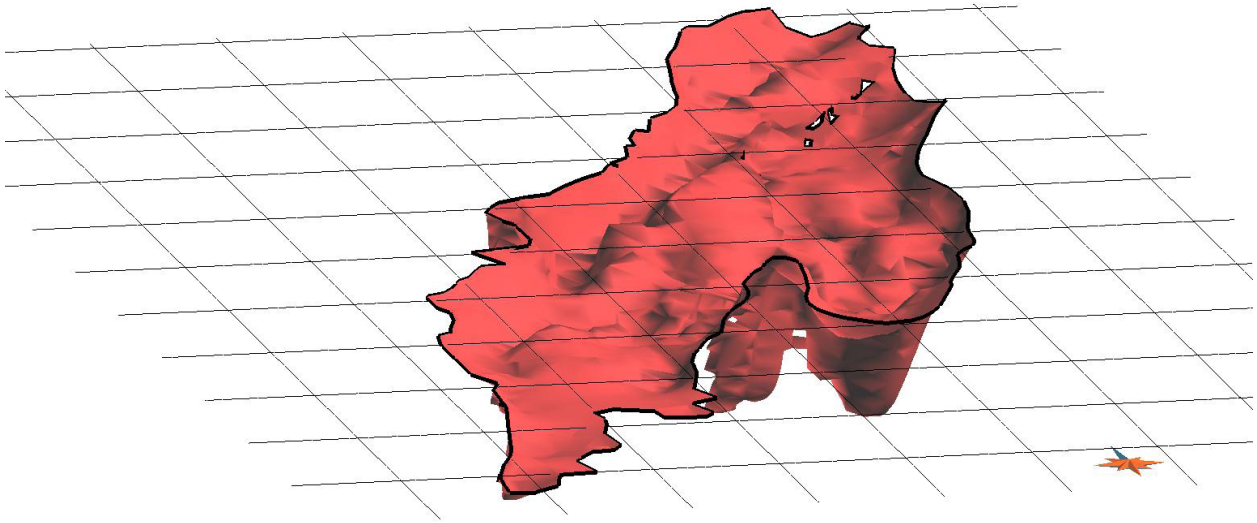

Figure 11. View of the tkc surface from the Ashanti Greenstone Belt model (from the south), showing an overall synformal curvature (vertical exaggeration x4).

Tarkwaian and differing axes of shortening (Perrouty et al., 2012). The cylindrical fold geometries are not expected for the same reasons. Therefore any use of models 31 and 12 (or others showing near-cylindricity) in further analysis should be performed with caution.

4.2. Gravity misfit comparison

Sensitivity analysis of all the gravity geodiversity metrics was performed to confirm that each metric has a similar variation to range ratio and that no correction was required to normalise any extremely high or low measurements. This was initially difficult to determine as each geophysical geodiversity measure has different units of measurement. Table 4 shows the comparison of metrics. The value to note is the range-standard deviation ratio, which is similar for all metrics (highlighted in grey within Table 4). This means that the degree of variability within each measure is proportional to its range and that comparison can be made between these metrics as end-members and no data levelling is required for PCA.

Geophysical response modelling is by no means the only method by which a model can be verified. For example, drill logs and/or field mapping can be integrated with geophysical observations to provide a less ambiguous solution. In practice though, geophysical data is often the only data set that has full coverage over the study area and subsequently suffices for first-pass model validation.

4.2.1. RMS misfit

Overall, the RMS misfit values are reasonably high for this kind of study. Obviously, one

Table 4. Statistical analysis of geophysical geodiversity metrics. A ratio of range to standard deviation has been calculated to evaluate whether the proportion of variation to range in the results across the model suite was the same, which appears to be the case with all metrics giving similar ratio values. This confirms that there is no metric that determines outliers (extremely high or low values) the presence of which may distort further analysis in PCA.

	Hausdorff distance	RMS	2D correlation coefficient	Entropy	Standard deviation
Range	4.9580	0.1967	0.0039	0.0358	0.1268
Standard deviation	1.1325	0.0424	0.00085	0.0081	0.0283
Range/standard deviation	4.3779	4.6392	4.5240	4.4164	4.4814
Mean	485.4841	8.4034	0.9482	1.8077	17.4716
Max	482.8557	8.4930	0.9503	1.8729	17.5306
Min	487.8138	8.2963	0.9465	1.7290	17.4038

would hope for slightly lower values, but the magnitude is also not high enough to reject the geology model outright. Figure 12 shows the difference between the end-member residual grids is not immediately obvious, though regions (indicated on the figure) through the centre and the edges of the Tarkwaian Basin appear to show the greatest variation. The highest magnitude anomalies appear to be concentrated in the northwest and southeast. The reason for this is that gravity in these areas respond to deeper Birimian-age structures (Perrouty et al., 2012) that were not included in the model, and this is subsequently reflected in the relatively high misfit values. The residual observed over the Tarkwaian is not as severe as in the northwestern and southeastern regions of the map, and the modelled geology appears to match the gravity data relatively well.

Low entropy ('*E*') reflects less randomness in the residual image. If the entire image has predictably (i.e. less random) high misfit values, then the misfit is predictably high. Therefore, low *E* values need to be considered in combination with the mean misfit value for the residual. A low RMS value reported with a high entropy value will represent an image with an overall low misfit but riddled with high magnitude anomalies. Choosing a model for further processing simply because it has a low RMS, without considering the corresponding entropy may prove problematic if high magnitude anomalies are present.

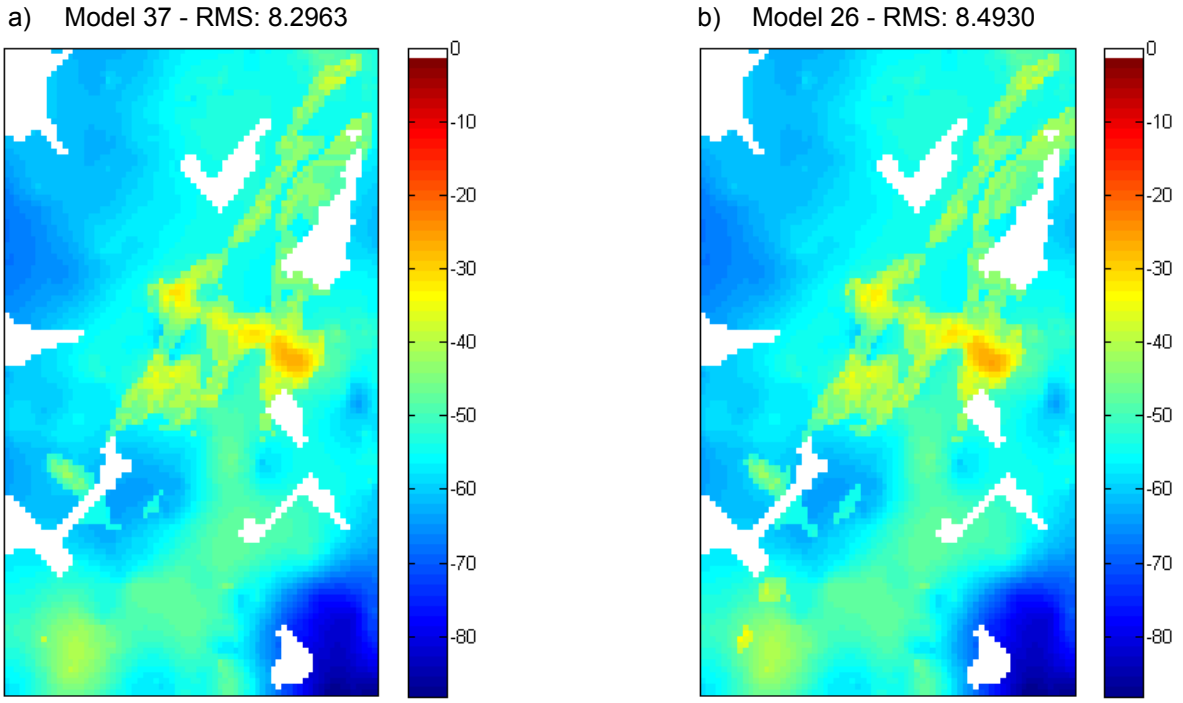

Figure 12. Residual grids from RMS misfit end-member models 37 (RMS: 8.2963) and 26 (RMS: 8.4930).

The remaining geophysical metrics produce a single scalar value that describes the phenomenon measured by each particular technique. The degree to which scores vary from the mean for each metric is relatively similar. Therefore we can expect that both techniques may be measuring relatively similar degrees of misfit for each calculated model response against the observed response. However, identical results have not been produced for a given model, meaning that each technique may be measuring different phenomena, as was hoped. The PCA should reveal what phenomena each geophysical metric is measuring, with the proviso that a companion geodiversity metric exists that also quantifies the same phenomena.

4.3. Combined Principal Component Analysis (PCA) and geodiversity metric relationships

PCA results are best analysed using a bi-plot diagram shown in Figure 13a. A short explanation is required to explain how to read a PCA bi-plot. The first two principal components are plotted along the X and Y axes respectively. The first two principal components together explain just under 50 percent of model suite variability (Figure 13b). The PCA plot shows each metrics contribution to model suite variability and how each model is represented in terms of model suite variability. The points represent models within the model suite and the distance of the point from the 0,0 intersection represents the distance of the model from the 'barycentre' of the model suite. The barycentre is a region containing models that share common characteristics, therefore the further away from the barycentre, the more diverse the models become. The models that plot around the edges of the diagram, the 'outliers', define the boundaries of model space. These outlier points represent the models that are dissimilar in terms of the geodiversity metrics that we have used to define the models within model space. The length and direction of the vectors extending from the 0,0 intersection represent how much they contribute to the principal components in the plot. Vector direction represents association with the component (or axis) the vector plots closest to. A long vector that plots close to the x-axis would shows a close association to the first principal component, representing a variable that contains a high proportion of model suite variability.

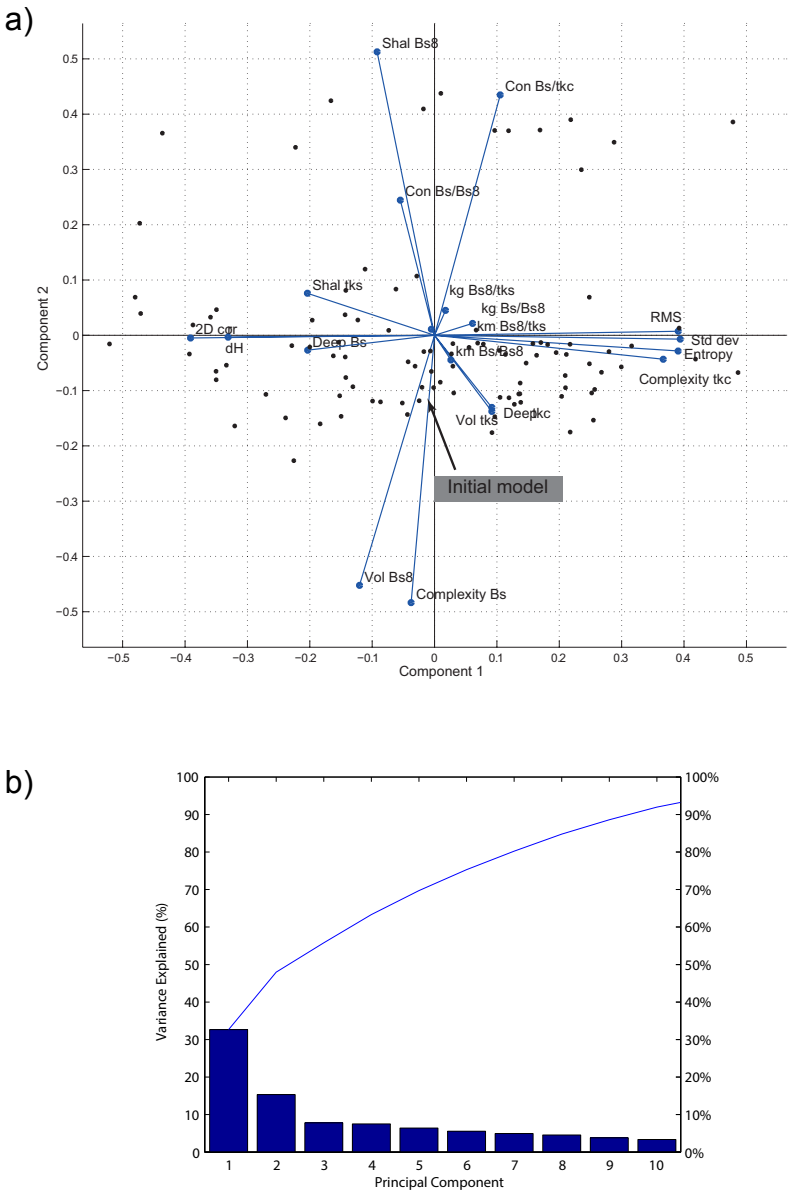

Figure 13. PCA for the Ashanti Greenstone Belt model suite and geodiversity metrics. a) Bi-plot diagram of the combined PCA showing that RMS, standard deviation, entropy geophysical metrics all measure similar variations between models as does the complexity metric of tkc. Note the location of the initial model. b) Pareto diagram of principal components and the variance explained. Almost half the variance observed by the geodiversity metrics within the model suite is explained by the first two components, negating the need to examine components three onwards.

4.4. Ashanti Greenstone Belt PCA

The most distinctive feature of this PCA diagram is the clustering of the RMS, standard deviation, entropy and complexity (***tkc***) vectors around the x-axis. The clustering shows that this group of metrics more effectively measure intrinsic model suite variability than the others in the diagram. Perhaps more interesting is that the geophysical gravity response of the model suite is linked with the complexity of ***tkc*** (Figure 14). Our original hypothesis that the volume of the base-

ment formations (***Bs*** or ***Bs8***) would be most influential over the geophysical response of the model has been proven false. The volume of ***Bs8*** is still influential in terms of model suite variability as it plots close to the y-axis (along with the complexity of the ***Bs*** / ***Bs8*** contact), but is not associated with the geophysical metrics. The remaining 2D correlation and Hausdorff distance geophysical metrics show no close association with other geometrical metrics, though they are almost covariant. The association the two metrics have with each other is due to their ability to recognise patterns within the data.

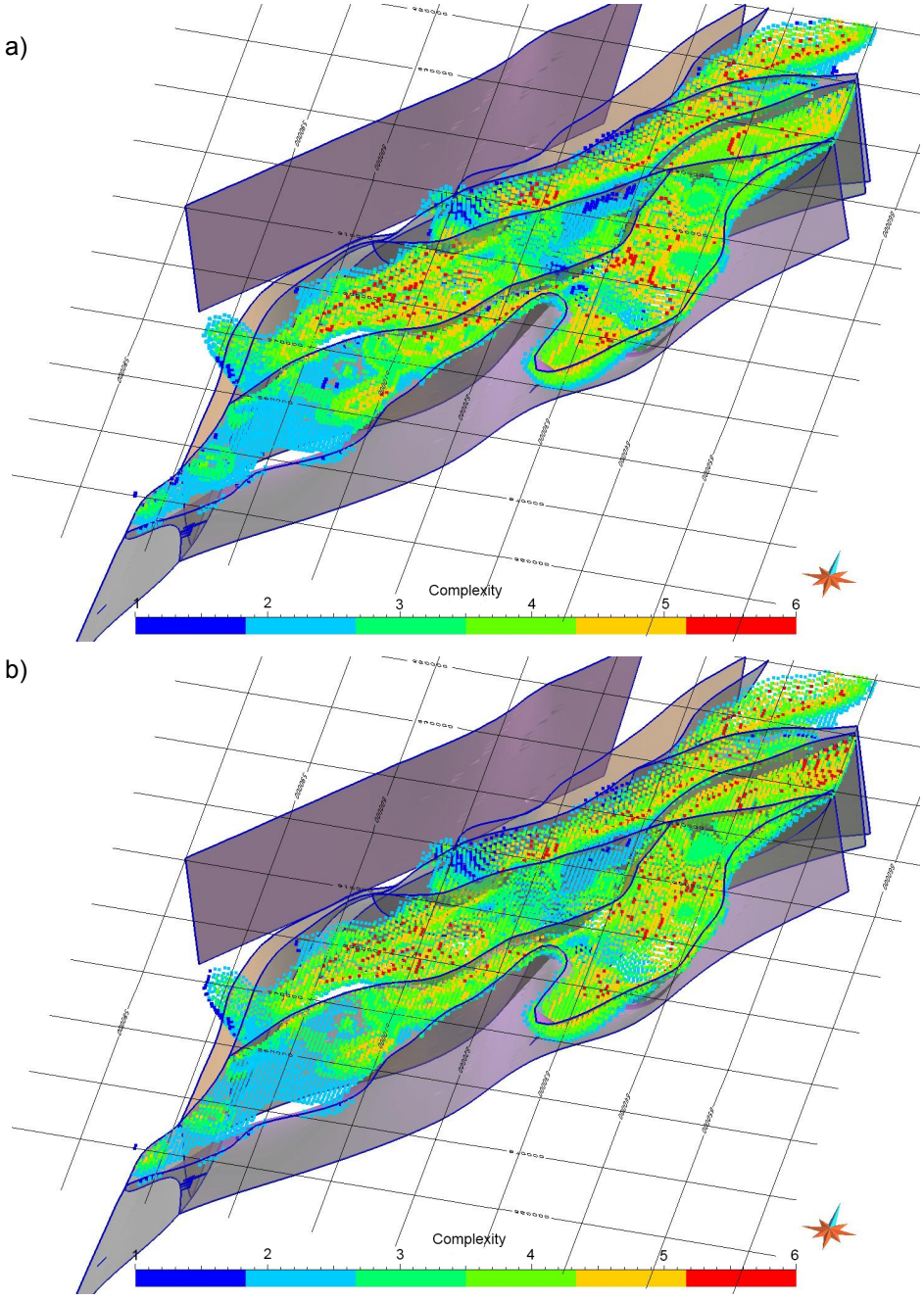

Figure 14. Complexity maps of tkc formation from models 70 (a) and 26 (b). Modelled fault surfaces (grey) and borders (blue) are shown.

The opposing direction of the vectors for 2D correlation and the Hausdorff distance to the other geophysical metrics is due the inverse relationship between these measures. For example, the Spearman's Rank between the RMS and Hausdorff distance is -0.81, showing a medium to high correlation (Figure 15). Table 3 shows that the RMS end-member representing the highest geophysical misfit is model 26, whereas the Hausdorff distance end-member representing the least distance from the observed grid is model 26. We suspect that this reversal of end-members is due to the Hausdorff distance metric recognising a pattern in the model 26 calculated grid that has a close resemblance to the pattern in the observed grid. This pattern may have been dilated or translated, as the RMS misfit is low, but may exhibit the same geometrical features. Identification of the exact transformation the Hausdorff distance has identified was not performed within this study, but would obviously be a useful outcome for future work.

The reason to construct this model was to better understand the geometrical nature of the Tarkwaian Basin, therefore little attention was paid to the underlying Birimian structures to accommodate petrophysical property heterogeneities in the Birimian basement. The complication is that if this model was subjected to geophysical inversion, Tarkwaian geometries may be adjusted beyond the boundaries of geological feasibility. As the Birimian geophysical response has not been adequately represented geometrically, the inversion process would likely adjust Tarkwaian structures or petrophysical properties. Tarkwaian structures are the only features that will likely

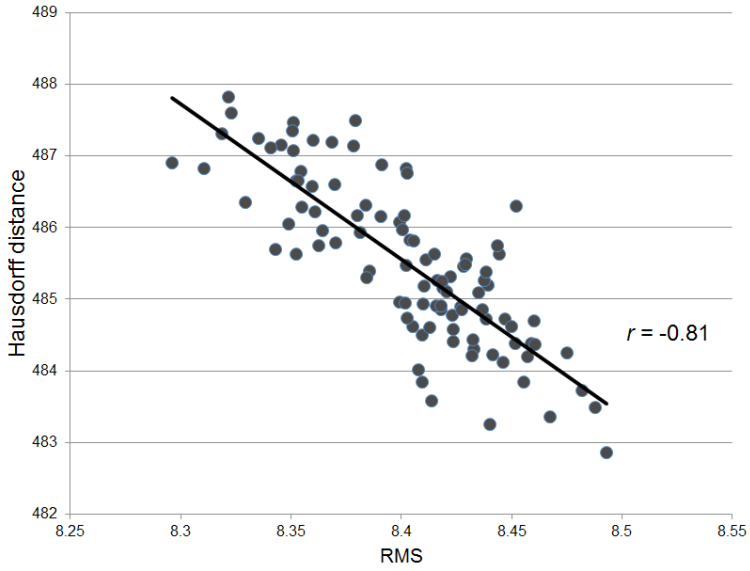

Figure 15. Comparison of RMS misfit scores and Hausdorff distances (y-axis) between calculated and observed geophysical grids for each model (x-axis). A reasonably strong negative correlation between both datasets (r = -0.81).

produce an improvement in misfit when adjusted in the model, and these changes may produce geologically unreasonable results. The obvious course of action is to better represent Birimian age structures in future model versions to avoid unnecessary adjustment of model attributes during inversion.

Hotelling's T^2 scores have been calculated to rank each model according to distance from the barycentre (Table 5). All outlier models (8, 84, 32, 61 and 37) feature in the end-member analysis (Table 3), though determining their influence on overall model suite variability is difficult to determine by simple ranking procedure. Model rank needs to be weighted according to the influence of the metric to overall model suite variability. A combined approach is needed to completely acknowledge all geodiversity within the model suite. Similar to results obtained in Lindsay et al. 2012b, the initial model does not feature in the bottom five ranked models. The initial model is reasonably close to the barycentre, being ranked in 88th position, but there are 13 other models that are considered more similar according to the geodiversity metrics used in this study. The necessity of employing modelling techniques producing multiple realisations of geological scenarios are supported by the results presented here. Modelling procedures may therefore benefit from probabilistic models, rather than models that have been produced from processes that optimise data.

5. Conclusion

Adding geophysical geodiversity metrics adds further information to model space exploration. The process of comparing different geophysical techniques has revealed that some are associated with the geological complexity of a gold prospective layer, ***tkc***, which forms the base of the Tarkwaian Basin. Complexity maps of the two end-member models (Figure 14) could provide useful input into prospectivity modelling, but also guide further modifications and changes to the initial model in combination with uncertainty analysis by identifying regions requiring specific focus.

The geophysical metrics included in this study have provided additional methods to calculate the misfit between calculated and observed grids. The pattern recognition feature of the Hausdorff distance provides a useful companion technique to typical RMS misfit calculations. The Hausdorff distance could be an inclusion for further studies due to its ability to detect patterns

Table 5. Hotelling's T^2 score rankings for the model suite. The top five models are those that exhibit the greatest distance from the model space barycentre. The bottom five models represent are closest to the barycentre. The ranking of the initial model is also shown.

Top 5	1	8
	2	84
	3	32
	4	61
	5	37
	88	**Initial model**
Bottom 5	97	50
	98	9
	99	67
	100	34
	101	11

in the observed response that may exist, translated, rotated or dilated, in the calculated response.

PCA has also revealed that the geophysical response is associated with a geometrical phenomenon. Further investigation of the model space through geophysical inversion can be streamlined by identifying models and elements that should be analysed. Based on the results obtained in the PCA, we suggest that geophysical inversion on ***tks***/***tkc*** or the ***Bs8***/***tkc*** contact may aid in producing a model honouring both geological and geophysical data. We can be more confident with the final result if models exhibiting both common (barycentre) and unusual (outlier) geometries are included in analysis. The inversion process can also be guided to focus on elements that have been determined to be important to reconcile when trying to obtain a model honouring both geological and geophysical data. This will be achieved by (1) eliminating model realisations that do not represent either the barycentre or outlier regions of model space and (2) identifying geometrical elements, while potentially important in other non-geophysical contexts, that do not contribute significantly to model suite variability. The production of models that best represent all input data and geological possibility will be aided by following the procedure outlined here.

Geodiversity PCA has implications for the future of 3D geological modelling. The initial model was found not to be the most representative model in the model suite. This finding exposes flaws in workflows that consider a single model to adequately represent geological possibility. We propose two processes that address these flaws: (1) Multiple models, identified through PCA and geodiversity analysis, to be produced as the product of simulation workflows and (2) a combina-

tion of all models in the model suite are combined to produce a probabilistic model, where surfaces and structures are represented by probability measures, rather than as discrete surfaces. The result from both proposals is that uncertainty inherent in geological studies is acknowledged and is communicated effectively.

Acknowledgements

Thanks go the Society of Economic Geologists Hugo Dummett Memorial Fund and Intrepid Geophysics for technical assistance and access to the 3D Geomodeller API (Application Programming Interface). Special thanks to Philip Chan of the Monash eResearch Centre for providing technical assistance with Monash Sun Grid computing.

3a

The geodiversity metrics demonstrated in Chapter 3 successfully identified important relationships within the Ashanti Greenstone Belt model suite. Firstly, large misfit anomalies resulted due to the model inadequately representing the Early Birimian Series. Secondly, the association of geometrical and geophysical covariance between models is difficult to predict. Differences in model element volumes were not found as influential in reflecting geophysical differences, as initially thought. Instead, geological complexity was identified as the most influential factor in variations between the gravity response, but also in overall model suite variability. Finally, principal component analysis again found that the initial model did not exhibit the most common geodiversity characteristics in the mode suite. These findings provide more supporting evidence for the production of multiple models in modelling workflows. The evidence is stronger as (1) it is corroborated by what was discovered in Chapter 2 and (2) the result was acquired using a different model suite with an expanded range of geodiversity metrics.

Producing multiple models from a modelling workflow advocates subjecting multiple a priori models to geophysical inversion. Chapter 4 demonstrates how this is achieved. Chapter 4 also provides how guidance for selection of inversion input data and parameter assignment is based on the techniques featured in Chapters 1, 2 and 3. Chapter 4 outlines a modelling workflow displaying how each technique developed in this research is complimentary. The aim is to produce a set of models that acknowledge model uncertainty and geological possibility. Chapter 4 shows that a geologically reasonable model can be generated while including appropriate geological constraints to an inverse problem. Chapter 4 is currently in preparation for submission to the Journal of Geophysical Research, Solid Earth.

4

Inversion and geodiversity: Searching model space for the answers

Mark D. Lindsay [a,b], Stephane Perrouty [b,c], Laurent Ailleres [a], Mark W. Jessell [b,c]

[a] School of Geosciences, Monash University, PO Box 28E, Victoria, 3800, Australia
[b] Université de Toulouse, UPS, (OMP), GET, 14 Av. Edouard Belin, F-31400, Toulouse, France
[c] IRD, GET, F-31400, Toulouse, France

In preparation for submission to the **Special Issue of Mathematical Geosciences on 3D Structural Modeling**.

Abstract

Geophysical inversion employs numerical methods to minimise the misfit between three-dimensional petrophysical distributions and geophysical datasets. Inversion techniques rely on many subjective inputs to provide a solution to a non-unique problem, including use of an a priori input model or model elements (a contiguous volume of the same litho-stratigraphic package) and inversion constraints. Inversions may produce a result that perfectly matches the observed geophysical data but still misrepresents the geological system. A workflow is presented that offers objective methods to provide inputs to inversion. First, simulations are performed to create a model suite that contains a range of geologically possible models. Next, uncertainty analysis is performed using stratigraphic variability to identify low certainty model regions and elements. 'Geodiversity' analysis is then conducted to determine the geometrical and geophysical extremes within the model space. Next, geodiversity metrics are then simultaneously analysed using principal component analysis to identify the geometrical and geophysical aspects that contribute most toward model suite variability. Principal component analysis determines which models exhibit common or diverse geological and geophysical characteristics, facilitating selection of models subjected to geophysical inversion. We apply this workflow to the Ashanti Greenstone Belt, southwestern Ghana in west Africa. The workflow described in this manuscript reduces the subjectivity during decision making, explores the range of geologically possible models and provides geological constraints to the inversion process with the aim of producing geologically and geophysically robust suites of models associated with an uncertainty grid.

Keywords: Uncertainty, 3D modelling, Geological constraints, Inversion, Ashanti Greenstone Belt

1. Introduction

Predicting the outcome of a set of measurements given a known set of parameters is called the forward problem, and results in a unique solution. Inverse problems can result in solutions that infer parameter values describing the system where parameters are not known, however inverse problems do not offer unique solutions (Tarantola and Valette, 1982a, b). Inverse problems are common in geoscience as knowledge of all parameters is rarely known. One such inverse problem is attempting to resolve the 3D geological architecture from a geophysical dataset. Knowledge of the parameters essential to formulating a forward problem (complete descriptions of shape, location and physical nature of all geological structures) are not explicitly known in geology (Frodeman, 1995). An inverse solution is required to determine the unknown parameters defining petrophysical distributions observed in the geophysical response.

Different schemes are available to solve geophysical inverse problems. Rock properties can be determined by minimising a model objective function dependent on finding a fit with the observed data (Li and Oldenburg, 1996, 1998). Monte Carlo methods, such as simulated annealing and genetic algorithms, employ an 'importance sampling' approach, where specially selected distribution properties are used to optimise simulations (Ji et al., 2002; Sambridge and Drijkoningen, 1992; Sambridge and Mosegaard, 2002). The least-squares method uses an iterative algorithm in which, at each iteration, the unknown problem parameters are estimated and evaluated to provide a solution (Tarantola, 1984; Tarantola and Valette, 1982a).

The least-squares method is used in this study to determine an appropriate solution to an under-defined geoscientific problem. Least-squares inversion is a process that conducts iterative forward modelling to resolve petrophysical distributions from a measured geophysical field (Fullagar et al., 2000; Jessell, 2001; Oldenburg, 1974). The a priori input for inversion is a starting model consisting of a selection of petrophysical properties and/or geological surfaces (Boschetti and Moresi, 2001; Fullagar et al., 2000; Gallardo and Meju, 2011; Guillen et al., 2008; Oldenburg et al., 1997). Estimation of rock property distributions produces a calculated response that is measured against the natural, or observed, geophysical response. Mathematical methods, such as residual

misfit and fit to data metrics, are used to assess whether the estimated rock property distribution adequately reflects the observed geophysical response. Estimation of rock properties distributions is performed using an objective function, however constraints (that are prone to error) such as petrophysical rock properties, are used to reduce the number of possible solutions (Boschetti and Moresi, 2001; Zelt, 1999).

Inversion parameters, such as fit to data thresholds; the structure of the starting model; the inversion scheme itself and what results constitute an adequate 'answer' are all chosen by the operator. Finding the optimal set of inversion parameters either requires sensitivity analysis through multiple inversion runs, or simultaneous examination of the input data and the required solution (Boschetti and Moresi, 2001; Gallardo and Meju, 2011; Zelt, 1999). Petrophysical constraints provide a sample of the natural world to guide the inversion process to provide geophysical contrast between different rock units (Fullagar et al., 2000; Fullagar et al., 2008; Guillen et al., 2008; Lane and Guillen, 2005; Lelièvre et al., 2009; McLean et al., 2008; Williams et al., 2009), but also contain error associated with specimen sampling (Worthington, 2002). The standard deviation of the sample is normally used to describe the petrophysical heterogeneity of the rock type, but can also infer the confidence one has with the sampling process. Petrophysical constraints also restrict geological elements from being attributed unrealistic values. Minimum and maximum petrophysical values can be assigned to model elements as lower and upper bounds that the inversion process cannot transgress in order to improve misfit (Fullagar et al., 2008). Some inversion schemes offer the opportunity to assign a probability density function to simulate property heterogeneities within model elements (Guillen et al., 2008).

Geometrical constraints are designed to stop large changes at shallow depths (Fullagar et al., 2008). Commonality constraints can be used where the geometrical modifications are kept within an assigned initial-model / final-model ratio (Geomodeller User Manual, 2012). Volume and shape ratios assigned by the operator ensure that model elements do not become unrealistically enlarged or distributed around the model in an attempt to lower misfit. A ratio can also be assigned to ensure that a unit cannot transgress set upper and lower depth bounds when modified by inversion (Fullagar et al., 2008). Davis et al. (2012) describe a technique that incorporates geological structural information as a constraint for inversion. Smoothness in the direction of the geological trend is imposed by an objective function that attributes structural information to the prisms sub-

jected to inversion. Geological constraints such as those offered by Fullagar et al. (2008) and Davis et al. (2012) do reduce the number of potential inverse solutions, but rely on geological information that contains its own uncertainty and error. Attempts to reduce the number of possible solutions through imposing geological constraints are achieved at the expense of adding further subjectivity.

Typical inversion procedures operate with a single a priori model, precluding other possible geological scenarios from being tested against the observed geophysical field (Boschetti and Moresi, 2001). Offering multiple starting points for a process intending to arrive at a single solution appears to overcomplicate an already complex process. A single a priori model also gives the perception that the final model will somehow resemble the pre-inversion model, giving confidence to the operator that the extensive geological knowledge that was used to build the model will be retained in the process. Ultimately, the inversion scheme assumes that the model input is the best geological solution. This assumption is flawed, as geological and geophysical problems are often as poorly parameterised as each other (Jessell et al., 2010; Mann, 1993; Thore et al., 2002). The operator is usually aware of the capability of the model to honour both geophysical and geological data as they have integrated all data into the model (Royse, 2010). The operator's opinion on model quality is important, but nonetheless subjective, biased and typically not based on any direct quantitative techniques, rendering the communication model quality to qualitative measures. Model quality is therefore a difficult property to transfer into inversion input parameters.

Qualitative assessment of inversion results is typically performed once the mathematically defined indicators of inversion success have been achieved. Completion of inversion requires review because results can bear little resemblance to what is considered a reasonable representation of geological reality. Situations such as this should not be unexpected. The solution has been produced automatically accommodating the defined input parameters and a-priori model. The algorithm has performed according to requirements, but as the solution is non-unique, the decision as to whether results are accepted rests with the operator (Polanyi, 1962; Torvela and Bond, 2010). Therefore, the role geological intuition plays is critical to the process, as geological idiosyncrasies that have not been retained during inversion may not be acknowledged as missing from the final result (Cooley, 2007). Intuition is based upon the education, experiences and background of the operator and is fundamentally a biased quality (Frodeman, 1995).

This manuscript presents a process that produces multiple geological realisations from the

same input dataset and subjects them to inversion. The process is tested for the Ashanti Greenstone Belt, southwestern Ghana in west Africa. Model uncertainty is calculated using techniques from Lindsay et al. (2012a) and described by stratigraphic variability. Geodiversity metrics are used to characterise the geophysical and geometrical aspects of each model. Metrics describe the volume, depth, curvature, contact relationships, complexity and geophysical responses of a model (Lindsay et al., 2012b; Lindsay et al., 2012c). Results are ranked to determine metric end-members and to identify inversion constraints. Principal component analysis (PCA) is used to analyse all metric results simultaneously in order to identify the configuration of model space and which geodiversity metric (or metrics) contribute most to model space variability. Models are selected from the PCA and selected geological elements are subjected to gravity inversion. Inversion parameters are obtained through analysis of petrophysical data and geodiversity. Inversion results are analysed individually and comparatively to access the viability of the presented technique. The primary aim is to produce model elements that honour both geological and geophysical data while removing some of the subjectivity from the inversion process. This can be achieved by: (1) providing multiple a priori models as inputs to inversion; (2) supplying relevant geological information as inversion parameters and (3) assessing the success of the inverse run through correlation with model uncertainty.

2. The Ashanti Greenstone Belt, southwestern Ghana

The Ashanti Greenstone Belt is a gold prospective Palaeoproterozoic granitoid-greenstone belt located in the south of the Leo-Man craton, West Africa (Figure 1). Figure 2a displays the stratigraphic column used in model construction. The Ashanti Greenstone Belt comprises a Palaeoproterozoic basement of Birimian Series metavolcanics overlain by metasediments (Adadey et al., 2009; Loh et al., 1999; Perrouty et al., 2012) in turn overlain by the Palaeoproterozoic Tarkwaian Series sediments (Junner, 1940; Kitson, 1928; Perrouty et al., 2012; Pigios et al., 2003). A steep regional gradient seen in the Bouguer gravity anomaly (Figure 3a) striking north-northeast south-southwest represents a faulted contact betwwen the Kumasi Group to the west and the Tarkwaian Series to the west, indicating the location of the Akropong and Ashanti faults. The Tarkwaian Series comprises a complex polydeformed sequence of dolerite sills, phyllites, conglomerates and sandstones (Eisenlohr and Hirdes, 1992; Feybesse et al., 2006). The Tarkwaian Series is represent-

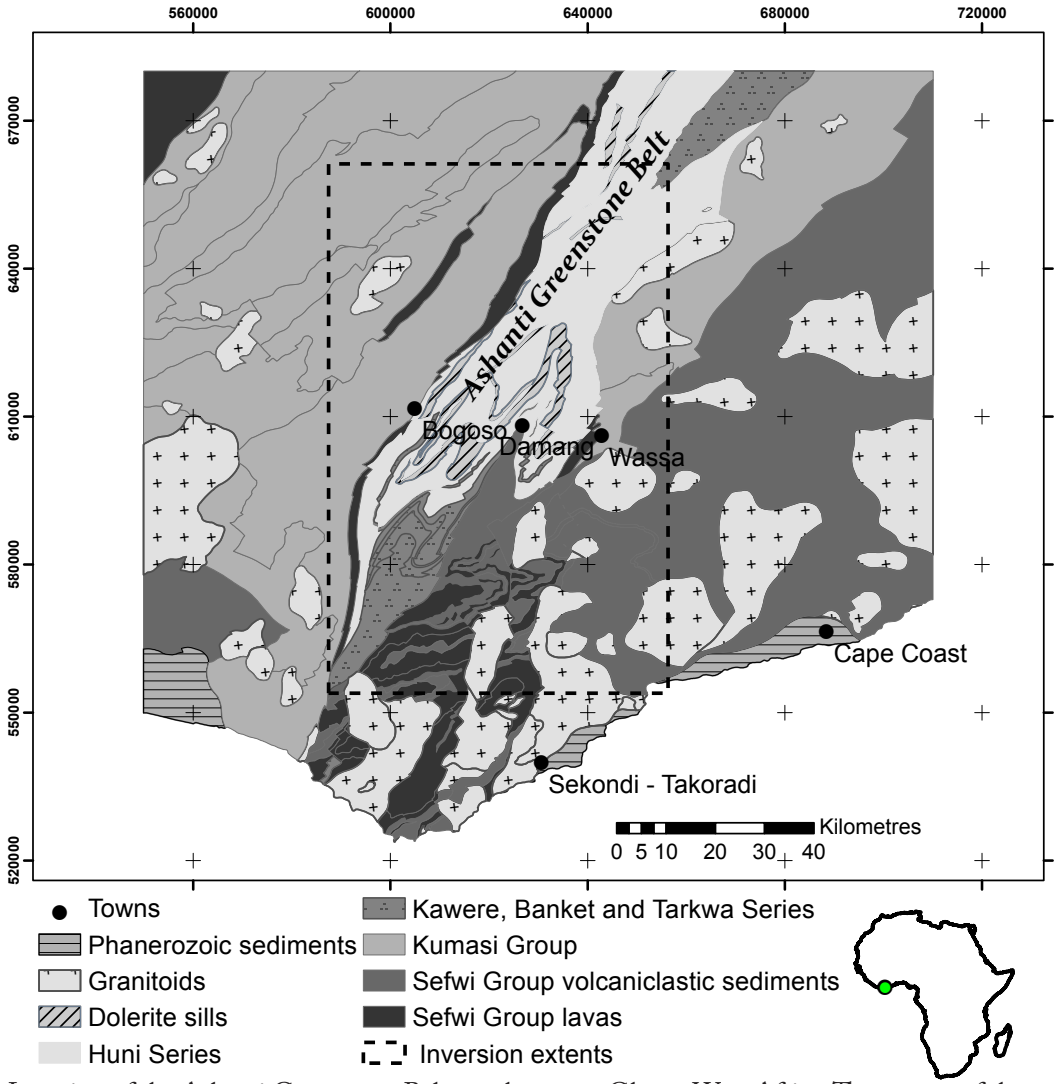

Figure 1. Location of the Ashanti Greenstone Belt, southwestern Ghana, West Africa. The extents of the geology in the top figure section correspond to the model extents. Note the inversion extents are defined by the dashed line. Modified after Perrouty et al. (2012)..

ed in the model by the conglomerates and dolerite sills. Dolerite dykes are common throughout the region and are noticeably represented in the aeromagnetic datasets (Figure 3b), though have not been included in the model. Granitoids have intruded the Birimian and Tarkwaian series during the Eoeburnean and Eburnean orogenic events. Eoeburnean grantoids (2180-2150 Ma), then Eburnean grantoids (2130-2070 Ma) were emplaced throughout the region (Perrouty et al., 2012). The Eoeburnean and Eburnean granitoids both display typical tonalite-trondhjemite-granodiorite (TTG) compostions. The south of the region also contains a suite of granitoids of more intermediate composition. For the purposes of the modelling exercise, granitoids have been separated into TTG-type Eoeburnean granitoids and Late Eburnean grantitoids rich in K-feldspar (Perrouty et al., 2012). The youngest modelled geological unit is a layer of Phanerozoic shales and sandstones, which predominantly crop out along coastal regions.

a)

Stratigraphic column			Assigned petrophysical properties: Density (gm/cm^3) mean ρ	Density σ	Mag. Susceptibiilty (SI) mean	Mag. Susceptibiilty σ
Phanerozoic Cover	st	**19**	2.55	0.001	0.002	0.001
Late Eburnean	granite_k	**18**	2.74	0.001	0.002	0.00001
Eoburnean	granitoid_ttg	**17**	2.78	0.05	0.005	0.00001
Tarkwaian Group	td	**16**	3.0	0.001	0.01	0.00001
Inversion input	tkc	**15**	2.7	0.005	0.005	0.0001
Late Birimian	lvbs	**14**	2.71	0.0001	0.001	0.00005
Mpohor mafic complex	Mpohor	**13**	2.75	0.2	0.05	0.0001
Early Birimian	bv5	**12**	2.81	0.05	0.02	0.0001
	bvc4	**11**	2.72	0.001	0.001	0.00001
	bv4	**10**	2.81	0.05	0.02	0.0001
	bvs	**9**	2.72	0.005	0.005	0.0001
	bvc3	**8**	2.72	0.005	0.001	0.0001
	bv3	**7**	2.81	0.05	0.02	0.0001
	bg	**6**	2.89	0.04	0.01	0.0001
	bv2	**5**	2.72	0.01	0.02	0.0001
	bvc2	**4**	2.72	0.05	0.001	0.0001
	bv1	**3**	2.81	0.05	0.02	0.001
	bvc1	**2**	2.72	0.04	0.001	0.0001
Micaschist basement	base	**1**	2.76	0.01	0.005	0.0001

b)

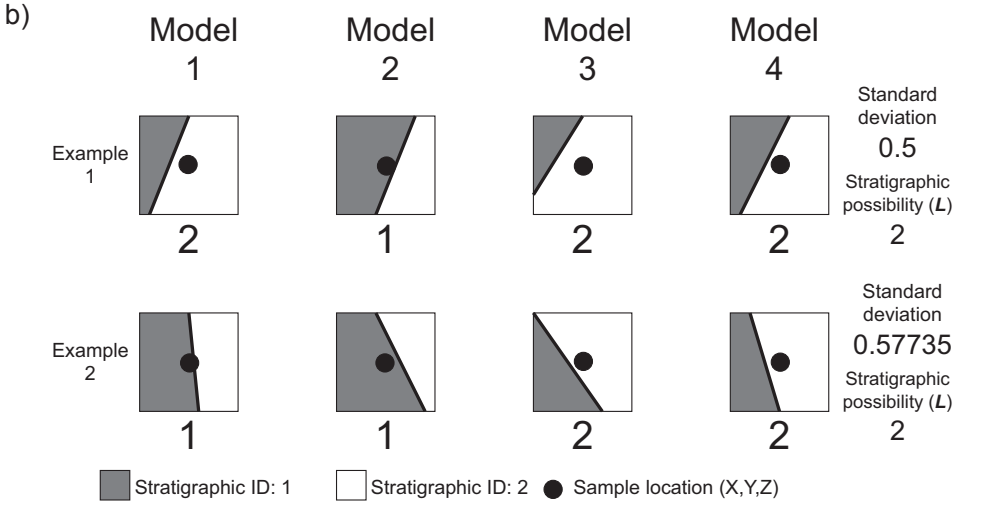

Figure 2. Model parameters and determination of model uncertainty. a) Stratigraphic column and stratigraphic identifier values (bold numbers). Assigned petrophysical values are listed to the right of each stratigraphic unit. Modified after Perrouty (2012). Note the base of ***tkc*** is used for inversion. b) Simplified synthetic example of how stratigraphic variability is determined to represent model uncertainty (after Lindsay et al., 2012a).

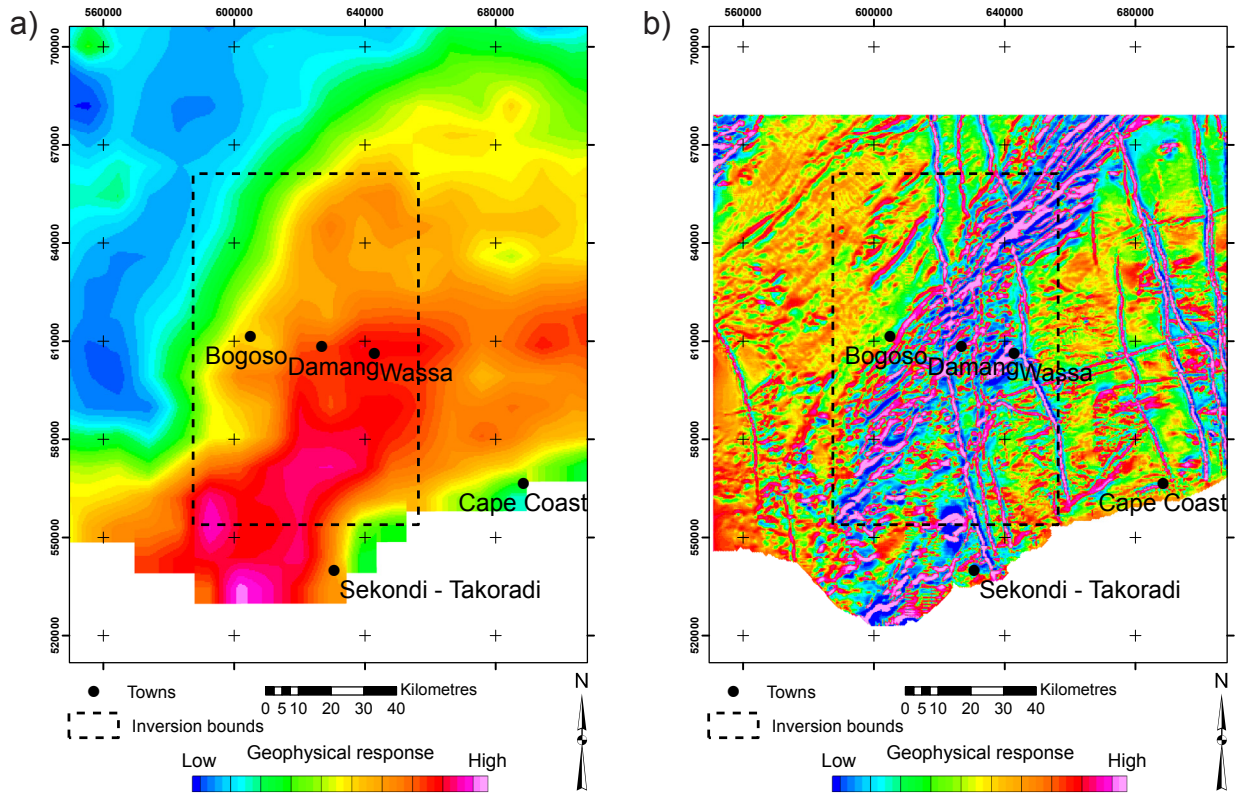

Figure 3. Geophysical grids used to construct the Ashanti Greenstone Belt model. a) Bouguer gravity anomaly image and b) reduced to the pole image of the total magnetic intensity. Modified after Perrouty et al. (2012).

3. 3D modelling workflow

Figure 4 describes an eight step workflow used to obtain the results discussed in this manuscript. Brief descriptions of steps one to six are performed here, though are provided in greater detail in Lindsay et al. (2012a), Lindsay et al. (2012b) and Lindsay et al. (2012c). Steps seven and eight, describing the inversion procedure and results analysis, are described in detail within this manuscript.

3.1. Model construction

The 3D geological model of the Ashanti Greenstone Belt was constructed using a combination of field, geophysical and remotely sensed data. Field data consisted of measurements obtained through the outcrop maps of Loh et al. (1999), BHP Billiton and Golden Star and data collected by Perrouty et al. (2012). Field data includes petrophysical measurements, structural observations, lithological descriptions and a revised stratigraphic column produced by Perrouty et al.

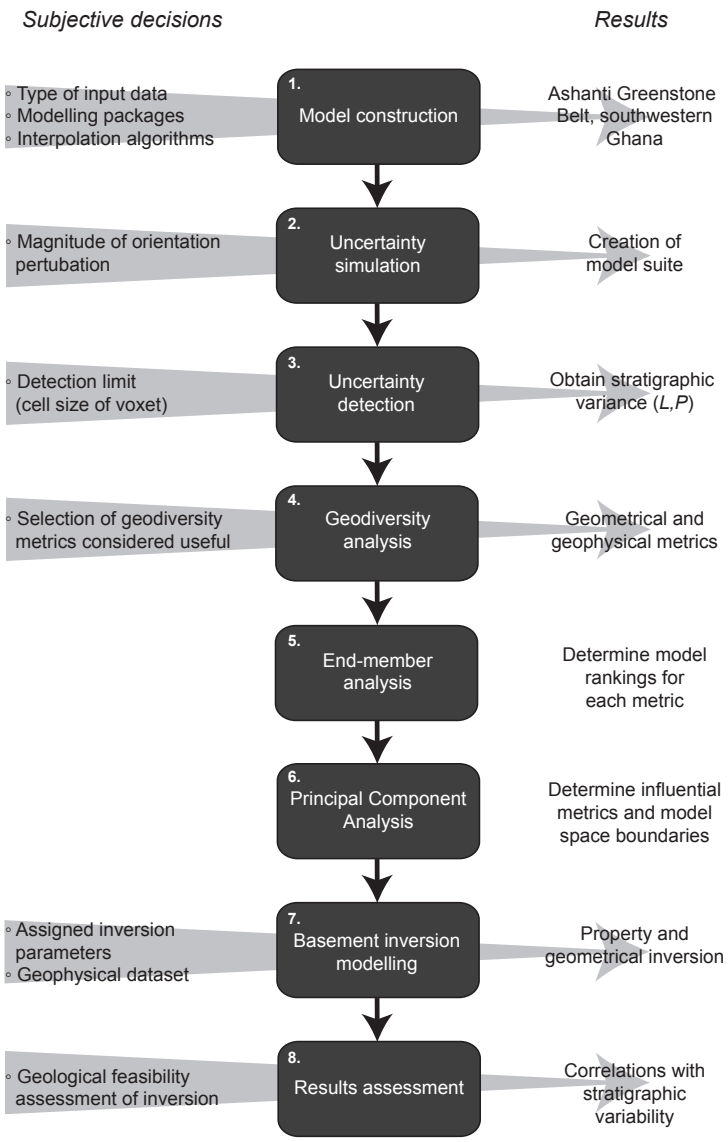

Figure 4. Workflow diagram depicting the steps taken during the procedure. The subjective decisions made in and results of each step of the workflow are shown.

(2012). Geophysical interpretation of potential field datasets was extensively employed to provide greater geological understanding over the study area. Geophysical datasets include gravity (Figure 3a) and aeromagnetic data (Figure 3b). Gravity data was obtained through the International Gravimetric Bureau (BGI, http://bgi.omp.obs-mip.fr/) and has a resolution of approximately 4.6 kilometres per pixel (2.5 arc-minutes). The gravity dataset contains a combination of Getech ground data (African Gravity Project 1986-1988, http://www.getech.com/history.htm), BGI off- and on-shore data and satellite gravity data. Aeromagnetic data was acquired from the Geological Survey of Ghana and was flown at a height of 80 metres, with line spacing at 200 metres, striking 135 degrees. The reduced-to-pole (RTP) grid was generated using International Geomagnetic Reference Field (IGRF) parameters at the time of the survey (1994 to 1996): magnitude – 31699

nT; inclination of -14.5 degrees and a declination of -6.5 degrees.

Input datasets were integrated into 3D Geomodeller™ (http://www.geomodeller.com/), a 3D geological modelling system. The modelling system is considered 'implicit' modeller as model elements are calculated using the potential field method (Lajaunie et al., 1997). The location of geological contacts, associated orientation measurements and the stratigraphic column are cokriged in combination to produce a scalar 'potential field' (not to be confused with a geophysical potential field) representing an interpolation of geology between data points. The 3D position of interpolated surfaces can be determined from the scalar potential field. The boundaries of the geological body are defined by 'iso-potential' surfaces and orientation is defined by gradients determined by the orientation measurements. The relationship of each geological body to the other is defined by the stratigraphic column. More complex relationships between model elements can be defined using 'onlap' (where a younger unit will onlap an older unit) and 'erode' (where a unit will erode an older unit) relationship options in the stratigraphic column. Fault networks can be defined to determine which faults to stop or cross-cut others, and which geological formations are affected by which fault. The combination of these options allows the definition of a particular model topology that can be configured to represent the tectonic evolution of the study area (refer to Calcagno et al. (2008), Lindsay et al. (2012a), Martelet et al. (2004), Maxelon et al. (2009), Schreiber et al. (2010) and Vouillamoz et al. (2012) for extensive examples and case studies).

3.2. Uncertainty simulation

3D geological models are built using sparse data sets that do not fully describe the entire geological system under study; in particular, there is almost no subsurface geological information. A number of assumptions and interpolations are therefore required to predict geology in regions not described by input data. Knowledge-driven and non-unique interpolation is typically employed to generate geological relationships between sparse data points. The modelling system assists in removing some subjectivity associated with knowledge-driven processes through interpolation of a repeatable objective function with the implicit method. However, what decisions regarding what data is included are made by the operator and thus subjective. These subjective decisions can significantly affect the resulting 3D architecture produced by the modelling application. Inherent error in

input data also produces model uncertainty (Jessell et al., 2010; Lindsay et al., 2012a; Wellmann et al., 2010). Finally, there is a question of whether the data collected adequately represents the actual architecture of the geological terrane. There are customisations that can be made to interpolation algorithms by the operator, such as variogram parameters, that influence the architecture of the resulting model. In general, however, the resulting model is a repeatable and objective representation of input data. Whether this data-driven model is an accurate representation of the geology is decided upon with knowledge-driven assessment by the operator. If the initial interpolation seems incorrect, subsequent addition or removal of data may be performed that fundamentally changes the geological representation of an area until the resulting model is acceptable. It is difficult to capture the reasoning behind an opinion of whether a model seems incorrect or correct, but producing a suite of models that may contain the 'correct' model is possible (Lindsay et al., 2012a).

Uncertainty simulation is employed in order to understand the role of the different datasets that are inputs into the modelling process. The orientation measurements that help the shape of model elements (i.e. the strike and dip of geological surfaces) are varied through Monte Carlo simulation. Each measurement, either defining geological contacts or fault orientation, are varied to within five degrees of the original value using psuedo-random equiprobable perturbation. For example, a measurement of 084/62E can be changed to 081/58E or 089/64E and so on, as long as the new measurement is within ± five degrees of the original.

3.3. Uncertainty detection

The original model, hereafter referred to as the 'initial model', has been calculated with the implicit method using datasets comprising unperturbed orientation measurements i.e. the best model according to the operator. The perturbed sets of orientation measurements are re-calculated to construct 'perturbed models', which, together with the initial model, collectively form a 'model suite' (Lindsay et al., 2012a). The next step is to characterise uncertainty within the model suite. Uncertainty exists in locations showing difference between models, for example, when a particular geological formation displays different geometries across the model suite.

Characterising the model uncertainty is performed by first discretising each model into a 'voxet', a collection of volumetric pixels (or 'voxels') that are attributed with a stratigraphic iden-

tifier. The stratigraphic identifier is an integer that represents the location of the unit within the stratigraphic column (Figure 2a) allowing easy calculation of the stratigraphic range ('L') between voxels (Figure 2b). Lindsay et al. (2012a) describe uncertainty using two different measures collectively called 'stratigraphic variability'. The number of stratigraphic units, 'L' at the same X,Y,Z location in each model throughout the model suite comprises the first component of 'stratigraphic variability'. The second part of stratigraphic variability, 'P' describes the deviation away from the most common stratigraphic unit at that X,Y,Z point throughout the model suite. The most common stratigraphic unit is determined from the 'modal model', a conceptual model that is calculated by determining the modal stratigraphic unit at each point within the voxet. Stratigraphic variability can be used to visualise the location and magnitude of uncertainty within a model.

3.3.1 Uncertainty in the Ashanti Greenstone Belt model

The location and magnitude of model uncertainty was determined using stratigraphic variability (Lindsay et al., 2012a). Figure 5 shows that levels of uncertainty > 4 tend to be associated with the Early Birimian surfaces and their contact with ***tkc***. A somewhat surprising result is only a small amount of uncertainty is associated with the many modelled faults. The only faults associated with uncertainty dip shallowly, while those with little uncertainty display high dip angles. A shallowly dipping fault is potentially longer and cross-cuts more volume of a model that is tile-shaped (i.e. wide and long but shallow - such as the Ashanti Greenstone Belt model), than a model volume that is prism-shaped (small on the x and y axes, but deep). In addition, high-angle fault will be shorter and subsequently cross-cut less of a tile-shaped model volume. Obviously, for the Ashanti Greenstone Belt model, any perturbation of a fault that cross-cuts more of the model will be associated with more uncertainty.

3.4. Geodiversity analysis

Uncertainty is detected in a model suite when differences have been detected between voxels in the model suite. Logically, these differences must be due to model elements changing shape or location. Unfortunately, stratigraphic variance does not describe how uncertainty changes the model geometrically. Quantitative analysis of the varied geometries exhibited by the model suite allows models to be compared and then ranked against each other. Geometrical analyses are

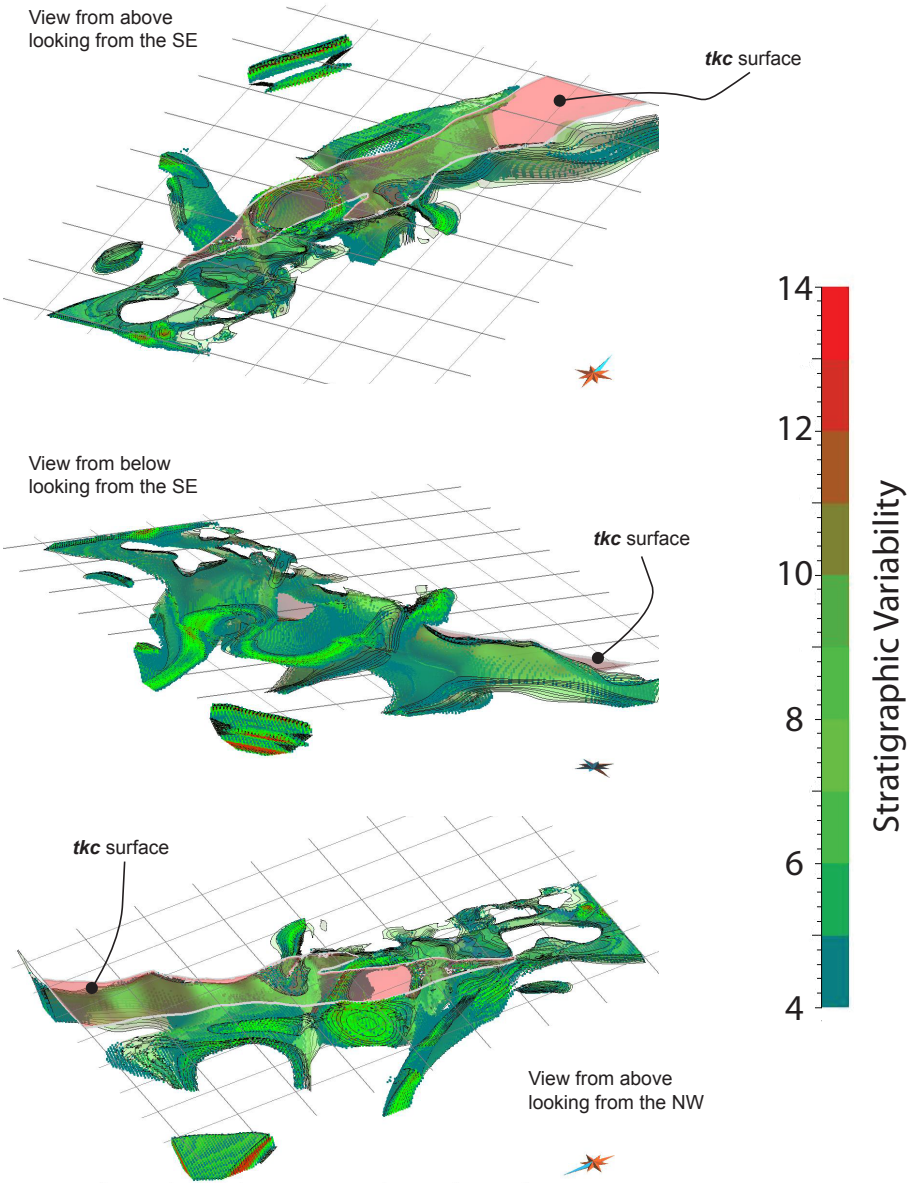

Figure 5. Uncertainty associated with the base of the Tarkwaian (*tkc*) and the Early Birimian Series. *tkc* is bordered in thick grey and the Early Birimian Series unit in black. Uncertainty is represented by points coloured according to stratigraphic variability. Higher magnitude stratigraphic variability has been displayed (>4). The *tkc* and Early Birimian structures have been obtained from model 92.

performed under a collection of geometrical analyses called 'geodiversity metrics' (Lindsay et al., 2012b) (Table 1). Included in the geodiversity metrics are methods to calculate the curvature of a model surface, finding the deepest and shallowest extent of a model element, the volume of a model element, the surface area of a geological contact and the complexity of a model element. The complexity of a model element is calculated by a nearest-neighbour calculation (six closest neighbours) that determines the number of different stratigraphic units that surround a given point. For example, if the complexity of a point is determined to equal three, then three different stratigraphic units surround that point, which would represent a relatively complex location within the model.

Table 1. Summary of geodiversity metrics and their function. Detailed descriptions of the geometrical metrics and their function can be found in Lindsay et al. (2012b). After Lindsay et al. (2012c).

Name	Subject	Measurement	Output
Geometrical geodiversity metrics			
Volume	Voxet	Metres^3	Volume for each formation
Depth	Voxet	Metres	Shallowest and deepest occurrence of each formation
Curvature	Surface	k_m: Mean curvature k_g: Gaussian curvature	Average k_m and k_g values for each formation
Contact relationships	Surface	Area (metres^2)	Contact surface area and contact relationships
Geological complexity	Voxet	Number of different lithologies around point-of-interest	Scalar value representing geological complexity
Geophysical geodiversity metrics			
Root mean square (RMS)	Residual grid	Global measure of geophysical misfit	Scalar value
Standard deviation	Calculated grid	Global measure of geophysical variability	Scalar value
Entropy	Residual grid	Global measure of geophysical variability	Scalar value
2D correlation coefficient	Comparison between observed and calculated grids	Global measure of geophysical covariance – recognises similar patterns	Scalar value
Hausdorff distance	Observed and calculated grids	Global measure of geophysical misfit – accounts for pattern translation, rotation and dilation	Scalar value

For more detailed explanations of geometrical geodiversity metrics see Lindsay et al. (2012b).

Average values of each metric from every stratigraphic unit are calculated to provide a representative value for the entire unit, not just individual points. A similar method is also employed by Lindsay et al. (2012c) when including geophysical metrics in geodiversity analysis. Geophysical metrics analyse the observed and calculated geophysical responses, and the difference between the observed and calculated response (the 'residual'). Image analysis and statistical techniques are used to measure different aspects of model geophysical representation, including root mean square (RMS), standard deviation (O'Gorman et al., 2008), entropy (Gonzalez et al., 2003; Wellmann

and Regenauer-Lieb, 2011), 2D correlation co-efficient and the Hausdorff distance (dH) (Huttenlocher et al., 1993). Each of these geophysical metrics is described with greater detail in Lindsay et al. (2012c). The aim of using geodiversity metrics is to provide a comprehensive description of geological and geophysical variation within the model suite.

3.4.1. End-member analysis

End-member analysis is conducted by ranking each model according to each geodiversity metric. For example, models with the smallest and largest volume of a particular model element, or the highest and lowest forward modelled gravity misfit within the model suite can be obtained. The end-member representatives for the Ashanti Greenstone Belt model suite are shown in Table 2. The selection of stratigraphic units shown was based which stratigraphic unit was the best representative of model suite variability. The end-member values for the depth of ***tkc*** show the range of possible depths of contact with the Early Birimian is 1,400 m (between 6650 and 8050 m). The inverted ***tkc*** models did not exceed the depth outlined in the end-member results, providing additional confidence that the result is geologically feasible.

The contact surface area (CSA) metric measures the surface area of a contact between two stratigraphic units. The most variable units were found within the Early Birimian series. There is a high range of CSA within the respective end-member representatives, which is reflected in the high degree of uncertainty associated with the Early Birimian surfaces.

The complexity metrics show similar ranges between each unit. The complexity of the Eoeburnean-age granites (***granite_ttg***) show similar ranges of complexity to the uncertain Early Birimian units ***bv4*** and ***bvc4***. The higher complexity of the Early Birimian can be attributed to the relatively high number of units (11) with which this series has been modelled. The result is that the units are thin and the potential for complexity increases in locations where the potential for surrounding units being adjacent increases, such as where these units are folded. In contrast, the complexity of the ***granite_ttg*** is due the unit being modelled as an intrusion and subsequently cross-cuts much of the modelled geology. In addition, some of the ***granite_ttg*** bodies outcrop at the surface and extend to the bottom of the model, so the likelihood of complexity is increased with the corresponding likelihood of cross-cutting other model elements.

The range of possible volumes for the Late Eburnean granites (granite_k) is 4677 $km^{3.}$ Model 86 displays the highest ***granite_k*** volume (15178 km^3) for the entire model suite, with the

range of being 31% of that value. This high variability (and therefore uncertainty) is not immediately obvious when visually assessing the modelled ***granite_k*** bodies' uncertainty (Figure 6). The granite_k bodies in the eastern section of the model do not appear to be uncertain, aside from where the Cape Coast Fault intersects a body in the southeastern quadrant. The majority of uncertainty is associated with the ***granite_k*** bodies located in the south and southwestern quadrants of the map, where they cross-cut the Early Birimian series units and are cross-cut by the Akropong Fault. Model uncertainty therefore cannot be estimated purely on the measurements from one stratigraphic unit. The interaction with other model elements also needs to be considered to develop a better understanding of the complex nature of model uncertainty. A topological measure of uncertainty (unfortunately beyond the scope of this study) would be desirable to aid this type of analysis.

The model uses a single stratigraphic unit to model the ***granite_k bodies***, where each these bodies would be more topologically accurate if represented individually. The modelling package and geodiversity assumes that a single stratigraphic unit is temporally contiguous, whereas in real-

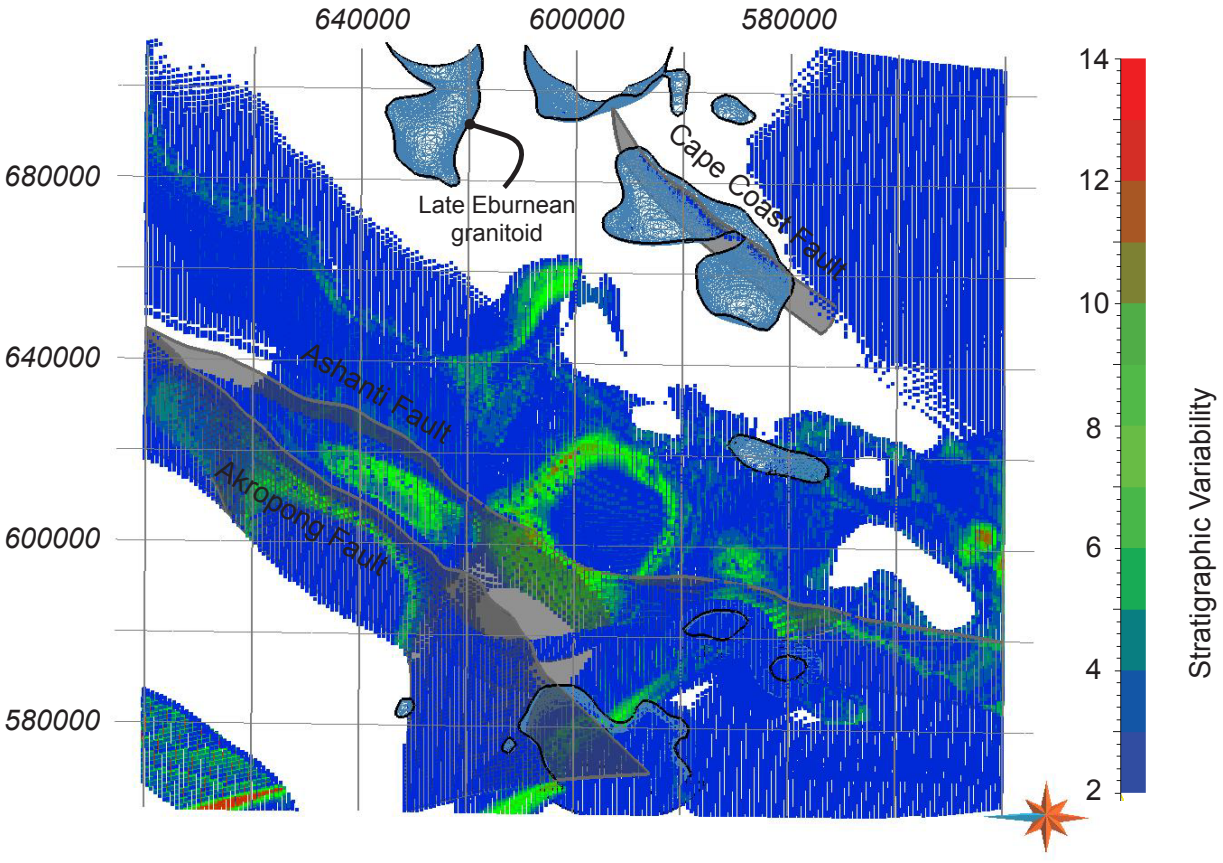

Figure 6. View from the west showing the lack of high uncertainty with the Late Eburnean granites ('***granite_k***'). The surface expression of the granites is shown with black borders. Faults are shown with grey borders. Stratigraphic variability shows low magnitudes (blue) through to extreme (red).

ity the Late Eburnean granitoid bodies display different ages (Loh et al., 1999; Oberthür et al., 1998; Perrouty et al., 2012). Modelling the Late Eburnean granites individually would reduce the high volume range shown in Table 2, avoid the suite of granites being mislabelled as highly uncertain, and rather than assuming the entire set is uncertain, would facilitate finding specific bodies displaying high uncertainty.

The RMS misfit values calculated by forward modelling are large; between 8.86 and 9.46 mGal for gravity (at most 15 percent of the 63.66 mGal dynamic range) and between 55.94 and 58.05 nT for magnetics (at most 12 percent of the 479.23 nT dynamic range). This large misfit is likely due to the lack of geological detail in the Tarkwaian Series units. By better modelling dense (2.87 – 2.90) and magnetically susceptible (15 – 78.8 x 10-3 SI) (Metelka et al., 2011; Perrouty et al., 2012) doleritic units in the Tarkwaian, large misfits could be avoided.

Variation between RMS misfit values obtained through aeromagnetic and gravity forward modelling show that the geophysical signature responds to uncertainty simulation. If there was no difference in RMS between models, it would suggest that differences between model architectures

Table 2. End-member representatives for the Ashanti Greenstone Belt model suite. Abbreviations are as follows: CSA = Contact surface area – voxels; Deep. = deepest part of unit – metres; k_m = mean curvature; k_g = Gaussian curvature; Comp. = complexity; Vol. = Volume (km^3); RMS = root-mean-square – mGals (gravity), nT (magnetic); dH = Hausdorff distance; Std. = standard deviation; 2D corr. = 2D correlation. The CSA metric measurement unit is in 'voxels' as an accurate estimate of surface area was not able to be obtained because the voxels have an irregular shape.

CSA ***bv1*** and ***bg***	CSA ***bvc1-bv2***	CSA ***bg-bv3***	Deep. ***tkc***	Deep. ***st***	k_m ***bv5-lbvs***	k_g ***bv5-lbvs***
165 (1)	51 (1)	4586 (89)	-6650 (17)	-9450 (25)	$-7.06x10^{-4}$ (53)	$-8.34x10^{20}$ (63)
4892 (72)	3847 (54)	7792 (1)	-8050 (91)	-11900 (61)	0.0013 (101)	$-4.07x10^{-7}$ (97)

Comp. ***granite_ttg***	Comp. ***bv4***	Comp. ***bvc4***	Vol. ***base***	Vol. ***granite_k***
1.46 (79)	1.55 (29)	1.62 (51)	145828 (1)	10501 (44)
2.21 (24)	2.30 (1)	2.50 (1)	174685 (50)	15178 (86)

RMS gravity	RMS magnetic	dH grav.	dH mag.	Std. grav	Std. mag	Entropy grav.	Entropy mag.	2D corr. grav	2D corr. mag
8.86 (78)	55.94 (75)	911.34 (99)	1501.30 (51)	20.13 (75)	29.83 (75)	0.35 (42)	1.05 (40)	-0.16 (1)	-0.19 (87)
9.46 (85)	58.05 (1)	934.03 (32)	1581.46 (36)	21.12 (1)	33.22 (1)	0.37 (6)	1.12 (62)	-0.17 (46)	-0.16 (1)

and petrophysical distributions had little influence over the geophysical response, and selection of model for input to inversion would have been arbitrary. As this is not the case, model selection is important. In addition, the petrophysical contrast for both density and magnetic suspectibility values are likely adequate for inversion.

Information entropy is a useful technique that reflects the roughness within an image and its overall information content (Gonzalez et al., 2003; O'Gorman et al., 2008; Shannon, 1948). An entropy metric is applied to the residual grid to discover whether it is 'rough', and contains high variability in values, or 'smooth' and contains little variability in values (Lindsay et al., 2012c). The entropy values of the aeromagnetic residual reveal a variety of results from relatively low entropy values (1.05 –model 40) indicating smooth residual images (i.e. displaying less large or frequent anomalies) to higher entropy values (1.12 – model 62), which indicate rougher or 'spikier' residual images. The gravity residual images show low entropy values for the residual grids (between 0.35 and 0.37) indicating the residual response fluctuates less than the aeromagnetic residual response. Less fluctuation in the gravity residual is likely due to the gravity signal being longer wavelength than the magnetic. Longer wavelengths of the gravity signature can be attributed to the gravity data being collected with larger station spacing (average of 10 km) than aeromagnetic flight lines (200 m) (Perrouty et al., 2012). In addition, magnetic petrophysics typically display a larger range of variation, especially in the presence of magnetically remanent geology (Muxworthy and McClelland, 2000). The higher entropy values do not mean a large misfit between observed and calculated response, rather sections of the model frequently differ in terms of misfit from each other. Figure 7 shows that several high-magnitude residual anomalies fall within the regions of the model that contain Tarkwaian series model elements, especially in the aeromagnetic case. In addition, the rougher parts of these images (i.e. where the entropy is higher) are associated with the same regions, indicating that the model is not representing the geology reflected by the geophysical dataset. There is a possibility that the model exhibits more model elements than are necessary to produce a geologically feasible response, resulting in the rough texture in the residual image. This is highly unlikely as there are just two stratigraphic units, td and ***tkc*** that represent the Tarkwaian series, so additional units would likely be required to match the higher frequency response shown in the observed aeromagnetic grid (Figure 3b). The additional units could be used to provide a more detailed realisation of the polydeformed sequence of dolerite sills, phyllites, conglomerates

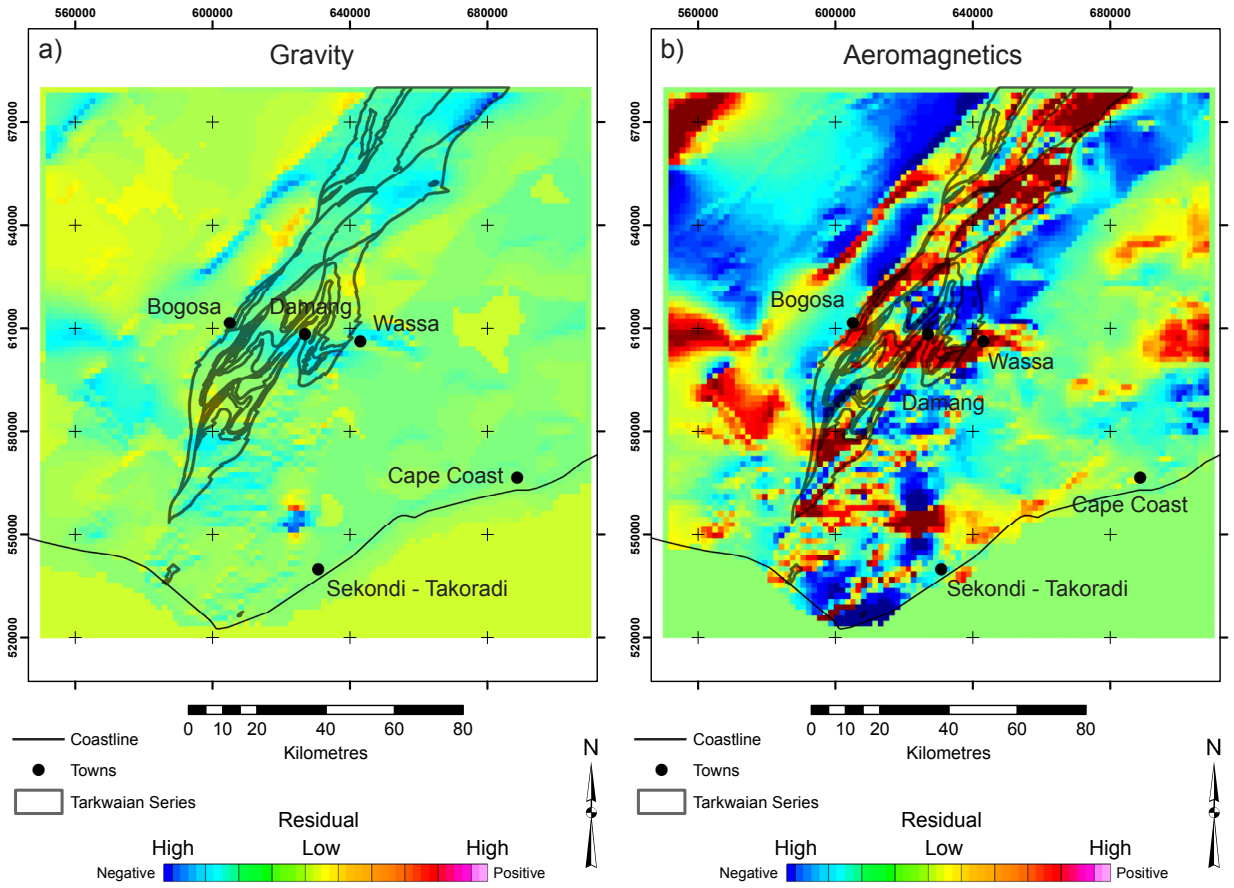

Figure 7. Analysis of residual image anomalies and regions that show the highest degree of misfit been the observed and calculated images. The main residual anomalies appear to be associated with the Early Birimian and Tarkwaian Series units.

and sandstones of the Tarkwaian Series (Perrouty et al., 2012).

The 2D correlation metric results support the Hausdorff distance (dH) metric results by showing that the observed and calculated responses for all models do not match very successfully. The dH results shown in Table 2 are high for both the aeromagnetic and gravity calculated responses, supporting the low correlation shown by the 2D correlation metric. Overall, the geophysical metric results suggest that it is very likely the Ashanti Greenstone is not representative of reality, and subsequently could be improved through geophysical inversion.

3.5. Principal component analysis

Ranking each model according to a geodiversity metric allows easy comparison of models, but only communicates which models are end-member representatives for that particular metric. To determine the ranking of models across the entire set of geodiversity metric requires a more sophisticated means of comparison than ordered lists. Simulatenous comparison of geodiversity

metrics is successfully achieved via Principal Component Analysis (PCA), a multivariate statistical technique (Jolliffe, 2002; Krzanowski, 1996). There are several reasons PCA was chosen to perform geodiversity metric analysis. Firstly, measurements with different units can be compared, for example volume (m^3), surface area (m^2), RMS misfit (mGals or nT) or depth (m). In addition, other metrics not included in this study can be easily included in future studies, regardless of the measurement type. Secondly, models can be ranked according to Hotelling's T^2 statistic (Hotelling, 1931; Krzanowski, 1995) to determine whether they exhibit typical or diverse characteristics and the configuration of model space can be determined, with diverse models defining the boundaries and models exhibiting typical characteristics populating the centre. Finally, the variance contained within each metric can be used by the PCA to identify which metric contributes most to model suite variability.

3.5.1. Geodiversity principal component analysis

PCA revealed two important aspects of the models within the Ashanti Greenstone Belt model suite. The first aspect was identifying the models with the most diverse and a common characteristic, the second aspect was identifying which geodiversity metrics most influence geodiversity. Hotelling's T^2 statistic was used, which identified models 3, 38 and 101 as the most diverse, in descending order of diversity. Models 92, 33 and 59 were identified as those sharing the most common characteristics, in descending order of commonality. Inverting similar models may seem unnecessary, as inversion would likely produce a similar result. The T^2 statistic for the similar models is not exactly the same, therefore these models do show differences. Subsequently, we were conservative by deciding to invert the similar models in case results did differ.

Identifying the most influential geodiversity metric was aided by 3D PCA visualisation. It was found that just under 50 percent of variance could be explained by the first three components, with the following 19 components explaining the remainder (Figure 8). Figure 9a shows a bi-plot, where points and vectors are plotted, each representing different aspects of PCA. This particular bi-plot is in 3D, as three principal components - one, two and three - are plotted on the x, y and z axes respectively. The distribution of points represents the relative distance each model has from the centre of the dataset. The coordinates for each point are scaled with respect to the influence of each metric, the axis that they are plotted along and the score obtained from PCA. The locations of these points in the bi-plot are therefore only representative, making Hotelling's T^2 statistic a more

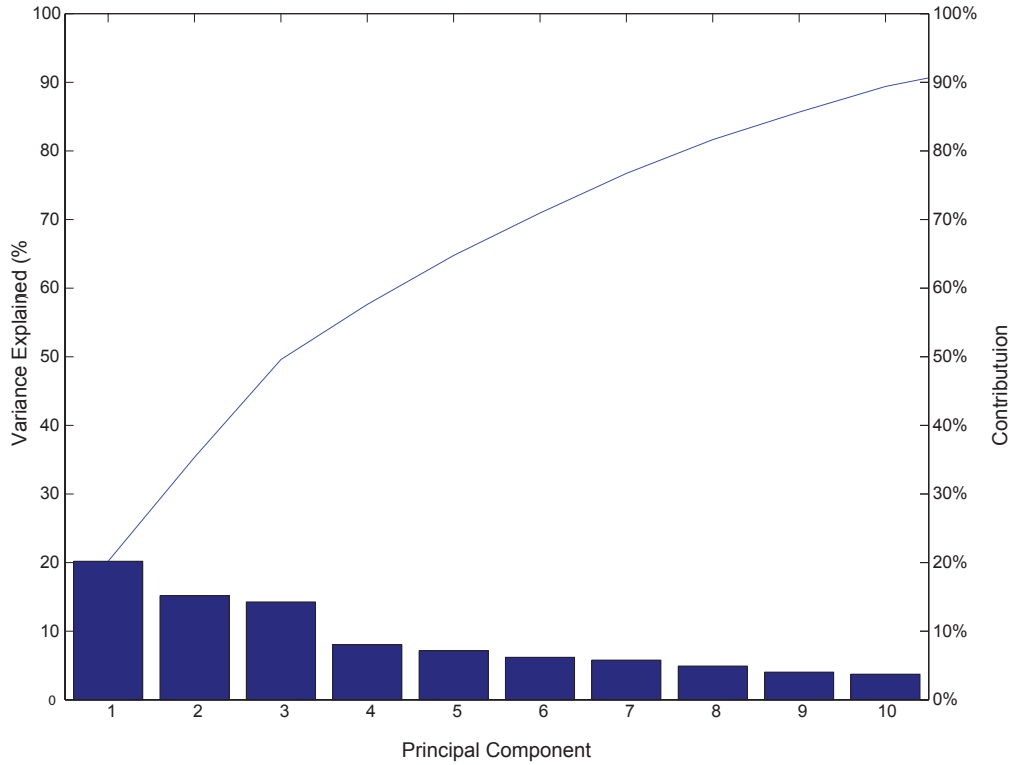

Figure 8. Cumulative distribution diagram showing that just under 50 percent of model suite variability is contained within the first three components. This requires the 3D visualisation of the first three components shown in Figure 12.

useful means of identifying common and diverse models.

Figure 9b-d shows 2D sections through the 3D plot to assist in visualising the somewhat complex arrangement of coefficient vectors. Note that each vector has been labelled according to the geodiversity metric it represents. The long vectors represent metrics that contain relatively higher model suite variability. Labels belonging to the shorter vectors have been removed to simplify the diagrams.

The distance a vector plots from the component axis represents the level of variance explained by that vector in that component. The closer a vector plots to a component axis, the closer the association. Vectors that plot on the right or upper side of the diagram have a positive association, those that plot to the left or lower side have a negative association. As shown in Figure 9, the largest amount of model suite variance is contained within Component 1 (~20 percent), therefore any vector with a close association with Component 1 (x-axis, Figure 12a and c) is of interest to explain model suite variability. Close associations to Component 1 are split between standard deviation of gravity; the contact surface area of ***bvc1-bv2*** and ***bv1-bg***; the aeromagnetic forward model RMS misfit and the aeromagnetic standard deviation.

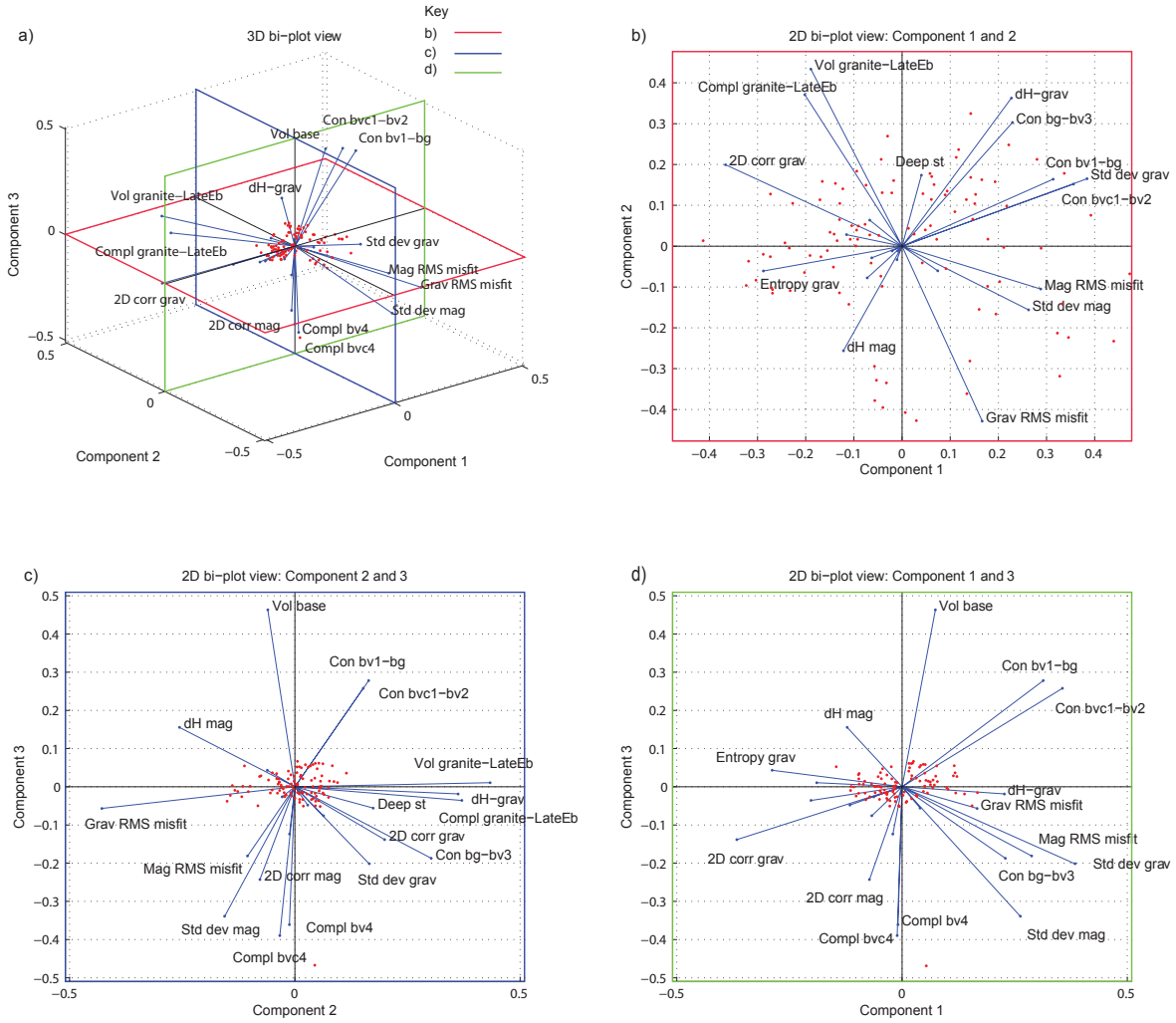

Figure 9. Results of combined principal component analysis on the Ashanti Greenstone Belt model suite. a) 3D bi-plot of the first three principal components. Component 1 is plotted on the x-axis, Component 2 on the y-axis and Component 3 on the z-axis. To aid visualisation each coloured section in a) represents the corresponding border of each 2D plot in b), c) and d).

Further insight into finding influential metrics is achieved by considering both Component 2 and Component 3. Figure 9b highlights the association of geophysical metrics (dH gravity, 2D correlation gravity) and the volume and complexity of the Late Eburnean granites with Component 2 model suite variability. Figure 9c and d support the association geophysical metrics have with model suite variability, along with the CSA within the Early Birimian Series.

Similarly oriented vector coefficients can be interpreted to be covariant, and usually this interpretation is used to identify redundant metrics that measure the same phenomena. Redundant metrics can then be removed from PCA to simplify the process. This analysis identifies vectors that plot in the same direction to guide understanding of the interaction between geometrical and geophysical metrics within the model suite. There appears to be some covariance between CSA (Con *bg-bv3*, Con *bvc1-bv2*) and gravity geophysical metrics (standard deviation and dH - Figure

9b). There also is covariance between the gravity geophysical metrics (2D correlation and dH), the volume and complexity of the Late Eburnean granites, and the CSA within the Early Birimian (Figure 9c). The covariance observed in the PCA bi-plot between these specific metrics confirms that the calculated gravitational response of the model suite is sensitive to geometrical variation within the models suite. It stands to reason that the gravity dataset will be useful as an input to the inversion process.

Gravity inversion of the ***tkc*** surface was performed to determine the depth and shape of the base of the Tarkwaian Series. The observations made during end-member analysis and PCA suggest that basement inversion on the ***tkc*** surfaces calculated from models 92, 33, 59 (typical model representatives) and models 3, 38 and 101 (diverse model representatives) may be successful. (1) ***tkc*** forms the basement of the Tarkwaian series and the interface between the Tarkwaian and the Early Birimian units. (2) ***tkc*** is associated with uncertainty. (3) End-member analysis identified that the depth of ***tkc*** is highly variable. (4) The depth of ***tkc*** affects the underlying Early Birimian units. The CSA of the Early Birimian units was identified by the PCA as influential in terms of overall model suite variability, therefore the depth of ***tkc*** is likely to be a primary cause of this variability. (5) Geophysical forward modelling of both aeromagnetics and gravity has shown that the largest variation in residual is associated with a region defined by the boundaries of ***tkc***. Inversion can be used with increased confidence to resolve some of the uncertainties in the model suite as the input has been chosen using an integrated analysis of geological factors.

3.6. Basement inversion

Commercial inversion packages now offer methods that jointly change both geometry and distribution of petrophysical properties (Fullagar et al., 2008; Guillen et al., 2008). VPmg ™ software (Fullagar et al., 2008) provides a means of defining the contribution of geometrical and property changes for each iteration of the inversion. This approach is useful as it does not assume the geometry of the model element is correct, nor the assigned petrophysical properties homogenous. The inversion procedure iteratively optimises the geometry, then property of the basement unit, independent of each other. Petrophysical properties cannot be changed during the geometry optimisation phase of the iteration and vice versa.

The inversion algorithm is performed on a discretised version of the 3D model. Discretisation is performed by subdividing the model into 1 km by 1 km prisms that extend from the Earth's surface to the base of the model. Each prism is further subdivided into two layers, one representing basement and the other representing cover. The observed Bouguer gravity response was assigned to each basement prism as a property. The Bouguer anomaly was chosen as the topography for the model is essentially flat (Figure 10). The contact location of a prism is changed during geometry optimisation to achieve a lower misfit between the forward modelled calculated response and the observed response. Geometrical perturbation is achieved by moving the subdivision boundary between cover and basement representatives along the z-axis in each prism. Density property perturbation is achieved by changing the assigned property value for each prism within the basement only. The solution of each phase of the iteration was selected according to the reduction of the forward response misfit and by the degree of fit to the data (the chi-squared data norm 'L2') (Fullagar, 2009). The objective of the inversion iteration is to halve the chi-squared data misfit using the smallest modification. The inversion will terminate if successive iterations do not result in reduced misfit, if a predetermined misfit threshold is obtained or if the maximum number of iterations is completed.

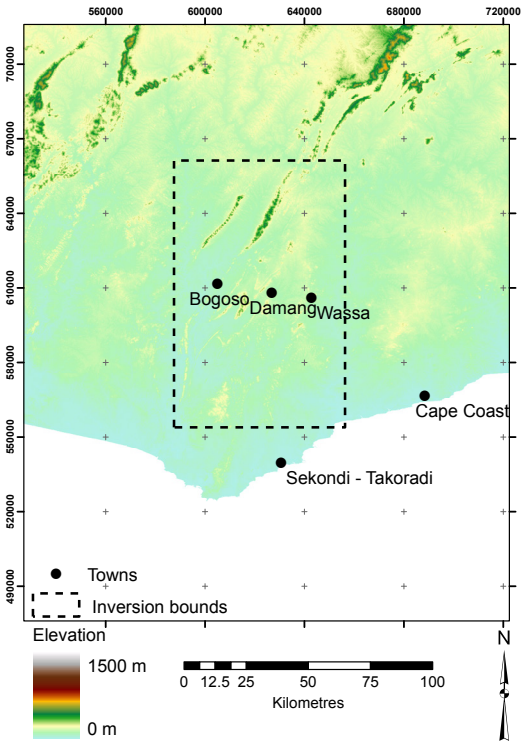

Figure 10. Digital Elevation Model (DEM) of southwestern Ghana displaying mostly flat topography over the region of interest. Data shown was obtained from the Shuttle Radar Topography Mission (SRTM) through CGIAR (http://srtm.csi.cgiar.org/).

Upper and lower density bounds were provided so that the inversion algorithm was restricted from using values outside of this range to achieve the necessary misfit reduction and data fit. The values used for density constraints were guided by data collected from rock samples (Figure 2a).

3.6.1. Inversion attempts using magnetic data

We investigated using magnetic data as a constraint for inversion, as in principal the finer resolution available should provide important local information (Aitken and Betts, 2009; Caratori Tontini et al., 2009; Williams et al., 2009). Using two independent potential field datasets should also reduce the ambiguity associated with using a geophysical dataset to constrain geology (Fullagar et al., 2004; Saltus and Blakely, 2011). The aeromagnetic data available was of sufficient quality and resolution, however was finally ill-suited for inversion purposes due to the pervasive presence of dolerite dykes (Figure 11a).

The magnetic susceptibility of the dolerite dykes is around two orders of magnitude higher than that of the surrounding sediments (~20x10-3 SI versus 0.1x10-3 to 0.5x10-3 SI) (Perrouty et al., 2012). An attempt was made to remove the influence of these dykes from the data. First, the dyke response was 'masked' using by selecting a ROI around each dyke and removing that region from the data set. These regions were then 'filled' using square roll-off interpolation to repopulate the masked regions. Figure 11b shows that the results were satisfactory and that the dolerite dykes

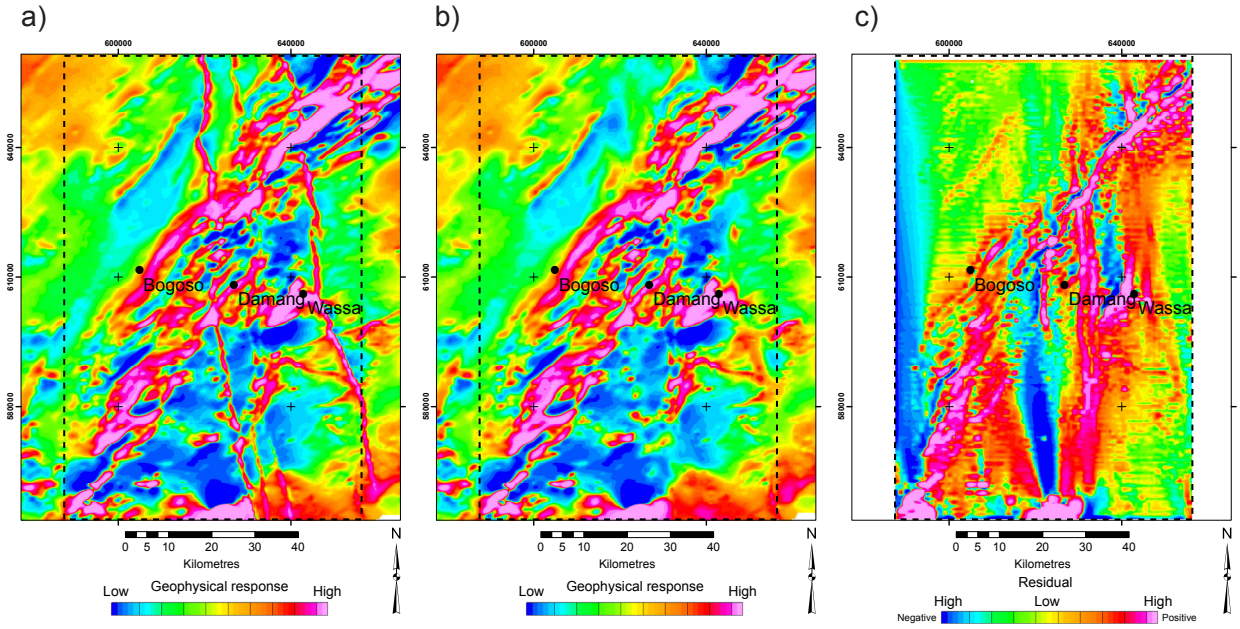

Figure 11. Aeromagnetic data and the influence of dolerite dykes. a) Pre-masked TMI aeromagnetic grid showing the presence of NNE and WSW-trending dolerite dykes b) TMI aeromagnetic grid after masking and filling c) residual grid of the magnetic basement inversion.

no longer dominated the grid, suggesting that the aeromagnetic dataset could be used for inversion. A trial inversion run was setup to test whether the aeromagnetic grid was appropriate to include in the models being analysed, and whether the inversion models providing reasonable insight into the geological architecture of the Ashanti Greenstone Belt.

The basement-style inversion was performed on the ***tkc*** surface rendered from the calculation of model 92. Inversion was attempted and results show that dyke removal was unsuccessful, so further inversion was stopped. Assessment of the inversion model residual grid shows that the influence of the dykes remains (Figure 11c).

3.6.2. Gravity inversion

The ***tkc*** surfaces from models 92, 33, 59, 3, 38 and 101 were subjected to inversion separately. Figure 12 shows the differences in geometry between the selected model ***tkc*** surfaces prior to inversion. Constraints were placed upon the edges of the ***tkc*** surfaces to prevent geometrical modification during inversion as the basal contact of the Tarkwaian is relatively well-defined from surface mapping, an assumption confirmed by field mapping and the relatively low uncertainty associated with the zero elevation part of ***tkc*** (Figure 5 – highlighted in grey). Density constraints are applied to both the cover layer (2.55 gm/cm^3) – taken from the Phanerozoic cover unit '***st***' and kept static through inversion) and ***tkc*** (2.7 gm/cm^3, Perrouty, 2012; Perrouty et al., 2012) to provide a starting property the inversion algorithm was allowed to modify. Each inversion run was set to execute 100 iterations, with each iteration first executing geometrical inversion, then property inversion, totalling 200 inversion operations. Each inversion run was executed in the VPmg™ inversion scheme.

The inversions were deemed successful as (1) both or one of the data norms L1 and L2 ≤ 1; (2) each modification saw a reduction in RMS misfit and chi-squared data misfit and (3) inversion convergence resulted in an RMS misfit that approximately equalled the standard deviation of the residual between the calculated and observed responses. All final produced final RMS errors of 0.20 mGal, except for model 101 where the final RMS error was 0.19 mGal. Inversion results are analysed in three ways: (1) the differences between inverted models; (2) what the inversion has modified (petrophysical property and geometry) to achieve a successful inversion and (3) what can be learned about the geology of the region from the modelling workflow presented in this manuscript.

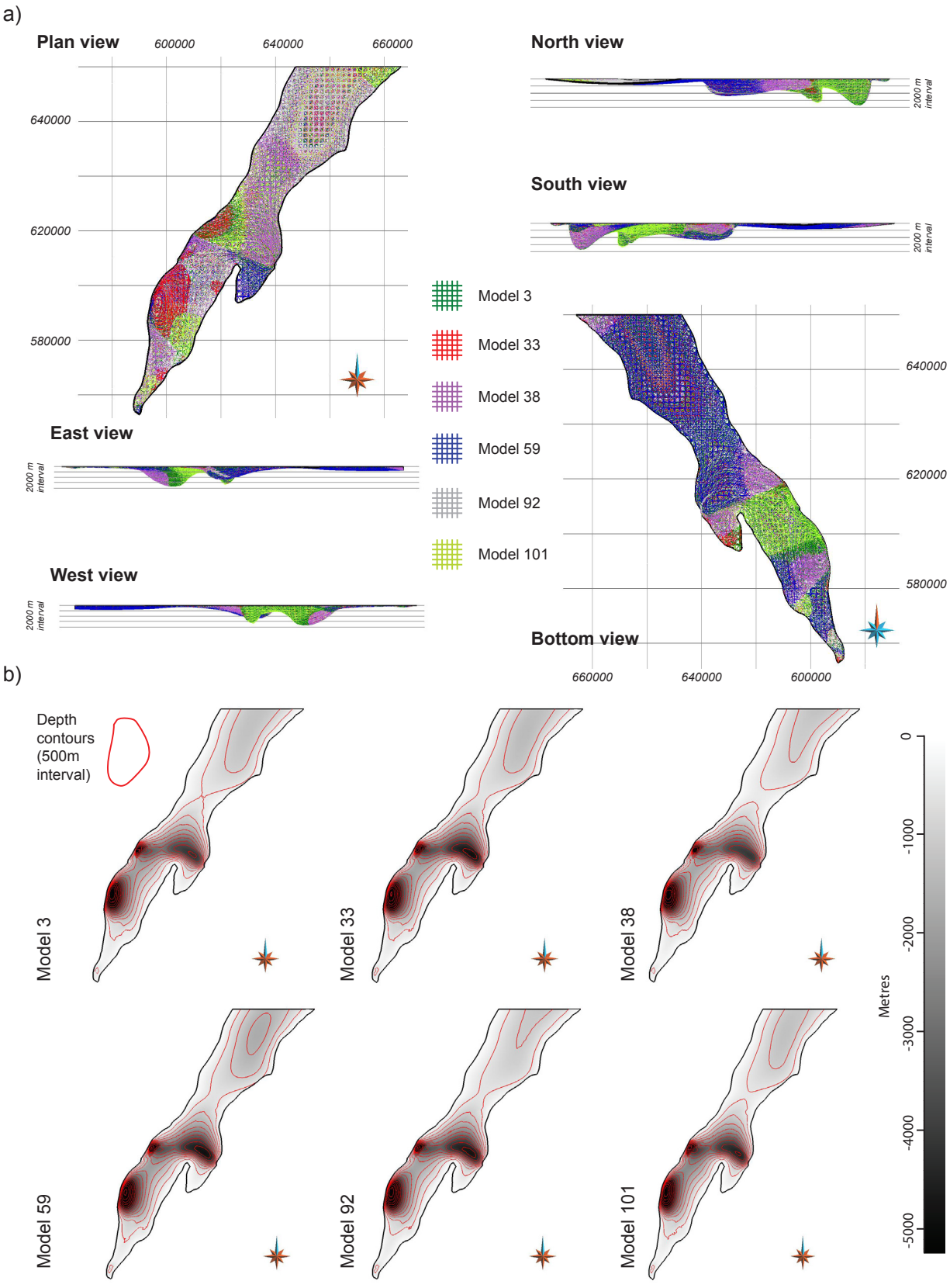

Figure 12. Comparison of ***tkc*** surfaces prior to inversion modelling. a) Each surface mesh has been colour-coded to assist comparison. The surface closest to the observer will show colour more dominantly. A selection of view directions have been provided to emphasise the geometrical variability between these surfaces. b) Map view showing colour coded depths. Red depth contours (500m interval) are shown to assist identification of differences.

3.6.3. Inversion differences

Variability maps were generated by calculating standard deviation maps from the six models generated after inversion (Figure 13) (Aitken et al., 2012). Values outside of the boundaries of ***tkc*** were masked to remove values outside the ***tkc*** region of interest. Figure 14 shows that the largest density differences between inversion results are located in the central west area and around Damang. Intermediate levels of difference are located in (1) the far northeastern corner, (2) five km of Bogosa and (3) south-southwest of Damang. The geometrical differences are less widespread than density differences, though a very high, localised anomaly is located near (1) Bogosa (the same region as a density difference anomaly), (2) south-southwest of Bogosa and (3) a lesser anomaly is located east of Damang. The results suggest that the inversion algorithm found it difficult to resolve regions where density and geometry modifications differ between models, and/or that the initial selected models played a significant role in the final result. It is possible that after five to ten iterations the input model still retained its original properties and influenced the inversion result. However, it is highly unlikely that after 100 iterations the initial model was still influential. A reason as to why the inversion algorithm has difficultly resolving the anomalous areas needed to be uncovered.

Correlation with uncertainty can assist in resolving this impasse. The 3D uncertainty grid (Section 3.3) was converted into a 2D representation by projecting the 3D grid onto a plane located at the topographic surface. The mean value of stratigraphic variability is used to incorporate the values in each column. The 2D stratigraphic variability grid shown in Figure 15 has been masked to remove values outside the region of interest defined by the borders of ***tkc***. The correlation

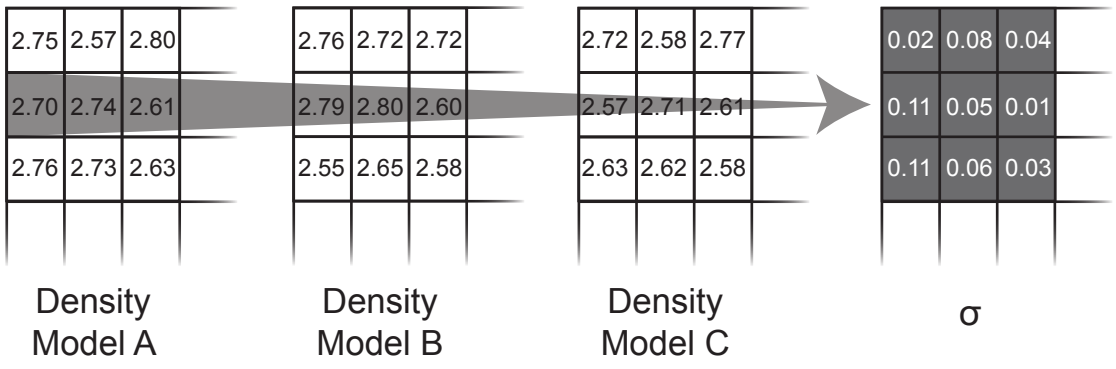

Figure 13. Comparison technique employed to detect variation between different inverted models. The example shown here uses density values (g/cm^3). Models A, B and C are fictitious inverted models and the cells shown are a sample of a larger grid. The 'σ' grid at right displays the standard deviation from the corresponding cell in each model i.e. the top-left cell (0.02) is the standard deviation of the top-left cell value from Model A (2.75), Model B (2.76) and Model C (2.72).

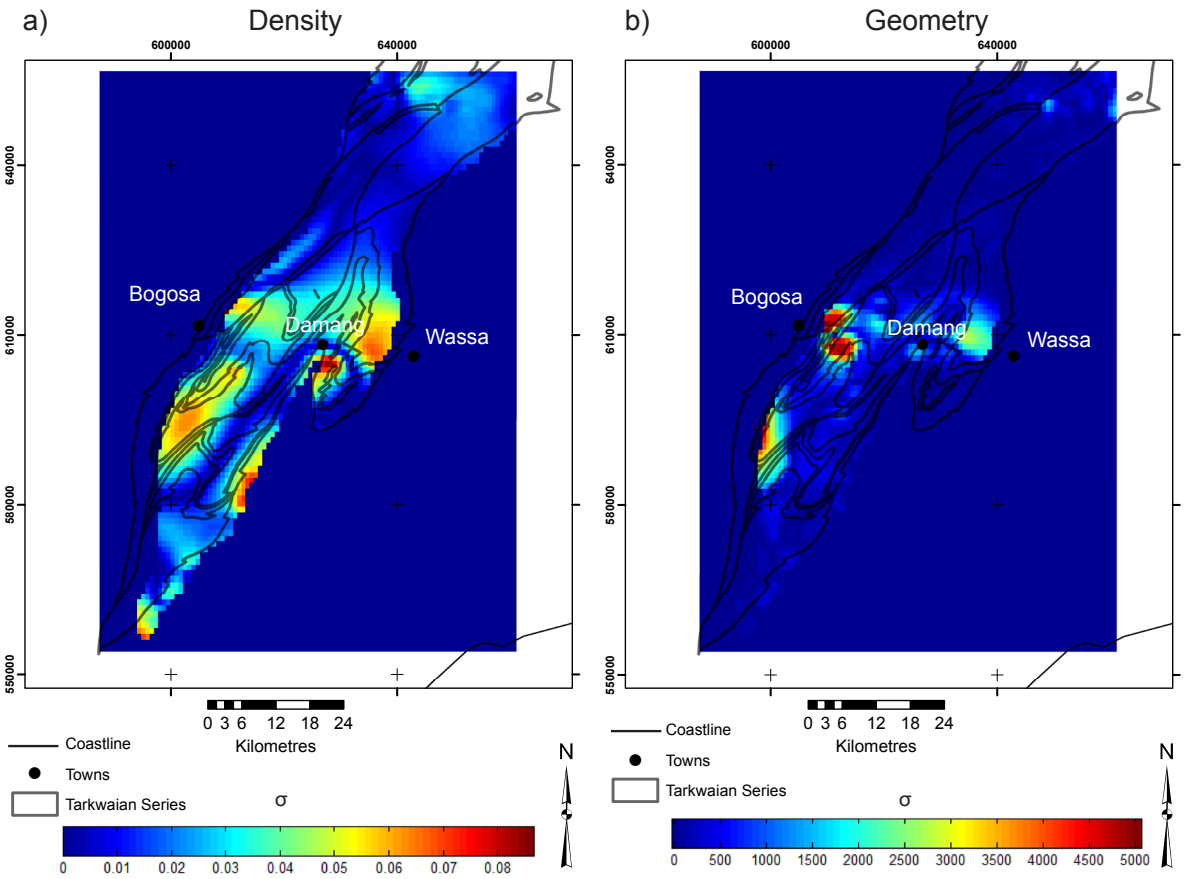

Figure 14. Variability map showing the differences between inversion results for (a) density and (b) geometry across inversion model results. Property values are used to calculate the density variability in (a) and depth values are calculate the geometrical differences in (b). The variability maps are generated using standard deviation value for each x,y point (see Figure 6).

coefficient for the differences in density between the inverted models and stratigraphic variability is 0.77 (Table 3). The correlation coefficient for the differences in geometry between the inverted models and stratigraphic variability is 0.67. These high coefficient values indicate that there is a link between locations identified as geologically uncertain, and locations geophysical inversion finds difficult to reconcile against the observed geophysical response. Thus the inversion algorithm could be guided by stratigraphic variability to focus on areas of high uncertainty to achieve higher confidence in inversion results (discussed further discussed in Section 5).

3.7.4. Geometrical and property modifications

Figure 16 shows variability maps for each input model displaying the modifications made to both density and geometry values during inversion. These maps display where modifications were made and the degree to which they were modified by comparing the input and inverted models. Visually there appears to be little difference between both the density and geometry map sets. The conclusion reached through visual inspection is confirmed by the correlation coefficient

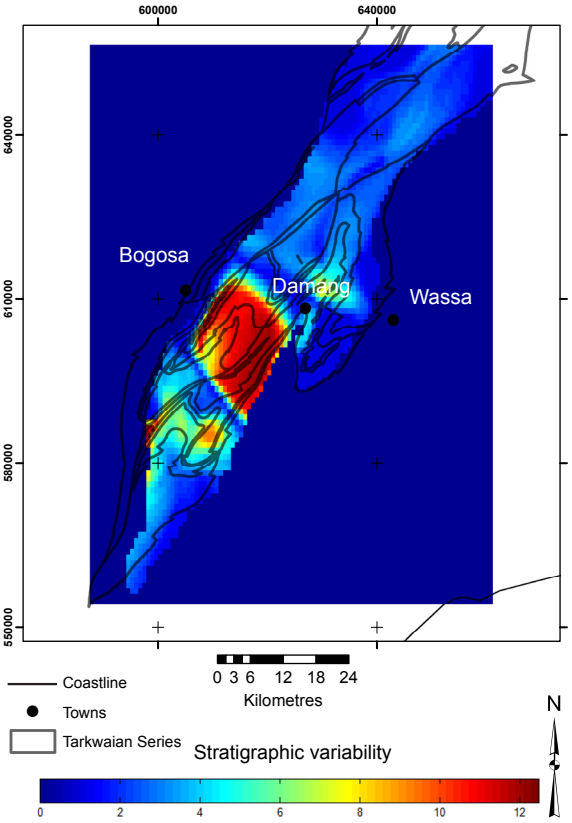

Figure 15. Image showing the projection of uncertainty (stratigraphic variability) onto a horizontal 2D surface. This image was used to correlate model uncertainty with various aspects of inversion modelling.

matrices shown in Table 4a and 4b. These display coefficients indicating the variability maps are almost identical. The inversion algorithm appears to address almost the exact same regions with very similar degrees of modification to achieve the respective inversion results. Table 3 shows that while there is some correlation between the respective inversion modification schemes and uncertainty,

Table 3. Correlation coefficients between inversion behaviour with model suite uncertainty (stratigraphic variability).

Variability between inverted models		
	Density correlation coefficient with stratigraphic variability	Geometrical correlation coefficient with stratigraphic variability
	0.77	0.67
Variability between input model and inverted model		
Model	Density correlation coefficient with stratigraphic variability	Geometry correlation coefficient with stratigraphic variability
3	0.62	0.50
33	0.61	0.49
38	0.61	0.50
59	0.61	0.50
92	0.60	0.49
101	0.64	0.52

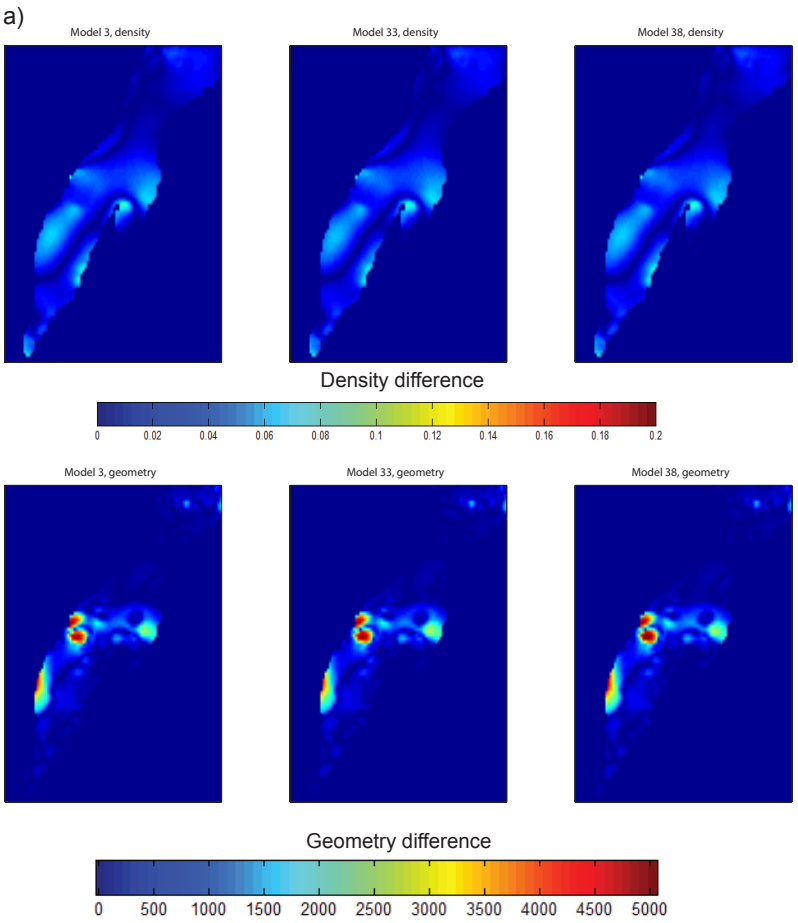

Figure 16. Variability maps showing the location and magnitude of modifications the inversion algorithm has performed to basement (density) and ***tkc*** surface (geometry). Each map is a comparison between the first iteration and the last iteration for both density and geometry. a) Models 3, 33 and 38. b) (next page) Models 59, 92 and 101. See Figure 6 for pre-inversion ***tkc*** surface geometry.

Table 4. Correlation coefficient matrices for (a) density and (b) geometry modification variability maps.

a)	3	33	38	59	92	101
3	1.0000					
33	0.9980	1.0000				
38	0.9992	0.9979	1.0000			
59	0.9982	0.9992	0.9974	1.0000		
92	0.9981	0.9992	0.9986	0.9982	1.0000	
101	0.9989	0.9960	0.9976	0.9962	0.9959	1.0000

b)	3	33	38	59	92	101
3	1.0000					
33	0.9965	1.0000				
38	0.9980	0.9965	1.0000			
59	0.9971	0.9990	0.9964	1.0000		
92	0.9972	0.9983	0.9981	0.9973	1.0000	
101	0.9982	0.9938	0.9955	0.9943	0.9941	1.0000

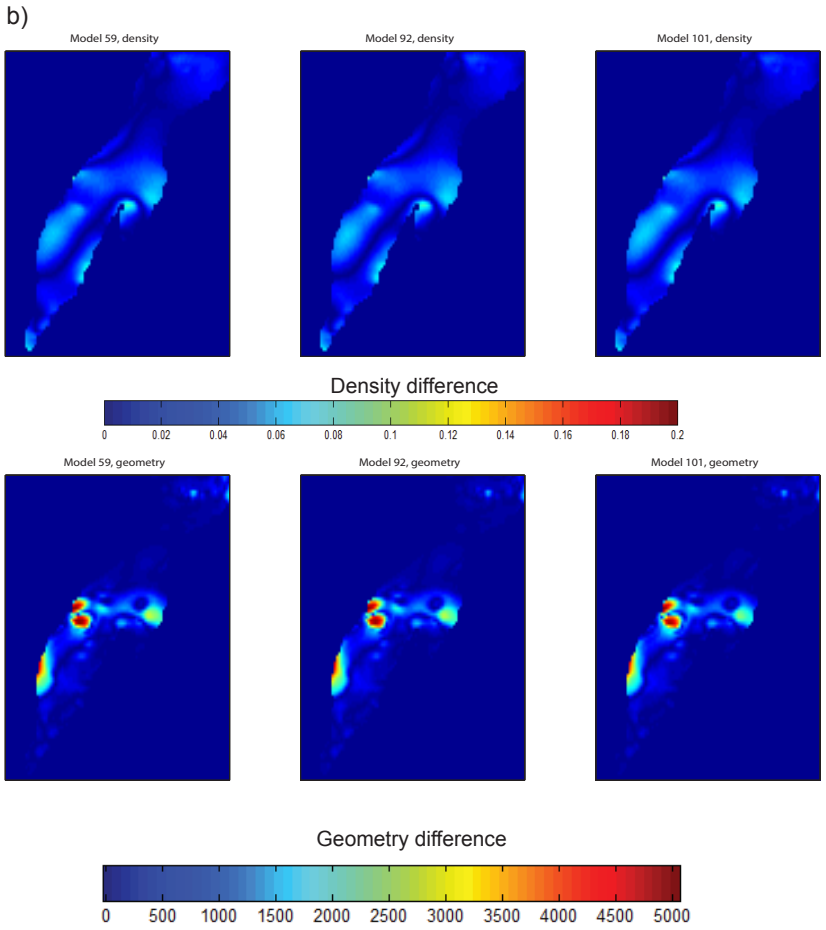

the coefficients are not high enough to suggest that modification schemes can confidently predict of regions of geological uncertainty.

4. Geological significance

Given the differences between inverted models have been determined to be low, we are confident that the inversion algorithm responded to geological structures existing in both the geological model and geophysical datasets. Cross-validation with the depth bounds discovered through end-member analysis (Table 2 – maximum depth of ***tkc*** = 8050 m) was performed and no part of the ***tkc*** surface exceeded this depth, removing the need to geologically justify the presence of anomalously deep sections of the Tarkwaian Series. The geometry of the ***tkc*** surface overall has been modified to be shallower. The greatest geometrical change, as identified in the variability maps, is located in the central western area close to the Ashanti Fault. A region of thick Tarkwaian Series sediments was not retained (Figure 17 - feature '1'), though a region of thicker sediments 23 km northeast along the strike of the Ashanti Fault near Bogoso has been thickened (Figure

17 – feature '2'). At this location three faults interact with the base of the Tarkwaian: the Ashanti Fault, striking northeast – southwest; an unnamed fault interpreted by Perrouty et al. (2012), striking west-southwest – east-northeast; and the fault-defined Tarkwaian/Early Birimian contact. The protrusion of the ***tkc*** surface through the fault-defined contact of the Tarkwaian/Early Birmian is not a reasonable geological proposition. The result was likely produced as the inversion algorithm is unaware of these faults and their topology,. Another possible solution can be offered geophysically. The inversion has modified the ***tkc*** surface to account for a low magntitude gravity anomaly in this location. A number of geological reasons can be made to account for this anomaly, including a thick layer of relatively unconsolidated basin infill (unlikely, given the age and metamorphic history of the region) or, (more likely) the presence of Late Eburnean granitoid near the unnamed fault which facilitated magma transport and emplacement.

The density distribution displayed in the ***tkc*** surface does not present too many obvious geological dilemmas. Possible Early Birimian structures beneath the ***tkc*** surface are reflected in the

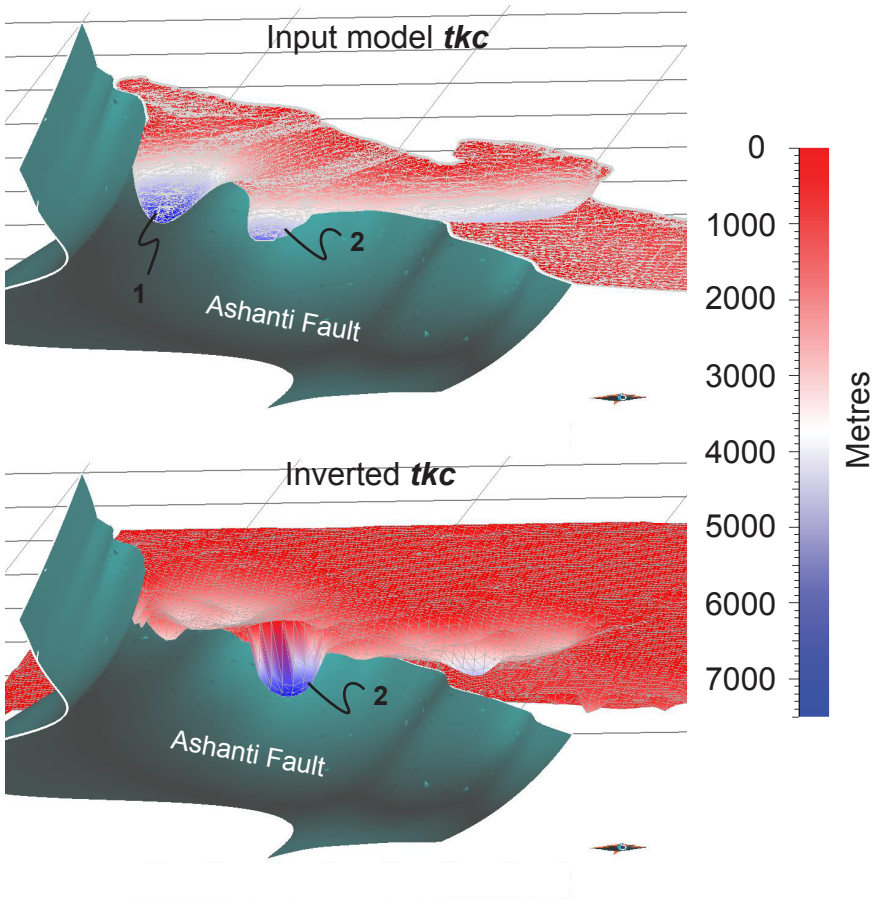

Figure 17. Inversion results showing geometrical changes near the Ashanti Fault (labelled). The input model and inversion surfaces have been painted according to their depth in metres (scale at right). Note feature 1 from the input model has not been retained during inversion modelling, while feature 2 has been thickened. The overall depth of the ***tkc*** surface has been shallowed during inversion.

density distribution and also correlate to the Early Birimian model elements (Figure 18). Folded surfaces can be interpreted in the density response. The large high-magnitude density anomaly between Wassa and Damang is spatially linked to a large-scale isoclinal fold in the model. The density anomaly may be due to either: higher volume of higher density stratigraphic units due to the presence of the fold; isoclinal folding may have produced an accumulation of higher density rocks, such as amphibolites, in the hinge zone and resulted in hinge thickening.

5. The future of geophysical inversion

In this section we assess the potential of 3D uncertainty grids to be used as guides for geophysical inversion. Geologically uncertain regions are correlated to regions that require heavy modification via geophysical inversion in order to achieve lower misfits between calculated and observed responses. The significance of this correlation is that a 3D uncertainty grid attributed with stratigraphic variability values is a novel approach that can assist inversion in two ways: (1) by focussing inversion on regions that are uncertain and (2) provide additional geological constraints to solve the inverse problem. Focussing inversion on uncertain areas will optimise the algorithm by supplying the locations that require modification, rather than relying on least-squares or stochastic methods to search for where and how modifications should be applied.

Additional inversion constraints are supplied by a 3D uncertainty grid via two sets of information that can be useful to inversion algorithms. The first set of information is the possible stratigraphic units at any given point, and the second is the proportion of each unit. Together this set of information defines a frequency histogram that describes geological probability at any given point. The inversion could perform modifications according to the frequency histogram, rather than relying on global constraints such as perturbation per iteration or petrophysical ranges (Figure 19). An uncertainty grid is a geological constraint that also acknowledges that there are multiple geological solutions as there are multiple geophysical solutions. The integration of an uncertainty grid into inversion would increase the likelihood of finding a solution that honours both geological and geophysical data.

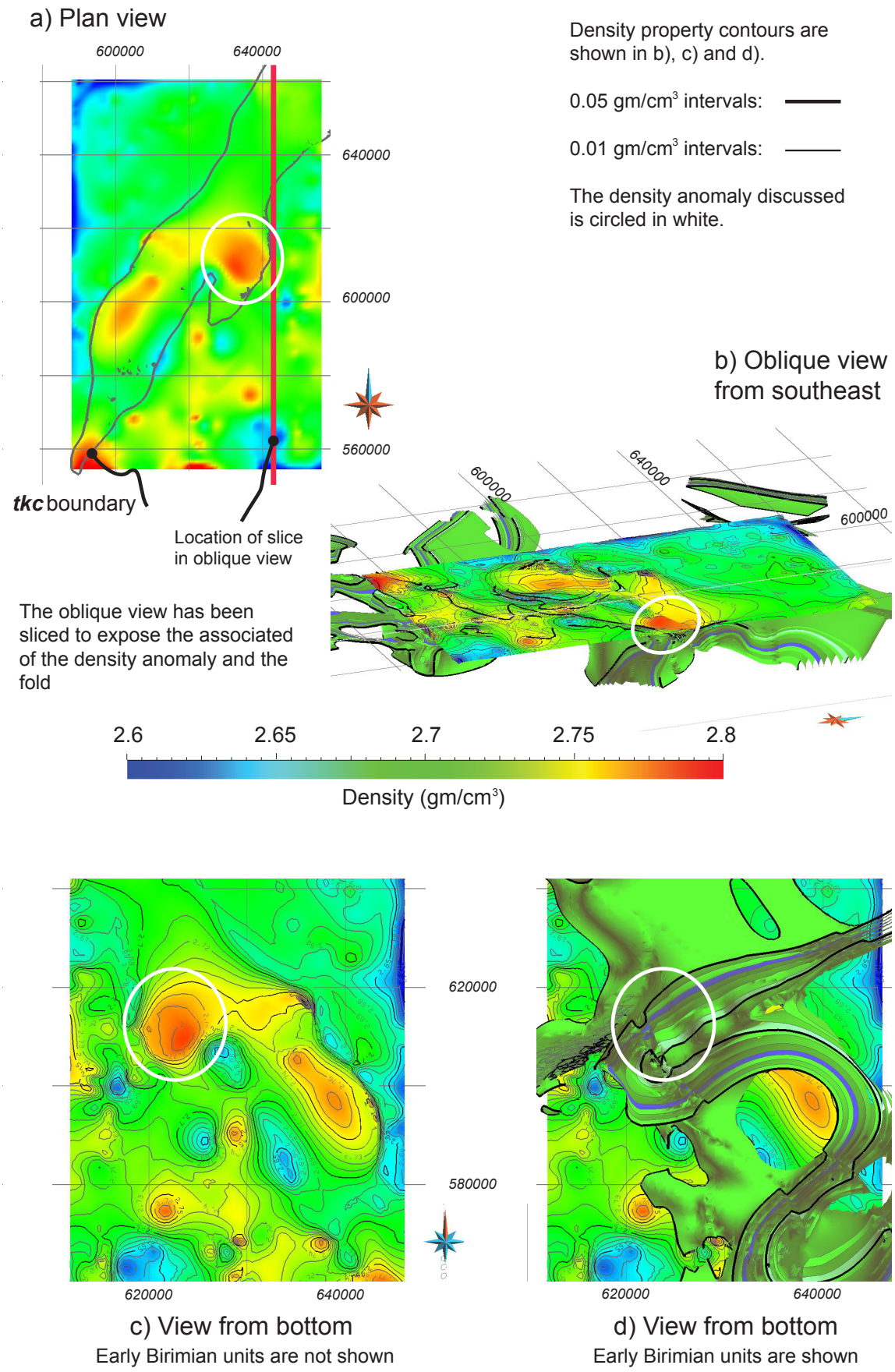

Figure 18. Model 92 inverted model density distribution. A large density anomaly is circled in white in all views. b) The model surfaces have been 'sliced' from the east to expose the centre east of the model. The location of the slice is shown in (a) with a red line.

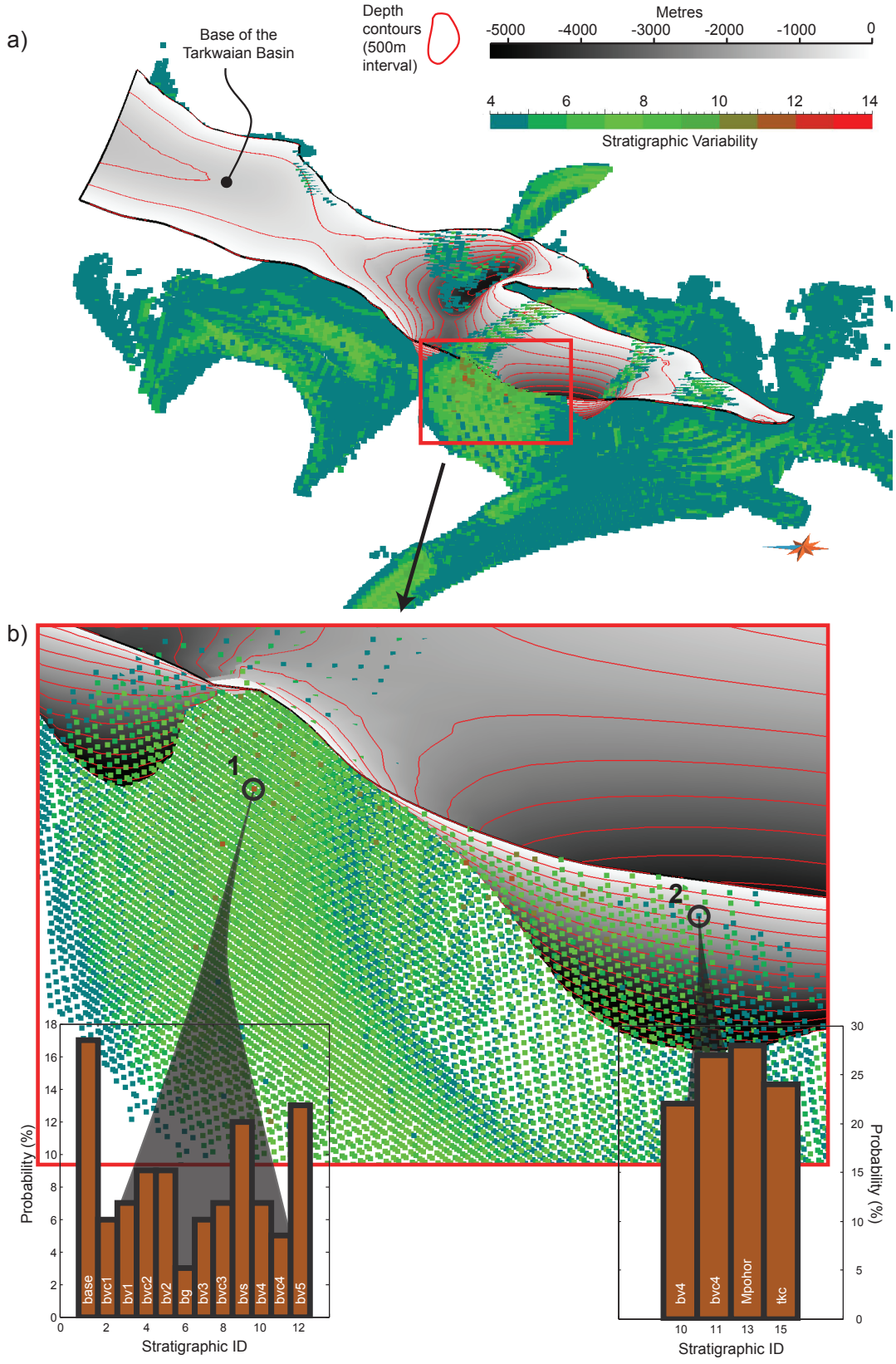

Figure 19. Example of how a 3D stratigraphic grid guides inversion. a) View from the west of a surface representing the base of the Tarkwaian Basin (*tkc*) overlain by the points representing stratigraphic variability. Note the depth and stratigraphic variability scales at the top-right. The red box indicates the location of b). Two locations shown in b) are highly uncertain (1) and less uncertain (2). The histograms display the stratigraphic identifier value of each different unit detected at these locations on the x-axis) (the corresponding unit name is labelled) and the probability of their occurrence on the y-axis. The combination of knowing which units are possible and their likelihood provides a powerful geological constraint for geophysical inversion.

6. Conclusions

The workflow described in this manuscript reduces subjectivity in the geophysical inversion process by (1) producing multiple geological realisations from input data and (2) guiding the choice of geophysical input data through geodiversity analysis. A model now has more use than just a reference point for the distribution of petrophysical properties. The operator is now informed of the geological and geophysical possibilities contained within the model, and geodiversity endmember analysis and PCA help to guide inversion and assist in results assessment. Complex interactions within the Ashanti Greenstone Belt model suite that were determined with the aid geodiversity analysis and PCA are the relationship between the gravitational response and the CSA of Early Biriman Series. This relationship supported the choice of gravity data for inversion. PCA of geodiversity metrics also provided the identification of models 92, 33, 59, 3, 38 and 101 that were input to inversion.

Visualisation of stratigraphic variability highlighted sources of uncertainty, such as our modelling whole collection of granite bodies as one geological unit, rather than as individual bodies. Perhaps most importantly, the 3D stratigraphic variability grid has been recognised as a new inversion constraint that can insert more geological information into a dominantly geophysical process. Although subjective decisions are still required by the operator, the objective techniques used in this workflow remove some subjectivity while simultaneously increasing the role of geological input. The results provided a geologically reasonable model of the Ashanti Greenstone Belt, southwestern Ghana.

Acknowledgements

Thanks go to Intrepid Geophysics for technical assistance and access to the 3D Geomodeller API (Application Programming Interface). Special thanks to Philip Chan of the Monash eResearch Centre for providing technical assistance with Monash Sun Grid computing.

Discussion

1. Uncertainty in three-dimensional geological modelling

The exponential increase in computing power has encouraged development of 3D modelling technologies and provided many applications that analyse a diverse range of geoscientific interests. Minerals exploration companies are now looking deeper into the Earth to find new prospects and resources, requiring 3D geological models for resource estimation and planning exploration activities (Dill, 2010; Malehmir et al., 2012). Large-scale 4D tectonic models can be tested within geodynamic simulation platforms such as 'Underworld' (Moresi et al., 2007) and '4DPlates' (Clark et al., 2012). The requirement for analysis of geological ambiguity and subsequent uncertainty increases correspondingly with increasing reliance on 3D modelling. Uncertainty has been found to have a wide range of effects, not just in local variations regarding the location of a fault or stratigraphic contact, but also in widespread geometrical variability throughout a model suite.

Stratigraphic variability and geodiversity have shown that the effect of orientation measurement uncertainty has a profound and complex effect on every model element. Lindsay et al. (2012) show that while uncertainty can be decreased with the inclusion of additional data, additional data is not a panacea for model uncertainty. Uncertainty will always exist in some form, therefore it is crucial to understanding the subsequent effects on the model. Geology is necessarily an interpretive science (Frodeman, 1995; Bárdossy and Fodor, 2001) where there is no right answer (Bond et al., 2010) and therefore uncertainty will always exist. One could argue that with complete knowledge of a geological system, where 100 percent data saturation is achieved, uncertainty would disappear. This argument is flawed however, as data are nonetheless uncertain due to measurement and sampling error. The most efficient way forward is to acknowledge that uncertainty exists and redirect efforts away from uncertainty removal towards understanding the implications of its subsidiary effects. Lindsay et al. (2012a), Lindsay et al. (2012c) and Lindsay et al. (2012d) reveal that the effects of uncertainty can be identified using geodiversity analysis, but differ between model suites. There is no single metric that will always be the most influential in terms of uncertainty and therefore no subsequent formula that applies to any given model. Geodiversity analysis is required for each model suite to appreciate the extents of geological possibility.

The current state of research shows increasing importance is being placed on the identification and quantification of uncertainty (Cherpeau et al., 2010; Jessell et al., 2010; Viard et al., 2010; Wellmann et al., 2010; Wellmann and Regenauer-Lieb, 2011; Goodfellow et al., 2012; Joly et al., 2012; Lallier et al., 2012; Lindsay et al., 2012a; MacCormack and Eyles, 2012; Woodward, 2012). Uncertainty results from many decisions made during modelling workflows, including the selection of modelling application and parameters (MacCormack and Eyles, 2012), sedimentary correlations (Lallier et al., 2012), input data (Putz et al., 2006; Jessell et al., 2010; Lindsay et al., 2012a) and tectonic evolution model (Cherpeau et al., 2010). History matching processes conducted after construction of the 3D model are also subject to uncertainties (Seiler et al., 2010; Cherpeau et al., 2012; Tavakoli et al. 2013). Quantification of uncertainty provides data that reflects the degree of confidence one can have when predictions from a particular dataset. Further, as uncertainty is unavoidable and pervasive in 3D models, the current form of 3D models can be viewed as redundant.

Current models display each element as a solid object, a necessary practice that ensures appropriate visualisation. Unfortunately, this practice can lead the observer to believe that the model element is truth (Tarantola, 2006). It is also possible that the observer will see the element as a prediction, as it should be observed, however as MacEachren et al. (1998), Thomson et al. (2005) and Viard et al. (2010) show, visualisation techniques are required to guarantee that model elements are viewed by everyone with the appropriate amount of scepticism. The techniques presented by these authors all suggest that either input data or the modelled results should be displayed on an uncertainty spectrum. Visually, the spectrum may be linked to transparency of the object, where less certainty is reflected in more transparency, or masking uncertain regions with an increasingly opaque pattern. Lindsay et al. (2012a) shows that stratigraphic variability reflects different levels of uncertainty in model elements with a probability measure.

The use of probabilistic elements is an effective means to store, visualise and represent geological models. In an ideal world, each element, be they volume, surface or point should be attributed with a probability value. The probability would then describe not just the probability of the most likely lithology, but all possible lithologies. Probability data exists in the uncertainty grid that is created from determination of stratigraphic variability, but could be integrated into model elements as a property, rather than existing as separate dataset. The geological study area would be

better represented by probabilistic models that describe what is known, rather than represented by a single version of what is thought to be known.

2. Falsification approach to modelling

The techniques presented in this thesis support Boschetti and Moresi (2001) and Tarantola (2006) by employing a falsification approach to geological and geophysical modelling. Rather than producing a single 'best' model, a selection of models that can be falsified is produced. The presentation of multiple realisations of the same input data set allows each model to be ranked and evaluated with the support of data obtained through stratigraphic variability and geodiversity metric analysis. Many solutions to the geological problem are therefore presented, and geodiversity can describe many of the geometrical and geophysical possibilities that are difficult to efficiently determine visually.The process of falsifying these models naturally requires the expertise of the operator, which introduces subjectivity to the decision. However, this subjectivity is mitigated by the presence of other models and geodiversity analysis with which the operator can use quantitative means to compare and contrast to make informed selections of models that reliably represent geology (Boschetti and Moresi, 2001).

A large component of this thesis has been dedicated to critiquing current approaches to 3D geological modelling. One of the arguments presented against the optimisation of input data by producing a single 'best' model is that the observer may place too much faith in the model architecture (Tarantola, 2006). Subsequently others within the geoscientific community observe 3D models as untrustworthy. Distrust of 3D models can be due to an inherent empirical bias and a belief that models can never represent all natural phenomena and are therefore inadequate. Unfortunately this somewhat fundamentalist attitude is difficult to combat as the argument is sound, but misplaced. Models are an abstraction and not a simulation. A select group of geological phenomena, appropriate to answer the prescribed question should be modelled. Attempts to model all geological phenomena (i.e. a simulation) will always end in failure as one component or another will appear to be false, and subsequent mistrust of everything else within the model will follow. Simulations of geology are a practical impossibility as the entire system will never be completely determined as they are in engineering or some physical applications (Caumon, 2010). Modelling

geology is the only practical method to make predictions about the earth and is enhanced through appropriate selection of boundary conditions, input and offering realistic solutions.

3. 3D geological modelling: workflows and accessibility to the scientific community

Producing a 3D model is a time consuming and sometimes frustrating task. Much time is spent in the data preparation stage, finding and filtering data appropriate for the study. There are time constraints that must be adhered to, and budgets and data propriety issues to accommodate. A broad knowledge base is required to be able to select geological data, process it in the appropriate software, produce a model and then perform assessment to ensure its geological feasibility. It is understandable that the successful construction of a model is received with excitement (and the thought of producing further versions is untenable). The automation of techniques presented in this thesis allows the production of an entire model suite with a disproportionately small increase in time than required by producing a single model. Perhaps the approaches described in this thesis can also reach a middle-ground on the 'scepticism spectrum' between those that trust models too much and those that do not trust at all. By producing multiple realisations of the same data set, those that trust too much can be presented with other possible models for examination before making further decisions. The model sceptics are also accommodated with the production of multiple models, an implicit acknowledgment that some models contain large error. However, this approach allows us to examine the possibilities using measures of geological uncertainty and geodiversity to guide us toward finding models with less error.

4. Model space

The techniques presented in this thesis provide insight into the nature and effects of uncertainty, however only a small (though important) section of model space has been examined. Varying orientation measurements by ± five degrees during uncertainty simulation was kept constant through all experiments, as was the size of the model suite (101), to avoid adding a confound-

ing variable when developing stratigraphic variability and geodiversity techniques. Increasing the perturbation value from ± five degrees, in combination with an increase in the number of model suite members from 101, would provide a more thorough examination of model space. Other methods of uncertainty simulation also need to be examined. Model topology can be changed, affecting fault-fault, stratigraphy-fault and stratigraphic relationships to allow the examination of alternate tectonic evolution models. The resulting collection of tectonic models and associated model suites can be compared using the workflow described in Lindsay et al. (2012d) to reveal a vast number of geological possibilities within multidimensional model space.

Conclusion

Uncertainty in 3D geological models has been characterised to gain better understanding of geological possibility. There are many sources of 3D model uncertainty, including sparse and under-sampled data, data sampling and processing techniques, interpolation algorithms and differing geological interpretations. Stratigraphic variability has allowed the detection and quantification of uncertainty within the Gippsland Basin and Ashanti Greenstone Belt models. Stratigraphic variability determines which geological units exist at any given location within a model and the probability of finding those units. Stratigraphic variability guided the addition of data in key locations to increase model reliability in the Gippsland Basin model. Geodiversity analysis provided geometrical and geophysical characterisation of 3D models to explore the effects of modelling uncertainty and the range of geological possibility. End-member analysis identified the extremes of geometrical and geophysical possibility, while principal component analysis (PCA) determined model space boundaries and which metrics contribute most to model uncertainty. Covariance between geometrical and geophysical metrics was identified although the relationships differed between model suites. In the case of the Chapter 3 version of the Ashanti Greenstone belt model, geological complexity was covariant with the gravitational response, while in Chapter 4 the gravity was covariant with the contact surface area. Significantly, geodiversity analysis also found that producing a single model from an input data set very likely misrepresents nature and supports the practice of constructing multiple geological models.

Geophysical inversion was performed on the Ashanti Greenstone Belt model to determine the geometry and location of the base of the Tarkwaian Basin. Inversion was prepared and executed using a workflow that integrated stratigraphic variability and geodiversity. Multiple starting points were provided with a set of models that were selected for inversion through PCA to more thoroughly explore model space. Model selection was based on which models exhibited the most common or diverse model characteristics. Inversion of gravity data produced a geologically reasonable model from a process that introduced additional geological constraints while reducing some subjectivity. Further, it was demonstrated that the stratigraphic variability grid could be used as a powerful geological constraint for inversion.

Different geological terranes can be examined, as shown in the analyses of the Gippsland Basin, southeastern Victoria and Ashanti Greenstone Belt, southwestern Ghana. The broad range of geodiversity metrics allows applied studies to reveal relevant characteristics of the model suite.

These aspects include, but are not restricted to, volume and depth calculations for an oil and gas prospective terrane (Gippsland Basin), or contact surface area and geological complexity for structurally-controlled gold deposits (Ashanti Greenstone Belt). The current stable of geodiversity metrics is not exhaustive, and new geodiversity metrics can be added to analyse model characteristics that were not addressed in this thesis. Nonetheless, while improvements can always be made, the techniques described in this thesis demonstrate that uncertainty and geodiversity analyses can be performed and used to guide geophysical inversion. These techniques uncover and highlight interesting and problematic features of a model suite, and should be employed when providing detailed assessment of 3D geological model space.

References Cited

Adadey, K., Clarke, B., Théveniaut, H., Urien, P., Delor, C., Roig, J. Y., and Feybesse, J.-L., 2009, Geological map explanation - Map sheet 0503 B (1:100 000), CGS/BRGM/Geoman, Geological Survey Department of Ghana (GSD). No MSSP/2005/GSD/5a.

Agresti, A., 2007, An introduction to catergorical data analysis, Hoboken, New Jersey, John Wiley & Sons, Inc.

Airo, M. L., 2002, Aeromagnetic And Aeroradiometric Response To Hydrothermal Alteration: Surveys in Geophysics, v. 23, no. 4, p. 273-302.

Aitken, A. R. A., 2010, Moho geometry gravity inversion experiment (MoGGIE): A refined model of the Australian Moho, and its tectonic and isostatic implications: Earth and Planetary Science Letters, v. 297, no. 1-2, p. 71-83.

Aitken, A. R. A., and Betts, P. G., 2008, High-resolution aeromagnetic data over central Australia assist Grenville-era (1300 Ma-1100 Ma) Rodinia reconstructions: Geophys. Res. Lett., v. 35.

-, 2009, Multi-scale integrated structural and aeromagnetic analysis to guide tectonic models: An example from the eastern Musgrave Province, Central Australia: Tectonophysics, v. 476, no. 3-4, p. 418-435.

Aitken, A. R. A., Betts, P. G., Schaefer, B. F., and Rye, S. E., 2008, Assessing uncertainty in the integration of aeromagnetic data and structural observations in the Deering Hills region of the Musgrave Province: Australian Journal of Earth Sciences, v. 55, no. 8, p. 1127 - 1138.

Aitken, A. R. A., Salmon, M. L., and Kennett, B. L. N., 2012, Australia's Moho: A test of the usefulness of gravity modelling for the determination of Moho depth: Tectonophysics, In Press, Accepted Manuscript: : doi 10.1016/j.tecto.2012.06.049.

Allibone, A. H., McCuaig, T. C., Harris, D., Etheridge, M. A., Munroe, S., Bryne, D., Amanor, J., and Gyapong, W., 2002, Structural controls on gold mineralization at the Ashanti gold deposit, Obuasi, Ghana, in Goldfarb, R. J., and Neilson, R. L., eds., Integrated Methods for Discovery: Global Exploration in the 21st Century, Society of Economic Geologists, p. 65-93.

Aug, C., 2004, Modélisation géologique 3D et caractérisation des incertitudes par la méthode du champ de potentiel [PhD]: École des Mines de Paris, 198 p.

Bárdossy, G., and Fodor, J., 2001, Traditional and new ways to handle uncertainty in geology: Natural Resources Research, v. 10, no. 3, p. 179-187.

Barritt, S. D., and Kuma, J. S., 1998, Constrained gravity models and structural evolution of the Ashanti Belt, southwest Ghana: Journal of African Earth Sciences, v. 26, no. 4, p. 539-550.

Bernecker, T., and Partridge, A. D., 2001, Emperor and Golden Beach Subgroups: the onset of Late Cretaceous sedimentation in the Gippsland Basin, in Hill, K. C., and Bernecker, T., eds., Eastern Australian Basins Symposium, a Refocused Energy Perspective for the Future, Petroleum Exploration Society of Australia, Special Publication, p. 391–402.

Bernecker, T., Woollands, M., Wong, D., Moore, D., and Smith, M., 2001, Hydrocarbon prospectivity of the deep water Gippsland Basin, Victoria, Australia: APPEA Journal, v. 41, p. 91-113.

Betts, P., Williams, H., Stewart, J., and Ailleres, L., 2007, Kinematic analysis of aeromagnetic data: Looking at geophysical data in a structural context: Gondwana Research, v. 11, no. 4, p. 582-583.

Betts, P. G., Valenta, R. K., and Finlay, J., 2003, Evolution of the Mount Woods Inlier, northern Gawler Craton, Southern Australia: an integrated structural and aeromagnetic analysis: Tectonophysics, v. 366, no. 1-2, p. 83-111.

Blenkinsop, T., Schmidt, M., Kumi, R., and Sangmoor, S., 1994, Structural geology of the Ashanti Goldmine, in Oberthür, T., ed., Geologisches Jahrbuch D100: Hannover, p. 131-153.

Bond, C. E., Lunn, R. J., Shipton, Z. K., and Lunn, A. D., 2012, What makes an expert effective at interpreting seismic images?: Geology, v. 40, no. 1, p. 75-78.

Bond, C. E., Philo, C., and Shipton, Z. K., 2010, When There isn't a Right Answer: Interpretation and reasoning, key skills for twenty-first century geoscience: International Journal of Science Education, v. 33, no. 5, p. 629-652.

Bond, C. E., Shipton, Z. K., Jones, R. R., Butler, R. W. H., and Gibbs, A. D., 2007, Knowledge transfer in a digital world: Field data acquisition, uncertainty, visualization, and data management: Geosphere, v. 3, no. 6, p. 568-576.

Bonham-Carter, G. F., 1994, Geographic information systems for Geoscientists: Modelling with GIS, Oxford, Pergamon Press.

Bosch, M., Guillen, A., and Ledru, P., 2001, Lithologic tomography: an application to geophysical data from the Cadomian belt of northern Brittany, France: Tectonophysics, v. 331, no. 1-2, p. 197-227.

Boschetti, F., and Moresi, L., 2001, Interactive inversion in geosciences: Geophysics, v. 66, no. 4, p. 1226-1234.

Bowden, R. A., 2007, Sources of uncertainty in the estimation and reporting of results from down hole gamma-ray and prompt fission neutron logging for uranium: Australasian Institute of Mining and Metallurgy Publication Series.

Braude, H., 2009, Clinical intuition versus statistics: different modes of tacit knowledge in clinical epidemiology and evidence-based medicine: Theoretical Medicine and Bioethics, v. 30, no. 3, p. 181-198.

Bremner, D., Demaine, E., Erickson, J., Iacono, J., Langerman, S., Morin, P., and Toussaint, G., 2005, Output-Sensitive Algorithms for Computing Nearest-Neighbour Decision Boundaries: Discrete & Computational Geometry, v. 33, no. 4, p. 593-604.

Brown, W. M., Gedeon, T. D., Groves, D. I., and Barnes, R. G., 2000, Artificial neural networks: a new method for mineral prospectivity mapping: Australian Journal of Earth Sciences, v. 47, no. 4, p. 757 - 770.

Calcagno, P., Chilès, J. P., Courrioux, G., and Guillen, A., 2008, Geological modelling from field data and geological knowledge: Part I. Modelling method coupling 3D potential-field interpolation and geological rules: Physics of the Earth and Planetary Interiors, v. 171, no. 1-4, p. 147-157.

Cameron, M. K., 2007, Seismic velocity estimation from time migration: Inverse Problems, v. 23, no. 4, p. 1329-1369.

Caratori Tontini, F., Cocchi, L., and Carmisciano, C., 2009, Rapid 3-D forward model of potential fields with application to the Palinuro Seamount magnetic anomaly (southern Tyrrhenian Sea, Italy): Journal of geophysical research, v. 114, no. B02103.

Caumon, G., 2010, Towards Stochastic Time-Varying Geological Modeling." Mathematical Geosciences 42, no. 5, p. 555-69.

Caumon, G., Collon-Drouaillet, P., Le Carlier de Veslud, C., Viseur, S., and Sausse, J., 2009, Surface-based 3D modeling of geological structures: Mathematical Geosciences, v. 41, p. 927-945.

Caumon, G., Tertois, A.-L., and Zhang, L., Elements for stochastic structural perturbation of stratigraphic models., in Proceedings Petroleum Geostatistics, Cascais, Portugal, 2007, EAGE.

Chen, X., and Schmitt, F., 1992, Intrinsic surface properties from surface triangulation, in Sandini, G., ed., Computer Vision — ECCV'92, Volume 588, Springer Berlin Heidelberg, p. 739-743.

Cherpeau, N., Caumon, G., and Lévy, B., 2010, Stochastic simulations of fault networks in 3D structural modeling (Simulations stochastiques de réseaux de failles en modélisation structurale 3D): Comptes Rendus - Geoscience, v. 342, no. 9, p. 687-694.

Cherpeau, N., Caumon, G., Caers, J., and Lévy, B., 2012, Method for Stochastic Inverse Modeling of Fault Geometry and Connectivity Using Flow Data: Mathematical Geosciences, v. 44, no. 2, p. 147-168.

Chilès, J. P., Aug, C., Guillen, A., and Lees, T., 2004, Modelling the geometry of geological units and its uncertainty in 3D from structural data: the potential-field method, in Proceedings Orebody Modelling and Strategic Mine Planning, Perth, WA, 22 - 24 November 2004, Australian Institute of Mining and Metallurgy Publication Series.

Chiles, J. P., and Delfiner, P., 1999, Geostatistics: modeling spatial uncertainty, New York, New York, Wiley.

Chugunov, N., Shepelyov, G., and Sternin, M., 2008, Probabilistic Methods for Uncertainty Quantification, Encyclopedia of Decision Making and Decision Support Technologies, IGI Global, p. 732-742.

Clark, D. A., 1983, Comments on magnetic petrophysics: Bulletin of the Australian Society of Exploration Geophysics, v. 14, p. 49–62.

-, 1997, Magnetic petrophysics and magnetic petrology: aids to geological interpretation of magnetic surveys: ASGO Journal of Australian Geology and Geophysics, v. 17, no. 2, p. 83–103.

Clark, S. R., Skogseid, J., Stensby, V., Smethurst, M. A., Tarrou, C., Bruaset, A. M., and Thurmond, A. K., 2012, 4DPlates: On the fly visualization of multilayer geoscientific datasets in a plate tectonic environment: Computers & Geosciences, v. 45, p. 46-51.

Cook, P. J., 2006, Carbon dioxide capture and geological storage: research, development and application in Australia: International Journal of Environmental Studies, v. 63, no. 6, p. 731 - 749.

Cooley, M., 2007, From judgment to calculation: AI & Society, v. 21, no. 4, p. 395-409.

Cox Jr, L. A., 1982, Artifactual uncertainty in risk analysis: Risk Analysis, v. 2, no. 3, p. 121-135.

Davis, J. C., 2002, Statistics and Data Analysis in Geology, New York, Wiley.

Davis, K., Oldenburg, D. W., and Hillier, M., 2012, Incorporating geologic structure into the inversion of magnetic data: ASEG Extended Abstracts, v. 2012, no. 1, p. 1-4.

de Kemp, E. A., 1999, Visualization of complex geological structures using 3-D Bézier construction tools: Computers & Geosciences, v. 25, no. 5, p. 581-597.

de Kemp, E. A., 2000, Three-dimensional integration and visualization of structural field data :tools for regional subsurface mapping = Integration et visualisation 3-D de données structurales de terrain : outils pour la cartographie géologique régionaleThèse de doctorat (Université du Québec à Chicoutimi) ;]: Chicoutimi : Université du Québec à Chicoutimi, 2000.

Dill, H. G., 2010, The «chessboard» classification scheme of mineral deposits: Mineralogy and geology from aluminum to zirconium: Earth-Science Reviews, v. 100, no. 1-4, p. 1-420.

Dong, C. S., and Wang, G. Z., 2005, Curvatures estimation on triangular mesh: Journal of Zhejiang University: Science, v. 6 A, no. SUPPL., p. 128-136.

Dumont, T., Champagnac, J.-D., Crouzet, C., and Rochat, P., 2008, Multistage shortening in the Dauphiné zone (French Alps): the record of Alpine collision and implications for pre-Alpine restoration: Swiss Journal of Geosciences, v. 101, no. 1, p. S89-S110.

Edmiston, M. A., Lepong, P., and Blenkinsop, T. G., 2008, Structure of the Isan Orogeny under cover to the east of the Mount Isa Inlier revealed by multiscale edge analysis and forward and inverse modelling of aeromagnetic data: Precambrian Research, v. 163, no. 1-2, p. 69-80.

Eisenlohr, B. N., and Hirdes, W., 1992, The structural development of the early Proterozoic Birimian and Tarkwaian rocks of southwest Ghana, West Africa: Journal of African Earth Sciences, v. 14, no. 3, p. 313-325.

Feltrin, L., McLellan, J. G., and Oliver, N. H. S., 2009, Modelling the giant, Zn-Pb-Ag Century deposit, Queensland, Australia: Computers & Geosciences, v. 35, no. 1, p. 108-133.

Feybesse, J.-L., Billa, M., Guerrot, C., Duguey, E., Lescuyer, J.-L., Milesi, J.-P., and Bouchot, V., 2006, The paleoproterozoic Ghanaian province: Geodynamic model and ore controls, including regional stress modeling: Precambrian Research, v. 149, no. 3-4, p. 149-196.

Foudil-Bey, N., 2012, Développement d'outils d'interprétation de données géophysiques [PhD] Université du Québec en Abitibi-Témiscamingue et Université de Lorraine.

Frank, T., Tertois, A.-L., and Mallet, J.-L., 2007, 3D-reconstruction of complex geological interfaces from irregularly distributed and noisy point data: Computers & Geosciences, v. 33, no. 7, p. 932-943.

Friedman, J. H., Bentley, J., and Finkel, R. A., 1977, An algorithm for finding best matches in logarithmic expected time: ACM Transactions on Mathematical Software, v. 3, no. 209.

Frodeman, R., 1995, Geological reasoning: Geology as an interpretive and historical science: Geological Society of America Bulletin, v. 107, no. 8, p. 960-968.

Fullagar, P. K., 2009, VPmg user documentation, version 5.2: Fullagar Geophysics.

Fullagar, P. K., Hughes, N. A., and Paine, J., 2000, Drilling-constrained 3D gravity interpretation: Exploration Geophysics, v. 31, p. 017-023.

Fullagar, P. K., Pears, G., Hutton, D., and Thompson, A., 2004, 3D gravity and aeromagnetic inversion for MVT lead-zinc exploration at Pillara, Western Australia: Exploration Geophysics, v. 35, no. 2, p. 142-146.

Fullagar, P. K., Pears, G. A., and McMonnies, B., 2008, Constrained inversion of geologic surfaces - pushing the boundaries: The Leading Edge, v. 27, no. 1, p. 98-105.

Gallagher, S. J., Smith, A. J., Jonasson, K., Wallace, M. W., Holdgate, G. R., Daniels, J., and Taylor, D., 2001, The Miocene palaeoenvironmental and palaeoceanographic evolution of the Gippsland Basin, Southeast Australia: a record of Southern Ocean change: Palaeogeography, Palaeoclimatology, Palaeoecology, v. 172, no. 1-2, p. 53-80.

Gallardo, L. A., and Meju, M. A., 2011, Structure-coupled multiphysics imaging in geophysical sciences: Reviews of Geophysics, v. 49, no. 1.

Gallerini, G., and De Donatis, M., 2009, 3D modeling using geognostic data: The case of the low valley of Foglia river (Italy): Computers & Geosciences, v. 35, no. 1, p. 146-164.

Gao, Y., and Leung, M. K. H., 2002, Face recognition using line edge map: Pattern Analysis and Machine Intelligence, IEEE Transactions on, v. 24, no. 6, p. 764-779.

Geomodeller User Manual, a., 2012, Forward modelling and inversion with 3D Geomodeller.

Gershon, N., 1998, Visualization of an imperfect world: Computer Graphics and Applications, IEEE, v. 18, no. 4, p. 43-45.

Gonzalez, R. C., Woods, R. E., and Eddins, S. L., 2003, Digital image processing using MATLAB, Volume 11: New Jersey, Prentice Hall.

Goodfellow, R., Albor Consuegra, F., Dimitrakopoulos, R., and Lloyd, T., 2012, Quantifying multi-element and volumetric uncertainty, Coleman McCreedy deposit, Ontario, Canada: Computers & Geosciences, v. 42, p. 71-78.

Goovaerts, P., 1998, Ordinary cokriging revisited: Mathematical Geology, v. 30, no. 1, p. 21-42.

Grant, F. S., 1985, Aeromagnetics, geology and ore environments, I. Magnetite in igneous, sedimentary and metamorphic rocks: An overview: Geoexploration, v. 23, no. 3, p. 303-333.

Gray, A., Abbena, E., and Salamon, S., 2006, Modern differential geometry of curves and surfaces with Mathematica, Chapman & Hall/CRC.

Gray, D. R., and Foster, D. A., 1998, Character and kinematics of faults within the turbidite-dominated Lachlan Orogen: implications for tectonic evolution of eastern Australia: Journal of Structural Geology, v. 20, no. 12, p. 1691-1720.

Groshong, R. H., 2006, Elements of map-scale structure, 3-D structural geology: A practical guide to quantitative surface and subsurface map interpretation: New York, Springer, p. 1-32.

Guillen, A., Calcagno, P., Courrioux, G., Joly, A., and Ledru, P., 2008, Geological modelling from field data and geological knowledge: Part II. Modelling validation using gravity and magnetic data inversion: Physics of the Earth and Planetary Interiors, v. 171, no. 1-4, p. 158-169.

Gunn, P. J., 1997, Quantitative methods for interpreting aeromagnetic data: a subjective review: AGSO Journal of Australian Geology and Geophysics, v. 17, p. 105-114.

Gunn, P. J., Maidment, D., and Milligan, P. R., 1997, Interpreting aeromagnetic data in areas of limited outcrop: AGSO Journal of Australian Geology and Geophysics, v. 17, no. 2, p. 175-185.

Haq, B. U., Hardenbol, J., and Vail, P. R., 1987, Chronology of Fluctuating Sea Levels Since the Triassic: Science, v. 235, no. 4793, p. 1156-1167.

Hastings, D. A., 1982, On the tectonics and metallogenesis of West Africa: A model incorporating new geophysical data: Geoexploration, v. 20, no. 3-4, p. 295-313,317-327.

Heidegger, M., 1962, Being and time, translated by J. Macquarrie and E. Robinson, New York, Harper & Row.

-, 1963, Sein und zeit:, Tübingen, Germany, Neomarius Verlag.

Hirdes, W., and Nunoo, B., 1994, The Proterozoic Paleoplacers at Tarkwa Gold Mine, SW Ghana: Sedimentology, Mineralogy, and Precise Age Dating of the Main Reef and West Reef, and Bearing of the Investigations on Source Area Aspects: Geologisches Jahrbuch, v. D100, p. 247-311.

Holdgate, G. R., Gallagher, S. J., and Wallace, M. W., 2002, Tertiary coal geology and stratigraphy of the Port Phillip Basin, Victoria: Australian Journal of Earth Sciences, v. 49, no. 3, p. 437-453.

Holstein, H., 2003, Gravimagnetic anomaly formulas for polyhedra of spatially linear media: Geophysics, v. 68, no. 1, p. 157-167.

Holstein, H., Schürholz, P., Starr, A., and Chakraborty, M., 1999, Comparison of gravimetric formulas for uniform polyhedra: Geophysics, v. 64, no. 5, p. 1438-1446.

Hotelling, H., 1931, The generalization of Student's Ratio: The Annals of Mathematical Statistics, v. 2, no. 3, p. 360-378.

Howard, A. S., Hatton, B., Reitsma, F., and Lawrie, K. I. G., 2009, Developing a geoscience knowledge framework for a national geological survey organisation: Computers & Geosciences, v. 35, no. 4, p. 820-835.

Huttenlocher, D. P., Klanderman, G. A., and Rucklidge, W. J., 1993, Comparing images using the Hausdorff distance: Pattern Analysis and Machine Intelligence, IEEE Transactions on, v. 15, no. 9, p. 850-863.

Jessell, M., 2001, Three-dimensional geological modelling of potential-field data: Computers & Geosciences, v. 27, no. 4, p. 455-465.

Jessell, M. W., Ailleres, L., and de Kemp, E. A., 2010, Towards an integrated inversion of geoscientific data: What price of geology?: Tectonophysics, v. 490, no. 3-4, p. 294-306.

Ji, C., Wald, D. J., and Helmberger, D. V., 2002, Source description of the 1999 Hector Mine, California, earthquake, part I: Wavelet domain inversion theory and resolution analysis: Bulletin of the Seismological Society of America, v. 92, no. 4, p. 1192-1207.

Jolliffe, I. T., 2002, Principal component analysis, second edition, New York, Springer.

Joly, A., Chen, Y., Faure, M., and Martelet, G., 2007, A multidisciplinary study of a syntectonic pluton close to a major lithospheric-scale fault - "Relationships between the Montmarault granitic massif and the Sillon Houiller Fault in the Variscan French Massif Central: 1. Geochronology, mineral fabrics, and tectonic implications: Journal of Geophysical Research, v. 112.

Joly, A., Martelet, G., Chen, Y., and Faure, M., 2008, A multidisciplinary study of a syntectonic pluton close to a major lithospheric-scale fault - Relationships between the Montmarault granitic massif and the Sillon Houiller Fault in the Variscan French Massif Central: 2. Gravity, aeromagnetic investigations, and 3-D geologic modeling: Journal of Geophysical Research, v. 113.

Joly, A., Porwal, A., and McCuaig, T. C., 2012, Exploration targeting for orogenic gold deposits in the Granites-Tanami Orogen: Mineral system analysis, targeting model and prospectivity analysis: Ore Geology Reviews, v. 48, p. 349-383.

Jones, R. R., McCaffrey, K. J. W., Wilson, R. W., and Holdsworth, R. E., 2004, Digital field data acquisition: towards increased quantification of uncertainty during geological mapping: Geological Society, London, Special Publications, v. 239, no. 1, p. 43-56.

Journel, A. G., 1983, Nonparametric estimation of spatial distributions: Journal of the International Association for Mathematical Geology, v. 15, no. 3, p. 445-468.

Junner, N., 1940, Geology of the Gold Coast and Western Togoland with revised geological map, v. Memoir 11, p. 40p.

Kasabov, N. K., 1996, Learning fuzzy rules and approximate reasoning in fuzzy neural networks and hybrid systems: Fuzzy Sets and Systems, v. 82, no. 2, p. 135-149.

Kaufmann, O., and Martin, T., 2008, 3D geological modelling from boreholes, cross-sections and geological maps, application over former natural gas storages in coal mines: Computers & Geosciences, no. 34, p. 278-290.

Kaufmann, O., and Martin, T., 2009, Reprint of «3D geological modelling from boreholes, cross-sections and geological maps, application over former natural gas storages in coal mines» (Comput. Geosci. 34 (2008) 278-290): Computers & Geosciences, v. 35, no. 1, p. 70-82.

Kaven, J. O., 2009, Curvature calculations on triangular 3D surfaces, Mathworks MATLAB.

Kearey, P., Brooks, M., and Hill, I., 2002, An Introduction to Geophysical Exploration, Malden, MA, USA, Blackwell Science Limited.

Kitson, S. A. E., 1928, Provisional geological map of the Gold Coast with Western Togoland with brief descriptive notes thereon, Gold Coast Geological Survey, Benham & Company Limited.

Krzanowski, W. J., 1995, Selection of variables, and assessment of their performance, in mixed-variable discriminant analysis: Computational Statistics & Data Analysis, v. 19, no. 4, p. 419-431.

Krzanowski, W. J., 1996, Principles of multivariate analysis: A user's perspective, New York, Oxford University Press.

Lajaunie, C., Courrioux, G., and Manuel, L., 1997, Foliation fields and 3D cartography in geology: Principles of a method based on potential interpolation: Mathematical Geology, v. 29, no. 4, p. 571-584.

Lallier, F., Caumon, G., Borgomano, J., Viseur, S., Fournier, F., Antoine, C., and Gentilhomme, T., 2012, Relevance of the stochastic stratigraphic well correlation approach for the study of complex carbonate settings: Application to the malampaya buildup (Offshore Palawan, Philippines), Volume 370, p. 265-275.

Lane, R., and Guillen, A., 2005, Geologically-inspired Constraints for a Potential Field Litho-inversion Scheme: Proceedings of IAMG'05: GIS and Spatial Analysis, v. 1, p. 181-186.

Lee, D. T., and Schachter, B. J., 1980, Two algorithms for constructing a Delaunay triangulation: International Journal of Parallel Programming, v. 9, no. 3, p. 219-242.

Lelièvre, P. G., Oldenburg, D. W., and Williams, N. C., 2009, Integrating geological and geophysical data through advanced constrained inversions: Exploration Geophysics, v. 40, no. 4, p. 334-341.

Li, Y., and Oldenburg, D. W., 1996, 3-D inversion of magnetic data: Geophysics, v. 61, no. 2, p. 394-408.

-, 1998, 3-D inversion of gravity data: Geophysics, v. 63, no. 1, p. 109-119.

Lindsay, M. D., Aillères, L., Jessell, M. W., de Kemp, E. A., and Betts, P. G., 2012a, Locating and quantifying geological uncertainty in three-dimensional models: Analysis of the Gippsland Basin, southeastern Australia: Tectonophysics, v. 546–547, no. 0, p. 10-27.

Lindsay, M. D., Jessell, M. W., Ailleres, L., Perrouty, S., de Kemp, E. A., and Betts, P. G., 2012b, Geodiversity: Exploration of 3D geological model space, Submitted - review pending: Tectonphysics; Chapter 2 [PhD] Monash University and Université Paul Sabatier (Toulouse III).

Lindsay, M. D., Jessell, M. W., Perrouty, S., Ailleres, L., de Kemp, E. A., and Betts, P. G., 2012c, Chapter 3 - The forward response of model space: Using geometrical and geophysical geodiversity metrics to categorise geological possibility, Enhancing potential field inversion techniques with geological uncertainty and model space exploration [PhD] Monash University and Université Paul Sabatier (Toulouse III).

Lindsay, M. D., Perrouty, S., Ailleres, L., Jessell, M. W., de Kemp, E. A., and Betts, P. G., 2012d, Chapter 4 - Using uncertainty, geodiversity and inversion to investigate the Tarkwaian Basin, Ashanti Greenstone Belt, southwestern Ghana, Enhancing potential field inversion techniques with geological uncertainty and model space exploration [PhD] Monash University and Université Paul Sabatier (Toulouse III).

Lisle, R. J., and Robinson, J. M., 1995, The Mohr circle for curvature and its application to fold description: Journal of Structural Geology, v. 17, no. 5, p. 739-750.

Lisle, R. J., and Toimil, N. C., 2007, Defining folds on three-dimensional surfaces: Geology, v. 35, no. 6, p. 519.

Loh, G., Hirdes, W., Anani, C., Davis, D. W., and Vetter, U. K., 1999, Explanatory notes for the geological map of Southwest Ghana 1: 100,000, Geologisches Jarhbuch, Reihe B, Heft 93, 150p, Bundesanstalt für Geowissenschaften und Rohstoffe.

Luyendyk, A. P. J., 1997, Processing of airborne magnetic data: AGSO Journal of Australian Geology and Geophysics, v. 17, no. 2, p. 31-38.

MacCormack, K. E., and Eyles, C. H., 2012, Assessing the impact of program selection on the accuracy of 3D geologic models: Geosphere, v. 8, no. 2, p. 534-543.

MacEachren, A. M., Brewer, C. A., and Pickle, L. W., 1998, Visualizing georeferenced data: representing reliability of health statistics: Environment and Planning A, v. 30, no. 9, p. 1547-1561.

Magurran, A. E., 2003, Measuring biological diversity, Oxford, Blackwell.

Malehmir, A., Juhlin, C., Wijns, C., Urosevic, M., Valasti, P., and Koivisto, E., 2012, 3D reflection seismic imaging for open-pit mine planning and deep exploration in the Kevitsa Ni-Cu-PGE deposit, northern Finland: Geophysics, v. 77, no. 5, p. WC95-WC108.

Mallet, J.-L., 2002, Geomodeling, New York, Oxford University Press, Applied Geostatistics Series.

Mallet, J. L., 1992, Discrete smooth interpolation in geometric modelling: Computer-Aided Design, v. 24, no. 4, p. 178-191.

Mann, J. C., 1993, Uncertainty in geology, Computers in geology - 25 years of progress: Oxford, Oxford University Press, p. 241-254.

Marinoni, O., 2000, Geostatistisch gestützte Erstellung baugeologischer Modelle am Beispiel des zentralen Bereiches von Berlin, Mensch-und-Buch-Verl.

-, 2003, Improving geological models using a combined ordinary-indicator kriging approach: Engineering Geology, v. 69, no. 1-2, p. 37-45.

Marjoribanks, R. W., Rutland, R. W. R., Glen, R. A., and Laing, W. P., 1980, The structure and tectonic evolution of the Broken Hill region, Australia: Precambrian Research, v. 13, p. 209–240.

Martelet, G., Calcagno, P., Gumiaux, C., Truffert, C., Bitri, A., Gapais, D., and Brun, J. P., 2004, Integrated 3D geophysical and geological modelling of the Hercynian Suture Zone in the Champtoceaux area (south Brittany, France): Tectonophysics, v. 382, no. 1-2, p. 117-128.

Maxelon, M., Renard, P., Courrioux, G., Brändli, M., and Mancktelow, N., 2009, A workflow to facilitate three-dimensional geometrical modelling of complex poly-deformed geological units: Computers & Geosciences, v. 35, no. 3, p. 644-658.

McLean, M. A., and Betts, P. G., 2003, Geophysical constraints of shear zones and geometry of the Hiltaba Suite granites in the western Gawler Craton, Australia: Australian Journal of Earth Sciences, v. 50, no. 4, p. 525 - 541.

McLean, M. A., Rawling, T. J., Betts, P. G., Phillips, G., and Wilson, C. J. L., 2008, Three-dimensional inversion modelling of a Neoproterozoic basin in the southern Prince Charles Mountains, East Antarctica: Tectonophysics, v. 456, no. 3-4, p. 180-193.

Meju, M. A., 2002, Geoelectromagnetic Exploration For Natural Resources: Models, Case Studies And Challenges: Surveys in Geophysics, v. 23, no. 2, p. 133-206.

Metelka, V., Baratoux, L., Naba, S., and Jessell, M. W., 2011, A geophysically constrained litho-structural analysis of the Eburnean greenstone belts and associated granitoid domains, Burkina Faso, West Africa: Precambrian Research, v. 190, no. 1-4, p. 48-69.

Miller, A. I., and Foote, M., 1996, Calibrating the Ordovician radiation of marine life: Implications for Phanerozoic diversity trends: Paleobiology, v. 22, no. 2, p. 304-309.

Milligan, P. R., and Gunn, P. J., 1997, Enhancement and presentation of airborne geophysical data: AGSO Journal of Australian Geology and Geophysics, v. 17, no. 2, p. 63-75.

Mitchell, J. K., Holdgate, G. R., and Wallace, M. W., 2007, Pliocene - Pleistocene history of the Gippsland Basin outer shelf and canyon heads, southeast Australia: Australian Journal of Earth Sciences: An International Geoscience Journal of the Geological Society of Australia, v. 54, no. 1, p. 49 - 64.

Moore, D., and Wong, D., 2002, Eastern and Central Gippsland Basin, Southeast Australia; Basement Interpretation and Basin Links: Victorian Initiative for Minerals and Petroleum Report 69: Department of Natural Resources and Environment.

Moresi, L., Quenette, S., Lemiale, V., Mériaux, C., Appelbe, B., and Mühlhaus, H. B., 2007, Computational approaches to studying non-linear dynamics of the crust and mantle: Physics of the Earth and Planetary Interiors, v. 163, no. 1–4, p. 69-82.

Morozov, I., Chubak, G., and Blyth, S., 2009, Interactive 3D/2D visualization for geophysical data processing and interpretation: Computers & Geosciences, v. 35, no. 7, p. 1397-1408.

Mosegaard, K., and Tarantola, A., 1995, Monte Carlo sampling of solutions to inverse problems: Journal of geophysical research, v. 100, no. B7, p. 12,431-412,447.

Moyen, R., 2005, Paramétrisation 3D de l'espace en géologie sédimentaire : le modèle GeoChron [PhD]: Université de Nancy, France.

Murphy, F. C., Rawling, T. J., Wilson, C. J. L., Dugdale, L. J., and Miller, J. M., 2006, 3D structural modelling and implications for targeting gold mineralisation in western Victoria: Australian Journal of Earth Sciences, v. 53, no. 5, p. 875 - 889.

Muxworthy, A. R., and McClelland, E., 2000, Review of the low-temperature magnetic properties of magnetite from a rock magnetic perspective: Geophysical Journal International, v. 140, no. 1, p. 101-114.

Mynatt, I., Bergbauer, S., and Pollard, D. D., 2007, Using differential geometry to describe 3-D folds: Journal of Structural Geology, v. 29, no. 7, p. 1256-1266.

Nabighian, M. N., Grauch, V. J. S., Hansen, R. O., LaFehr, T. R., Li, Y., Peirce, J. W., Phillips, J. D., and Ruder, M. E., 2005, The historical development of the magnetic method in exploration: Geophysics, v. 70, no. 6, p. 33ND-61ND.

Nettleton, L. L., 1942, Gravity and magnetic calculations: Geophysics, v. 7, no. 3, p. 293-310.

O'Dell, M., and Lamers, E., 2005, Subsurface Uncertainty Management and Development Optimization in the Harweel Cluster, South Oman: SPE Reservoir Evaluation and Engineering, v. 8, no. 2, p. 164-168.

O'Gorman, L., Sammon, M. J., and Seul, M., 2008, Practical algorithms for image analysis : description, examples, programs, and projects, New York, Cambridge University Press.

Oberthür, T., Vetter, U., Davis, D. W., and Amanor, J., 1998, Age constraints on gold mineralization and Palaeoproterozoic crustal evolution in the Ashanti belt of southern Ghana: Precambrian Research, v. 89, p. 129-143.

Okabe, M., 1979, Analytical expressions for gravity anomalies due to homogeneous polyhedral bodies and translations into magnetic anomalies: Geophysics, v. 44, no. 4, p. 730-741.

Oldenburg, D. W., 1974, Inversion and interpretation of gravity anomalies: Geophysics, v. 39, no. 4, p. 526-536.

Oldenburg, D. W., Li, Y., and Ellis, R. G., 1997, Inversion of geophysical data over a copper gold porphyry deposit: A case history for Mt. Milligan: Geophysics, v. 62, no. 5, p. 1419-1431.

Olson, C. F., and Huttenlocher, D. P., 1997, Automatic target recognition by matching oriented edge pixels: Image Processing, IEEE Transactions on, v. 6, no. 1, p. 103-113.

Perrouty, S., 2012, Chapter 4 - 3D modelling of the Ashanti Belt, southwest Ghana, and lithostratigraphic control on hold occurences within the Sefwi Group, Evolution Structurale de la Ceinture Minéralisée d'Ashanti, Sud-Ouest Ghana, [PhD] Université Paul Sabatier (Toulouse III).

Perrouty, S., Aillères, L., Jessell, M. W., Baratoux, L., Bourassa, Y., and Crawford, B., 2012, Revised Eburnean geodynamic evolution of the gold-rich southern Ashanti Belt, Ghana, with new field and geophysical evidence of pre-Tarkwaian deformations: Precambrian Research, v. 204-205, p. 12-39.

Pigios, J.-P., Groves, D. I., Fletcher, I. R., McNaughton, N. J., and Snee, L. W., 2003, Age constraints on Tarkwaian palaeoplacer and lode-gold formation in the Tarkwa-Damang district, SW Ghana: Mineralium Deposita, v. 38, p. 695-714.

Plouff, D., 1976, Gravity and magnetic fields of polygonal prisms and application to magnetic terrain corrections: Geophysics, v. 41, no. 4, p. 727-741.

Polanyi, M., 1962, Tacit knowing: Its bearing on some problems of philosophy: Reviews of modern physics, v. 34, no. 4, p. 601-616.

Popper, K., 1983, A proof of the impossibility of inductive probability [7]: Nature, v. 302, no. 5910, p. 687-688.

Prutkin, I., and Casten, U., 2009, Efficient gravity data inversion for 3D topography of a contact surface with application to the Hellenic subduction zone: Computers & Geosciences, v. 35, no. 2, p. 225-233.

Putz, M., Stüwe, K., Jessell, M., and Calcagno, P., 2006, Three-dimensional model and late stage warping of the Plattengneis Shear Zone in the Eastern Alps: Tectonophysics, v. 412, no. 1-2, p. 87-103.

Rahmanian, V. D., Moore, P. S., Mudge, W. J., and Spring, D. E., 1990, Sequence stratigraphy and the habitat of hydrocarbons, Gippsland Basin, Australia: Geological Society, London, Special Publications, v. 50, no. 1, p. 525-544.

Rawling, T. J., Schaubs, P. M., Dugdale, L. J., Wilson, C. J. L., and Murphy, F. C., 2006, Application of 3D models and numerical simulations as a predictive exploration tool in western Victoria: Australian Journal of Earth Sciences, v. 53, no. 5, p. 825 - 839.

Ray, T., 2009, Rethinking Polanyi's concept of tacit knowledge: From personal knowing to imagined institutions: Minerva, v. 47, no. 1, p. 75-92.

Reid, A. B., Allsop, J. M., Granser, H., Millett, A. J., and Somerton, I. W., 1990, Magnetic interpretation in three dimensions using Euler deconvolution: Geophysics, v. 55, no. 1, p. 80-91.

Rix, G., and Liévre, P., 2008, Towards a codification of practical knowledge: Knowledge Management Research Practices, v. 6, no. 3, p. 225-232.

Roy, K., and Foote, M., 1997, Morphological approaches to measuring biodiversity: Trends in Ecology and Evolution, v. 12, no. 7, p. 277-281.

Royer, J.-J., Mallet, J.-L., Cognot, R., and Moyen, R., Geochron: a framework to estimate fracturation of deformed sedimentary layers, in Proceedings International Association for Mathematical Geology: XIth International Congress, Université de Liège, Belgium, September, 3rd to 8th 2006, International Association for Mathematical Geology.

Royse, K. R., 2010, Combining numerical and cognitive 3D modelling approaches in order to determine the structure of the Chalk in the London Basin: Computers & Geosciences, v. 36, no. 4, p. 500-511.

Rucklidge, W. J., 1997, Efficiently locating objects using the Hausdorff distance: International Journal of Computer Vision, v. 24, no. 3, p. 251-270.

Saltus, R. W., and Blakely, R. J., 2011, Unique geologic insights from "non-unique" gravity and magnetic interpretation: GSA Today, v. 21, no. 12, p. 8.

Samadi, A., Amiri-Tokaldany, E., and Darby, S. E., 2009, Identifying the effects of parameter uncertainty on the reliability of riverbank stability modelling: Geomorphology, v. 106, no. 3-4, p. 219-230.

Sambridge, M., and Drijkoningen, G., 1992, Genetic algorithms in seismic waveform inversion: Geophysical Journal International, v. 109, no. 2, p. 323-342.

Sambridge, M., and Mosegaard, K., 2002, Monte Carlo methods in geophysical inverse problems: Reviews of Geophysics, v. 40, no. 3, p. 3-1 - 3-29.

Schmidt, P. W., and McDougall, I., 1977, Palaeomagnetic and potassium-argon dating studies of the Tasmanian Dolerites: Journal of the Geological Society of Australia, v. 24, no. 5, p. 321-328.

Schreiber, D., Lardeaux, J.-M., Martelet, G., Courrioux, G., and Guillen, A., 2010, 3-D modelling of Alpine Mohos in Southwestern Alps: Geophysical Journal International, v. 180, no. 3, p. 961-975.

Seiler, A., Aanonsen, S. I., Evensen, G., and Riven, J. C., 2010, Structural surface uncertainty modeling and updating using the ensemble kaiman filter: SPE Journal, v. 15, no. 4, p. 1068-1082.

Sestini, G., 1973, Sedimentology of a paleoplacer: the gold-bearing Tarkwaian of Ghana, Ores In Sediments Springer, p. 275-305.

Shannon, E., 1948, A mathematical theory of communication: Bell Systems Technical Journal, v. 27, p. 379-423.

Shcheglov, V., 1991, Errors in determining boundaries of stratified deposits: Mathematical Geology, v. 23, no. 1, p. 77-85.

Sim, D.-G., Kwon, O.-K., and Park, R.-H., 1999, Object matching algorithms using robust Hausdorff distance measures: Image Processing, IEEE Transactions on, v. 8, no. 3, p. 425-429.

Simpson, E. H., 1949, Measurement of diversity [16]: Nature, v. 163, no. 4148, p. 688.

Singer, D., and Menzie, W., 2010, Quantitative mineral resource assessments: an integrated approach, Oxford, Oxford University Press.

Sloan, S. W., 1993, A fast algorithm for generating constrained delaunay triangulations: Computers & Structures, v. 47, no. 3, p. 441-450.

Smirnoff, A., Boisvert, E., and Paradis, S. J., 2008, Support vector machine for 3D modelling from sparse geological information of various origins: Computers & Geosciences, v. 34, no. 2, p. 127-143.

Smith, M. A., Bernecker, T., Liberman, T., Moore, D., and Wong, D., 2000, Petroleum prospectivity of the deep-water gazettal areas V00-3 and V00-4, southeastern Gippsland Basin, Victoria, Australia: Department of Natural Resources and Environment.

Stewart, J. R., and Betts, P. G., 2010, Implications for Proterozoic plate margin evolution from geophysical analysis and crustal-scale modeling within the western Gawler Craton, Australia: Tectonophysics, v. 483, no. 1-2, p. 151-177.

Strykowski, G., Boschetti, F., and Papp, G., 2005, Estimation of the mass density contrasts and the 3D geometrical shape of the source bodies in the Yilgarn area, Eastern Goldfields, Western Australia: Journal of Geodynamics, v. 39, no. 5, p. 444-460.

Susini, S., and De Donatis, M., 2009, 3D model of a sector of the South Scotia Ridge (Antarctica): Computers & Geosciences, v. 35, no. 1, p. 83-91.

Suzuki, S., Caumon, G., and Caers, J., 2008, Dynamic data integration for structural modeling: model screening approach using a distance-based model parameterization: Computational Geosciences, v. 12, no. 1, p. 105-119.

Talbot, J.-Y., 2000, AMS study of the Pont-de-Montvert-Borne porphyritic granite pluton (French Massif Central) and its tectonic implications: Geophysical journal international, v. 140, no. 3, p. 677-686.

Talbot, J.-Y., Martelet, G., Courrioux, G., Chen, Y., and Faure, M., 2004, Emplacement in an extensional setting of the Mont Lozère-Borne granitic complex (SE France) inferred from comprehensive AMS, structural and gravity studies: Journal of Structural Geology, v. 26, no. 1, p. 11-28.

Tangestani, M. H., and Moore, F., 2001, Porphyry copper potential mapping using the weights-of- evidence model in a GIS, northern Shahr-e-Babak, Iran: Australian Journal of Earth Sciences, v. 48, no. 5, p. 695-701.

-, 2003, Mapping porphyry copper potential with a fuzzy model, northern Shahr-e-Babak, Iran: Australian Journal of Earth Sciences, v. 50, no. 3, p. 311-317.

Tarantola, A., 1984, Inversion of seismic relfection data in the acoustic approximation: Geophysics, v. 49, no. 8, p. 1259-1266.

Tarantola, A., 2005, Inverse problem theory and methods for model parameter estimation, Society for Industrial and Applied Mathematics.

Tarantola, A., 2006, Popper, Bayes and the inverse problem: Nature Physics, v. 2, no. 8, p. 492-494.

Tarantola, A., and Valette, B., 1982a, Generalized nonlinear inverse problems solved using the least squares criterion: Reviews of Geophysics and Space Physics, v. 20, no. 2, p. 219-232.

-, 1982b, Inverse problems = quest for information: Journal of Geophysics - Zeitschrift fur Geophysik, v. 50, no. 3, p. 159-170.

Tavakoli, R., Pencheva, G., Wheeler, M. F., and Ganis, B., 2013, A parallel ensemble-based framework for reservoir history matching and uncertainty characterization: Computational Geosciences, v. 17, no. 1, p. 83-97.

Telford, W. M., Geldart, L. P., and Sheriff, R. E., 1990, Applied Geophysics, Cambridge, UK, Cambridge University Press.

Thomson, J., Hetzler, E., MacEachren, A., Gahegan, M., and Pavel, M., A typology for visualizing uncertainty, in Proceedings Proceedings of SPIE - The International Society for Optical Engineering, Jena, Germany, 2005, Volume 5669, p. 146-157.

Thore, P., Shtuka, A., Lecour, M., Ait-Ettajer, T., and Cognot, R., 2002, Structural uncertainties: Determination, management, and applications: Geophysics, v. 67, no. 3, p. 840-852.

Torvela, T., and Bond, C. E., 2010, Do experts use idealised structural models? Insights from a deepwater fold-thrust belt: Journal of Structural Geology, v. 33, no. 1, p. 51-58.

Tunks, A. J., Selley, D., Rogers, J. R., and Brabham, G., 2004, Vein mineralization at the Damang Gold Mine, Ghana: controls on mineralization: Journal of Structural Geology, v. 26, p. 1257-1273.

Veevers, J. J., 1986, Breakup of Australia and Antarctica estimated as mid-Cretaceous (95 ± 5 Ma) from magnetic and seismic data at the continental margin: Earth and Planetary Science Letters, v. 77, no. 1, p. 91-99.

Veevers, J. J., Powell, C. M., and Roots, S. R., 1991, Review of seafloor spreading around Australia. I. synthesis of the patterns of spreading: Australian Journal of Earth Sciences: An International Geoscience Journal of the Geological Society of Australia, v. 38, no. 4, p. 373 - 389.

Viard, T., Caumon, G., and Lévy, B., 2010, Adjacent versus coincident representations of geospatial uncertainty: Which promote better decisions?: Computers & Geosciences, v. 37, no. 4, p. 511-520.

Vouillamoz, N., Sue, C., Champagnac, J. D., and Calcagno, P., 2012, 3D cartographic modeling of the Alpine arc: Tectonophysics.

Wang, L., and Suter, D., 2007, Learning and Matching of Dynamic Shape Manifolds for Human Action Recognition: Image Processing, IEEE Transactions on, v. 16, no. 6, p. 1646-1661.

Wellmann, F. J., Horowitz, F. G., Schill, E., and Regenauer-Lieb, K., 2010, Towards incorporating uncertainty of structural data in 3D geological inversion: Tectonophysics, v. 490, no. 3-4, p. 141-151.

Wellmann, J. F., and Regenauer-Lieb, K., 2011, Uncertainties have a meaning: Information entropy as a quality measure for 3-D geological models: Tectonophysics, v. 526-529, p. 207-216.

White, S. H., Rothery, E., Lips, A. L. W., and Barclay, T. J. R., 1995, Broken Hill area, Australia, as a Proterozoic fold and thrust belt: implications for the Broken Hill base-metal deposit: Transactions of the Institution of Mining and Metallurgy. Section B. Applied Earth Science, v. 104, p. B1-B17.

Wijns, C., and Kowalczyk, P., 2007, Interactive geophysical inversion using qualitative geological constraints: Exploration Geophysics, v. 38, no. 3, p. 208-212.

Williams, H. A., Betts, P. G., and Ailleres, L., 2009, Constrained 3D modeling of the Mesoproterozoic Benagerie Volcanics, Australia: Physics of the Earth and Planetary Interiors, v. 173, no. 3-4, p. 233-253.

Williams, N. C., Applying UBC-GIF potential field inversions in greenfields or brownfields exploration, in Proceedings AESC2006, Melbourne, Australia, 2006.

Willman, C. E., VandenBerg, A. H. M., and Morand, V. J., 2002, Evolution of the southeastern Lachlan Fold Belt in Victoria: Australian Journal of Earth Sciences, v. 49, no. 2, p. 271-289.

Woodward, N. B., 2012, Evaluation, analysis and prediction of geologic structures: Journal of Structural Geology, v. 41, p. 76-85.

Worthington, P. F., 2002, A validation criterion to optimize core sampling for the characterization of petrophysical facies: Petrophysics, v. 43, no. 6, p. 477-493.

Wu, Q., Xu, H., and Zou, X., 2005, An effective method for 3D geological modeling with multi-source data integration: Computers & Geosciences, v. 31, no. 1, p. 35-43.

Wycisk, P., 2009, High-resolution 3D spatial modelling of complex geological structures for an environmental risk assessment of abundant mining and industrial megasites: Computers & Geosciences, v. 35, no. 1, p. 165-182.

Xue, Y., Sun, M., and Ma, A., 2004, On the reconstruction of three-dimensional complex geological objects using Delaunay triangulation: Future Generation Computer Systems, v. 20, no. 7, p. 1227-1234.

Yeten, B., Brouwer, D. R., Durlofsky, L. J., and Aziz, K., 2004, Decision analysis under uncertainty for smart well deployment: Journal of Petroleum Science and Engineering, v. 43, no. 3-4, p. 183-199.

Zanchi, A., Francesca, S., Stefano, Z., Simone, S., and Graziano, G., 2009, 3D reconstruction of complex geological bodies: Examples from the Alps: Computers & Geosciences, v. 35, no. 1, p. 49-69.

Zelt, C. A., 1999, Modelling strategies and model assessment for wide-angle seismic traveltime data: Geophysical Journal International, v. 139, no. 1, p. 183-204.

Zuk, T., and Carpendale, S., 2006, Theoretical analysis of uncertainty visualizations, in Erbacher, R. F., Roberts, J. C., Gröhn, M. T., and Börner, K., eds., Proceedings of SPIE-IT&T Electronic Imaging, SPIE, p. 66-79.